PHYSICO-CHEMICAL STUDIES ON THE SYSTEMS, OXYGEN AND COBALT-SCHIFF BASE COMPLEX [Co(SALEN)] AND ITS DERIVATIVES

BY

NOBUHIRO KURIYAMA

GOVERNMENT INDUSTRIAL RESEARCH INSTITUTE, OSAKA

AGENCY OF INDUSTRIAL SCIENCE AND TECHNOLOGY

Doctoral Committee

Professor Michio Sorai

Professor Shichio Kawai

Professor Michihiko Kishita

Professor Hiroshi Suga

Acknowledgements

I wish to express sincere thanks to Professor Michio Sorai and Associate Professor Minoru Sakiyama for their kind guidance, encouragement and stimulative discussions. I also wish to thank to Professor Hiroshi Suga for encouragement and helpful suggestions to my work.

Measurement of magnetic susceptibility in this thesis was performed at Kishita Laboratory of collage of general education of Osaka University. I would like to express my acknowledgement to Professor Michihiko Kishita, Dr. Wasuke Mori, Dr. Hirokazu Nakayama and Dr. Taro Eguchi for their kind agreement concerning the apparatuses of the magnetic susceptibility measurement, their helpful advice, their fruitful discussions and encouragement.

I wish to thank to the late Professor Yoich Simura, Professor Sumio Kaizaki and Dr. Kazuaki Yamanari for permission to use their visible-ultraviolet spectrometer.

Infrared measurements were performed by Mr. Shin-ichi Ishikawa, Raman measurements by Mr. Mitsuo Oohama, and elemental analysis by Mr. Masakazu Okumiya. I am very grateful to them for their kindness.

After my leaving Osaka University and joining in Government Industrial Research Institute, Osaka (GIRIO), I had opportunity for engaging in the project on oxygenation reactions of solid-state materials by kind arrangement of Dr. Ryozo Hayami, the then director-general, Dr. Reikichi Iwamoto, the then senior officer for research planning and Dr. Hiroshi Sano, the then director of material chemistry department. I also wish to express sincere thanks to Dr. Toru Komiyama, director-general, Dr. Teruo Kodama,

senior officer for research planning, Dr. Yoshiko Nakahara, director of material chemistry department, and Dr. Masaki Haruta, deupty officer for research planning, for much encouragement and kind arrangement of opportunity for studying at Osaka University.

I am deeply gratful to Dr. Hiroshi Ishikawa, leader of chemical metallurgy section for encouragement, Dr. Tetsuo Sakai, senior researcher of the section, and Mr. Hiroshi Miyamura, researcher of the section, for heartfelt encouragement and useful discussion. Their attitude toward research works stimulated me to perform my works. I also wish to thank to the researchers of material chemistry department for much encouragement.

I would like to express my gratitude to the members of Microcalorimetry Center and Suga laboratory for valuable discussion and hearty encouragement.

Abstract

Physico-chmical studies were carried out on gas-solid reaction systems between dioxygen (O_2) and a series of solid-state synthetic oxygen carriers; [Co(SALEN)], [Co(3-RO-SALEN)] (R=CH_3 and C_2H_5), which form dimeric oxygenated species having a Co-O-O-Co linkage. Special attention was paid to cooperativity in their nonstoichiometric phases and intramolecular motion in the [Co(3-RO-SALEN)]-O_2 systems.

The partial molar Gibbs energy, enthalpy and entropy of oxygenation were determined by means of equilibrium pressure measurement and gas-solid reaction calorimetry. Magnetic and spectroscopic properties and powder X-ray diffractions as a function of dioxygen content and temperature were measured in order to obtain structural informations on the complexes and the distribution of dioxygen moities in their crystals. Lattice dynamical calculation was performed on finite random lattices which are models of the studied systems in order to estimate the effect of Co-O-O-Co linkages on their thermodynamic functions and cooperativity in them.

Two kinds of [Co(SALEN)] samples which were prepared from its pyridine and chloroform adducts were studied. They reacted with dioxygen up to Co:O_2=2:1, and gave similar phase relation, a two-phase region in lower dioxygen contents and an one-phase nonstoichiometric region in higher dioxygen content, although small differences were found in their thermodynamic and magnetic properties which are attributable to slight difference in molecular packing. In their nonstoichiometric phases, their partial molar enthalpies were independent of dioxygen content,

while cooperativity in those systems was observed. On the other hand, increase in their partial molar entropies with increasing dioxygen content decreased, that is, the dioxygen content dependences of the entropy terms were found to be an origin of their cooperativity. These variations in thermodynamic functions were explained as effect of change in lattice spectrum due to linkage formation between two adjacent complexes by a dioxygen through the lattice dynamic calculation.

In chapter 5, studies on two types each of [Co(3-MeO-SALEN)] ("ME" and "MM") and of [Co(3-EtO-SALEN)] ("ET" and "EM") are described, where ME and ET are the fresh samples annealed prior to every oxygenation run, while MM and EM are the samples stored for 1 year in their oxygenated forms. The systems between dioxygen and those samples consist of a nonstoichiometric phase for which random mixing of oxygenated and unoxygenated complex molecules was suggested from dioxygen content dependence of magnetic susceptibility. However, the systems indicated appreciable difference in thermodynamic quantities, magnetic susceptibility, vibrational and electronic spectra, and X-ray diffraction patterns. The difference between those fresh sample (ME and ET) and stored sample (MM and EM) would be attributable to difference in packing of the alkoxy groups. The ME-O_2 system exhibited considerable temperature dependence of the partial enthalpy and entropy between 274.75 K and 293.15 K. At 293.15K, these thermodynamic values were almost independent of dioxygen content, while those increased about 20kJmol^{-1} (in enthalpy) and 60 kJmol^{-1}K^{-1} (in entropy) with increasing dioxygen content. However, the MM-O_2 system did not indicate appreciable temperature and dioxygen content dependence between 274.75 K and

293.15 K. The ET-O_2 system did not show dioxygen content dependence at both 293.15 K and 323.15 K. However, the EM-O_2 system showed quite different dioxygen content dependence of thermodynamic values between 293.15 K and 323.15 K, which is similar to those for the ME-O_2 system.

The cooperativity observed in the system was attributed to contribution from the entropy term resulted from the dimerization of the complex molecules by dioxygens, as suggested from the lattice dynamics described in chapter 4. Since the partial molar Gibbs energies of the ME-O_2, MM-O_2, ET-O_2 and EM-O_2 systems showed similar dioxygen content dependence, the dioxygen content dependences of partial molar equantities of the systems compensate each other, and cooperative interaction by dioxygen binding would be also suggested for the systems. For the ET-O_2 system and the ME-O_2 system (at 293.15 K), estimation of the partial molar entropy excluding the statistical entropy of random distribution of dioxygen suggested positive contributions to the partial molar quantities through oxygenation.

Temperature dependences of vibrational spectra for the unoxygenated and oxygenated samples of the systems suggested that the positive contribution to partial molar enthalpy and entropy was attributable to excitation of intramolecular motions of the chelate skeleton of the complex molecules. For the ME-O_2, ET-O_2 and EM-O_2 systems, the experimental results agreed well with trends of the positive shift of the partial molar quantities expected from the temperature dependence of vibrational spectra for the unoxygenated and oxygenated samples of the systems. For the MM-O_2 system, the motions would contribute to the partial molar quantities.

Contents

Chapter 1 Introduction

Reversible reactions of dioxygen* (O_2) with metal complex are of crucial importance to animal life through the transport and storage of dioxygen by metalloprotain oxygen carriers, for example, hemoglobin, myoglobin and hemocyanin. Therefore the structure of the proteins, the property of the metal-dioxygen bond and the cooperative nature of dioxygen absorption found in hemoglobin and hemocyanin have been studied for many years by means of various techniques. Moreover, many metal complex molecules with reactivity toward dioxygen have been also synthesized, and studied extensively as models of the biological oxygen carriers[1,2].

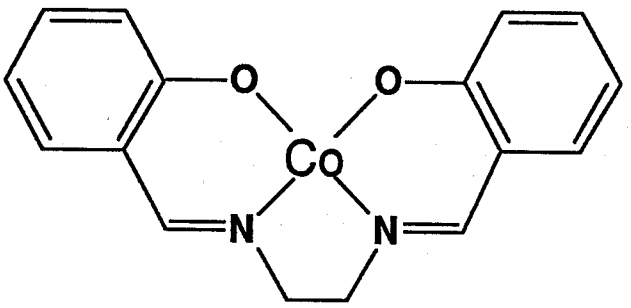

Fig.1.1 [Co(SALEN)]

Crystals of several synthetic oxygen carriers, as well as their solution, are known to react with dioxygen reversibly. N,N'-entylenebis(salicylideneiminato) Cobalt(II), [Co(SALEN)] (Fig.1.1), is the first synthetic reversible oxygen carrier. Its reactivity to dioxygen was found by Tumaki[3] in 1938 for its crystal. Calvin et al.[4] and Diehl et al.[5] synthesized various [Co(SALEN)] derivatives which react with gaseous dioxygen in their solid state, and studied their properties extensively.

Calvin et al. also reported the existence of a nonstoichiometric phase in the [Co(SALEN)]-O_2 system, and their isotherms of the systems of gaseous oxygen and [Co(SALEN)] derivatives. Since then, the nature of their dioxygen-metal ion bond in their solution and solid states have been extensively studied[1,2]. Recently, a series of iron(II) picket fence porphyrin complex derivatives as synthetic solid-state oxygen carriers were reported by Jameson *et al.*[6]. The systems between dioxygen and these oxygen carriers exhibit nonstoichiometry over entire composition, and the isotherms of some of them shows a sigmoidal curve which indicate a cooperative interaction between the oxygenated complex molecules as observed in hemoglobin[7].

Nonstoichiometry in gas-solid reaction systems is familiar for many metal-oxygen[8] and metal-hydrogen[9] systems for which solid phases of the systems are ionic or metallic crystal. In the systems, the thermodynamic properties of their nonstoichiometric phases are controlled by Coulomb interaction between ionic defects (metal-oxygen system)[10] or interaction between dissolved species through conduction electrons and lattice strain (metal-hydrogen system)[9]. On the other hand, crystal with no ionic defects and conduction electrons. [Co(SALEN)] is a molecular crystals. Therefore, it is interesting to see what is the interaction which dominantry controls the thermodynamic properties in the systems of gaseous dioxygen and derivatives of [Co(SALEN)] and iron(II) picket fence porphyrin. However, physico-chemical properties of the gas-solid reaction systems between gaseous dioxygen and those solid-state oxygen carriers, especially those in the nonstoichiometric phases, have not been elucidated.

In this thesis, physico-chemical properties of the systems between dioxygen and [Co(3-X-SALEN)] (X=H, OCH_3 and OC_2H_5), especially their nonstoichiometric phases, are studied, because of their simple molecular structure and easines of their synthesis. One of difficulties to study the systems is that the partial molar enthalpy determined from temperature dependence of the equilibrium pressure depends on the temperature range of the equilibrium data[4]. In order to overcome this difficulty, partial molar enthalpy of the systems was directly determined by means of gas-solid reaction calorimetry. This technique and simultaneous equilibrium measurement enable to determine all thermodynamic functions at a given temperature for the systems between dioxygen and [Co(3-X-SALEN)] (X=H, OCH_3 and OC_2H_5). According to the thermodynamic results and other physico-chemical informations, the thermodynamic properties of the nonstoichiometric phases, cooperativity** (or cooperative interaction between oxygenated complex molecules) and intramolecular motion in those systems are discussed.

In chapter 2, preparation of materials, apparatuses and experimental techniques used in this thesis are described. In chapter 3, partial molar enthalpy of [Co(SALEN)]-O_2 system is directly determined by gas-solid reaction calorimetry, and its thermodynamic properties are discussed. In chapter 4, effect of linking of adjacent complexes by dioxygen bridge to lattice energy and entropy is calculated for finite cubic lattices, and cooperativity in the thermodynamic functions of the lattices is discussed. In chapter 5, thermodynamic functions of [Co(3-RO-SALEN)] (R=CH_3 and C_2H_5)-O_2 systems are directly determined, and cooperativity and intramolecular motion in these systems are

discussed. In chapter 6, results and discussions in this thesis are summarized.

* The term "dioxygen" will be employed in this thesis in order to distinguish molecular oxygen (O_2) from atomic oxygen.[2)]

** The term "cooperativity" means the interaction which decrease partial molar Gibbs energy or equilibrium pressure of a system with increasing a parameter (for example, compositon).

References to Chapter 1

1. R.D.Jones, D.A.Summerville and F.Basolo, *Chem.Rev.*, 79, 139 (1979) and references therein.
2. E.C.Niederhoffer, J.H.Timmens and A.E.Martell, *Chem.Rev.*, 84, 137 (1984) and references therein.
3. T.Tsumaki, *Bull.Chem.Soc.Jpn.*, 13, 252 (1938).
4. M.Calvin, R.H.Bailes and W.K.Wilmarth, *J.Am.Chem.Soc.*, 68, 2254 (1946) and successive 5 articles; R.H.Bailes and M.Calvin, *ibid.*, 69, 1886 (1947).
5. H.Diehl, L.M.Ligget, G.Harrison, C.Hach and R.Curtis, *Iowa State Coll.J.Sci.*, 22, 165 (1948), and 13 preceding papers.
6. G.B.Jameson,F.S.Molinaro, J.A.Ibers, J.P.Collman, J.I.Brauman, E.Rose and K.S.Suslick, *J.Am.Chem.Soc.*, 100, 6769 (1978).
7. J.P.Collman, J.I.Brauman, E.Rose and K.S.Suslick, *Proc. Natl.Acad.Sci. U.S.A*, 75, 1052 (1978); G.B.Jameson, F.S.Molinaro, J.A.Ibers, J.P.Collman, J.I.Brauman, E.Rose and K.S.Suslick, *J.Am.Chem.Soc.*, 102, 3224 (1980).
8. "*Non-Stoichiometric Compounds*", ed. Mandelcorn, Academic Press, New York (1964); P.Gerdanian, *Adv.Solid-State Chem.*, 1,

225 (1989).

9. "*Hydrogen in Metals*", Vol.I and II, eds. G.Alefeld and J.Volkl, Springer-Verlag, Berlin, Heidelberg, New York (1978).

10. L.M.Atlas, *J.Phys.Chem.Solids*, 29, 91 (1968); *ibid.*, 29, 1349 (1968) and references therein.

Chapter 2. Materials, Apparatus and Experimental procedures

2.1 Introduction

In this thesis, various experimental methods were applied to study [Co(3-X-salen)](X=H,MeO,EtO)-dioxygen(O_2) systems and some of them were devised especially for the study of such nonstoichiometric systems which are unstable in atmosphere and at room temperature. In this chapter, all apparatuses and experimental procedures common to chapter 3 and chapter 5 and the preparation of materials are described.

2.2 Materials

The oxygen active [Co(SALEN)] derivatives studied in this thesis were prepared according to literature[1].

a) N,N'-Ethylenebis(salicylideneimine) : H_2SALEN

A solution of salicylaldehyde (Wako, GR grade, 48 g) and ethylenediamine (Wako, GR grade, 11.6 g) in 500 cm^3 of ethanol was prepared at 60 °C, and the mixture was cooled to room temperature. Yellow precipitate of H_2SALEN soon formed, was filtered, washed with cold ethanol. The crude H_2SALEN was recrystalized from ethanol solution.

Analysis Calcd. : C:71.62%, N:10.44%, H:6.01%.

Found : C:71.77%, N:10.41%, H:6.00%.

b) [Co(SALEN)] dimer : $[Co(SALEN)]_2$

H_2SALEN (40 g) was dissolved in 500 cm^3 of boiling ethanol. Cobaltous acetate tetrahydrate (36 g) was dissolved in boiling water (250 cm^3), and poured into the solution of H_2SALEN under

nitrogen stream. At first, red gelatinous product was precipitated, which changed to fine red crystals by keeping the mixture at 60 °C for 12 hours. After cooling, the crystals were filtered, washed with water and ethanol under nitrogen stream, and dried in a vacuum desiccator.

Analysis Calcd. : Co:18.12%, C:59.09%, N:8.61%, H:4.34%.

Found : Co:18.05%, C:59.15%, N:8.56%, H:4.38%.

c) [Co(SALEN)] pyridine adduct: [Co(SALEN)]py and oxygen active form prepared from it

(the latter sample is abbreviated as "SP").

A solution of $[Co(SALEN)]_2$ in pyridine (130 cm^3) was refluxed for 30 min. under nitrogen. After all precipitates had been dissolved, the solution was kept at a temperature slightly lower than its boiling point, and then monopyridine adduct was precipitated as needle crystals. After cooling the solution, the crystals were filtered off and washed with water under nitrogen stream. The crystals of [Co(SALEN)]py were dried in an oven 70 °C *in vacuo*.

Analysis Calcd. : Co:14.58%, C:62.38%, N:10.39%, H:4.74%.

Found : Co:14.51%, C:62.44%, N:10.41%, H:4.75%.

Oxygen active [Co(SALEN)] (SP) was prepared by heating [Co(SALEN)]py at 170 °C for 2 hours *in vacuo*. The completion of removal of pyridine was confirmed by elemental analysis. The ratio of carbon, nitrogen and hydrogen was determined since it was difficult to avoid oxygenation of the complex during the elemental analysis.

Analysis : Calcd. : C:N:H = 1:0.1457:0.0734

Found : C:N:H = 1:0.1465:0.0734

d) [Co(SALEN)] chloroform adduct: $[Co(SALEN)]CHCl_3$, and oxygen active form prepared from it

(the latter sample is abreviated as "SC").

Dissolution of $[Co(SALEN)]_2$ (1 g) in boiling chloroform (200 cm^3) gave dark purple needle crystals of $[Co(SALEN)]CHCl_3$ by removing the solvent at 40 °C under reduced pressure. The crystals were filtered, washed with a small amount of cold chloroform, and dried in a desiccator.

Analysis Calcd.: C:45.92%, N:6.31%, H:3.40%.

Found : C:46.36%, N:6.44%, H:3.47%.

Oxygen active form, [Co(SALEN)] (SC) was prepared by heating [Co(SALEN)]py at 100 °C for 2 hours *in vacuo*.

Analysis Calcd. : C:N:H = 1:0.1457:0.0734

Found : C:N:H = 1:0.1459:0.0733

e) N,N'-Ethylenebis(3-methoxysalicylideneimine) : H_2(3-MeO-SALEN)

To a solution of 3-methoxysalicylaldehyde (Tokyo Kasei, EP grade, 50 g) in a 3:1 ethanol-water mixture, ethylenediamine (10g) was added at 65 °C. Small yellow crystals precipitated immediately, was seperated from the solution and was recrystalized four times from ethanol solution.

Analysis Calcd. : C:65.84%, N:8.53%, H:6.14%,

Found : C:65.53%, N:8.42%, H:6.25%.

f) N,N'-Ethylenebis(3-methoxysalicylideneiminato) Cobalt(II) monohydrate : $[Co(3\text{-}MeO\text{-}SALEN)]H_2O$

To a boiling solution of H_2(3-MeO-SALEN) (25 g) and sodium acetate trihydrate (80 g) in a mixture of ethanol (700 cm^3) and

water (100 cm^3), cobaltous acetate tetrahydrate (19 g) was dissolved in boiling water (250 cm^3) was added rapidly under nitrogen stream. Yellow crystals precipitated after standing at room temperature overnight, were filtered out under nitrogen stream, washed with aqueous ethanol and were dried in vacuo at room temperature.

Analysis Calcd. : Co:14.61%, C:53.60%, N:6.95%, H:5.00%

Found : Co:14.42%, C:53.56%, N:7.00%, H:5.00%

g) N,N'-Ethylenebis(3-methoxysalicylideneiminato) Cobalt(II) form 1 (this sample is abbreviated as "ME").

Oxygen active [Co(3-MeO-SALEN)](ME) was prepared by heating [Co(3-MeO-SALEN)]H_2O at 150 °C for 2 hours in vacuo.

h) N,N'-Ethylenebis(3-methoxysalicylideneiminato) Cobalt(II) form 2 (this sample is abbreviated as "MM").

[Co(3-MeO-SALEN)](MM) was prepared by keeping oxygenated [Co(3-MeO-SALEN)](ME) for 1 year at room temperature.

i) N,N'-Ethylenebis(3-ethoxysalicylideneimine) : H_2(3-EtO-SALEN)

To a solution of 3-ethoxysalisylaldehyde (Tokyo Kasei, EP, 25 g) in boiling ethanol (400 cm^3), ethylenediamine (10.1 g) was added. After Cooling the solution, fine needle crystals formed were filtered off. After recrystallization from the solution in 1:1 mixture of ethanol and water, long needle crystals were obtained.

Analysis Calcd. : C:67.40, N:7.86, H:6.79,

Found : C:67.47, N:7.76, H:6.87

j) N,N'-Ethylenebis(3-ethoxysalicylideneiminato) Cobalt(II) monohydrate : [Co(3-EtO-SALEN)]H_2O

To a solution of H_2(3-EtO-SALEN) (10 g) and sodium acetate trihydrate (28g) in a mixture of ethanol (300 cm^3) and water (5 cm^3), cobaltous acetate tetrahydrate (7.5 g) dissolved in boiling water (100 cm^3) was added under nitrogen stream. After removing 160 cm^3 of ethanol, red purple crystals were precipitated, which were filtered off under nitrogen stream, washed with aqueous ethanol, and dried *in vacuo* at room temperature.

Analysis Calcd. : Co:13.66%, C:55.69%, N:6.49%, H:5.61%

Found : Co:13.42%, C:55.45%, N:6.44%, H:5.55%

k) N,N'-Ethylenebis(3-ethoxysalicylideneiminato) Cobalt(II) form 1 (this sample is abbreviated as "ET")

Oxygen active [Co(3-EtO-SALEN)](ET) was prepared by heating [Co(3-EtO-SALEN)]H_2O at 150 °C for 2 hours *in vacuo*.

l) N,N'-Ethylenebis(3-ethoxysalicylideneiminato) Cobalt(II) form 2 (this sample is abbreviated as "EM").

[Co(3-EtO-SALEN)](EM) was prepared by keeping oxygenated [Co(3-EtO-SALEN)](ET) for 1 year at room temperature.

m) N,N'-Ethylene-d_4-bis(3-methoxysalicylideneiminato) Cobalt(II) : [Co(3-MeO-SALEN-d_4)]

The deuterated ligand was prepared by condensation of 3-methoxysalicylaldehyde and ethylenediamine with deuterated methylene groups, and [Co(3-MeO-SALEN-d_4)] was prepared in a similar manner as in f). Preparation of deuterated ethylenediamine is described.

1,2-Dibromoethane-d_4

Conc. sulfuric acid (30 g) was slowly added to a mixture of ethylene glycol-d_4 (5 g), potassium bromide (22 g) and water (8 cm^3) under cooling by crashed ice. The mixture was refluxed for 30 min, and distilled. Lower layer of the distillate at about 105°C was washed with 20 cm^3 of conc. sulfuric acid, 10% NaOH and water, and then dried over calcium chloride. Yield was 1.6 g.

Ethylenediamine-d_4

A mixture of 1,2-dibromoethane-d_4 (1.6 g), potassium phthalimide (1.9 g) and DMF (6 cm^3) was kept at 90°C for 3 hours. After cooling to 40 °C, 20 cm^3 of 50% NaOH was added to it. The mixture was stirred overnight, and distilled. The distillate containing ethylenediamine-d_4 was directly used for the preparation of H_2(3-MeO-SALEN-d_4).

2.3 Gas-Solid Reaction Calorimetry

2.3.1 Gas-Solid Reaction Calorimetry System[2)]

A schematic diagram of the system is shown in Fig.2.1. This system consists of a calorimetric section and a gas-manipulation one.

Calorimetric section

In this section, a Tian-Calvet microcalorimeter[3)] (Setaram, low temperature model, from 77 to 473 K) with a sensitivity of about 60 $\mu V.mW^{-1}$ and two identical reaction vessels are included. In the experiments, the temperature of the isothermal block of the calorimeter was controlled by use of a proportional-integral temperature controller (Setaram RT-3000), under cooling with cold nitrogen gas flow (flow-mode) when required.

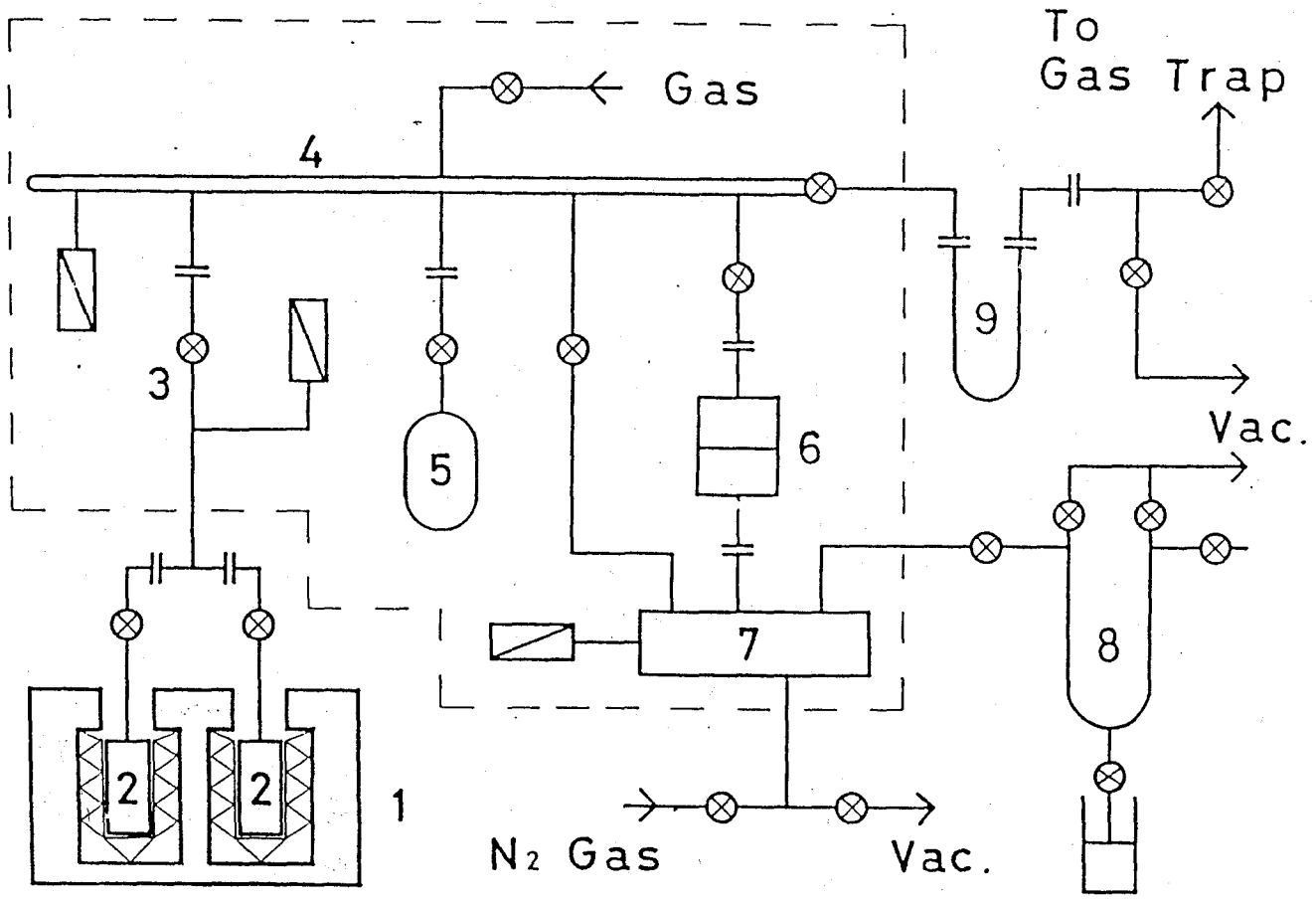

Fig.2.1 Schematic diagram of the gas-solid reaction calorimetry system : [- - - -], air thermostat; ⊗, greaseless stop-cock; ⊣⊢ ,joint; ▭, pressure gauge (strain gauge type) ; 1, calorimeter; 2, reaction vessel; 3, needle cock; 4, gas-manipulation line; 5, reference volume vessel; 6, differential pressure gauge (MKS); 7, ballast tank; 8, Hg manometer; 9, cold trap.

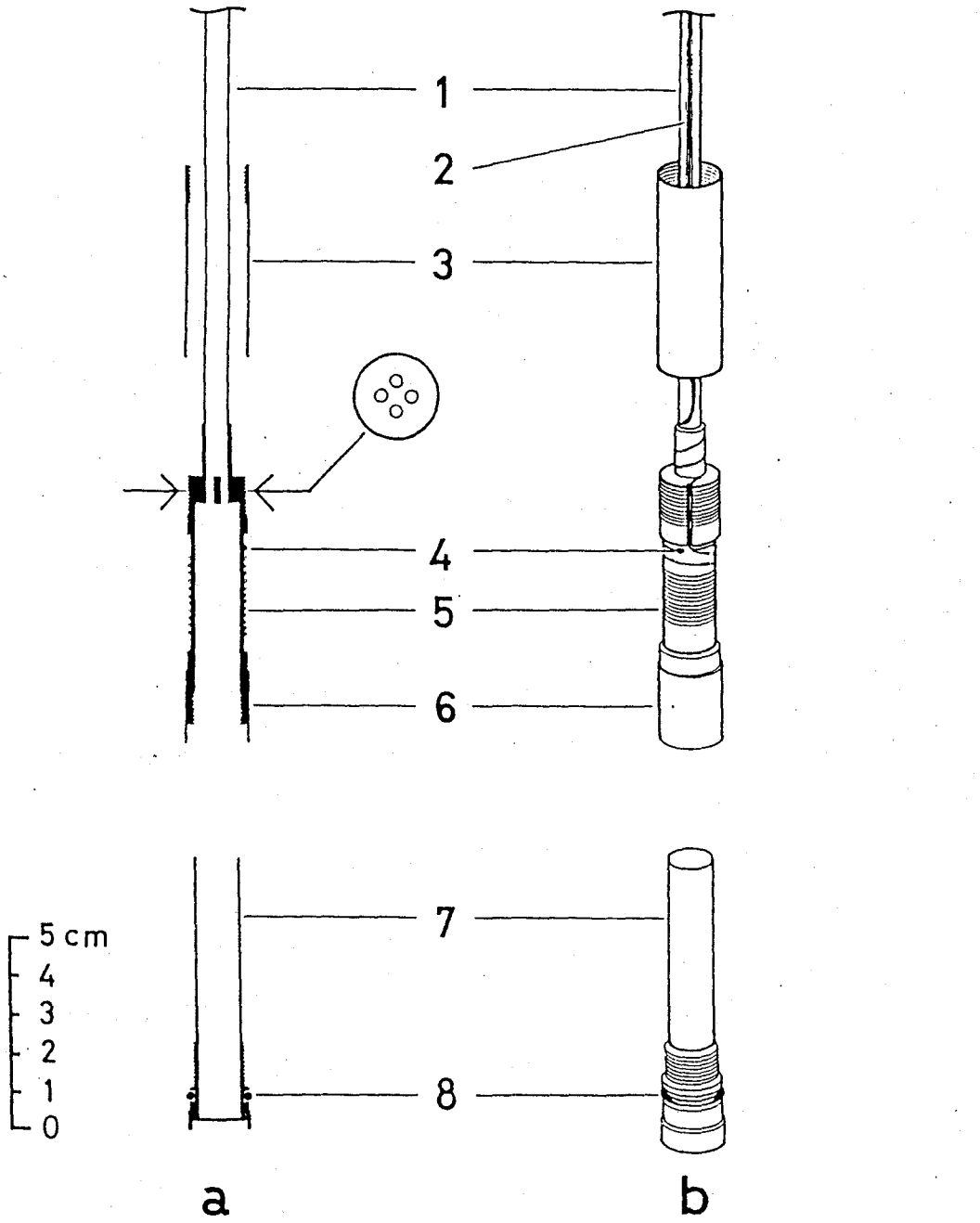

Fig.2.2 Side and cross-sectional views of the reaction vessel: 1, stainless-steel tube; 2, lead wire; 3, cover; 4, thermocouple; 5, heater wire; 6, reaction vessel; 7, sample container; 8, O-ring

Cross-sectional and side views of the reaction vessel are shown in Fig.2.2. The vessel is connected to the gas-manipulation section through a greaseless stop-cock on its top and a stainless steel tube with internal diameter of 2 mm and length of 100 cm. The reaction vessel proper (6) and the sample container (7) are made of stainless steel. At the neck of the reaction vessel proper, there are four small holes, through which gas enters or leaves the vessel. The internal volume below the neck is about 6.7 cm^3. The vessel is equipped with a calibration heater (Nichrome V, about 500 ohm) wound around the external surface of the reaction vessel proper, and a thermocouple junction (chromel to constantan) for temperature measurement.

Output voltage from the calorimeter was measured with a 6.5 digits digital multimeter (Keithley 181) and, at the same time, recorded on a strip-chart recorder. The digital data acquisition and processing were carried out with a personal computer (NEC PC-8001).

Gas-manipulation section

This section consists of a Pyrex glass tube ("line") (4 in Fig.2.2) about 100 cm^3 in volume, vessel (5) (98.630±0.019) cm^3 in volume, and pressure measurement facilities (6,7,8). The section can be evacuated to 2×10^{-4} Pa. The whole section, except the mercury manometer (8), was placed in an air thermostat kept within (301±0.05) K. Temperatures were measured at both sides of the tube and the average of the two was adopted as the temperature of gas in this section.

The pressure of gas in this section was determined by measuring the pressure difference between the line and ballast tank (7) with a capacitance pressure gauge (MKS type 222A, 1.333

kPa in full scale, ±1.5% of reading in accuracy) and the pressure in the ballast tank with a mercury manometer (8). The capacitance gauge was placed in the air-thermostat and calibrated against the mercury manometer. By this procedure, the inaccuracy of the gauge was decreased to 0.7% of the reading. By use of the mercury manometer, pressures up to 66.6 kPa were measured with a resolution of 1.3 Pa and those between 35 kPa and 160 kPa were measured with a resolution of 13 Pa, which is the resolution of a mercury barometer. The section is equipped with three auxiliary strain-gauge-type pressure gauges in order to monitor the pressure in each part, as shown in Fig.2.1.

2.3.2 Gas-Solid Reaction Calorimetry

The amount of gas reacted $\Delta_r n(\text{gas})$ was determined as the decrease in the one of gas in the gas-manipulation line $\Delta_r n(\text{line})$ minus the increase in the reaction vessel and the inlet tube $\Delta_r n(\text{vessels})$:

$$\Delta_r n(\text{gas})) = \Delta_r n(\text{line}) - \Delta_r n(\text{vessels}). \qquad \text{(eq.2.1)}$$

For the calculation of amount of gas the following equation of state was employed :

$$pV = nRT \cdot Z(p,T), \qquad \text{(eq.2.2)}$$

where V is the volume of gas at temperature T and pressure p and n is the amount of gas. $Z(p,T)$ is the compressibility factor defined as

$$Z(p,T) = 1 + \frac{9(p/p_c)}{128(T/T_c)}\left\{1 + \left(\frac{T}{T_c}\right)^2\right\}, \qquad \text{(eq.2.3)}$$

where T_c and p_c are the critical temperature and pressure, (T_c=154.6 K and p_c=5.05 MPa for oxygen gas), respectively.

The volume of the gas-manipulation line V_L was determined to be (93.033±0.070) cm^3, by expansion of helium from the line to the reference volume vessel. Since a temperature gradient is present along the reaction vessels and inlet tubes, the sample side volume shown in Fig.2.3 was divided into four sections (see Fig.2.3), V(reaction vessels) (V_r = 13.4 cm^3 - V_{sample} , at T_r), V(reaction vessels to outside of calorimeter) ($V_1=f_1 \cdot V_x$ at $T_1=(T_r+T_{room})/2$), V(at room temperature) ($V_2=f_2 \cdot V_x$ at $T_2=T_{room}$) and V(within the air thermostat) ($V_3=f_3 \cdot V_x$ at $T_3=T_{therm}$), where f_1=0.2148, f_2=0.4629, f_3=0.3223, and V_x was determined by expansion of helium from the line to the sample side at each calorimeter temperature.

Gas-solid reaction calorimetry was carried out on six Co(II) Schiff base complexes (SP, SC, ME, MM, ET and EM; see section 3.2) by similar procedure, and the temperatures measurements were conducted at 284.75 K and 293.15 K for SP and SC, 273.15K and 293.15K for ME and MM, and 293.15 K and 323.15 K for ET and EM.

Tablets (10 mm in diameter) of each sample were charge into the sample container, and it was sealed under nitrogen (Fig.2.4). After weighing, the sample container was attached to the reaction vessel and the vessel was kept at 130 °C *in vacuo* for 2 hours, for ME and ET, followed by annealing at 100 °C *in vacuo* for 1 day. Then the vessel was attached to the sample side thermopile of the calorimetric system, and another reaction vessel containing stainless steel rods with a volume similar to the one of the sample tablets[4]. Prior to calorimetry, the whole system was evacuated to $2x10^{-4}$ Pa.

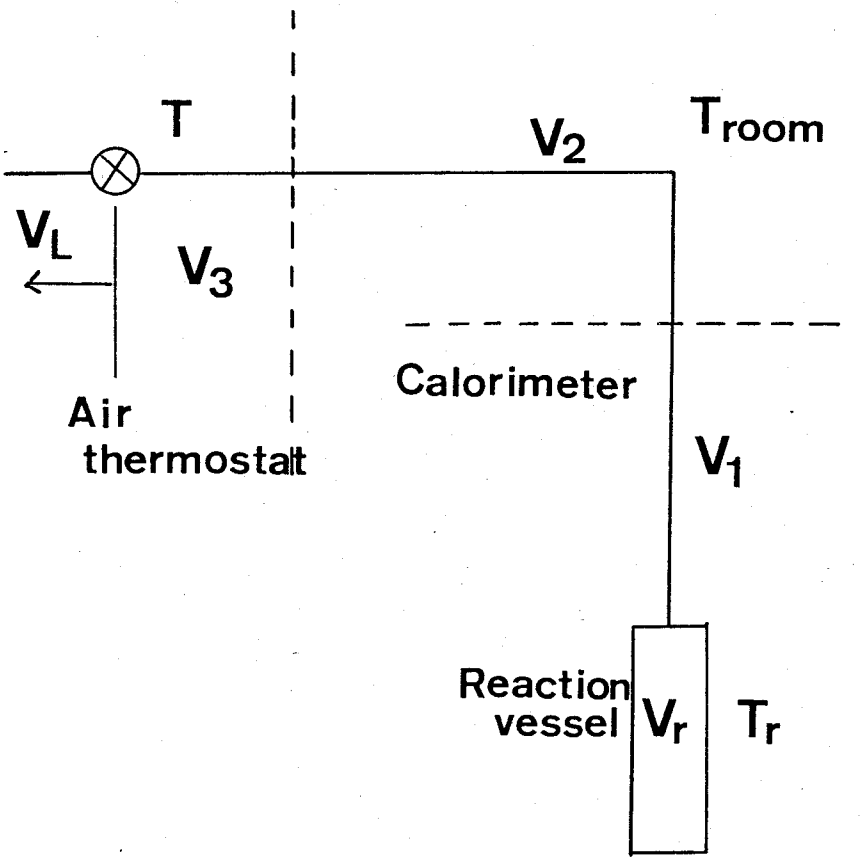

Fig.2.3 Division of the sample side volume into four sections; V_r, V_1, V_2, and V_3.

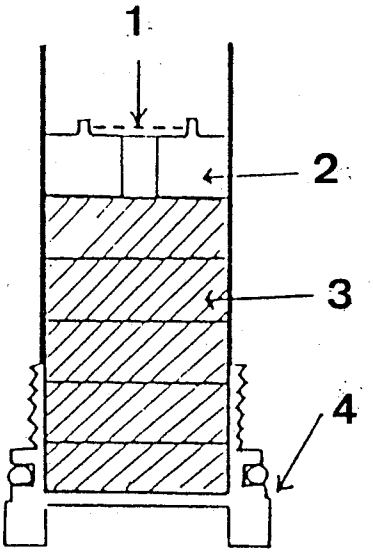

Fig.2.4 The sample container charged with sample pellets: 1, stainless-steel net; 2, stainless-steel ring; 3, sample pellets; 4, sample container.

Calorimetry on oxygenation reaction of the Co(II)-Schiff base complexes was carried out by step-by-step introduction of dioxygen from the gas-manipulation line to the reaction vessel (gas titration technique), that is, a sample was made to react with a small amount of dioxygen to change its composition, the heat evolved during the reaction being measured. Since the reaction rate was slow and it took at least 1 day until a significant heat effect was not observed, dioxygen pressure in the vessel was decreased to accelerate establishment of equilibrium after a prescribed amount of oxygen was reacted. Gradual drift in the pressure in the system was observed after output voltage of the thermopile had returned to the initial value, the pressure was further decreased until no pressure drift was observed. It took 4 or 6 hours for calorimetry and another 20 hours to confirm equilibrium.

Calibration on the sample-side reaction vessel was carried out after the first reaction step of every series by use of a built-in heater wound around the vessel (5 in Fig.3.2). In order to correct the energy equivalent E_b, thus obtained for systematic error associated with it, heat effect Q during the reaction was determined as follows;

$$Q = -a.E_b \cdot S \quad , \qquad \text{(eq.2.4)}$$

where S is the integrated voltage from the thermopile with respect to time, and a is the correction factor, which was found to be 0.9751[2] from the comparison of E_b with the equivalent obtained by using an oil-immersed heater placed in the reaction vessel. The latter had been shown to be accurate for the reaction: $NiCl_2(cr) + 6NH_3(g) = Ni(NH_3)_6Cl_2(cr)$ at 298.15 K[5].

2.4 Gas Titration System for Preparing Partially Oxygenated Sample

A simple gas titration system (Fig.2.5) was constructed to prepare partially oxygenated Co^{2+}-Schiff base complex for measuring magnetic susceptibilities, diffuse reflectance spectra, infrared spectra, Raman spectra and X-ray diffraction patterns. The system consists of a constant temperature water bath controlled at (293.15±0.02) K and a Pyrex glass tube (33.989±0.041) cm^3 equipped with a reference volume vessel (47.779±0.026) cm^3, a capacitance pressure gauge (MKS model 127A, 0 to 133 kPa, resolution 13 Pa), which are placed in an air thermostat at (304.5±1.0) K. The volume of the glass tube and reaction vessels was determined with helium based on the reference volume vessel. Procedure for the determination of the amount of gas reacted was similar to that described in section 3.3.2.

2.5 Magnetic Susceptibility

2.5.1 Dioxygen Content Dependence of Magnetic Susceptibility

Dioxygen content dependence of molar magnetic susceptibility of the complexes at room temperature was measured by Gouy method. A sample (about 0.3 g) was charge into a sealable quartz tube (Fig.2.6 Cell 1). After reaction with a prescribed amount of oxygen, the tube was sealed, and kept at 293.15K for more than 12 hours to homogenize the sample composition. Deionized water was used as reference material of susceptibility measurement, and the magnetic field strength was about 20 kGauss.

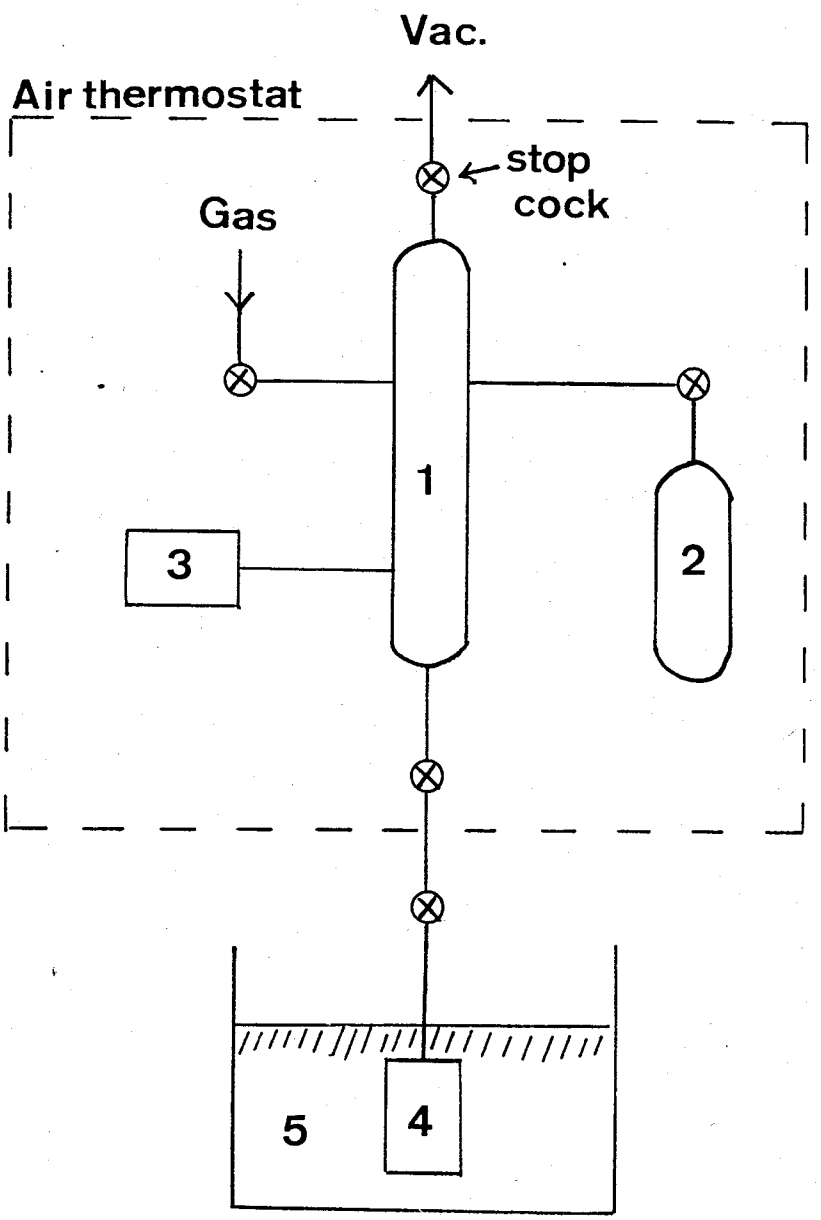

Fig.2.5 A gas-titration system for nonstoichiometric sample preparation: 1, Pyrex glass tube; 2, reference volume vessel; 3, pressure gauge (MKS 127A); 4, reaction vessel; 5, water thermostat.

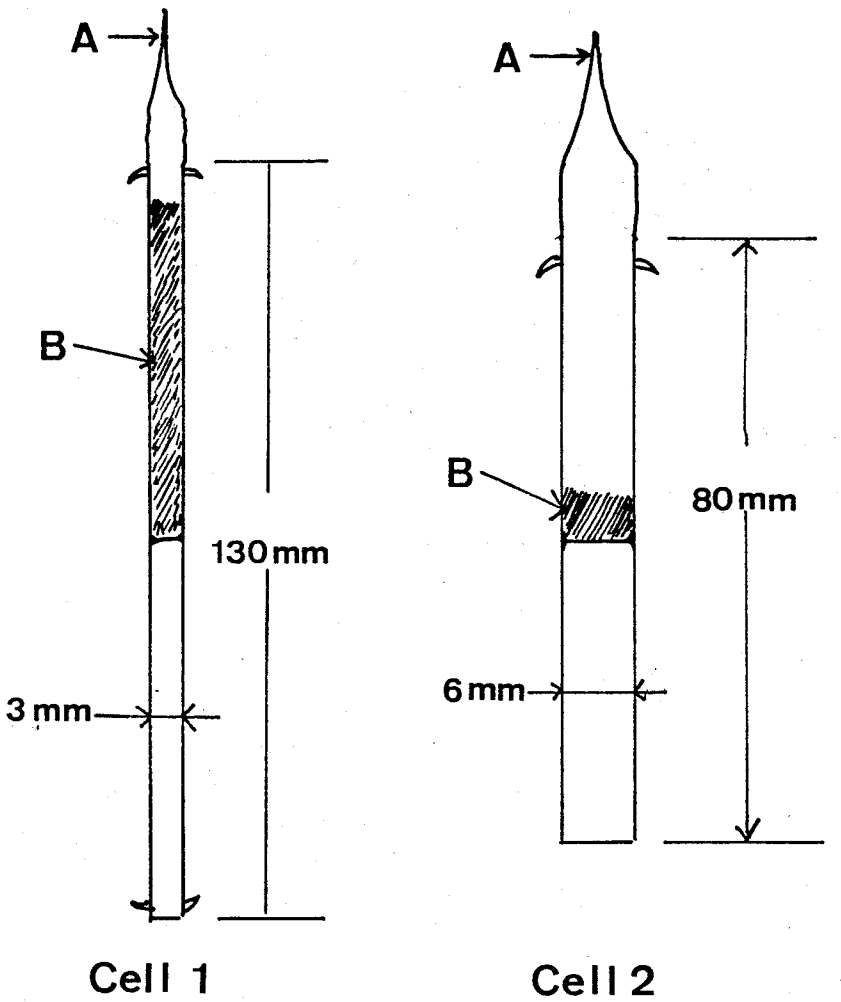

Fig.2.6 Sealable quartz cells, Cell 1 and Cell 2, for dioxygen content and temperature dependence measurements of magnetic susceptibility of the nonstoichiometric samples, respectively. Before the dioxygen content of the sample is changed, the cells is opened by cutting the capillary A. B is the sample.

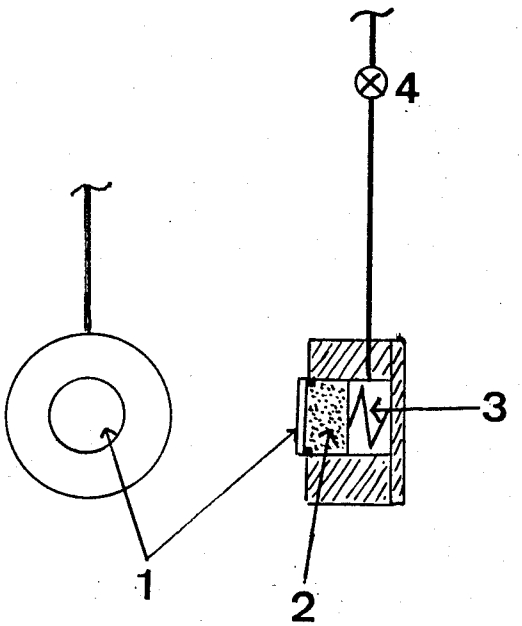

Fig.2.7 A cell for diffuse reflectance spectral: 1, quartz window; 2, sample; 3, spring; 4, stop cock.

2.5.2 Temperature Dependence of Magnetic Susceptibility

Temperature dependence of molar magnetic susceptibility was measured from 4.2 K to 297 K by the Faraday method. A sample (about 0.2g) was charged into a sealable quartz tube (Fig.2.6 Cell 2). Oxygenation was carried out as described in section 3.5.1. Molar susceptibility determined at room temperature was used as reference. The susceptibilities determined for a variety of amounts of [Co(3-EtO-SALEN)] agreed with each other within 1% above 17 K, in spite of the fact that the contribution of the cell to the measured susceptibility was of considerable magnitude (about 10 % at 200 K).

2.6 Diffuse Reflectance Spectra

An air-tight cell with a quartz window and a stop cock (Fig.2.7) was used for diffuse reflectance spectroscopic measurement for the cobalt complex samples with various oxygen contents. Oxygenation of samples were carried out as described in section 3.5.1. Spectra from 400 nm to 1500 nm were recorded at 295K by use of a HITACHI model 330 spectrometer.

2.7 Infrared and Raman Spectrum

Infrared spectra of the samples with various dioxygen contents were measured as nujol mull. Spectra from 400 cm^{-1} to 1800 cm^{-1} were recorded by a NIHON BUNKOU model DS-402G spectrometer and those from 30 cm^{-1} to 400 cm^{-1} by a HITACHI model FIS-1 spectrometer, both spectrometers being equipped with facilities for temperature variation.

Raman spectra were recorded for KBr pellet of the samples on a glass plate which was sealed in a glass tube. Excitation at 514.5 nm was made by an Ar ion laser (100 mW).

2.8 X-ray Diffraction

X-ray diffraction experiment by Cu-K_α radiation for the samples with at various dioxygen content were carried out by use of a RIGAKU X-ray diffraction system (RAD-B and Rotaflex RH-200) equipped with an air-tight goniometer and a temperature controller. Diffraction patterns were recorded at every 0.02° from 3° to 53°.

References to Chapter 2.

1. R.H.Bails and M.Calvin, *J.Am.Chem.Soc.*, 69, 1886 (1947).
2. N.Kuriyama and M.Sakiyama, *Thermochim. Acta*, 132, 75 (1988).
3. E.Calvet and H.Prat, "Recent Progress in Microcalorimetry", Pergamon, Oxford, (1963).
4. J.J.Murray, M.L.Post and J.B.Taylor, *J. Less-Common. Met.*, 80, 201 (1981).
5. N.Kuriyama and M.Sakiyama, *J.Chem.Thermodyn.*, 20, 729 (1988).

Chapter 3 Physico-chemical Studies on [Co(SALEN)]-O_2 Systems.

3.1 Introduction

[Co(SALEN)] (Fig.3.1a) was reported at the first time by Tumaki[1] in 1938 to be a solid state oxygen carrier. This complex forms adducts by recrystallization from solutions in pyridine, chloroform, benzene and so on[2]. Calvin *et al.*[2] and Aymes *et al.*[3] reported that its oxygen active forms prepared by thermal decomposition of the pyridine adduct and benzene adduct reacted with dioxygen in the ratio: Co:O_2=2:1, although Tsumaki[1] reported that [Co(SALEN)] prepared by decomposition of its chloroform adduct reacts with dioxygen in the ratio: Co:O_2=3:1. Calvin *et al.* also found a nonstoichiometric phase in the system, [Co(SALEN)]-O_2, for the complex prepared from its pyridine adduct[4]. Many studies on the complex in the solid state have been perfomed on the unoxygenated form and the fully oxygenated form, and it has been shown that two [Co(SALEN)] molecules react with an O_2 molecule to form a O_2-bridged dimer (Fig.3.1b) in many diamagnetic oxygenated crystals of the complex[5,6]. However, the behavior of the [Co(SALEN)]-O_2 system, especially in the nonstoichiometric phase, has not been studied in detail, and the origin of the difference in the ratios, Co:O_2, depending on sample preparation also has not been clarified.

In the present study, this system was studied by the thermodynamic (reaction-calorimetric and equilibrium) method and also studied by magnetic and spectroscopic methods to interpret the thermodynamic findings. The samples prepared from pyridine and chloroform adducts, "SP" and "SC", respectively, were used in

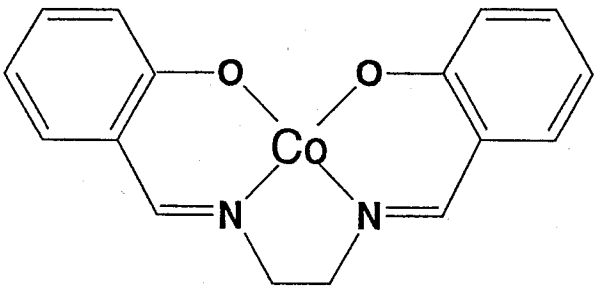

Fig.3.1a [Co(SALEN)]

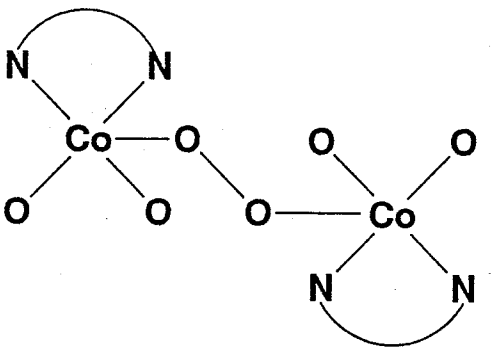

Fig.3.1b [Co(SALEN)]O_2[Co(SALEN)]

this study in order to clarify the difference in the maximum ratios of O_2 molecules to cobalt ions . Details of materials and experimental technques were described in chapter 2.

3.2 Experimental and Results

3.2.1 Gas-Solid Reaction Calorimetry on the Systems; O_2 and Two Types of [Co(SALEN)] (SP and SC)

Thermodynamic measurements on the systems were conducted for absorption run at 284.75 K and 293.15 K. The results are summarized in Table 3.1, where the dioxygen content, x, is indicated by the molar ratio of dioxygen moiety to [Co(SALEN)] in the oxygenated crystal. x_e indicates the dioxygen content at which equilibrium pressure has been determined, and x_m is the mean of initial and final dioxygen contents for a calorimetric run. Partial molar entropy at x_m were calculated from partial molar enthalpy and Gibbs energy at x_m determined by interpolation of experimental values. Standard state pressure is 100 kPa in this study. The equilibrium pressures, partial molar enthalpies and entropies of the systems are shown in Fig.3.2, Fig.3.3 and Fig.3.4, respectively.

As shown in Fig.3.2, each the SP-O_2 and SC-O_2 systems consists of a two-phase region characterized by a plateau reagion below about x=0.2, and a nonstoichiometric one-phase region where the equilibrium pressure increases monotonously with x. The phase boundaries were graphically determined as x=0.20 for the SP-O_2 system and x=0.25 for SC-O_2 at 293.15 K, and x=0.23 for SP-O_2 and x=0.26 for SC-O_2 at 284.75 K. The equilibrium pressure in the plateau of the SC-O_2 system was about 15% higher than that of SP-

O_2, but that in the one-phase region was lower above x=0.3 at 293.15 K and x=0.4 at 284.75 K.

Partial molar enthalpies in both the systems (Fig.3.3) were independent of x, while small discontinuity was found at their phase boundaries. As a result, partial molar entropies in the nonstoichiometric region decreases with increasing x. Thus, the variation of equilibrium pressure in both the systems results from the dioxygen content dependence of the entropy term. Mean value of the equilibrium pressure in their plateau and partial molar enthalpy in their plateau regions and the nonstoichiometric regions are summarized in Table 3.2. Partial molar entropies of the SP-O_2 system were by about 1 $kJmol^{-1}$ higher than those of the SC-O_2 system.

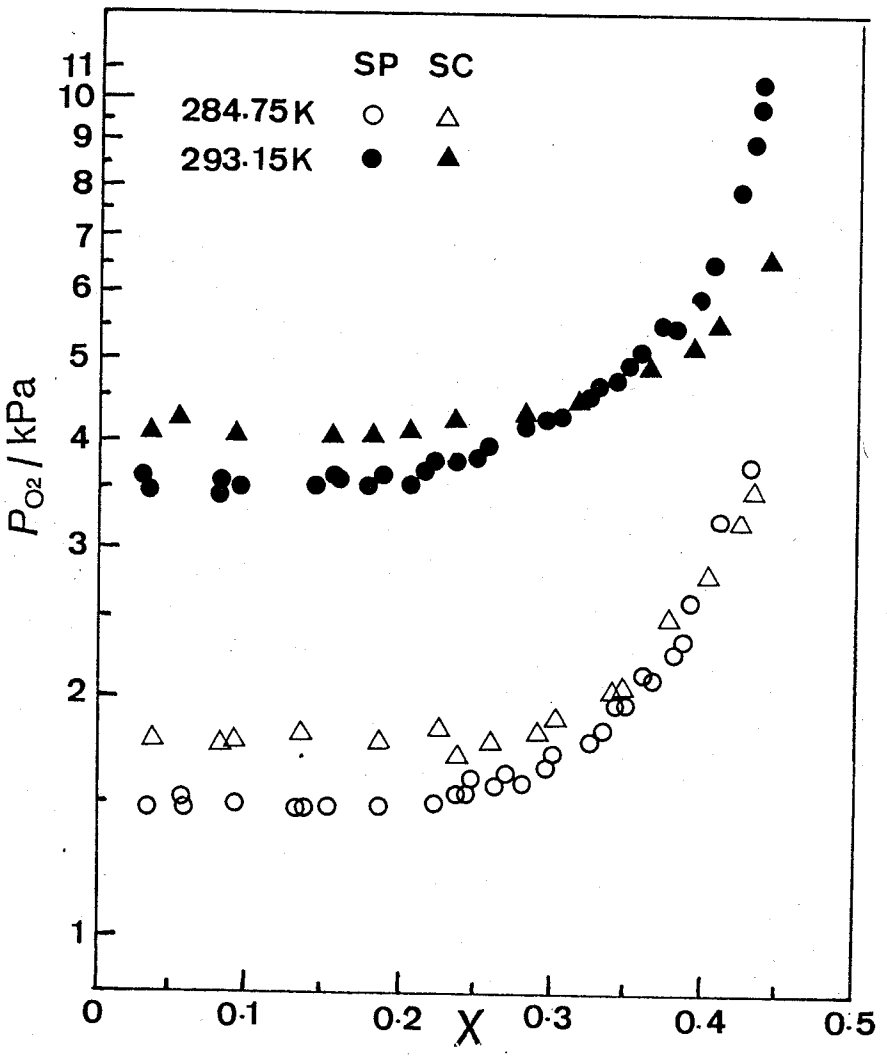

Fig.3.2 Equilibrium pressure of the SP-O_2 (circles) and SC-O_2 (triangles) systems at 284.75K (open marks) and 293.15K (filled marks).

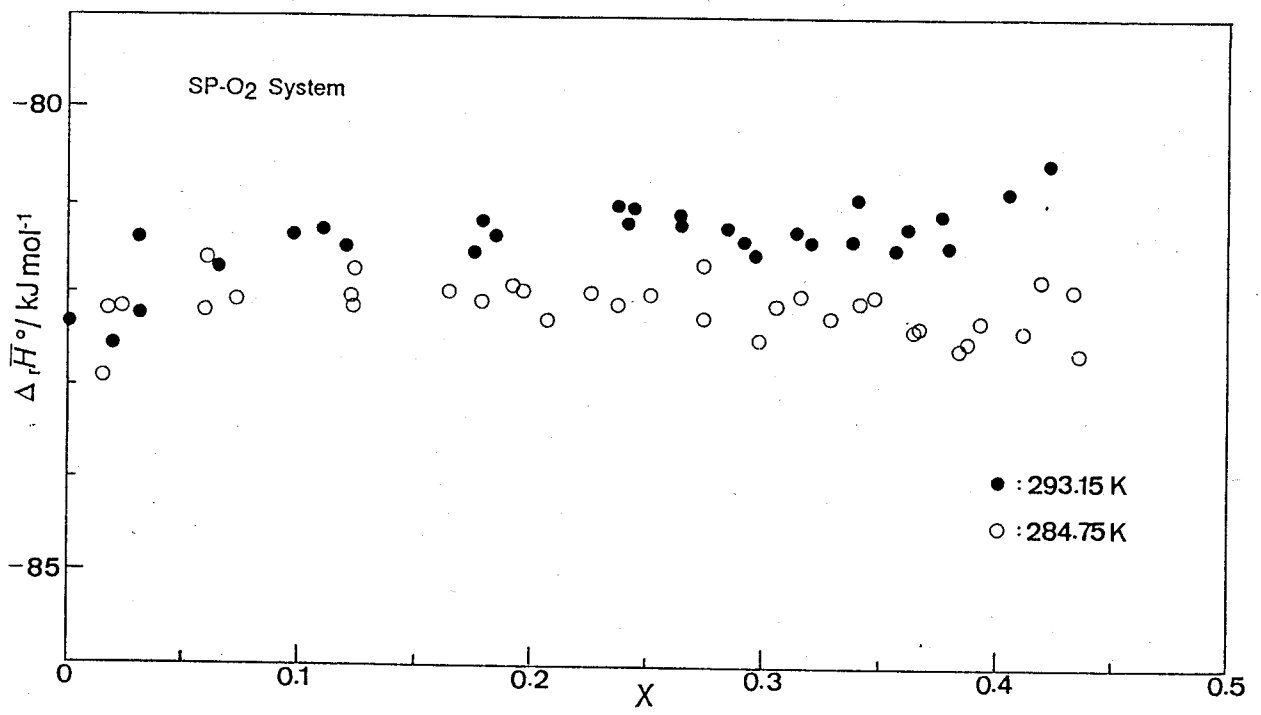

Fig.3.3a Partial molar enthalpy of oxygenation for the SP-O_2 system at 284.75K (open circles) and 293.15K (filled circles).

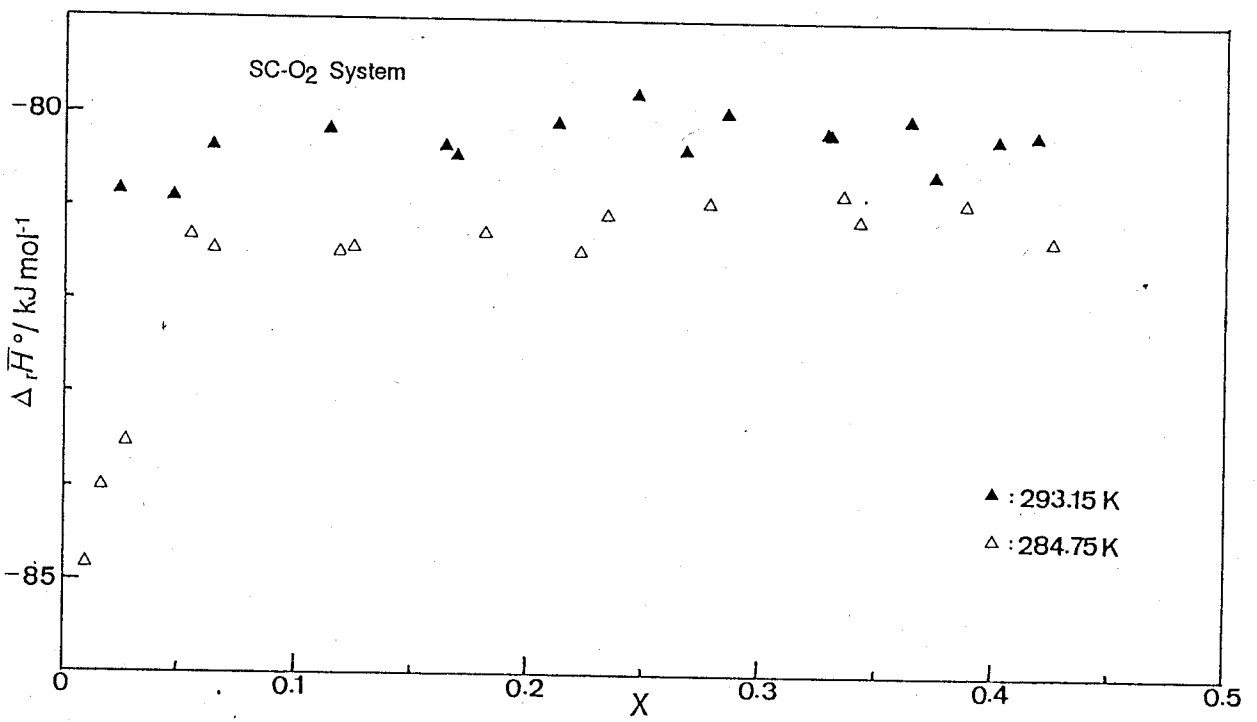

Fig.3.3b Partial molar enthalpy of oxygenation for the SC-O_2 system at 284.75K (open triangles) and 293.15K (filled triangles).

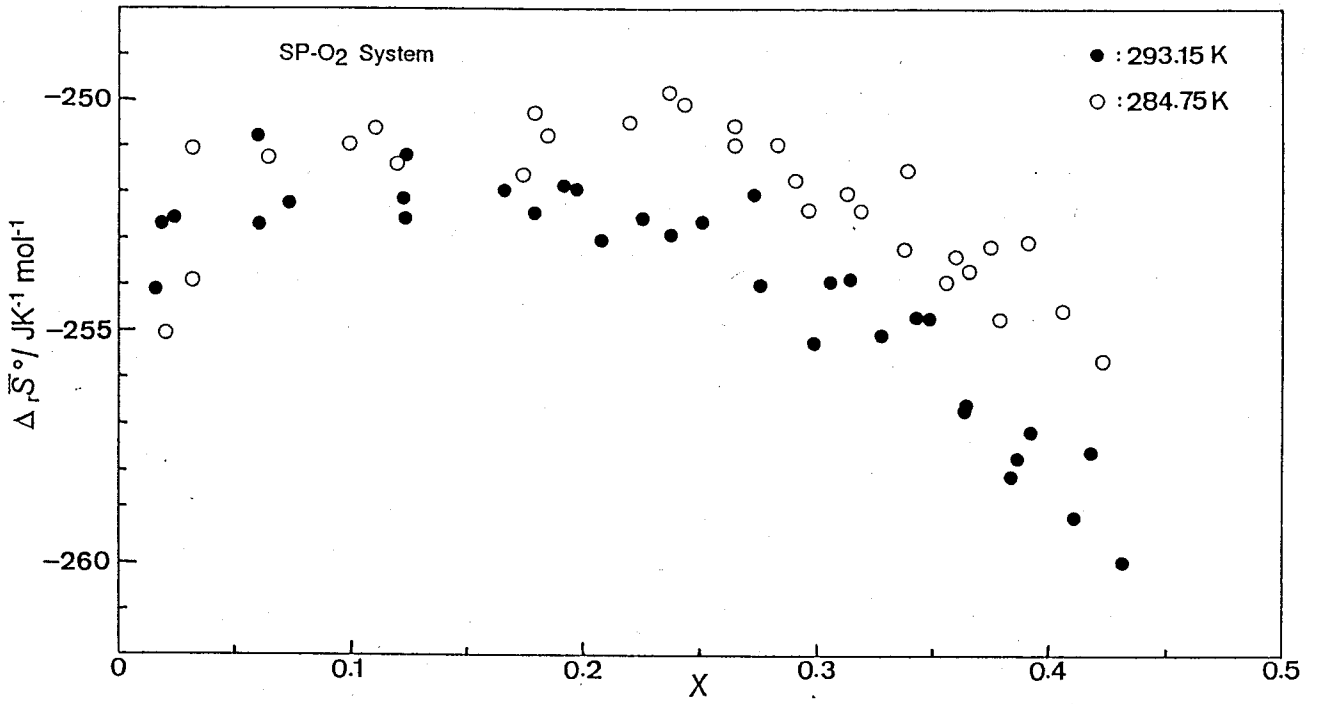

Fig.3.4a Partial molar entropy of oxygenation for the SP-O_2 system at 284.75K (open circles) and 293.15K (filled circles).

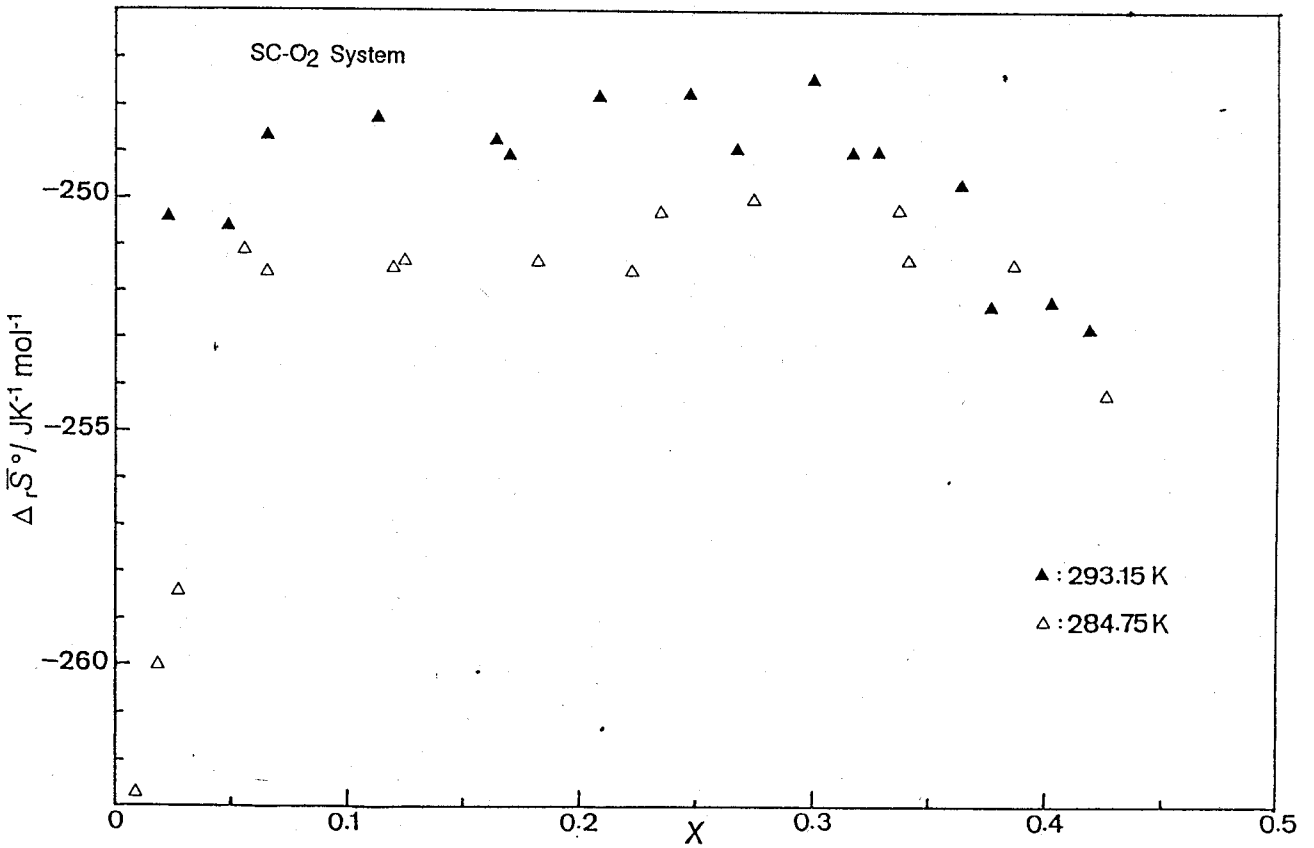

Fig.3.4b Partial molar entropy of oxygenation for the SC-O_2 system at 284.75K (open triangles) and 293.15K (filled triangles).

Table 3.1a Equilibrium pressure P_{eq}, partial molar Gibbs energy $\Delta_r \overline{G}^\circ$ and excess partial molar Gibbs energy $\Delta_r \overline{G}^E$ at dioxygen content x_e of the SP-O_2 system.

No.	x_e	P_{eq} / kPa	$\Delta_r \overline{G}^\circ$ / kJmol^{-1}	$\Delta_r \overline{G}^E$ / kJmol^{-1}
Series 1	at 284.75K			
1	0.03655	1.482	-9.971	---
2	0.09346	1.497	-9.948	---
3	0.13986	1.475	-9.982	---
4	0.22446	1.496	-9.950	-9.497
5	0.24586	1.540	-9.881	-9.803
6	0.24909	1.610	-9.775	-9.758
7	0.27308	1.634	-9.732	-10.171
8	0.30168	1.698	-9.649	-10.641
Series 2	at 284.75K			
1	0.05781	1.525	-9.904	---
2	0.13521	1.478	-9.978	---
3	0.21727	1.504	-9.937	-9.313
4	0.26401	1.574	-9.830	-10.095
5	0.28717	1.647	-9.722	-10.626
6	0.32432	1.783	-9.534	-10.986
7	0.34860	1.965	-9.303	-11.278
8	0.36717	2.099	-9.147	-11.555
9	0.36602	2.339	-8.891	-11.779
Series 3	at 284.75K			
1	0.05912	1.482	-9.972	---
2	0.15456	1.489	-9.960	---
3	0.18830	1.485	-9.967	---
4	0.24193	1.537	-9.886	-9.733
5	0.28268	1.577	-9.824	-10.447
6	0.30423	1.713	-9.629	-10.673
7	0.32814	1.829	-9.473	-11.004
8	0.34285	1.952	-9.319	-11.166
9	0.36223	2.137	-9.105	-11.394
10	0.38081	2.262	-8.971	-11.721
11	0.39350	2.603	-8.638	-11.731
12	0.41025	3.242	-8.118	-11.116
13	0.42938	3.752	-7.772	-12.045

Table 3.1a (continued)

No.	x_e	P_{eq} / kPa	$\Delta_r \overline{G}^\circ$ / kJmol^{-1}	$\Delta_r \overline{G}^E$ / kJmol^{-1}
Series 4	at 293.15K			
1	0.00021	1.113	-10.964	---
2	0.02997	3.623	-8.087	---
3	0.08340	3.634	-8.080	---
4	0.15581	3.648	-8.070	---
5	0.22093	3.844	-7.942	-7.373
6	0.27326	4.045	-7.818	-8.273
7	0.33005	4.696	-7.455	-9.073
8	0.35800	5.171	-7.220	-9.473
9	0.40449	6.510	-6.659	-10.177
10	0.47949	9.039	-5.859	-10.263
11	0.48709	10.707	-5.446	-10.170
Series 5	at 293.15K			
1	0.00056	1.899	-9.662	---
2	0.04550	3.613	-8.094	---
3	0.09381	3.548	-8.138	---
4	0.14375	3.557	-8.132	---
5	0.17953	3.556	-8.143	---
6	0.20613	3.540	-8.143	-7.279
7	0.28577	3.809	-7.965	-7.687
8	0.25806	3.954	-7.874	-8.031
9	0.28251	4.169	-7.745	-8.382
10	0.30750	4.317	-7.660	-8.801
11	0.34275	4.783	-7.410	-9.309
12	0.37981	5.534	-7.054	-9.859
13	0.40065	6.633	-6.613	-10.012
Series 6	at 293.15K			
1	0.00062	1.794	-9.800	---
2	0.03367	3.511	-8.164	---
3	0.07971	3.480	-8.185	---
4	0.15913	3.568	-8.124	---
5	0.19524	3.623	-8.087	-6.899
6	0.21788	3.442	-7.987	-7.357
7	0.25005	3.842	-7.944	-7.945
8	0.29998	4.237	-7.705	-8.592
9	0.32668	4.584	-7.514	-9.058
10	0.35053	4.943	-7.330	-9.407
11	0.37155	5.517	-7.062	-9.651
12	0.39601	5.929	-6.886	-10.145
13	0.42452	7.922	-6.180	-10.390
14	0.43447	10.110	-5.586	-10.196

Table 3.1a' Partial molar enthalpy, entropy, Gibbs energy and excess partial molar entropy of the SP-O_2 system at mean dioxygen content x_m for each reaction.

No.	x_m	$\Delta_r \overline{H}^\circ$ / kJmol^{-1}	$\Delta_r \overline{G}^\circ$ / kJmol^{-1}	$\Delta_r \overline{S}^\circ$ / JK^{-1}mol^{-1}	$\Delta_r \overline{S}^E$ / JK^{-1}mol^{-1}
Series 1 at 284.75K					
1	0.02057	-82.59	-9.971	-255.0	---
2	0.06440	-81.73	-9.968	-252.0	---
3	0.11950	-81.54	-9.967	-251.4	---
4	0.18462	-81.37	-9.967	-250.8	---
5	0.23758	-81.04	-9.902	-249.8	-250.7
6	---	---	---	---	---
7	0.26391	-81.18	-9.829	-250.6	-249.7
8	0.29054	-81.46	-9.769	-251.8	-249.1
Series 2 at 284.75K					
1	0.03156	-81.45	-9.905	-251.3	---
2	0.09933	-81.42	-9.952	-251.0	---
3	0.17915	-81.24	-9.965	-250.3	---
4	0.24340	-81.05	-9.884	-250.1	-250.5
5	0.28292	-81.29	-9.823	-251.0	-248.8
6	0.31308	-81.35	-9.587	-252.0	-247.7
7	0.33879	-80.99	-9.362	-251.6	-245.6
8	0.35984	-81.29	-9.140	-253.4	-244.5
9	0.37819	-81.53	-9.005	-254.7	-245.3
Series 3 at 284.75K					
1	0.03224	-82.25	-9.972	-253.8	---
2	0.11004	-81.32	-9.960	-250.6	---
3	0.17417	-81.62	-9.964	-251.6	---
4	0.21850	-81.28	-9.939	-250.5	---
5	0.26539	-81.28	-9.815	-251.0	-249.9
6	0.29623	-81.60	-9.729	-252.4	-249.3
7	0.31870	-81.45	-9.561	-252.5	-247.8
8	0.33748	-81.49	-9.375	-253.3	-247.2
9	0.35499	-81.53	-9.218	-253.9	-246.5
10	0.37499	-81.16	-9.101	-253.1	-243.9
11	0.39072	-80.79	-8.732	-253.1	-242.5
12	0.40444	-80.91	-8.298	-255.0	-243.6
13	0.42200	-80.61	-7.906	-255.3	-241.3

Table 3.1a' (continued)

No.	x_m	$\Delta_r \overline{H}^\circ$ / kJmol^{-1}	$\Delta_r \overline{G}^\circ$ / kJmol^{-1}	$\Delta_r \overline{S}^\circ$ / JK^{-1}mol^{-1}	$\Delta_r \overline{S}^E$ / JK^{-1}mol^{-1}
Series 4 at 293.15K					
1	0.00013	-123.4	---	---	---
2	0.01703	-82.93	-8.449	-255.3	---
3	0.05986	-81.64	-8.132	-250.7	---
4	0.12350	-81.77	-8.134	-251.2	---
5	0.19196	-81.92	-8.093	-251.9	---
6	0.25106	-81.99	-7.935	-252.6	-252.6
7	0.30483	-82.12	-7.669	-254.0	-250.3
8	0.34687	-82.05	-7.367	-254.8	-248.0
9	0.38356	-82.69	-7.015	-258.1	-248.2
10	0.41826	-81.85	-6.330	-257.6	-244.0
11	0.43490	-82.65	-5.563	-263.0	-249.2
Series 5 at 293.15K					
1	0.00028	-89.07	---	---	---
2	0.02420	-82.15	-8.168	-252.6	---
3	0.07330	-82.10	-8.168	-252.2	---
4	0.12254	-82.05	-8.134	-252.2	---
5	0.16534	-81.99	-8.117	-252.0	---
6	0.19651	-81.97	-8.109	-252.0	---
7	0.22487	-82.00	-7.948	-252.6	-254.3
8	0.25025	-82.00	-7.942	-252.6	-252.6
9	0.27419	-81.70	-7.811	-252.1	-250.5
10	0.29789	-82.52	-7.694	-255.3	-252.0
11	0.32820	-82.27	-7.487	-255.1	-249.7
12	0.36330	-82.43	-7.158	-256.8	-248.6
13	0.39232	-82.30	-6.925	-257.1	-246.4
Series 6 at 293.15K					
1	0.00031	-82.32	---	---	---
2	0.01999	-82.21	-8.164	-252.6	---
3	0.05988	-82.10	-8.132	-252.7	---
4	0.12293	-82.16	-8.134	-252.5	---
5	0.17888	-82.11	-8.100	-252.5	---
6	0.20757	-82.31	-8.124	-253.1	---
7	0.23759	-82.12	-7.962	-253.0	-253.8
8	0.27551	-82.27	-7.800	-254.0	-252.3
9	0.31420	-82.04	-7.609	-253.9	-249.6
10	0.34268	-82.38	-7.144	-257.7	-248.3
11	0.36452	-82.38	-7.144	-256.7	-248.4
12	0.38613	-82.54	-6.989	-257.7	-247.6
13	0.41052	-82.42	-6.515	-258.9	-246.1
14	0.43145	-81.94	-5.751	-259.9	-244.6

Table 3.1b Equilibrium pressure P_{eq}, partial molar Gibbs energy $\Delta_r \overline{G}^\circ$ and excess partial molar Gibbs energy $\Delta_r \overline{G}^E$ at dioxygen content x_e of the SC-O_2 system.

No.	x_e	P_{eq} / kPa	$\Delta_r \overline{G}^\circ$ / kJmol^{-1}	$\Delta_r \overline{G}^E$ / kJmol^{-1}
Series 1 at 284.75K				
1	0.03958	1.769	-9.553	---
2	0.08502	1.762	-9.562	---
3	0.13712	1.806	-9.503	---
4	0.18535	1.763	-9.560	---
5	0.22557	1.820	-9.484	---
6	0.26175	1.774	-9.546	-9.769
7	0.30411	1.884	-9.403	-10.444
8	0.34721	2.061	-8.752	-11.134
9	0.42396	3.223	-8.132	-12.200
Series 2 at 284.75K				
1	0.09303	1.776	-9.543	---
2	0.23894	1.701	-9.645	-9.436
3	0.29154	1.803	-9.508	-10.302
4	0.34215	2.036	-9.210	-11.051
5	0.40220	2.790	-8.474	-11.821
6	0.43316	3.498	-7.938	-12.363
Series 3 at 293.15K				
1	0.05254	4.246	-7.700	---
2	0.18371	4.105	-7.708	---
3	0.28233	4.336	-7.649	-8.283
4	0.39065	5.159	-7.225	-10.329
Series 4 at 293.15K				
1	0.03666	4.106	-7.782	---
2	0.09081	4.124	-7.771	---
3	0.15513	4.082	-7.796	---
4	0.20592	4.110	-7.780	---
5	0.23050	4.241	-7.703	-7.420
6	0.31725	4.486	-7.566	-5.910
7	0.36422	4.904	-7.349	-9.754
8	0.40886	5.542	-7.051	-10.709
9	0.44251	6.580	-6.633	-11.607
Series 5 at 293.15K				
1	0.01993	4.066	-7.806	---
2	0.09038	4.081	-7.797	---
Series 6 at 293.15K				
1	0.00407	4.047	-7.817	---

Table 3.1b' Partial molar enthalpy, entropy, Gibbs energy and excess partial molar entropy of the SC-O_2 system at mean dioxygen content x_m for each reaction.

No.	x_m	$\Delta_r \overline{H}^\circ$ / kJmol^{-1}	$\Delta_r \overline{G}^\circ$ / kJmol^{-1}	$\Delta_r \overline{S}^\circ$ / JK^{-1}mol^{-1}	$\Delta_r \overline{S}^E$ / JK^{-1}mol^{-1}
Series 1 at 284.75K					
1	0.02275	-80.85	-9.553	-250.4	---
2	0.06455	-80.37	-9.558	-248.7	---
3	0.11252	-80.22	-9.525	-248.3	---
4	0.16379	-80.36	-9.534	-248.7	---
5	0.20799	-80.08	-9.518	-247.8	---
6	0.24652	-79.66	-9.612	-247.8	---
7	0.28495	-79.99	-9.516	-247.5	-245.2
8	0.32835	-80.20	-9.286	-249.0	-243.6
9	0.36385	-80.05	-8.942	-249.7	-241.6
10	0.40228	-80.28	-8.472	-252.2	-240.4
Series 2 at 284.75K					
1	0.04821	-80.92	-9.555	-250.6	---
2	0.16943	-80.46	-9.541	-249.1	---
3	0.26743	-80.43	-9.538	-249.0	-247.8
4	0.31863	-80.24	-9.333	-249.0	-244.3
5	0.37333	-80.66	-8.800	-252.4	-243.4
6	0.41836	-80.20	-8.220	-252.8	-239.2
Series 3 at 293.15K					
1	0.02706	-83.55	-7.795	-258.4	---
2	0.11898	-81.52	-7.782	-251.5	---
3	0.23412	-81.08	-7.707	-250.3	-251.4
4	0.33712	-80.90	-7.474	-250.5	-244.4
Series 4 at 293.15K					
1	0.01875	-84.02	-7.806	-256.0	---
2	0.06464	-81.49	-7.731	-251.6	---
3	0.12379	-81.47	-7.784	-251.4	---
4	0.18154	-81.30	-7.783	-251.4	---
5	0.22205	-81.49	-7.738	-251.6	---
6	0.27749	-80.96	-7.655	-250.1	-248.2
7	0.34147	-81.13	-7.454	-251.3	-244.9
8	0.38710	-80.95	-7.242	-251.4	-241.2
9	0.42602	-81.35	-6.838	-254.2	-239.6
Series 5 at 293.15K					
1	0.01057	-84.84	-7.812	-262.8	---
2	0.05556	-81.33	-7.708	-251.2	---
Series 6 at 293.15K					
1	0.00221	-98.63	-7.812	-309.81	---

Table 3.2 Composition at phase boundaries in the SP-O_2 and SC-O_2 systems, and mean equilibrium pressure and partial molar enthalpy in their two-phase region and averaged partial molar enthalpy in the nonstoichiometric phase.

	two-phase region			Nonstoichiometric
	Phase boundary x	P_{eq} / kPa	$\Delta_r \overline{H}^\circ$ / kJmol^{-1}	$\Delta_r \overline{H}^\circ$ / kJmol^{-1}
SP-O_2 system				
at 284.75 K	0.23	1.489 ±0.011	-81.46 ±0.11	-81.20 ±0.12
at 293.15 K	0.20	3.570 ±0.042	-82.04 ±0.12	-82.21 ±0.12
SC-O_2 system				
at 284.75 K	0.26	1.769 ±0.026	-80.35 ±0.09	-81.06 ±0.11
at 293.15 K	0.23	4.107 ±0.009	-81.42 ±0.09	-80.25 ±0.16

3.2.2 Magnetic Properties

Dioxygen content (x) dependence of molar magnetic susceptibility (x_m) of the SP-O_2 and SC-O_2 systems were measured at (285.0±1.6) K and (287.9±2.5) K, respectively. The results are shown in Fig.3.5 together with molar susceptibilities of the paramagnetic species, $X_m/(1-2x)$, which corresponds to those of unoxygenated cobalt ions because of diamagnetism of oxygenated [Co(SALEN)][7]. In the SP-O_2 system, Xm decreased linearly as reported by Calvin *et al.*[7], and $X_m/(1-2x)$ was independent of x,

with the value: $(2.463\pm0.039)\times10^{-3}$ emu·mol(Co)$^{-1}$. On the other hand, the plots of X_m with respect to x for the SC-O_2 system shown in Fig.3.5 indicated a bend at about x=0.25 which agrees with the phase boundary between the one-phase and two-phase regions. The $X_m/(1-2x)$ vs. x plots for the system also shows a bend at the same dioxygen content (x) and a constant value [$(3.026\pm0.054)\times10^{-3}$ emu·mol(Co)$^{-1}$] for x>0.25 which is larger than the value at x=0, $(2.478\pm0.077)\times10^{-3}$ emu·mol(Co)$^{-1}$. The oxygenated complex molecules for both the SP-O_2 and SC-O_2 systems are diamagnetic, because those $X_m/(1-2x)$ vs. x plots is possible to be extrapolated to X_m=0 at full oxygenation (x=0.5).

Temperature dependence of magnetic susceptibility at various dioxygen contents was measured using the susceptibility at room temperature as a reference. The effective magnetic moments of an unoxygenated cobalt ion are shown in Fig.3.6. It is noticeable in Fig.3.6 that the effective magnetic moments for partially oxygenated sample of both SP and SC behave similarly with respect to temperature, and that the magnetic moments for the same sample show no dioxygen content dependence above 180K for both the SP-O_2 and SC-O_2 systems. Decrease in the magnetic moment in the lower temperatures may suggest the existence of diamagnetic interaction between cobalt ions.

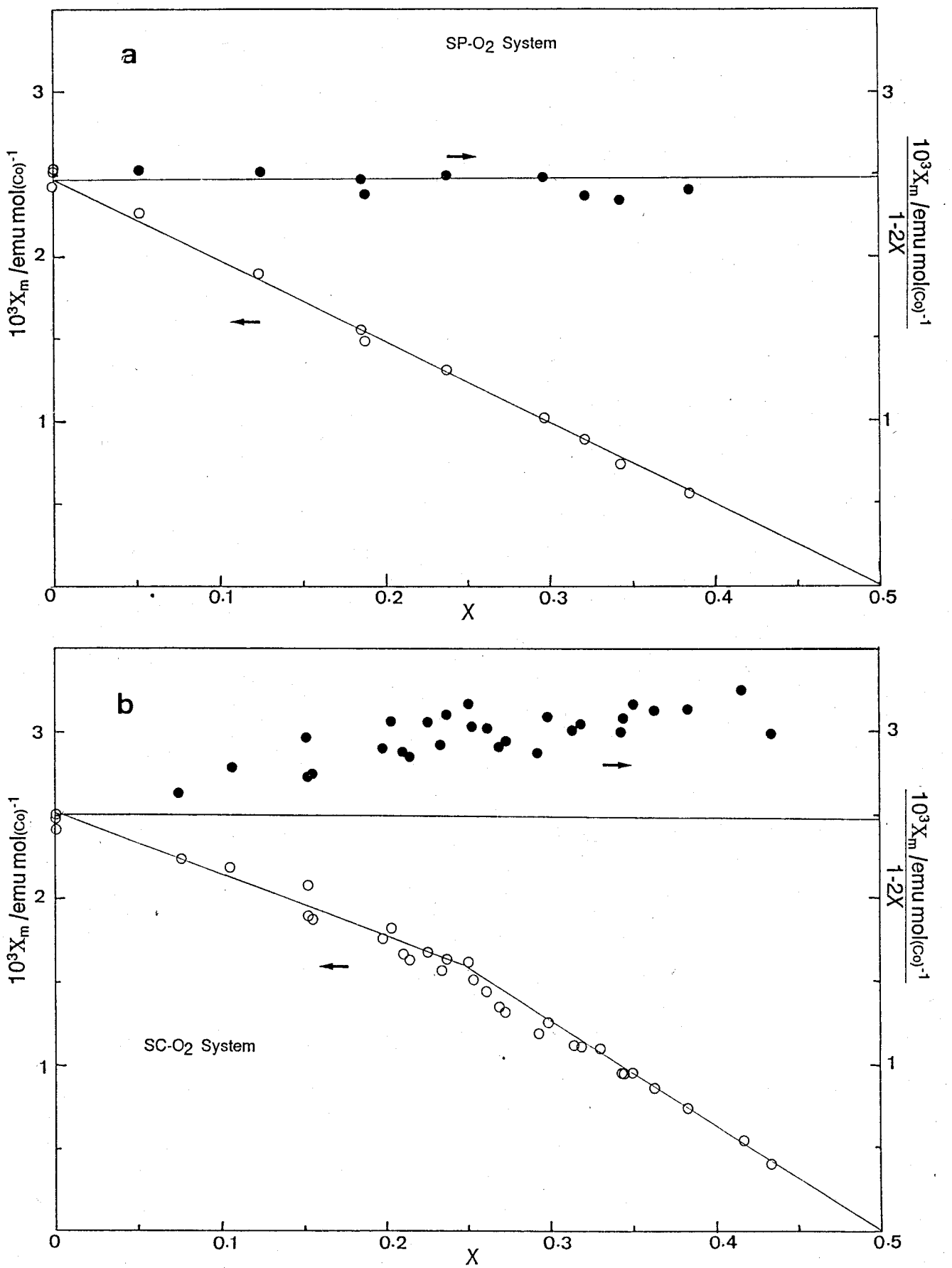

Fig.3.5 Dioxygen content dependence of molar magnetic susceptibility of the whole (open circles) and paramagnetic (filled circles) for cobalt ions in the complex: a, SP-O_2 system at (284.9±1.0)K; and b, SC-O_2 system at (287.9±2.5)K. Solid lines indicate the values without formation of the species with higher susceptibility.

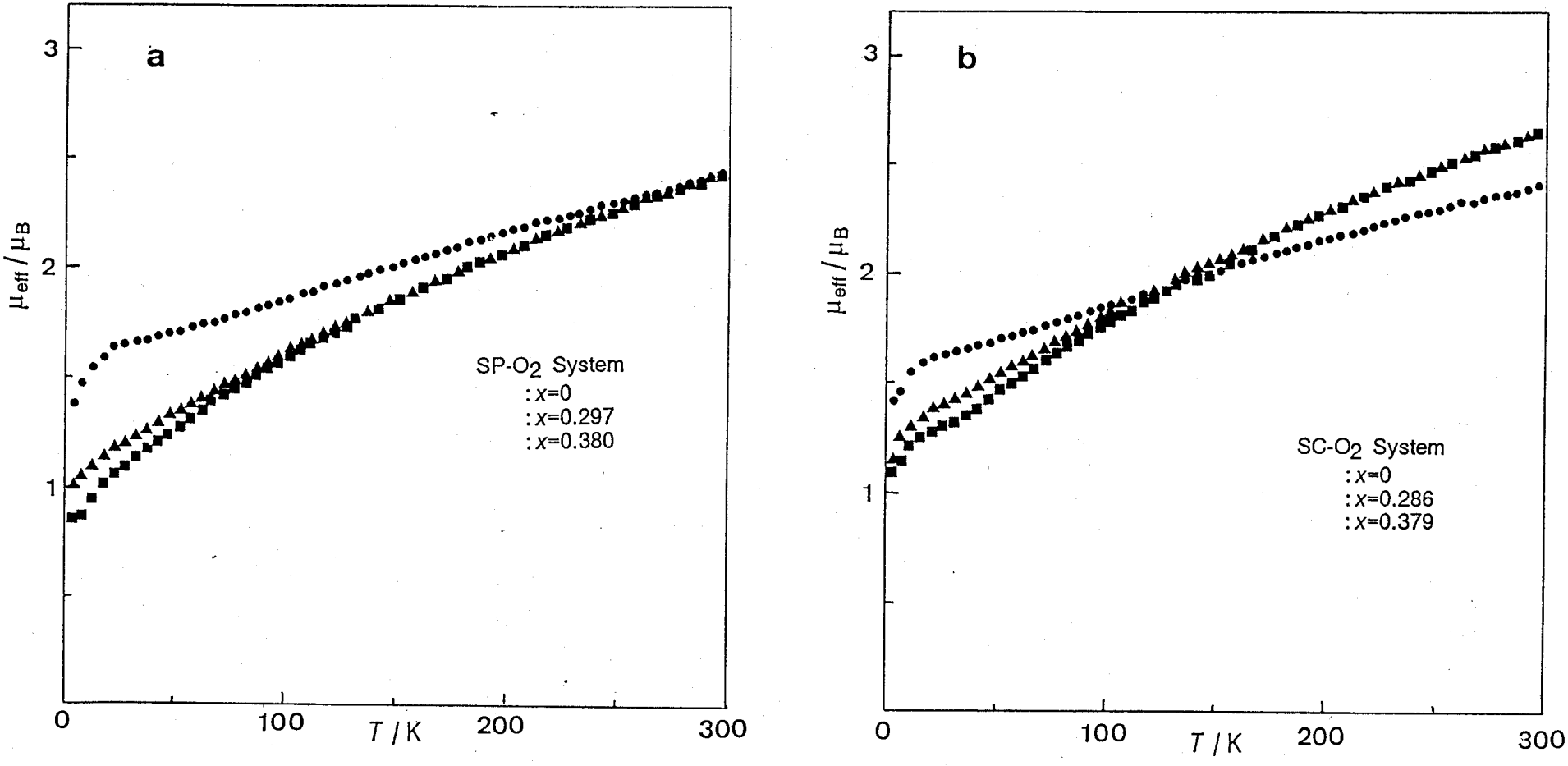

Fig.3.6 Temperature dependence of effective magnetic moment of paramagnetic species for the SP-O_2 (a) and SC-O_2 (b) systems at various dioxygen contents.

3.2.3 X-ray Diffraction

Powder X-ray diffraction patterns of the SP-O_2 and SC-O_2 systems were recorded at 293 K for unoxygenated samples, the samples in two-phase region and the fully oxygenated samples. The fully oxygenated samples were prepared by leaving unoxygenated samples for 2 days in dry air at 293 K, and the dioxygen content which were gravimetrically determined were x=0.45 and x=0.46 for the SP-O_2 and SC-O_2 systems, respectively. The samples in the two-phase region were obtained by placing the fully oxygenated samples in the sample chamber filled with nitrogen for 24 hours at 293 K. The unoxygenated samples were prepared by keeping partially oxygenated samples at 373 K in vacuo for 2 hours.

Diffraction patterns were shown in Fig.3.7 (SP-O_2 system) and Fig.3.8 (SC-O_2 system). In Fig.3.7b and Fig.3.8b, diffractions from both unoxygenated and fully oxygenated crystals are observed. Hence, the patterns are attributable to those of the samples in the two-phase region. The diffraction patterns were indexed as an orthorhombic system, and the lattice parameters and the lattice volume are shown in Table 3.3. The lattice of the SC-O_2 system was slightly smaller than that of the SP-O_2 system. Difference in intensity of diffractions between the systems was also observed below 12° and at about 18° and 26° in 2θ.

Since the shifts of strong diffractions, 020 and 210, were negligible in the nonstoichiometric region , the volume changes in the region was determined from the shift of 004 diffraction which are shown in Table 3.4. Although the changes in the spacing of the 004 plane in both the systems were less than 0.25%, those values can be regarded as significant, because the 004 diffraction was sharp and the values at the same composition

agreed with each other in successive measurements, moreover composition was varied without removing a sample holder.

Table 3.3 Lattice parameters and cell volume at 293 K of the SP-O_2 and SC-O_2 systems in the unoxygenated and oxygenated states. All diffraction patterns were indexed as an othorhombic system.

System and Dioxygen content x	Latticd parameters a / nm	b / nm	c / nm	Cell volume V_{cell} / nm^3
SP-O_2 x=0	0.8021	2.617	0.6774	1.414
x=0.45	1.569	2.646	1.450	6.021
SC-O_2 x=0	0.8000	2.610	0.6773	1.414
x=0.46	1.553	2.604	1.444	5.840

Table 3.4 Volume changes in nonstoichiometric phase of the SP-O_2 and SC-O_2 systems at 293 K between the phase boundary and fully oxygenated state. V_{cell}(av.) is a mean cell volume between the phase boundary and the observed highest dioxygen content.

System	Dioxygen content x Phase boundary	Fully oxygenated	$100\Delta V_{cell} / V_{cell}$(av.)
SP-O_2	0.20	0.45	0.12%
SC-O_2	0.23	0.46	0.24%

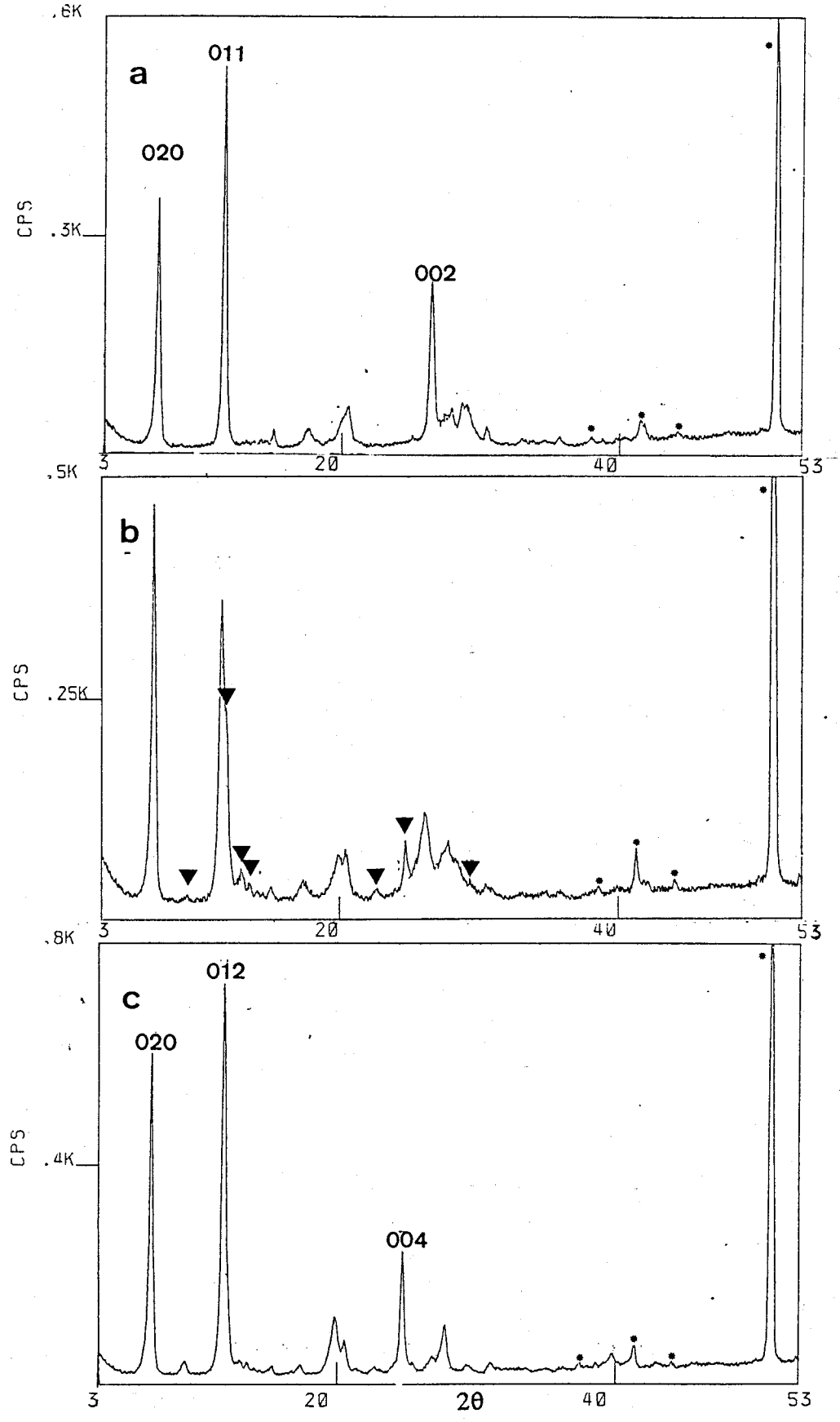

Fig.3.7 X-ray diffraction patterns of the SP-O_2 system at various dioxygen contents at 293K; a: unoxygenated sample, b: the sample in two phase region, c: x=0.45. Triangles in b indicate unique diffractions from the nonstoichiometric phase. The diffractions from the sample holder are indicated by asterisk(*).

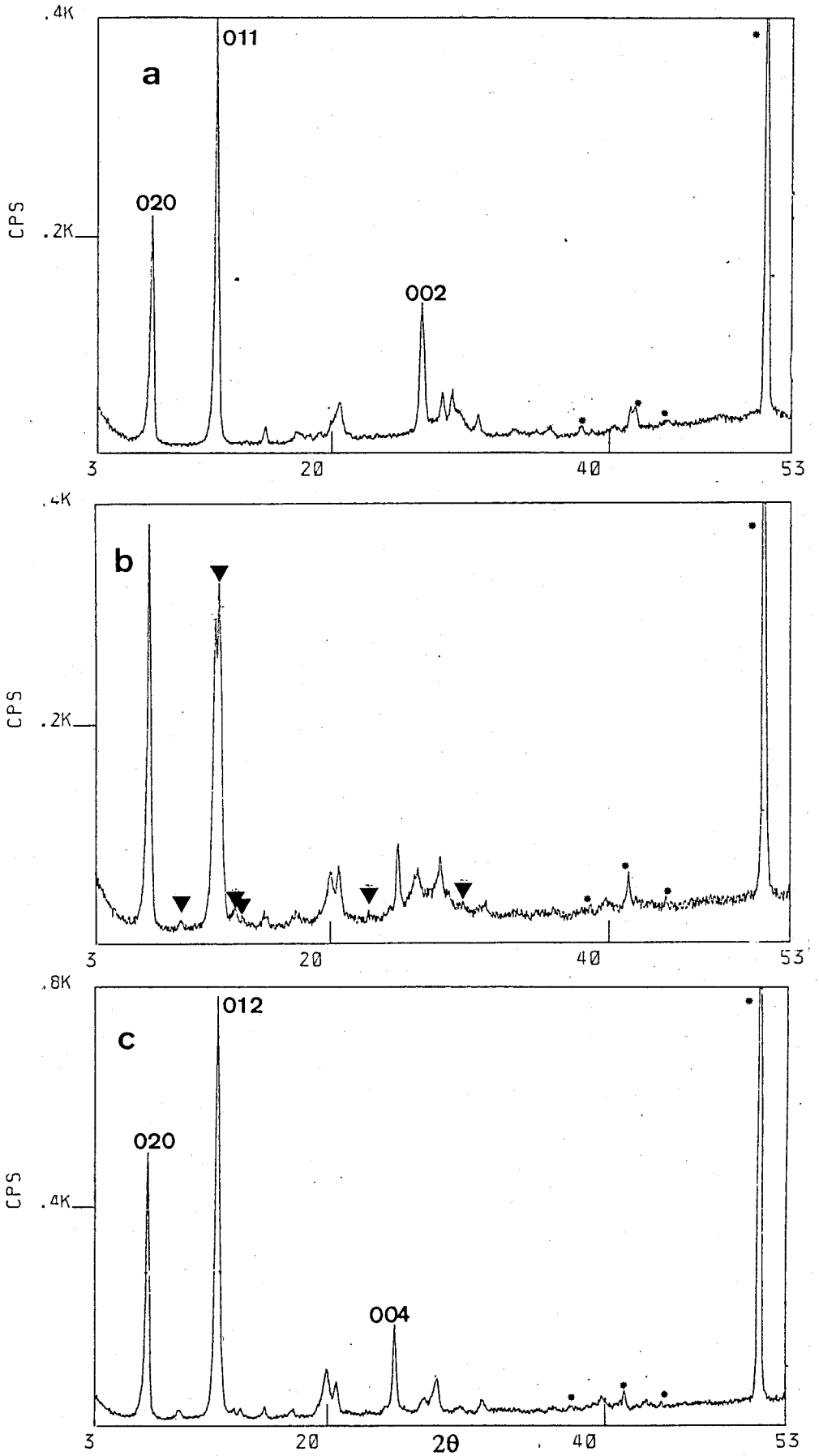

Fig.3.8 X-ray diffraction patterns of the SC-O_2 system at various dioxygen contents at 293K; a: unoxygenated sample, b: the sample in two phase region, c: x=0.46. Triangles in b indicate unique diffractions from the nonstoichiometric phase. The diffractions from the sample holder are indicated by asterisk(*).

3.2.4 Infrared Spectra

Infrared spectra in the 30-700 cm^{-1} and 1100-1300 cm^{-1} regions at various dioxygen contents at 298 K are shown in Fig.3.9 (SP-O_2 system) and Fig.3.10 (SC-O_2 system). In the one-phase region (x>0.25), it was noticeable that the intensity and wave number of most of absorption bands were unchanged by a change in the dioxygen content (x). In the far-infrared region, the spectra show no dependence on x in the nonstoichiometric samples of both the systems. Spectra in the 400-700 cm^{-1} and 1100-1300 cm^{-1} regions for the dimer, $[Co(SALEN)]_2$ and the five-coordinated pyridine adduct, [Co(SALEN)]py at 298 K are shown in Fig.3.11a and Fig.3.11b, respectively.

3.2.5 Diffuse Reflectance Spectra

Diffuse reflectance spectra recorded from 2000 nm to 500 nm at 295K at various dioxygen contents are shown in Fig.3.12. Spectra and their dependence on x were similar for the SP-O_2 and SC-O_2 systems. The spectra of unoxygenated samples of the both systems were similar to that of [Co(SALEN)] dissolved in chloroform[8]. By increasing the dioxygen content, a new band appeared at about 730 nm, but its intensity was decreased in the one-phase region. This fact suggests that the electronic state of the unoxygenated cobalt ions in the nonstoichiometric region are influenced.

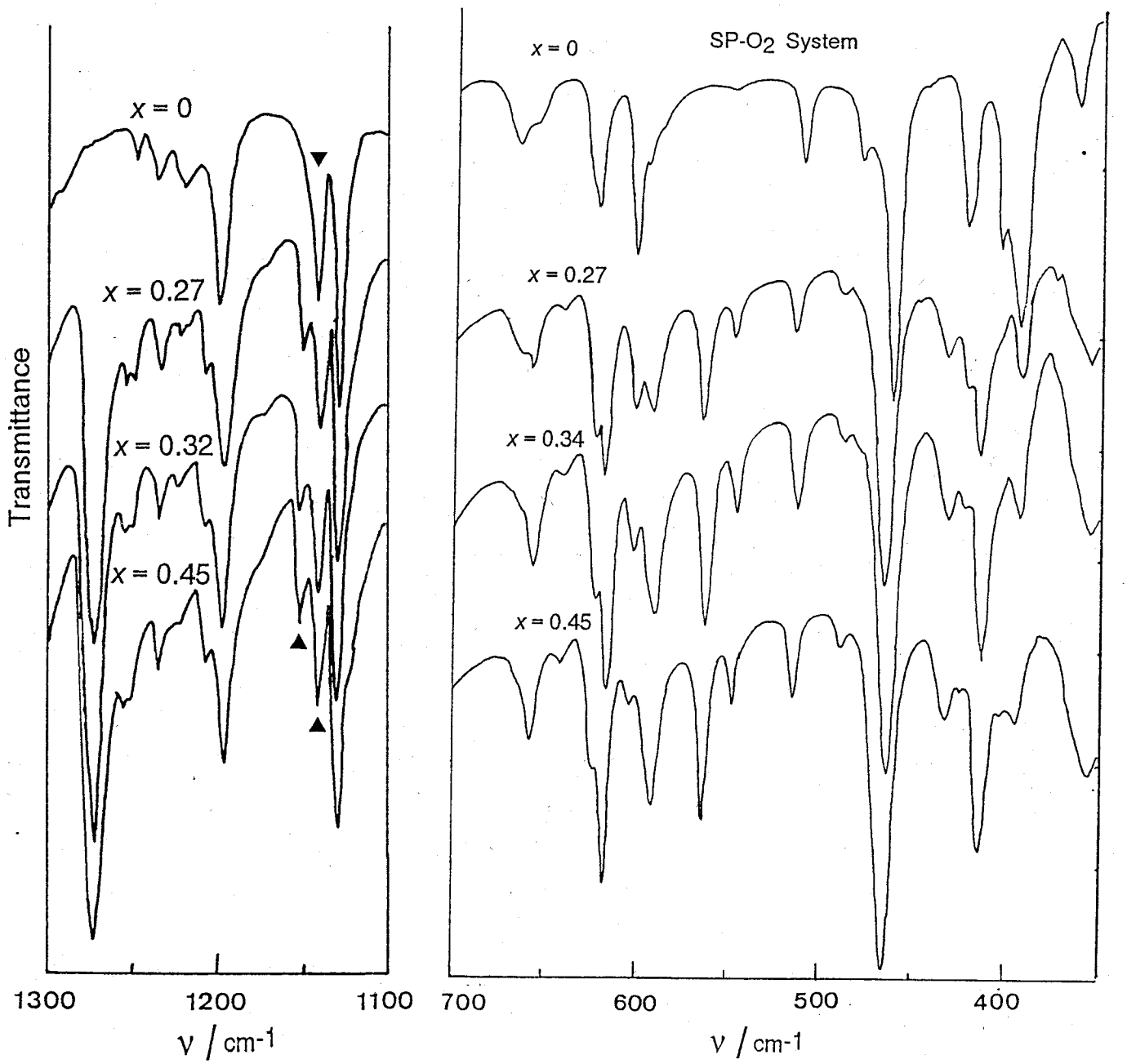

Fig.3.9a Dioxygen content dependence of infrared spectrum (350-700cm^{-1} and 1100-1300cm^{-1}) of the SP-O_2 system at 298K. Filled triangles indicate the C-O stretching bands.

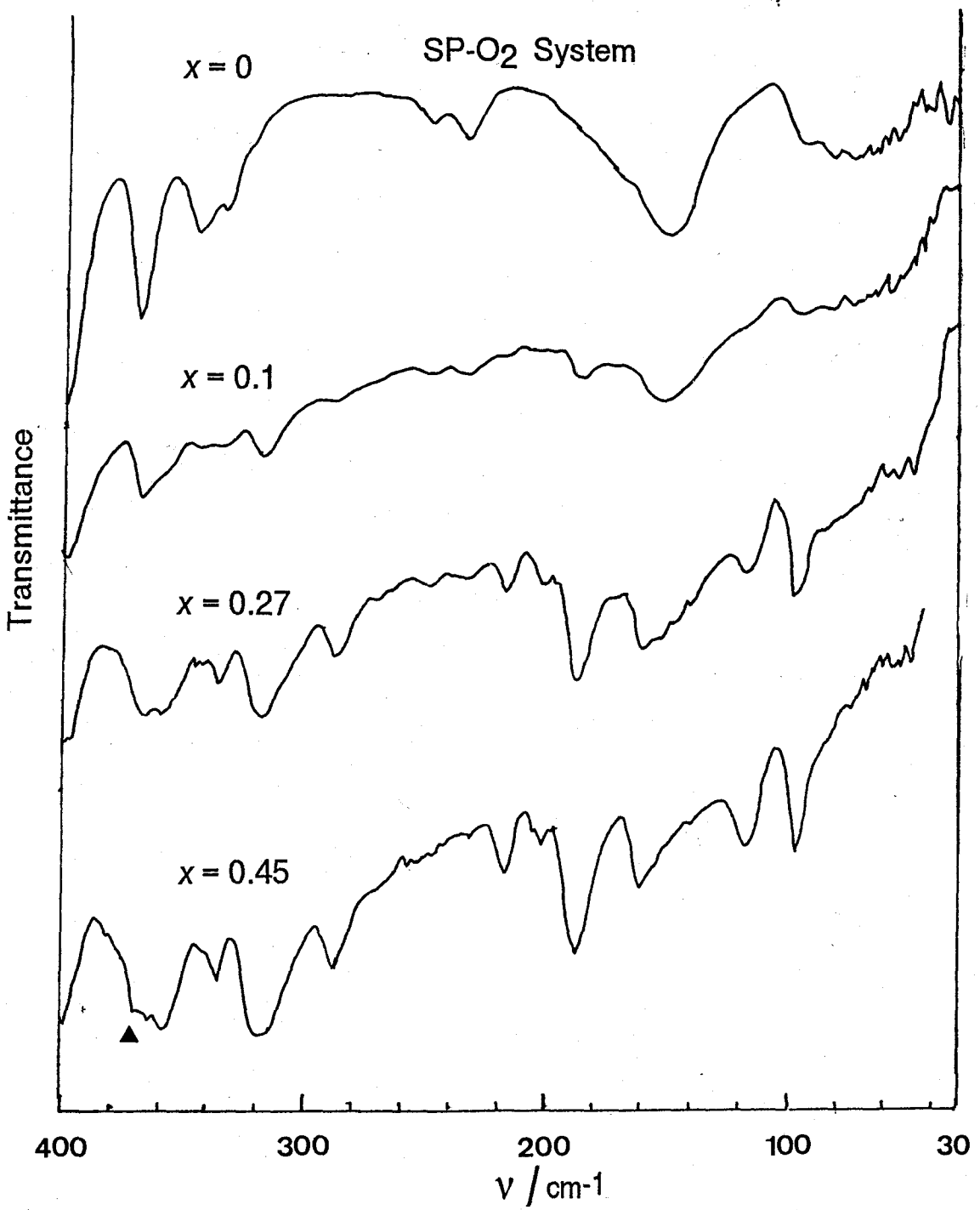

Fig.3.9b Dioxygen content dependence of far infrared spectrum (30-400cm^{-1}) of the SP-O_2 system at 298K. Triangles indicate the peaks which showed a change in transmittance in the nonstoichiometric phase.

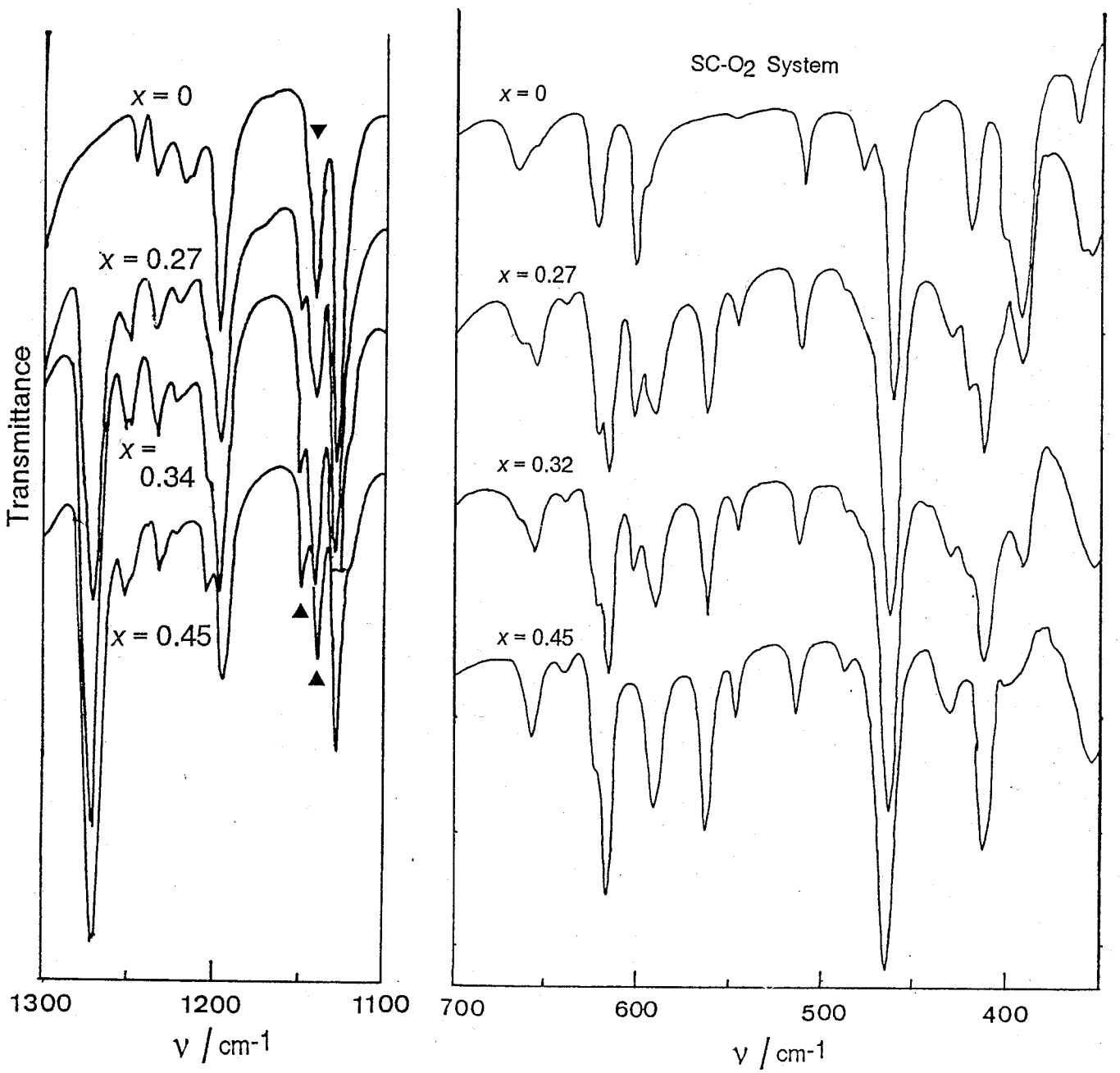

Fig.3.10a Dioxygen content dependence of infrared spectrum (350-700cm^{-1} and 1100-1300cm^{-1}) of the SC-O_2 system at 298K. Filled triangles indicate the C-O stretching bands.

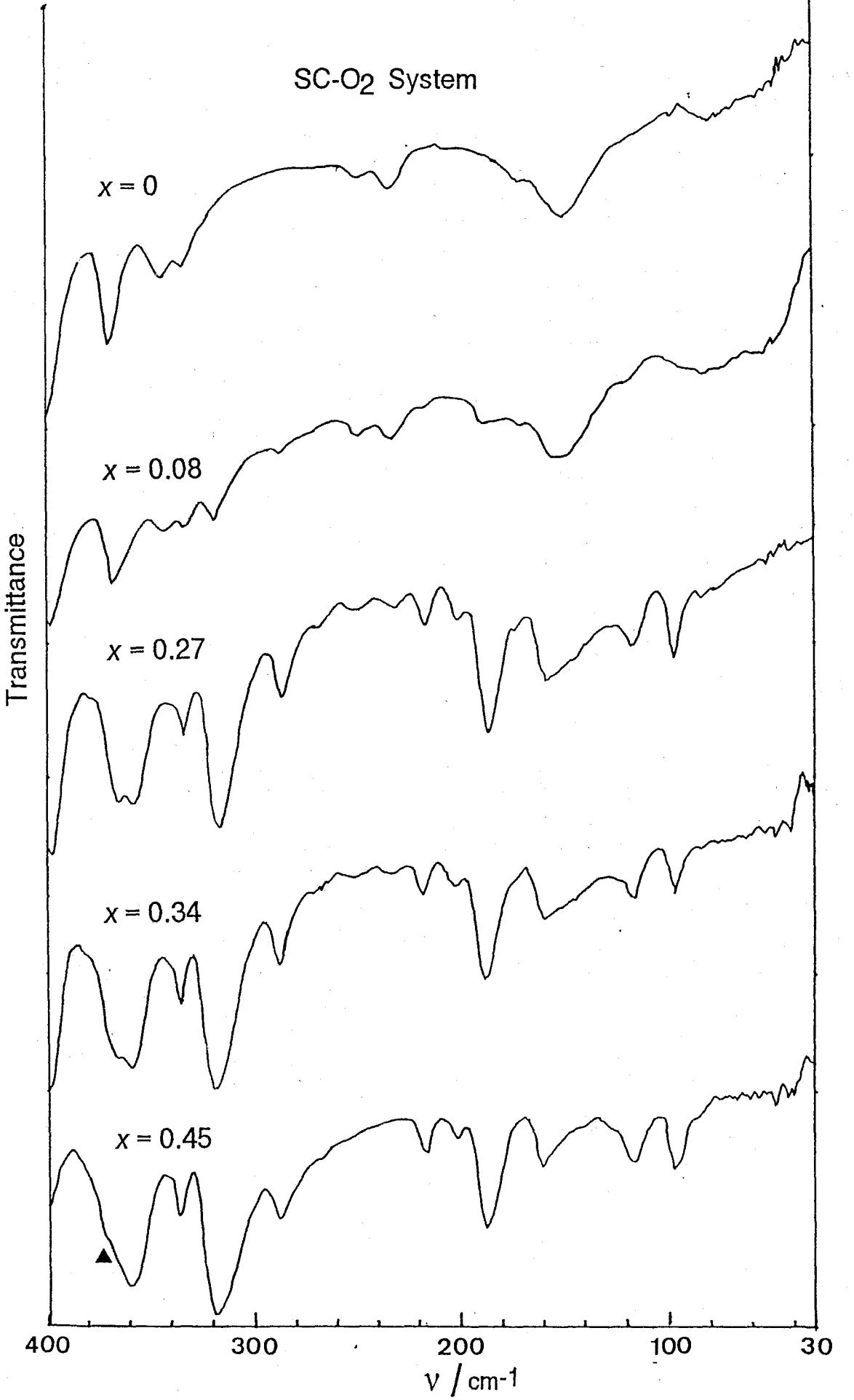

Fig.3.10b Dioxygen content dependence of far infrared spectrum (30-400cm^{-1}) of the SC-O_2 system at 298K. Triangles indicate the peaks which showed a change in transmittance in the nonstoichiometric phase.

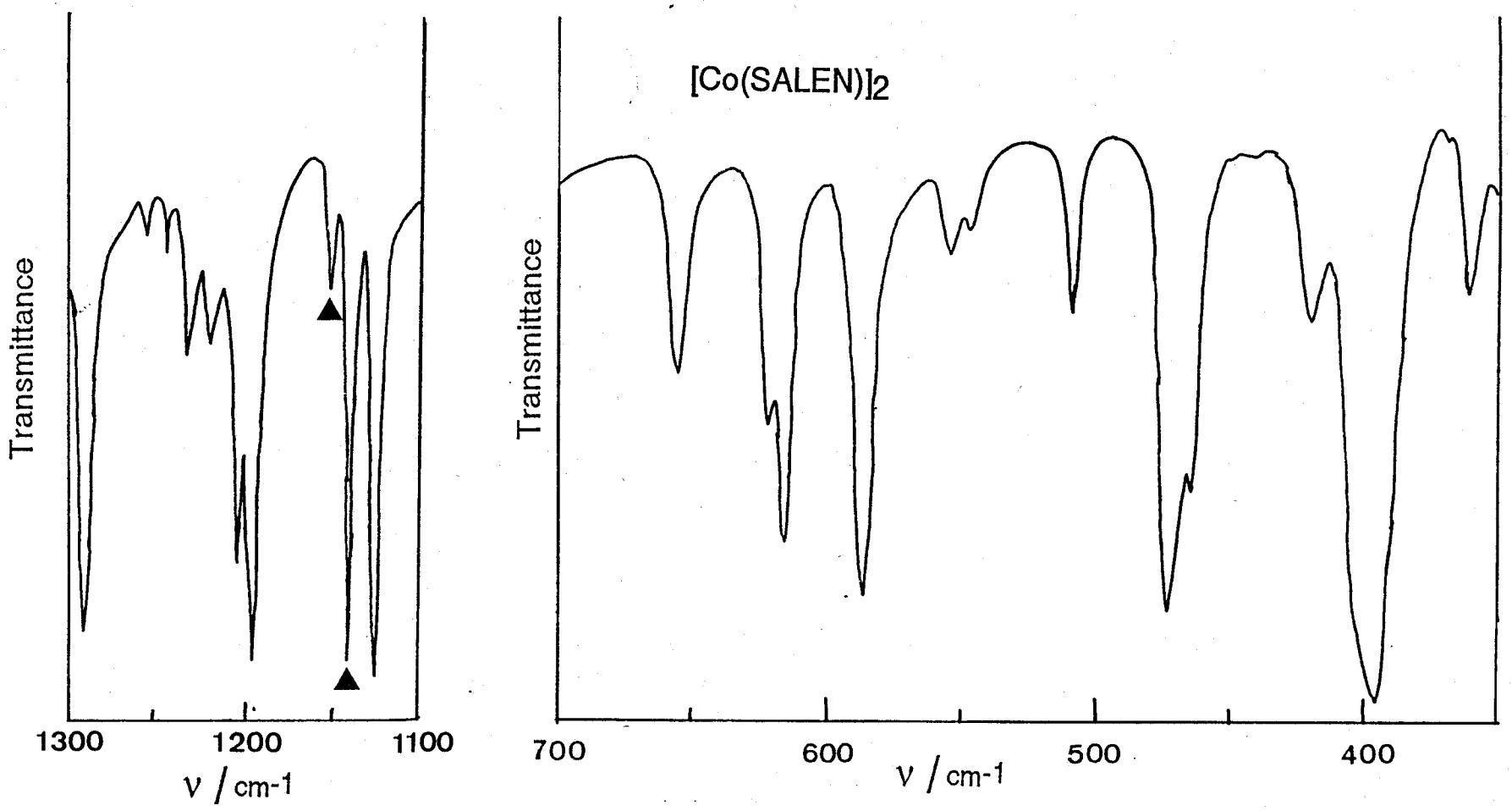

Fig.3.11a Infrared spectra of $[Co(SALEN)]_2$
($350\text{-}700cm^{-1}$ and $1100\text{-}1300cm^{-1}$) at 298K.
Filled triangles indicate the C-O stretching bands.

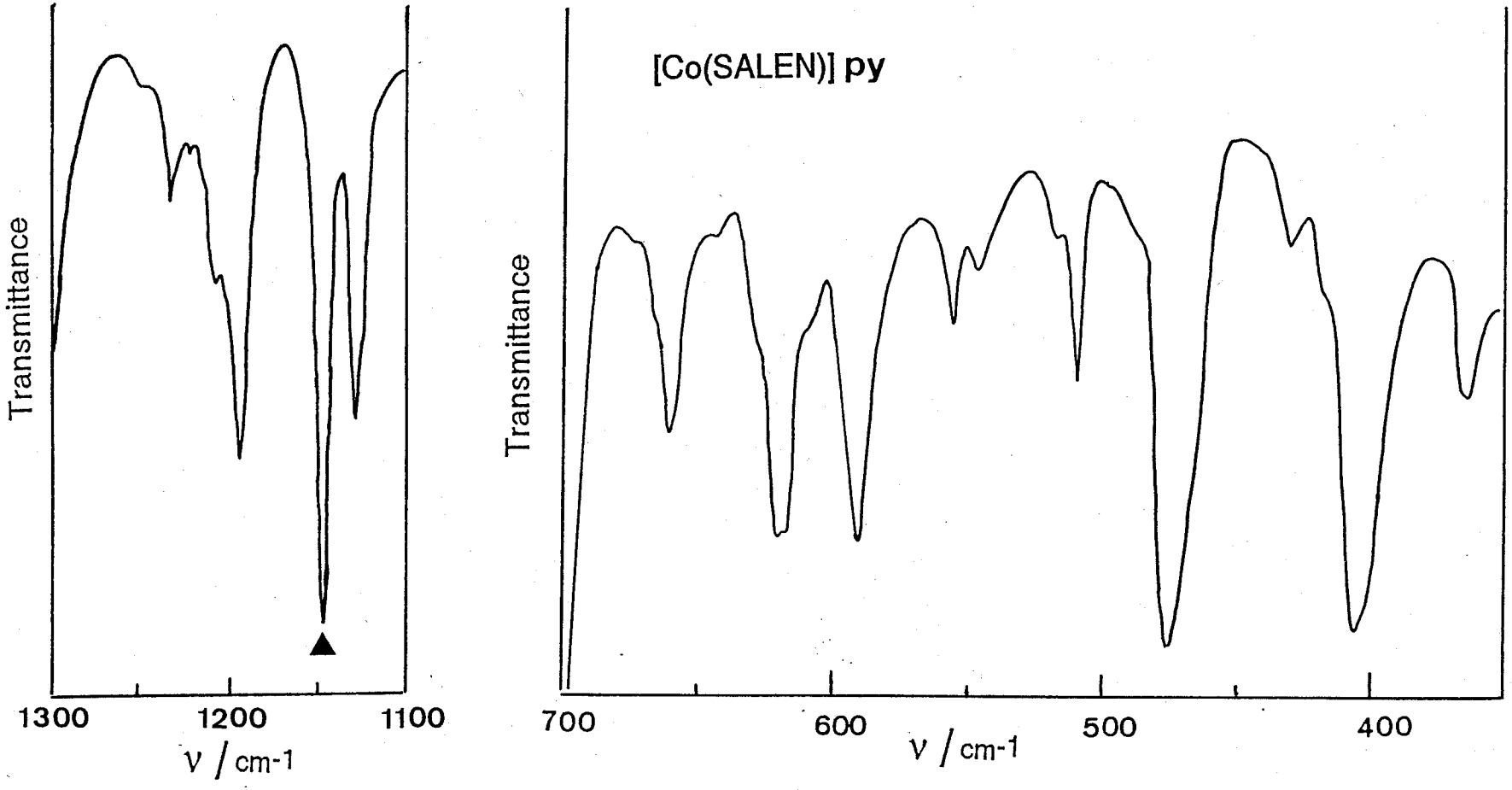

Fig.3.11b Infrared spectra of [Co(SALEN)]py
(350-700cm^{-1} and 1100-1300cm^{-1}) at 298K.
A filled triangle indicates the C-O stretching band.

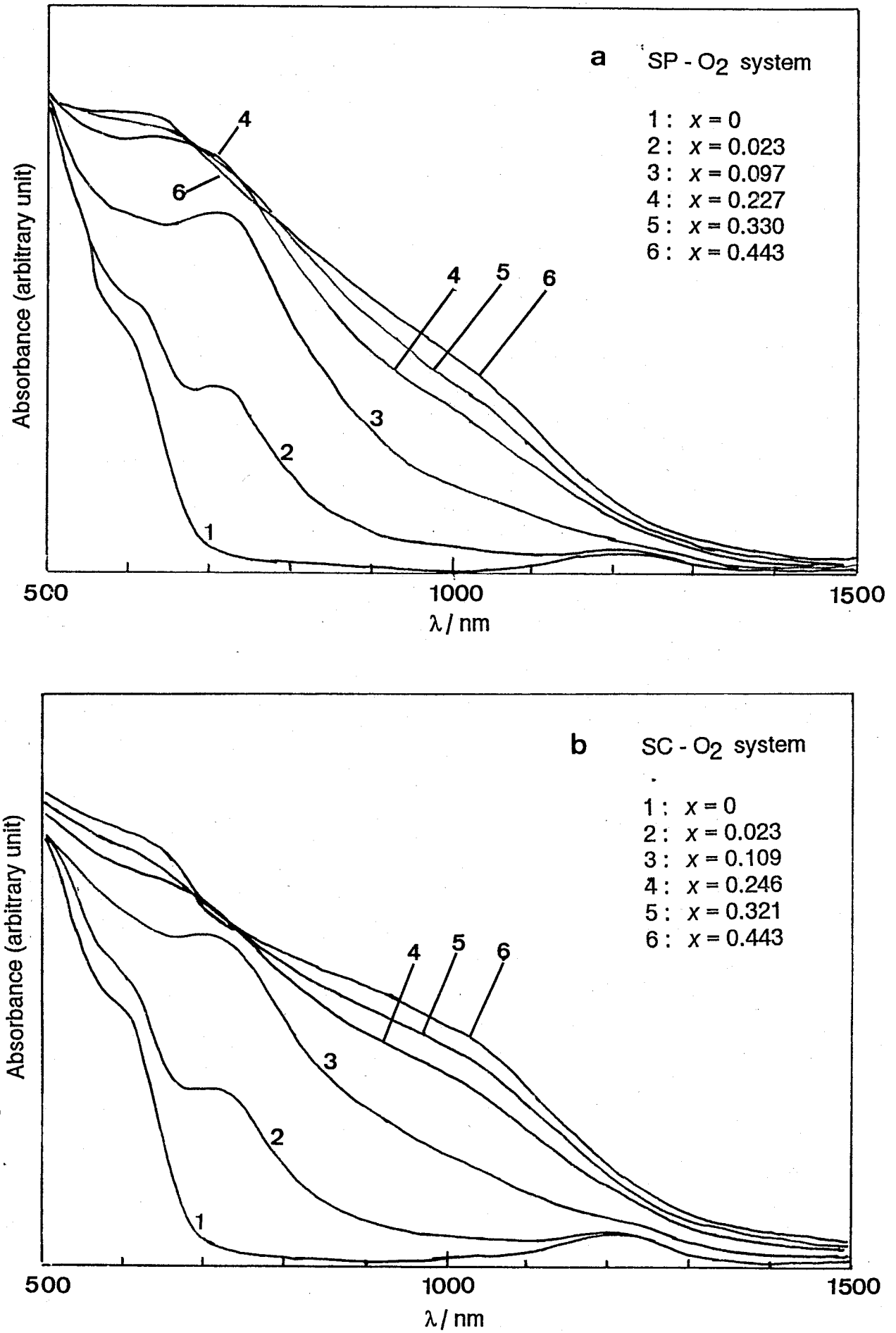

Fig.3.12 Diffuse reflectance spectra of the SP-O_2 (a) and SC-O_2 (b) systems at various dioxygen contents at 298K.

3.3 Discussion

3.3.1 Structure and Distribution of Dioxygens in the Nonstoichiometric Phase.

In the nonstoichiometric regions of both the SP-O_2 and SC-O_2 systems, magnetic susceptibilities of the unoxygenated cobalt ions, $X_m/(1-2x)$ (Fig.3.6), are independent of dioxygen content x, and temperature dependences of $X_m/(1-2x)$ ($x>0.25$) above 180K agreed well between the samples with different x, though the temperature dependence is steeper than those of corresponding unoxygenated samples. These facts show that cobalt ions in the nonstoichiometric crystals are more strongly perturbed than cobalt ions in the unoxygenated crystal. This conclusion is supported by the results of the visible and near-infrared spectra as described in section 3.2.5. Antiferromagnetic interaction between cobalt ions stronger than that of the unoxygenated phase would suggest Co-Co interaction between adjacent complex molecules similar to that in $[Co(SALEN)]_2$ dimer crystal where cobalt ions are coordinated with an oxygen atom of the ligand of the adjacent complex molecule (Fig.3.13a)[9] and enhancement of antiferromagnetic interaction between the two cobalt ions was reported[10].

Existence of perturbed [Co(SALEN)] in the nonstoichiometric phase is also supported by infrared spectra in the region assigned to metal-ligand bond stretching and chelate skeleton vibrations[11,12]. As described in section 3.2.4, intensities and wave numbers of most of bands from 400 cm^{-1} to 700 cm^{-1} were almost independent of x in the phase, and similar to those of $[Co(SALEN)]_2$ dimer.

The C-O bonds of the [Co(SALEN)] moiety of the dimer molecule (Fig.3.13a) are not equivalent crystallographically owing to the coordination of the adjacent [Co(SALEN)] to the cobalt ion[9], while those of the pyridine adduct (Fig.3.13b) are equivalent[13]. Corresponding to the difference in their C-O bond charactor, the band at 1150 cm^{-1} of [Co(SALEN)]py splits into two bands at 1140 cm^{-1} and 1152 cm^{-1} for the dimer, $[Co(SALEN)]_2$. Since these bands at about 1140 cm^{-1} are assigned to the C-O stretching bands according to the assignment on a derivative of [Co(SALEN)], N,N'-bis(salicylidene)-1,1-(dimethyl)ethylenediammine cobalt[12], the splitting of the band at about 1140cm^{-1} shows nonequivalent C-O bonds due to dimerization of the [Co(SALEN)] molecules.

A C-O stretching band of the complex molecules in the unoxygenated crystal for both the SP-O_2 ans SC-O_2 systems was observed at 1142 cm^{-1} as shown in Fig.3.9a (x=0). This is consistent with the square planer structure of the unperturbed molecule in the unoxygenated crystal which was suggested by Nishikawa et al.[8] according to its near-infrared diffuse reflectance spectrum. On the other hand, the C-O stretch band splitted into two bands at 1138 cm^{-1} and 1150 cm^{-1} for the nonstoichiometric region of both the systems. Comparing this result and infrared spectra of $[Co(SALEN)]_2$ and [Co(SALEN)]py, the phenolic oxygen atoms of the complex molecules in the nonstoichiometric region are not equivalent like those in $[Co(SALEN)]_2$.

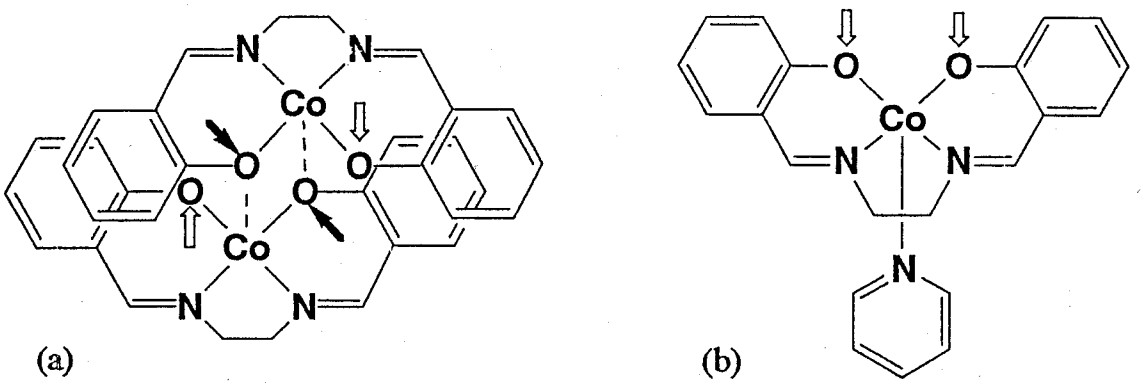

Fig.3.13 [Co(SALEN)]$_2$ (a) and [Co(SALEN)]py (b). The oxygen atoms with a open arrow coordinate to a cobalt ion. On the other hand, those with a filled arrow coordinate to two cobalt ions.

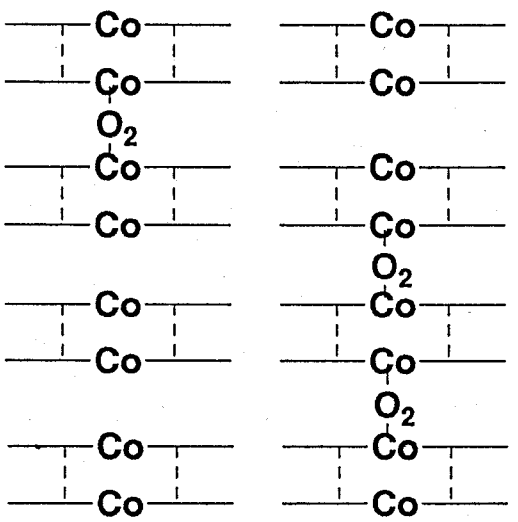

Fig.3.14 A structural model for [Co(SALEN)]$(O_2)_X$

Considering the antiferomagnetic interaction between cobalt ions and the nonequivalence of the phenolic C-O bonds of the complex molecules, it is concluded that the unoxygenated complex molecules in the nonstoichiometric phase have a dimeric structure similar to the $[Co(SALEN)]_2$ dimer.

Since 2 mol of active form [Co(SALEN)] reacts with 1 mol of dioxygen and [Co(SALEN)] molecules in the nonstoichiometric phase interact with each other as discussed above, dioxygens are considered to be distributed over the sites formed by dimerized [Co(SALEN)] molecules (Fig.3.14), where the number of sites is half of the number of complex molecules. The discussion to be given in chapter 5 suggests that deviation from complete random distribution of dioxygens is negligible.

3.3.2 Cooperativity in $[Co(SALEN)]$-O_2 System

From the discussion in the previous section, one can employ a model in which n dioxygen are randomly distributed over $(N/2)$ sites, where N is the number of [Co(SALEN)] complex molecules. According to this model, partial molar entropy of distribution is expressed as follows:

$$\Delta_r \bar{S}_{dis} = -R \ln\left(\frac{2x}{1-2x}\right), \qquad \text{(eq.3.1)}$$

where dioxygen content (x) is defined as n/N. If one can neglect the dioxygen content dependence of partial molar enthalpy and entropy except the contribution from eq.3.1, partial molar Gibbs energy can be written as follows:

$$\Delta_r \bar{G}^\circ = \text{const.} + RT \ln\left(\frac{2x}{1-2x}\right). \qquad \text{(eq.3.2)}$$

Since cooperativity in a system is defined as an interaction which decreases partial molar Gibbs energy from the value given by eq.3.2 when dioxygen content is increased, magnitude of cooperativity will be shown by that of decrease in excess partial molar Gibbs energy:

$$\Delta_r \bar{G}^E = \Delta_r \bar{G}^\circ - RT \ln\left(\frac{2x}{1-2x}\right). \qquad \text{(eq.3.3)}$$

Excess partial molar Gibbs energies for the SP-O_2 and SC-O_2 systems in their nonstoichiometric phases shown in Fig.3.15 and Table 3.1 indicate cooperativity in the both systems. Since no appreciable composition dependence as observed in the partial molar enthalpies as shown in Fig.3.3, the cooperativity in the systems is attributable to the entropy term of their Gibbs energy. Indeed deviations from eq.3.1, excess partial molar entropies increased linealy with x as shown in Fig.3.16 with parameters given in Table 3.5. The increase results in decrease in partial molar Gibbs energy.

Large composition dependence of the excess partial molar entropy may result from change in the density of state of low-frequency vibrations such as lattice vibration. Since no appreciable shift of any infrared absorption band was observed, the contribution from low-frequency intramolecular vibrations is considered to be small.

There are two additional possible entropy terms related to the lattice vibration in this gas-solid reaction system, (1) partial molar entropy change arising from the volume expansion associated with insertion of dioxygens as analogy of hydrogen-metal systems[14,15] and (2) the one arising from the linkage of adjacent

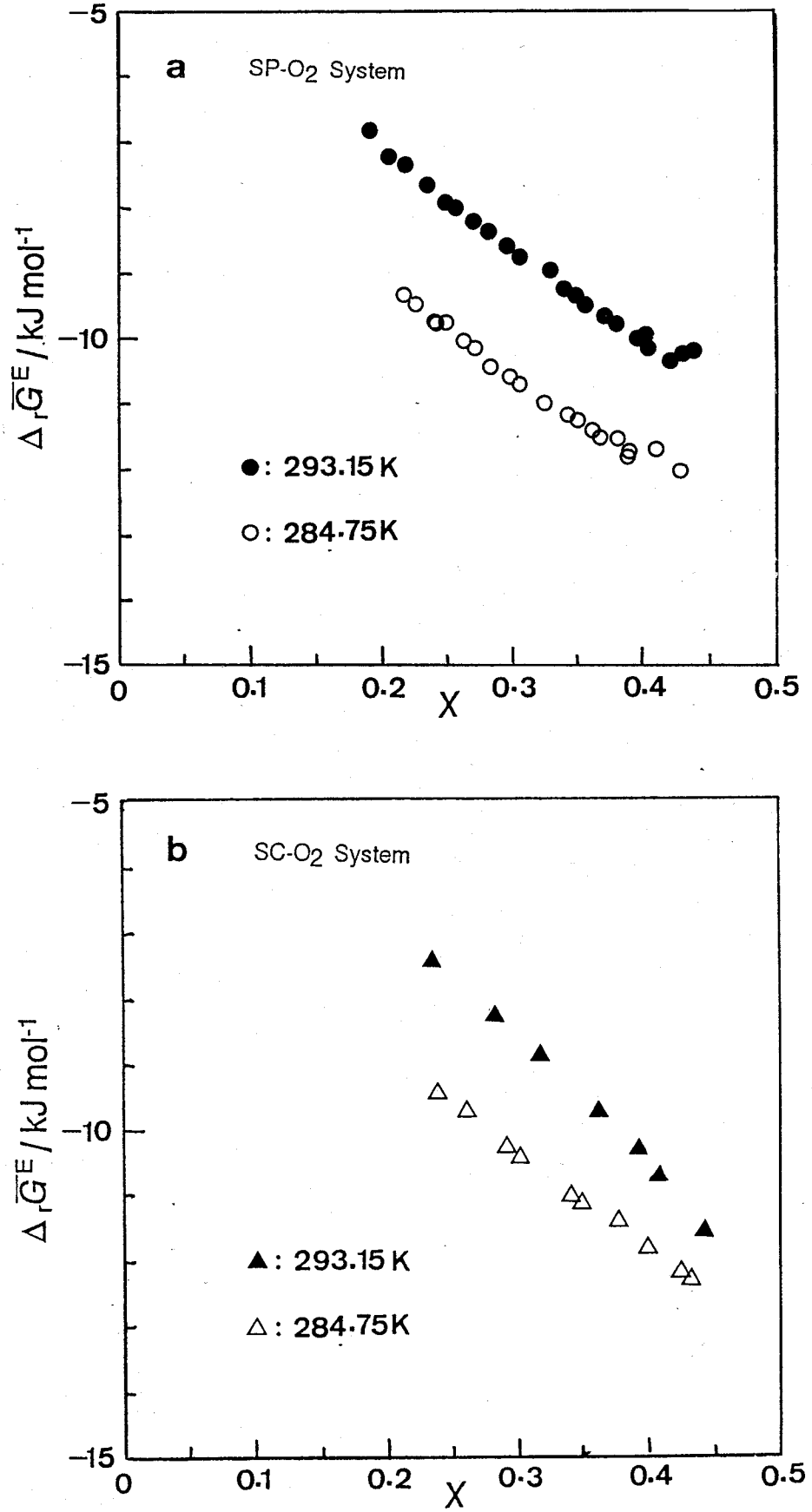

Fig.3.15 Excess partial molar Gibbs energy of the SP-O_2 (a) and SC-O_2 (b) systems at 274.75K (open marks) and 293.15K (filled marks).

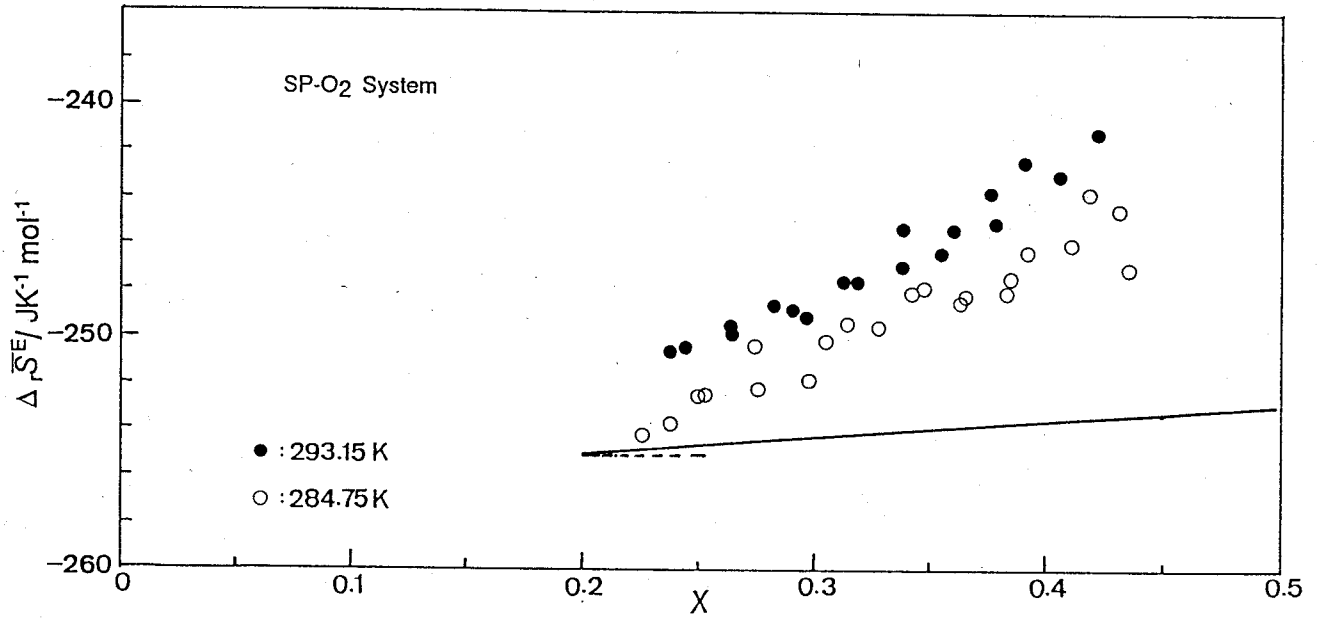

Fig.3.16a Excess partial molar entropy of the SP-O_2 system at 284.75K (open circles) and 293.15K (filled circles). The solid line shows the slope estimated from the volume expansion of the sample (see text).

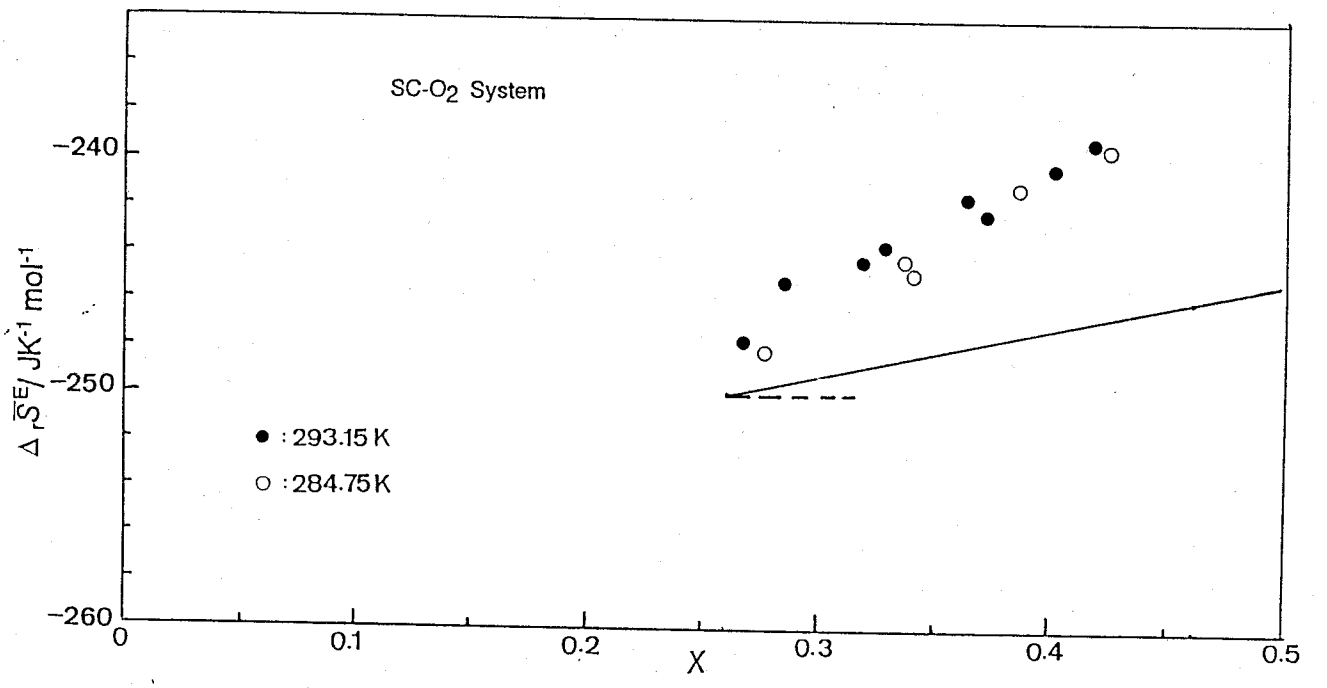

Fig.3.16b Excess partial molar entropy of the SC-O_2 system at 284.75K (open triangles) and 293.15K (filled triangles). The solid line shows the slope estimated from the volume expansion of the sample (see text).

Table 3.5 Patameters for $\Delta_r \overline{S}^E$ fitted by $\Delta_r \overline{S}^E = ax+b$.

	SP-O_2 system		SC-O_2 system	
	at 284.75 K	at 293.15 K	at 284.75 K	at 293.15 K
a / $JK^{-1}mol^{-1}$	41.6	39.4	48.6	61.8
b / $JK^{-1}mol^{-1}$	-260.5	-262.6	-259.9	-265.6

Table 3.6 $(\partial S/\partial V)_T$ of some organic and inorganic materials.

material	$(\partial S/\partial V)_T$ / $JK^{-1}cm^{-3}$
benzoic acid	1.85
naphthalene	1.94
anthracene	1.73
anthraquinon	1.50
sodium chloride	2.9
copper	2.33

two complex molecules by a dioxygen bridge described in chapter 4.

At room temperature, volume dependences of internal energy U and entropy (S) arising from lattice vibration can be expressed with an accuracy of up to 10-20% for most of organic crystals by the following equations[16]:

$$\left(\frac{\partial U}{\partial V}\right)_T = -6RT\left(\frac{\partial \ln \Theta_D}{\partial V}\right)_T, \qquad \text{(eq.3.4a)}$$

and

$$\left(\frac{\partial S}{\partial V}\right)_T = -6R\left(\frac{\partial \ln \Theta_D}{\partial V}\right)_T, \qquad \text{(eq.3.4b)}$$

respectively, where R is the gas constant and Θ_D is the Debye temperature of the crystal. Since these equations include the same term with respect to volume, the enthalpy and entropy would contribute to free energy by similar magnitudes and their composition dependences would be similar. This estimation is in conflict with the experimental findings that the partial molar enthalpy was almost independent of x, while the partial molar entropy increased with increasing x.

Quantitative estimation of the volume expansion term in partial molar entropy also shows that this term is a minor contribution to the partial molar entropy. The partial molar entropy term can be written as follows:[14,15,16]

$$\Delta_r \bar{S}_V = \frac{\alpha}{\beta}\left(\frac{\partial V}{\partial x}\right), \qquad \text{(eq.3.5)}$$

where α is the volume thermal expansion coefficient, and β is the isothermal compressibility. α/β values for some organic crystals fall in a narrow range around 2 $JK^{-1}cm^{-3}$ as summarized in Table 3.6[16,17]. Even for inorganic crystals (ionic and metallic), the values are not so much different from those of organic crystals. Thus the average value for organic crystals in Table 3.6, (1.8±0.3) $JK^{-1}cm^{-3}$ was adopted in this estimation. For the estimation of the contribution from this cause, the molar volume at about x=0.45, volume change by reaction given in Table 3.3 and Table 3.4 and x at the phase boundaries written in section 3.2.1 were used. The estimated volume expansion terms of partial molar entropy were (1.8±0.3) $JK^{-1}mol^{-1}$ and (4.0±0.7) $JK^{-1}mol^{-1}$ for the SP-O_2 and SC-O_2 systems, respectively, at about 293 K, if the term is independent of x. If the term has a first-order dependence on x like experimental results of excess partial molar entropy, the dioxygen content dependence can be shown as solid lines in Fig.3.16a and b, where it is assumed that the cell volume increases quadratically with respect to x and $\partial V/\partial x$=0 at the phase boundary. The slope of the experimental results is twice or three times steeper than the estimated volume expansion term. Furthermore smaller slope than the estimated one may be expected, because volume expansion in their nonstoichiometric phase is very small and deviation from Vegard's rule would not be so large. Therefore the volume expansion is considered to be a minor contribution to dioxygen content dependence of the excess partial molar entropy.

Although quantitative estimation on the effect of linkage formation between complex molecules by dioxygen moieties has not been carried out, the prerequisite in the calculation to be given

in the next chapter 4 (model A') that the lattice is made of dimerized atoms, is satisfied in the SP-O_2 and SC-O_2 system as discussed in section 3.3.1. As will be shown in Fig.4.8b and Fig.4.9b, the dioxygen content dependence in partial molar enthalpy and excess entropy agrees qualitatively with the results of the calculation on model A'. Therefore the linking by dioxygens in a dimer lattice can be proposed as a major part of the dioxygen content dependence of excess partial molar entropy which leads to cooperativity in the SP-O_2 and SC-O_2 system.

3.3.3 Differences between the SP-O_2 and SC-O_2 Systems

Different O_2/Co ratios for the full oxygenation of SP and SC had been reported by Calvin *et al.*[2] (Co:O_2=2:1 for the SP-O_2 system) and by Tsumaki[1] (Co:O_2=3:1 for the SC-O_2 system). However, in the present study, the isotherms of both the systems resemble each other as shown in Fig.3.2. Furthermore, extrapolation of magnetic susceptibility to the dioxygen content for Co:O_2=2:1 (x=0.5) indicated disappearance of paramagnetic complex molecules at x=0.5, which shows that all complex molecules form [Co(SALEN)]O_2[Co(SALEN)] dimers shown in Fig.3.1b. Thus, it is concluded that the maximum dioxygen content for both the systems is x=0.5 or Co:O_2=2:1. The above-mentioned ratio, Co:O_2=3:1, for the SC-O_2 system would be attributed to the neglect of the existence of the nonstoichiometric phase.

Although similar vibrational and electronic spectra were observed for both the SP-O_2 and SC-O_2 systems (Figs.3.9, 3.10 and 3.12), those systems indicated slightly different behavior in thermodynamic values (Figs.3.2, 3.3, 3.4, 3.15 and 3.16) and the magnetic susceptibility (Figs.3.5 and 3.6) in their

nonstoichiometric regions. The similarity in vibrational spectra shows that the molecular structure of the complex is scarcely different between them. Considering a few differences observed for X-ray diffraction pattern as described in section 3.2.3, a slight difference in molecular packing in the crystals would be envisaged. This would affect interaction between the complex molecules forming a dimer in the nonstoichiometric regions, and change in the electronic state of the cobalt ions which lead to a different magnetic behavior between the systems. The steeper slope in the dioxygen content dependence of excess partial molar entropy for the SC-O_2 system (Table 3.5) than that of the SP-O_2 system would also arise from the slight difference in their crystal structure, because the dioxygen content dependence is attributable to a change in the lattice vibration by oxygenation as described in the previous section.

References to Chapter 3.

1. T.Tsumaki, *Bull.Chem.Soc.Jpn.*, 13, 252 (1938).
2. R.H.Bailes and M.Calvin, *J.Am.Chem.Soc.*, 69, 1886 (1947).
3. D.J.Aymes, B.Bolloto and M.R.Paris, *J.Mol.Catal.*, 7, 289 (1980).
4. O.L.Harle and M.Calvin, *J.Am.Chem.Soc.*, 68, 2267 (1946).
5. R.D.Jones, D.A.Summerville and F.Basolo, *Chem.Rev.*, 79, 139 (1979).
6. E.C.Niederhoffer, J.H.Timmens and A.E.Martell, *Chem.Rev.*, 84, 137 (1984).
7. M.Calvin and C.H.Barkelew, *J.Am.Chem.Soc.*, 68, 2267 (1946).
8. N.Nishiyama and S.Yamada, *Bull.Chem.Soc.Jpn.*, 37, 8 (1964).

9. a)S.Burker, M.Calligaris, G.Nardin and L.Randaccio, *Acta Cryst.*, B25, 1671 (1969); b)R.Deiasi, S.L.Holt and B.Post, *Inorg.Chem.*, 10, 1498 (1971).

10. G.O.Carlisle, G.D.Simpson, W.E.Hatfield, Van H.Carwford and R.F.Drake, *Inorg.Chem.*, 14, 843 (1971).

11. K.Ueno and A.T.Martell, *J.Phys.Chem.*, 60, 1370 (1956).

12. J.A.Faniran, K.S.Patel and J.Bailar.Jr., *J.Inorg.Nucl.Chem.*, 36, (1547 (1974).

13. M.Calligaris, D.Minichelli, G.Nardin and L.Randaccio, *J.Chem.Soc.*(A), 2411 (1970).

14. C.Wagner, *Acta Metall*, 19, 843 (1971).

15. O.J.Kleppa, P.Dentzer and M.E.Melnichak, *J.Chem.Phys.*, 61, 4048 (1974).

16. A.I.Kitaigorodsky, "Molecular Crystals and Molecules", Academic Press, New York and London, 1973, Chap.6.

17. "Landolt-Boernstain Zahlen Werte und Function aus Physik, Chemie, Astronomie, Geophysik und Technik", 6 Aufl., II Band, 1 Teil, s.449-718, (1971); and Neue Serie Gruppe IV, Band 4, s.120-131, (1980), Springer Verlag.

Chapter 4 Cooperativity in Disordered Lattices Modeled after the [Co(SALEN)]-O_2 System.

4.1 Introduction

Interatomic interactions in the nonstoichiometric oxygen-metal[1] and hydrogen-metal systems[2] are dominated by long range forces, for example, Coulomb, electronic and elastic interactions, which cause appreciable composition dependence of partial molar enthalpy and entropy.[3,4] Since [Co(SALEN)] is a molecular crystal, Coulomb and electronic interactions would be a minor contribution to the interaction in the [Co(SALEN)]-O_2 system. Thus the system is characterized by the formation of a linkage between the cobalt atoms by a dioxygen bridge, like [Co(SALEN)]-O_2-[Co(SALEN)], which would affect its lattice vibration considerably. In this chapter, effects of the linkage formation on lattice vibration spectrum and derived thermodynamic quantities in finite cubic lattices of monoatomic molecules in which some interatomic bonds are randomly strengthened will be calculated and discussed as a model system for the [Co(SALEN)]-O_2 system.

Lattice dynamic calculation for lattices disordered in atomic mass, force constant and/or orientation of bonds has difficulties from absence of structural periodicity. One of them is that we cannot use familiar concepts associated with regularity, for example, unit cell and phonon. Direct numerical approach for calculation of vibrational spectra of finite disordered harmonic lattices was developed in 1960's[5] by Dean et al.. They used "negative eigen-value theorem"[6] which decreases the amount of computation to determine lattice spectrum from a proper equation

of large order. The method developed by Dean was employed in this chapter.

4.2 Models and Calculation of Lattice Spectra and Thermodynamic Properties

[Co(SALEN)] is a large plane molecule, and crystals containing such flat molecules are likely to have a column structure of the molecules in which the ligand planes are faced each other.[7-11] A similar crystal structure (Fig.4.1) may be expected to take place in the crystals of the oxygen-active and oxygenated forms of the complex. This supposition was supported by the analysis of powder X-ray diffraction pattern of the crystal[7] and the structure analysis of a parent compound of the active form[10] and an oxygenated derivative.[11] Thus, for the present lattice spectrum calculation, we used a simple cubic lattice consisting of point masses connected to their nearest neighbors by springs in stead of the real molecules. Dioxygen (O_2) moieties bonded to cobalt ions of adjacent complex molecules were approximated simply as stronger bonds than other ones, since mass of a dioxygen is at least ten times smaller than that of the complex. It was assumed that all the strengthened bonds are directed along the same axis, and they never neighbor each other in the bond direction because two dioxygen moieties cannot form a bond with one and the same cobalt ion simultaneously (Fig.4.2). Here we define "dioxygen content, x", as the ratio of number of the strengthened bonds to that of all the available bonds parallel to the strengthened one.

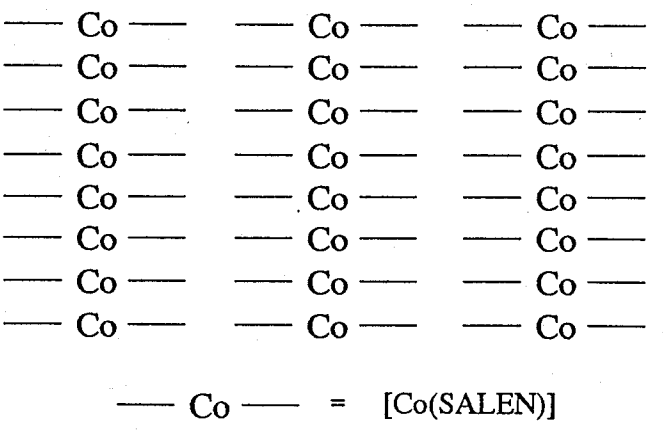

Fig.4.1 An expected column structure in oxygen active [Co(SALEN)].

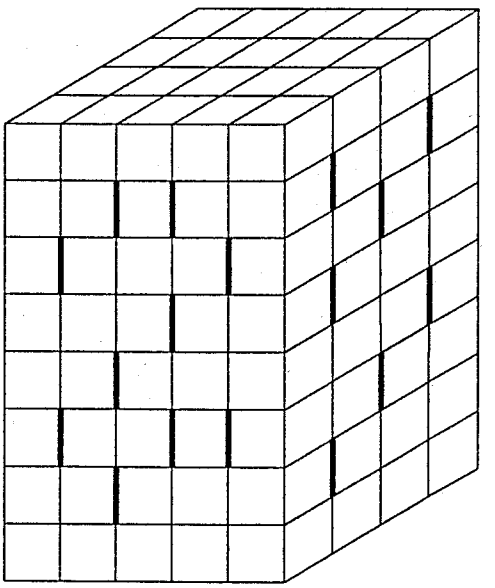

Fig.4.2 A distribution of dioxygen bonds (bold line) on a simple cubic lattice. All dioxygen bonds are directed along the same axis, and never adjacent to each other in the bond direction.

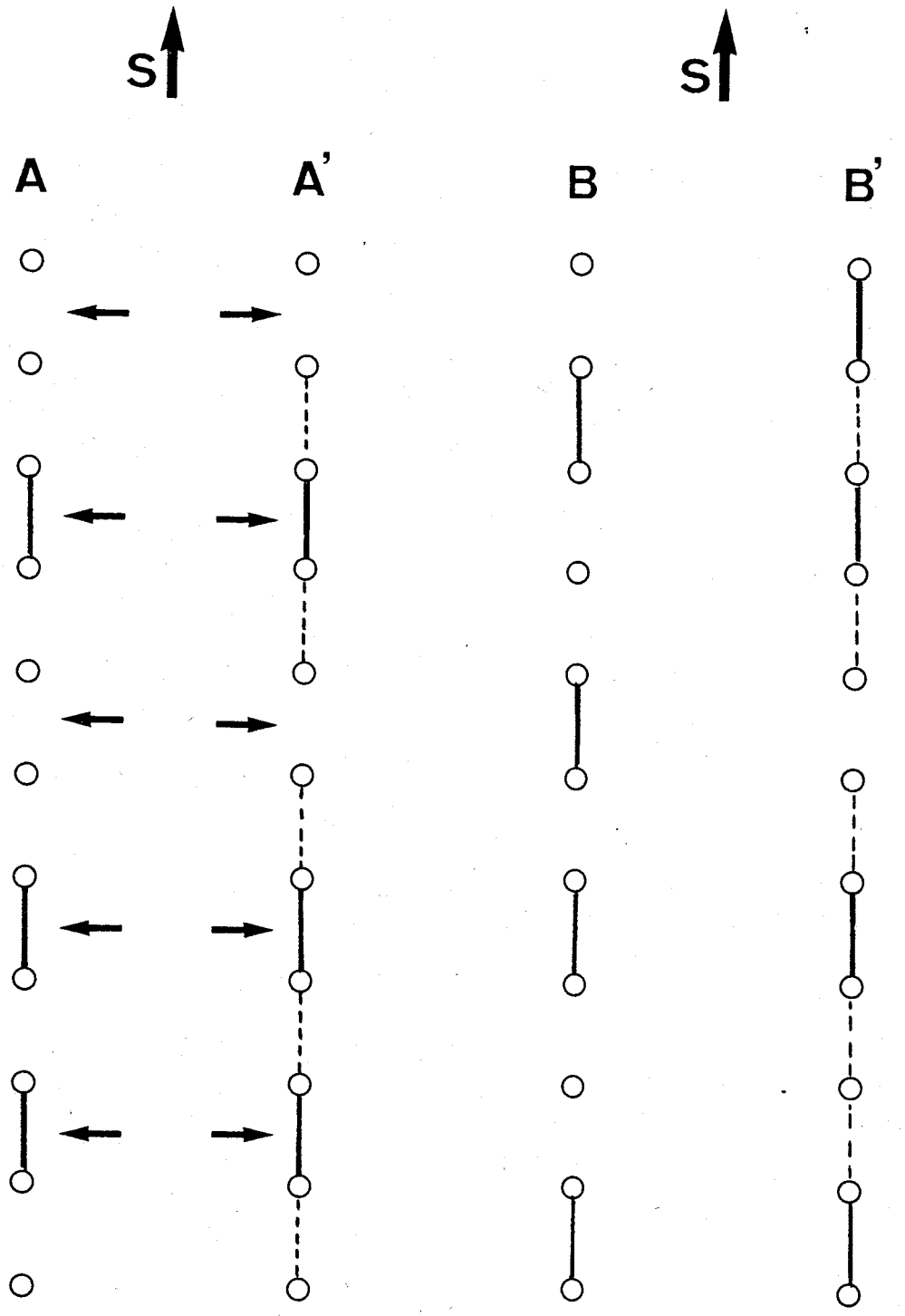

Fig.4.3 Schematic figures of the distribution of dioxygen bonds (bold line) directed along the **s** vector. In the models A and A′, dioxygen bonds are fixed at the sites shown by arrows. On the other hand, dioxygen bonds are placed everywhere except at their neighbor in the models B and B′. In the model A′, atoms are dimerized by moderately strengthened interatomic bonds (broken line). In the Model B′, the bonds adjacent to dioxygen bonds (broken line) are strengthened.

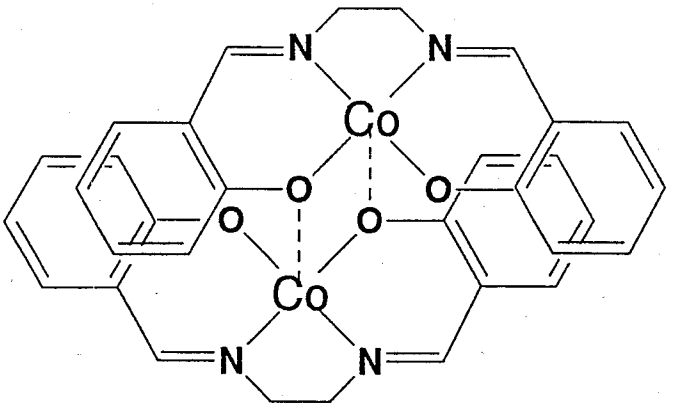

Fig.4.4a [Co(SALEN)]$_2$ dimer

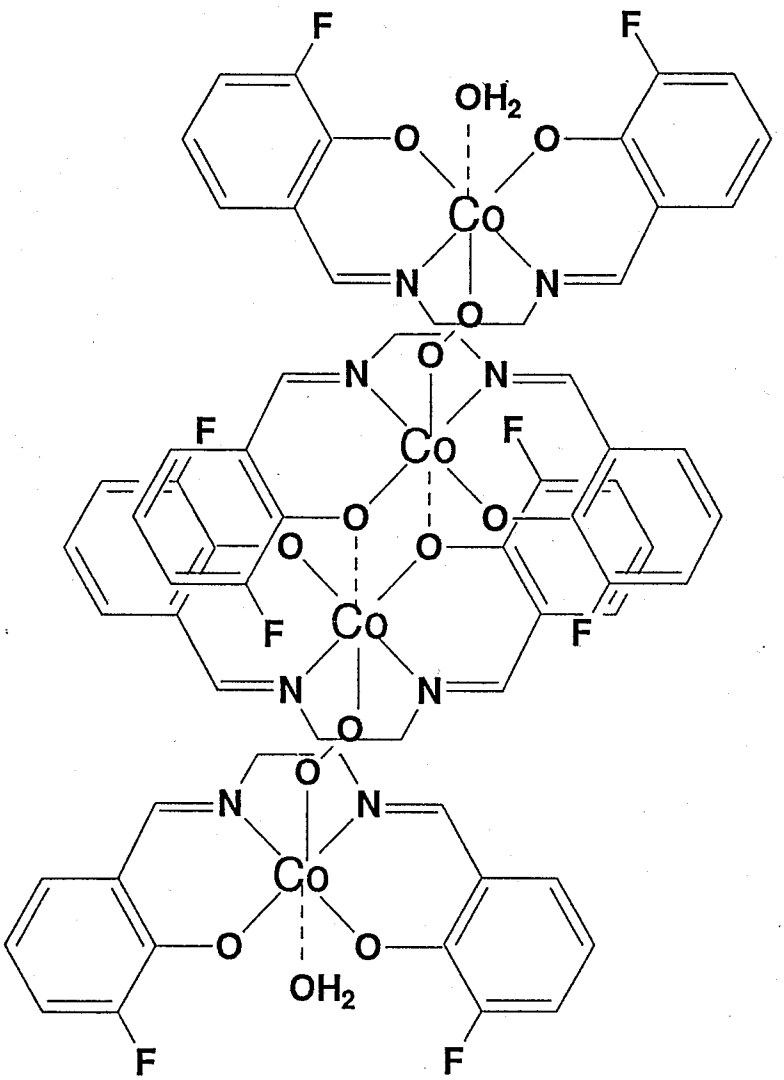

Fig.4.4b {H_2O[Co(3-FSALEN)]O_2[Co(3-FSALEN)]}$_2$

Disordered model lattices were constructed according to two types of arrangement of strengthened bonds; fixed site model (Fig.4.3 model A) and unfixed site model (Fig.4.3 model B). In model A, the formation of strengthened bonds are allowed only to every second bond, while this restriction is removed in model B. Coordination to a cobalt ion by a salicylic oxygen atom of a neighboring [Co(SALEN)] molecule were found in oxygen-inactive [Co(SALEN)] crystal[8,9] and $\{H_2O[Co(3\text{-}FSALEN)]O_2[Co(3\text{-}FSALEN)]\}_2(CHCl_3)_2py$ crystal[11] (Fig.4.4). Thus we calculated lattice spectra for additional two models in which interaction between complex molecules are incorporated. One (Fig.4.3 model A') is a model in which force constants for every gap never oxygenated in model A are moderately strengthened, while the other (Fig.4.3 model B') is a model in which force constants for pairs adjacent to oxygenated ones in model B were moderately strengthened. We used a model for force constants[12] in which an atom in the lattice is connected to their nearest neighbors by two types of springs with force constants r and r' as shown in Fig.4.5, where r' is a force constant for the net displacements along Z-axis between a particle and one of the neighbors on the same X-Y plane. In a three-dimensional simple cubic lattice, this model results in the simplification that the motions in each Cartesian coordinate direction are independent, and reduces the number of coupled variables of a three-dimensional lattice of N atoms from $3N$ to N.

The equation of motion for an atom in the mxmxn lattice (Fig.4.6) is, in harmonic approximation,

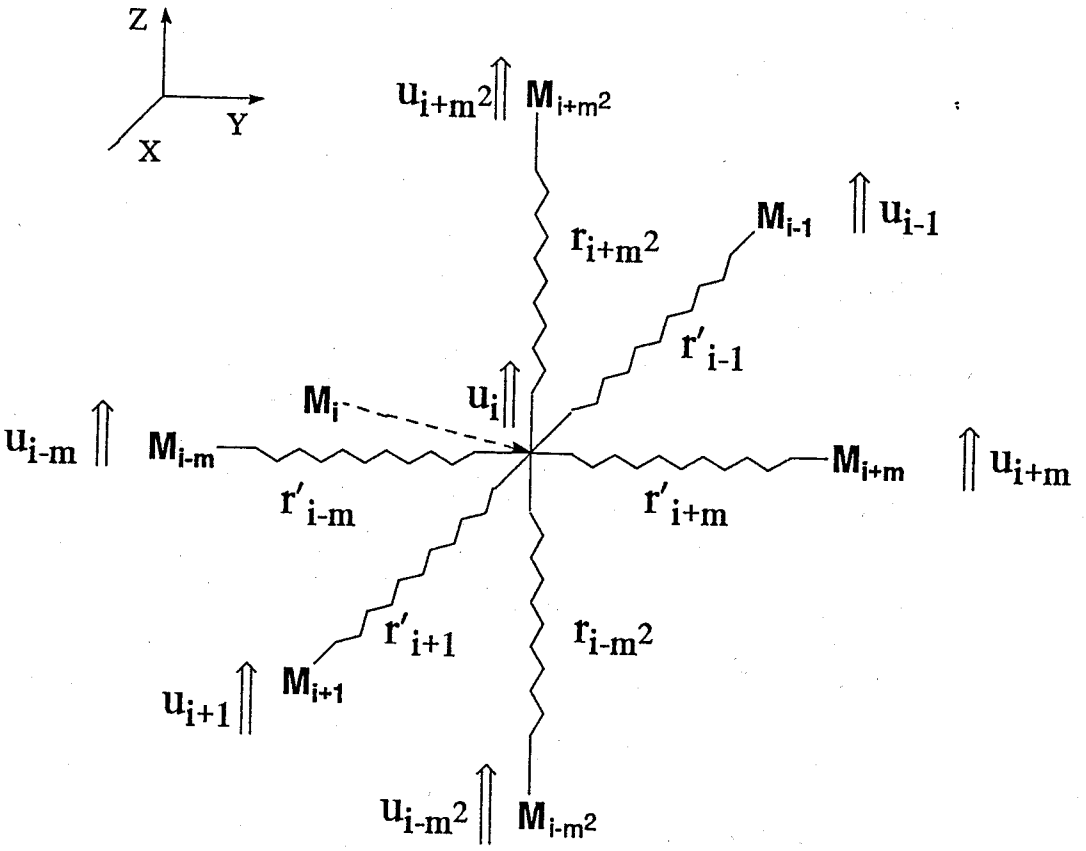

Fig.4.5 Displacement (u) of atoms (M), and central and noncentral force constants (r and r').

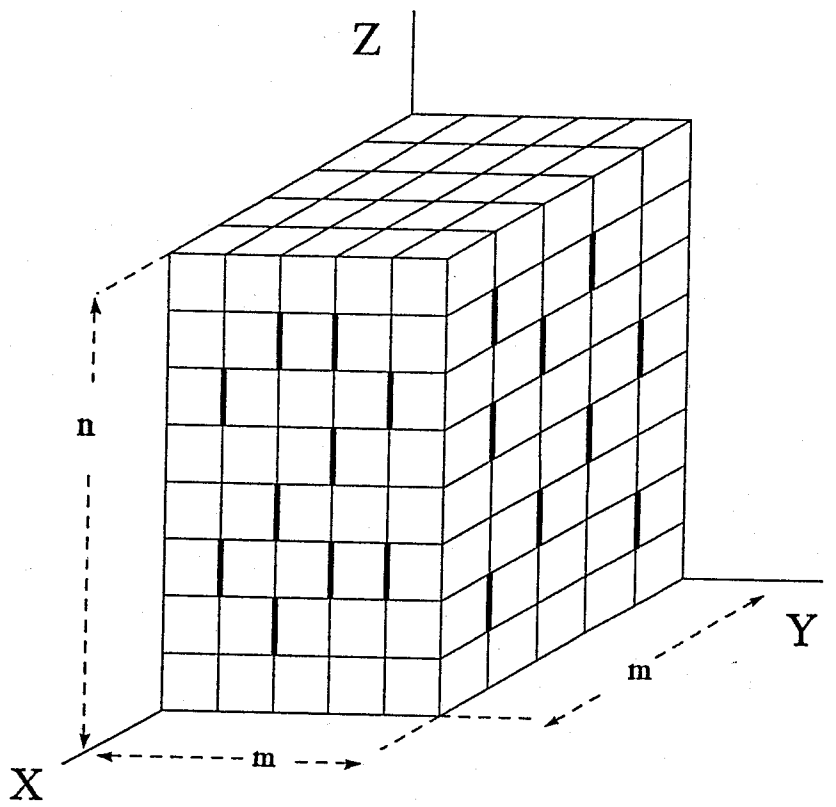

Fig.4.6 The model simple cubic (m,m,n) lattice used for the lattice vibration spectra calculation.

$$M_i \ddot{u}_i = r'_{ii+1}\cdot(u_{i+1} - u_i) + r'_{ii-1}\cdot(u_{i-1} - u_i)$$
$$+ r'_{ii+m}\cdot(u_{i+m} - u_i) + r'_{ii-m}\cdot(u_{i-m} - u_i) \qquad \text{(eq.4.1)}$$
$$+ r_{ii+m^2}\cdot(u_{ii+m^2} - u_i) + r_{ii-m^2}\cdot(u_{i-m^2} - u_i) \ ,$$

where M is the mass of the atoms, u_i is the displacement of the ith atom from an equilibrium position in a direction parallel to one of the cube edges as shown in Fig.4.5. Inserting $u_i = A_0 \exp(i\omega t)$ into eq.2.1 and dividing by $M^{1/2}$, the equation of motion for the whole atoms in the lattice is, in matrix notation,

$$[M_S - \omega^2 I]\cdot u = 0 \ , \qquad \text{(eq.4.2)}$$

where M_S is the dynamical matrix of the three-dimensional simple cubic lattice and its right upper half block can be written as follows:

$$M_S = \begin{pmatrix}
a_1 & b_2 & 0 & 0 & c_{m+1} & 0 & 0 & d_{m^2+1} & 0 & 0 & 0 & 0 & 0 & 0 \\
 & a_2 & \cdot & & & \cdot & & & \cdot & & & & & 0 \\
 & & \cdot & \cdot & & & \cdot & & & \cdot & & & & 0 \\
 & & & \cdot & \cdot & & & \cdot & & & d_i & & & 0 \\
 & & & & \cdot & \cdot & & & \cdot & & & \cdot & & 0 \\
 & & & & & \cdot & \cdot & & & \cdot & & & \cdot & 0 \\
 & & & & & & \cdot & \cdot & & & c_i & & & d_{m^2n} \\
 & & & & & & & \cdot & \cdot & & & \cdot & & 0 \\
 & & & & & & & & \cdot & \cdot & & & \cdot & 0 \\
 & & & & & & & & & \cdot & b_i & & & c_{m^2n} \\
 & & & & & & & & & & a_i & \cdot & & 0 \\
 & & & & & & & & & & & \cdot & \cdot & 0 \\
 & & & & & & & & & & & & \cdot & b_{m^2n} \\
 & & & & & & & & & & & & & a_{m^2n}
\end{pmatrix} \ , \qquad \text{(eq.4.3)}$$

where $a_i = (r'_{ii-1} + r'_{ii+1} + r'_{ii-m} + r'_{ii+m} + r_{ii-m^2} + r_{ii+m^2})/M$, $b_i = -r'_{ii+1}/M$, $c_i = -r'_{ii+m}/M$, $d_i = -r'_{ii+m^2}$, $r_{ij} = r_{ji}$, $r'_{ij} = r'_{ji}$ and $r_{ik}/M = r_{ki}/M = 0$ for $k=0$ and $k > m^2n$

In eq.4.3, we employed regid wall boundary condition in the Z direction of the lattice and a toroidal boundary condition in the X and Y directions[13] (for example, the atoms $c\cdot m$ and $c\cdot m^2$ have

noncentral interaction with the atoms $c \cdot m+1$ and $c \cdot m^2+1$, respectively, where c is an integer).

Using the negative eigenvalue theorem to eq.4.2 for a given dioxygen content x_k, the number of modes blow ω_l^2, $G(x_k, \omega_l^2)$, is obtained for the vibration in the z direction. The density of state (DOS) between ω_{l-1}^2 and ω_l^2, $g(x_k, \bar{\omega}_l 2)$, or ω_{l-1} and ω_l, $g(x_k, \bar{\omega}_l)$ can be obtained by eq.4.4 and eq.4.5,

$$g(x_k, \bar{\omega}_l^2) = \frac{1}{N} \frac{G(x_k, \omega_l^2) - G(x_k, \omega_{l-1}^2)}{\omega_l^2 - \omega_{l-1}^2} \quad , \qquad \text{(eq.4.4)}$$

and

$$g(x_k, \bar{\omega}_l) = \frac{\dfrac{G(x_k, \omega_l^2) - G(x_k, \omega_{l-1}^2)}{\omega_l^2 - \omega_{l-1}^2}}{\sum_l \dfrac{G(x_k, \omega_l^2) - G(x_k, \omega_{l-1}^2)}{\omega_l^2 - \omega_{l-1}^2}} \quad , \qquad \text{(eq.4.5)}$$

where $\bar{\omega}_l^2 = (\omega_{l-1}^2 + \omega_l^2)/2$, $\bar{\omega}_l = (\omega_{l-1} + \omega_l)/2$ and N is the number of atoms. The thermodynamic functions, entropy $S(x_k, \omega_0)/R$ and internal energy function $U(x_k, \omega_0)/RT$, were calculated by assigning an Einstein partition function with the degree of freedom, $N_A \cdot g(x_k, \bar{\omega}_l)$, as follows :

$$\frac{S(x_k, \omega_0)}{R} = \sum_l g(x_k, \bar{\omega}_l) \left[\frac{\bar{\omega}_l / \omega_0}{\exp(\bar{\omega}_l / \omega_0) - 1} - \ln\{1 - \exp(-\bar{\omega}_l / \omega_0)\} \right], \qquad \text{(eq.4.6)}$$

and

$$\frac{U(x_k,\omega_0)}{RT} = \sum_l g(x_k,\bar{\omega}_l)\left\{\frac{1}{2}\cdot\frac{\bar{\omega}_l}{\omega_0} + \frac{\bar{\omega}_l / \omega_0}{\exp(\bar{\omega}_l / \omega_0) - 1}\right\}, \qquad \text{(eq.4.7)}$$

where T is the temperature of the system, $\omega_0=kT/h$, and N_A is Avogadoro's constant. The partial molar functions for $S(x_k,\omega_0)/R$ and $U(x_k,\omega_0)/RT$ were determined as the slope of the straight line calculated from the values for five points from x_{k-2} to x_{k+2}. In the models for the [Co(SALEN)]-O_2 system, the strengthened bonds are directed to the same direction. Thus we carried out calculations on both the lattices in which the direction of the bonds is parallel to the Z-axis of the lattice (**s**//Z type distribution), and is perpendicular to the Z-axis (**s**⊥Z type distribution); in the latter case, the strengthened bonds are directed to the X-axis in this calculation. In order to avoid abrupt change in the spectrum, we did not change the strength of the force constants (r and r') associated with the atoms on the first and nth layer in the Z-axis and the force constants (r') of the edge of the layers. According to Dean[5], the spectra for lattices of 6x6x25 atoms disordered in their mass are scarcely different from those for larger lattices and they should represent well the general features of the spectrum of larger three-dimensional disordered lattice. Therefore we employed 5x5x35 and 5x5x43 lattices for the calculation of the **s**//Z type distribution and 5x5x43 and 5x5x53 ones for the **s**⊥Z type lattice.

M=2 for the mass of the atom and r=r'=0.25 for the original force constants of the lattice were used in our calculation. Four times stronger force constant was employed as the dioxygen bridge, and twice stronger one for the strengthened complex-

complex interaction. Dioxygen content (x) was varied by every 0.025 from 0 to 0.5.

The calculation of lattice spectra was executed on a NEC PC9801RA personal computer (CPU 80386 20MHz) with a numeric data processor (80387), utilizing a source program written in C language. The calculational time required for a lattice of 5x5x43 atoms was about 8 sec for one ω_1. Programs for preparation of the matrix Ms and calculation of thermodynamic functions were written in BASIC.

4.3 Results and Discussion

Some calculated spectra for model A, A', B and B' are shown in Fig.4.7. Generally, an incrase in dioxygen content (x) resulted in the reinforcement of diffuse nature of the spectrum. The spectra for the s⊥z type lattice of model A' and B' are characterized by road double lump structure and the disappearance of a central peak (at about ω_1=1) above x=0.3, whilst the features of the spectra for other type of lattices at the same dioxygen content was not appreciably different from each other. The DOS of the lowest frequency region became considerably large with increase in dioxygen content. Since this effect was outstanding in the case of the lattices with bigger dioxygen content as shown in Fig.4.7, it would be caused by the vibration of atoms dimerized by dioxygen bonds with mass, 2M.

The thermodynamic functions were calculated at ω_0=1.5 (ω_0^2=2.25). Since Debye temperature of most of organic crystals (about 100K and about 250K in case of crystals involving intermolecular hydrogen bonds[14]) is considered to be lower than room temperature, ω_0=1.5 may correspond to room temperature for

the calculated spectra of which the maximum of density of state is located at about ω_0=1. The dioxygen content dependences in entropy, S/R and internal energy function, U/RT are shown in Fig.4.8, where the thermodynamic functions of the s//z type lattice and the s⊥z one are denoted by subscript z and x, respectively.

All thermodynamic functions, S_z/R, S_x/R, U_z/RT and U_x/RT, were found to decreased monotonously with increase in dioxygen content (x). For models A (Fig.4.8a) and B (Fig.4.8c) in which only the dioxygen bond was considered, S_z/R decreased more steeply in bigger dioxygen content, while S_x/R, U_z/RT and U_x/RT changed linealy with dioxygen content. This variation in S_z/R results in a more enhanced increase in free energy in larger dioxygen content. On the other hand, for models A' (Fig.4.8b) and B' (Fig.4.8d) in which the strengthened interatomic bond other than the dioxygen bond was included, only S_x/R decreased less steeply at bigger dioxygen content, while U_z, U_x and S_z changed linealy with dioxygen content. This variation results in a monotonous increase in derived partial molar quantities as shown in Fig.4.9. These tendencies are independent of their lattice size and random numbers used in the calculations.

From the relation, $A = U - TS$, increase in partial molar entropy results in decrease in partial molar free energy. Thus the trend of the partial molar entropy observed in models A' and B' shows that cooperativity exists in the system described by those models, that is, partial molar free energy of the systems will be additionally lowered or the system is more remarkably stabilized with increasing dioxygen content than expected from the trend in the low dioxygen content region. On the other hand,

plots of internal energy for the models A' and B' with respect to dioxygen content increases linealy with dioxygen content. This shows that the partial molar quantity is independent of dioxygen content, that is, the internal energy term did not participate in cooperativity in the system. In the systems described by models A and B, internal energy functions also formed straight lines with respect to dioxygen content, while in contrast to models A' and B', dioxygen content dependence of the partial molar entropy for the **s**//Z lattice decreased in larger dioxygen content. Therefore the models A and B give an increase in the partial molar free energy in larger dioxygen content, which shows "negative" cooperativity.

Consequently, cooperativity from entropy term with respect to dioxygen content (x) results from the models A' and B' in which bonds adjacent to dioxygen bonds are strengthened or atoms are dimerized by stronger bonds than original one. On the other hand, the models A and B in which effect of the dioxygen bonds to the adjacent interatomic bonds are not incorporated gives "negative" cooperativity. In the nonstoichiometric phases of SP-O_2 system and SC-O_2 one, volume expansion in the phases was very small, and $U \approx H$ is considered to be a good approximation in solid phases. Therefore discussion in this chapter can be applied to cooperativity in the SP-O_2 and SC-O_2 systems. Since model A' well reflects the situation in the nonstoichiometric phase in those systems discussed in Chapter 3 and cooperativity in the systems arising not from the enthalpy term but from the entropy term, the cooperativity is attributable to effect of linking complex molecules with dioxygens in the phase consisting of dimerized complex molecules.

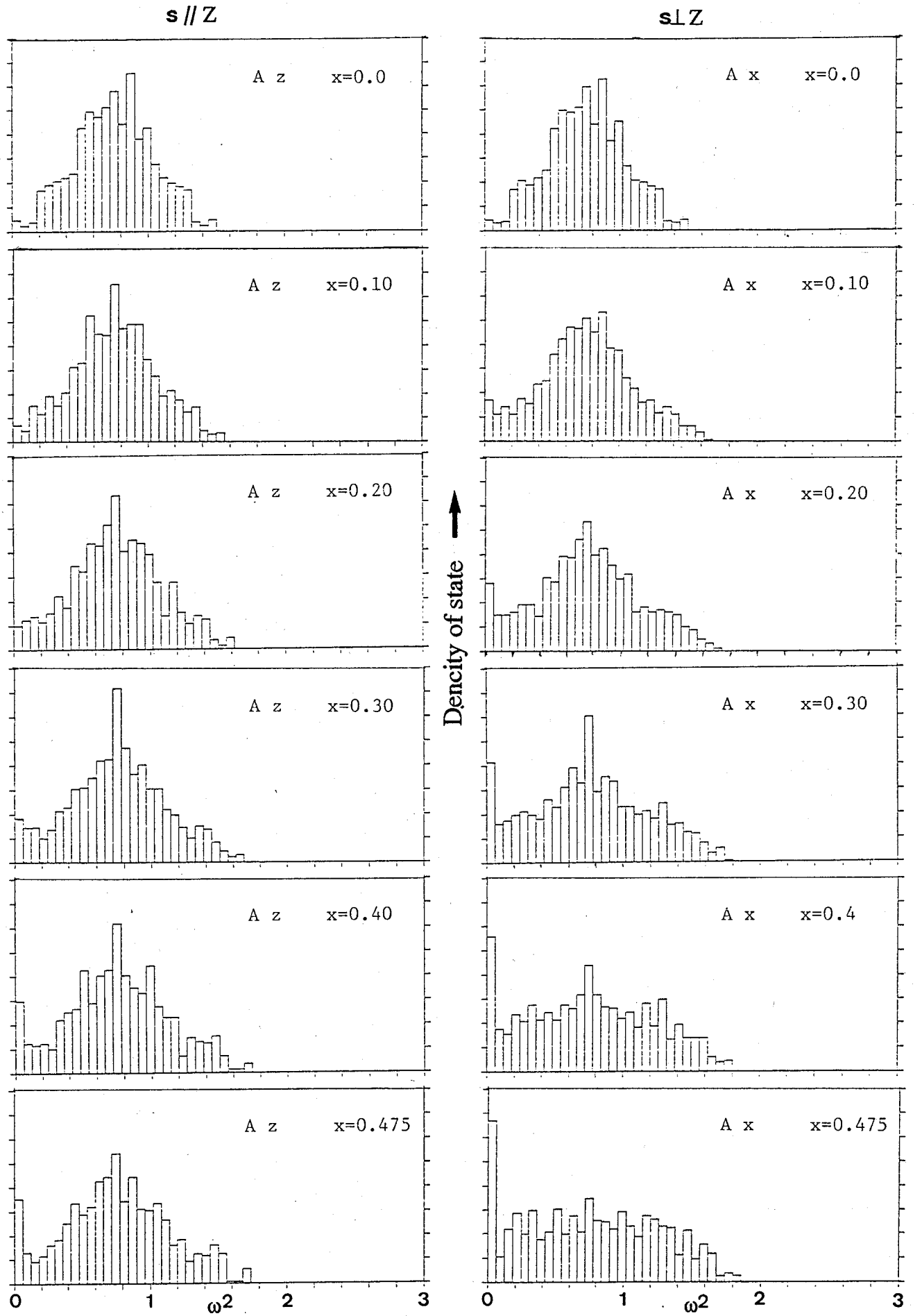

Fig.4.7a Lattice spectra for Model A at various content of dioxygen bonds, x.
The left column shows the spectra in case of **s** // Z, and the right column, **s**⊥Z.

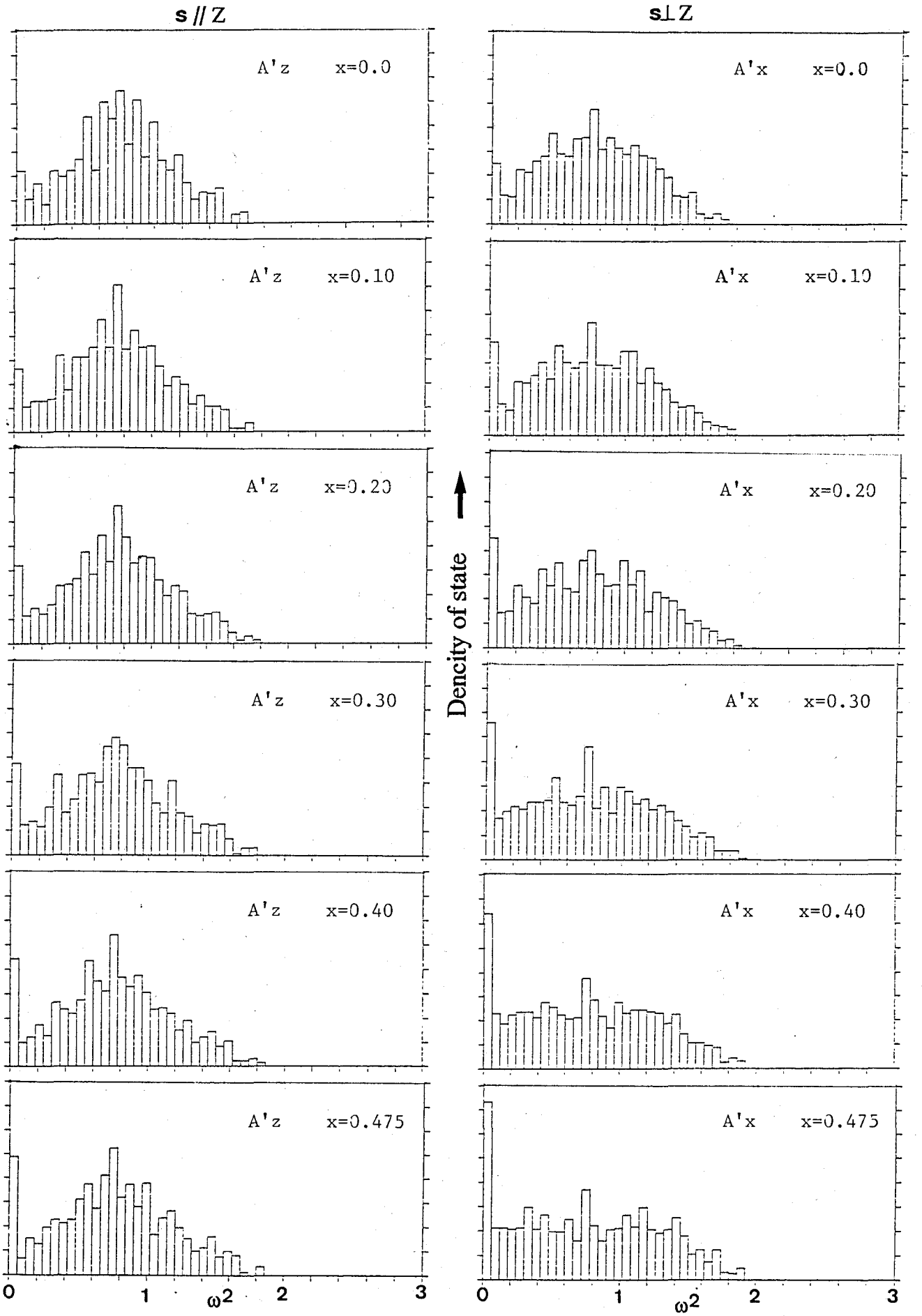

Fig.4.7b Lattice spectra for Model A′ at various content of dioxygen bonds, x.
The left column shows the spectra in case of s // Z, and the right column, s⊥Z.

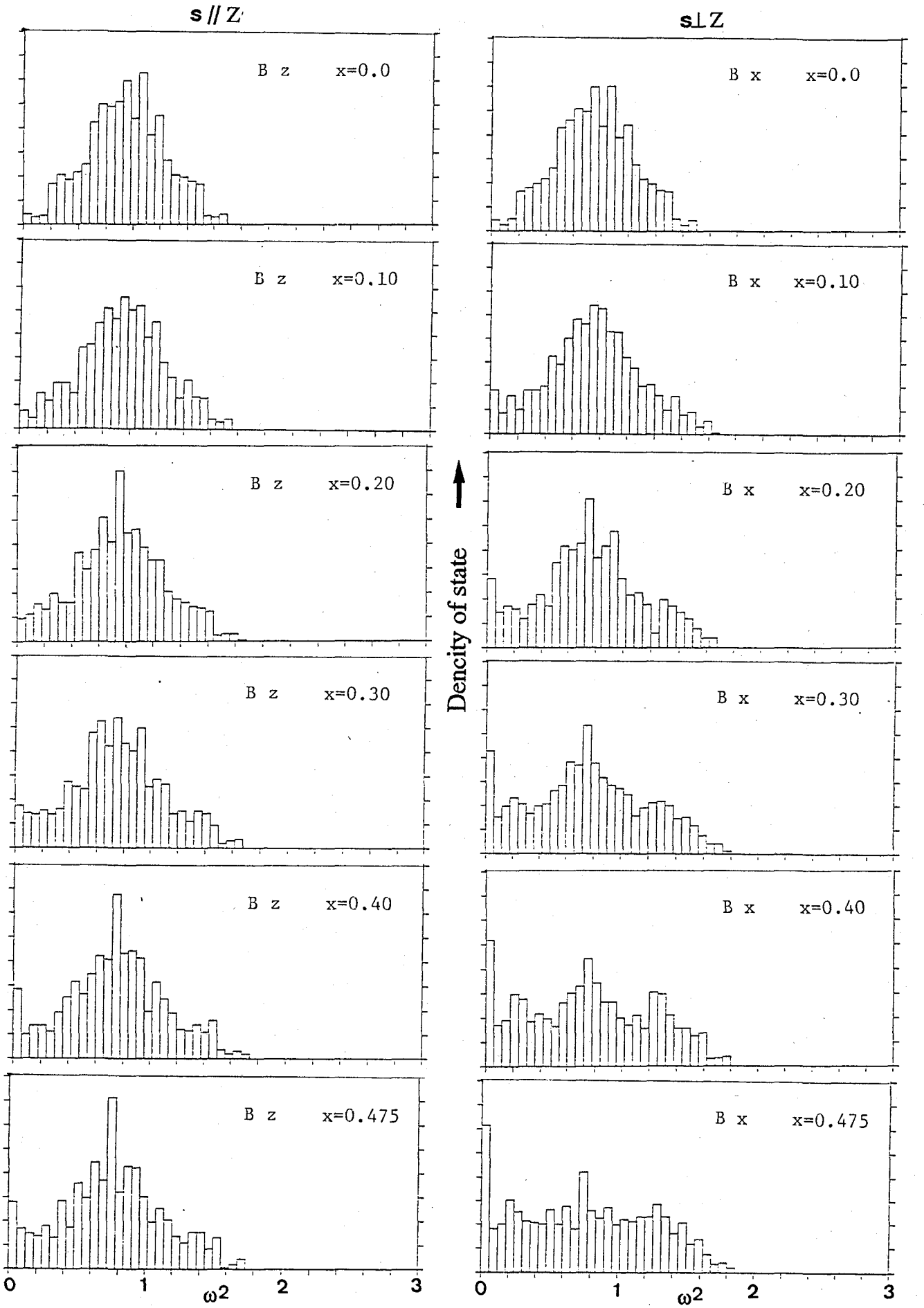

Fig.4.7c Lattice spectra for Model B at various content of dioxygen bonds, x.
The left column shows the spectra in case of s // Z, and the right column, s⊥ Z.

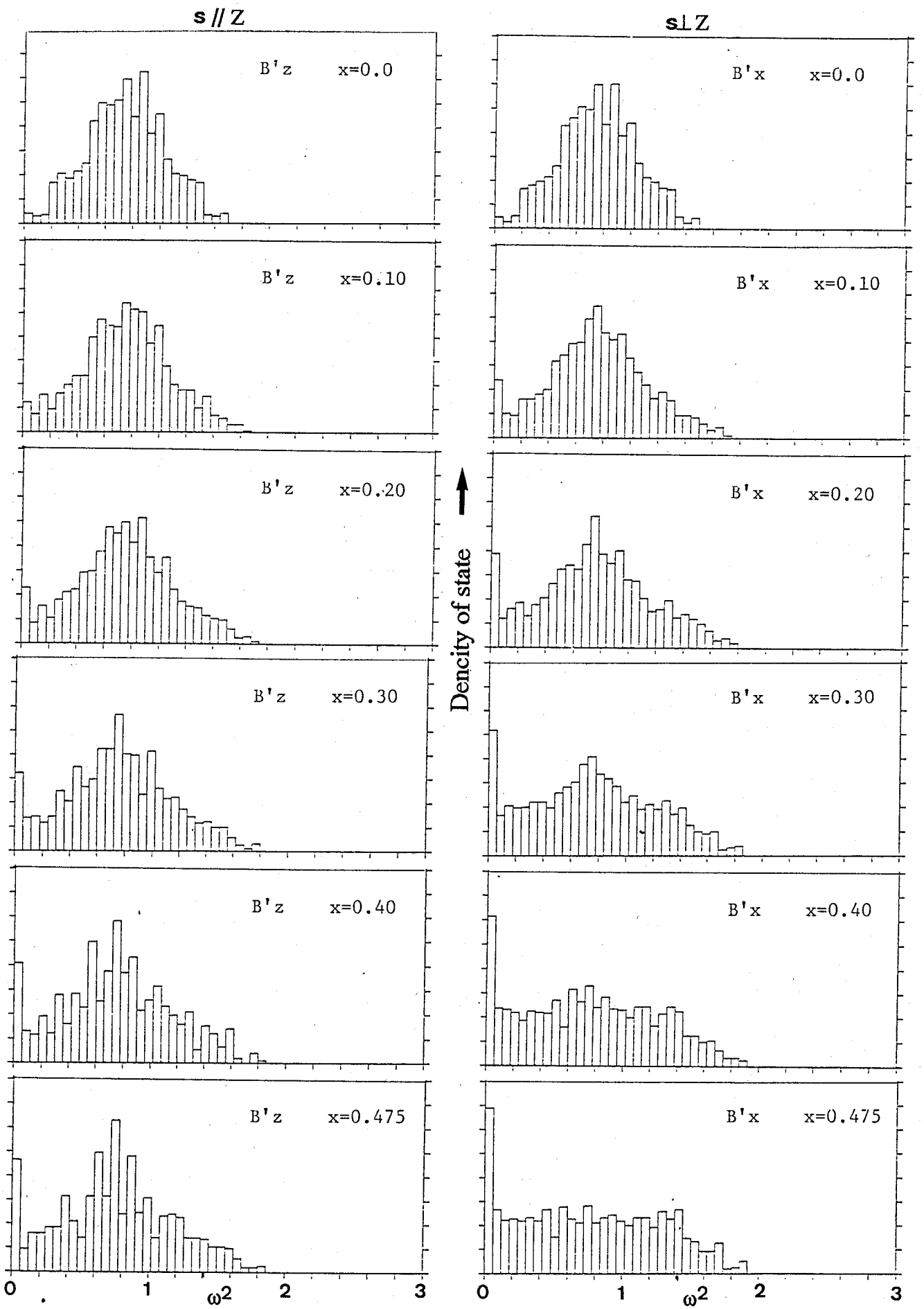

Fig.4.7d Lattice spectra for Model B′ at various content of dioxygen bonds, x.
The left column shows the spectra in case of **s** // Z, and the right column, **s**⊥ Z.

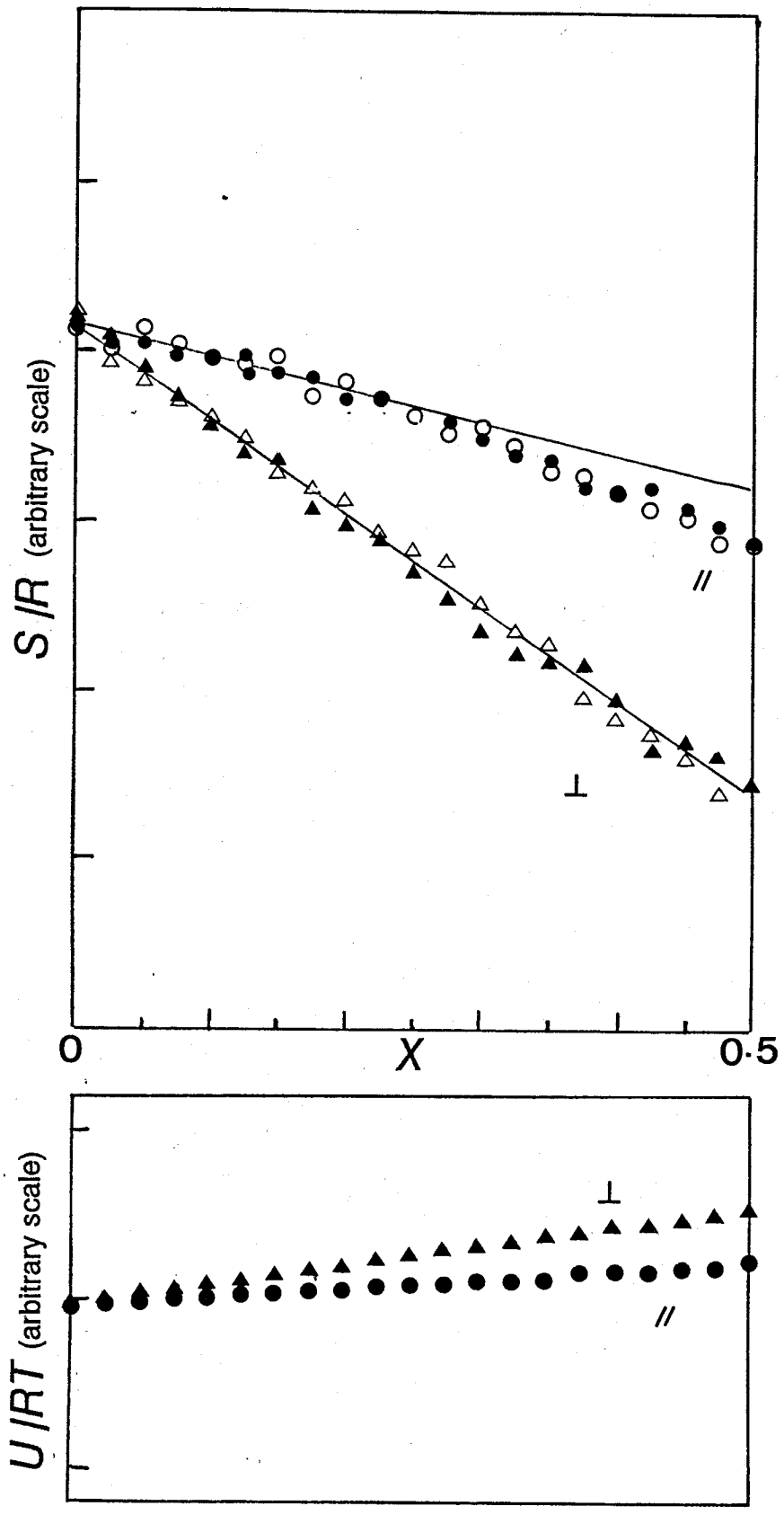

Fig.4.8a Calculated lattice entropy (top) and internal energy function (bottom) at various X based on the Model A. Circles indicate the values for the lattice, **s** // Z axis, and triangles the values for **s** ⊥ Z axis (see Fig.4.3). The values based on different random number series are shown by open and filled marks. Solid lines are drawn for the eye.

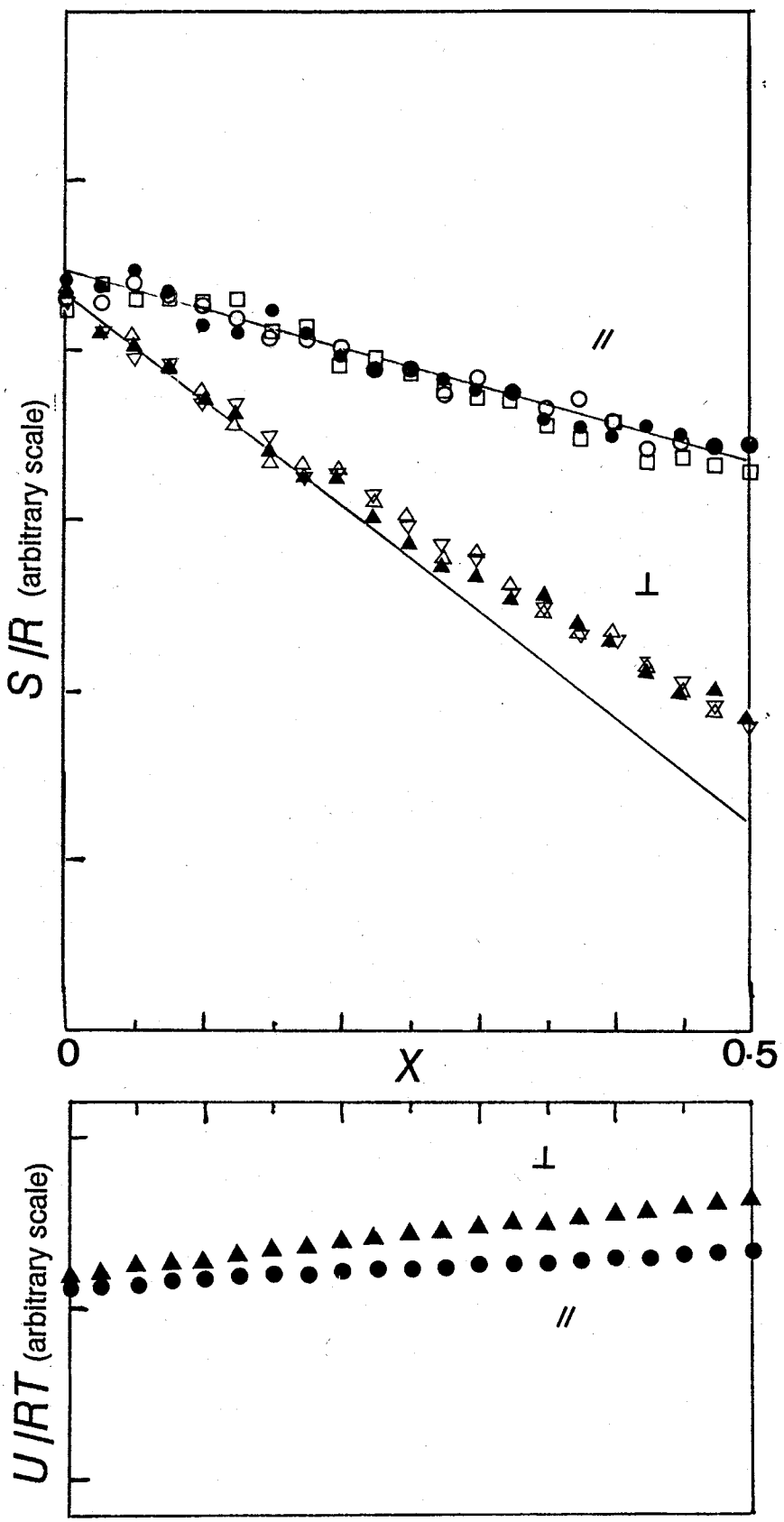

Fig.4.8b Calculated lattice entropy (top) and internal energy function (bottom) at various contents of dioxygen bonds (X) based on the model A'. Circles indicate the values for the lattice, **s** // Z axis, triangles the values for **s** ⊥ Z axis (see Fig.4.3), and squares (**s** // Z) and inverted triangles (**s** ⊥ Z) indicate the values for lattices larger than the former two cases. The values based on different random number series are shown by open and filled marks. Solid lines are drawn for the eye.

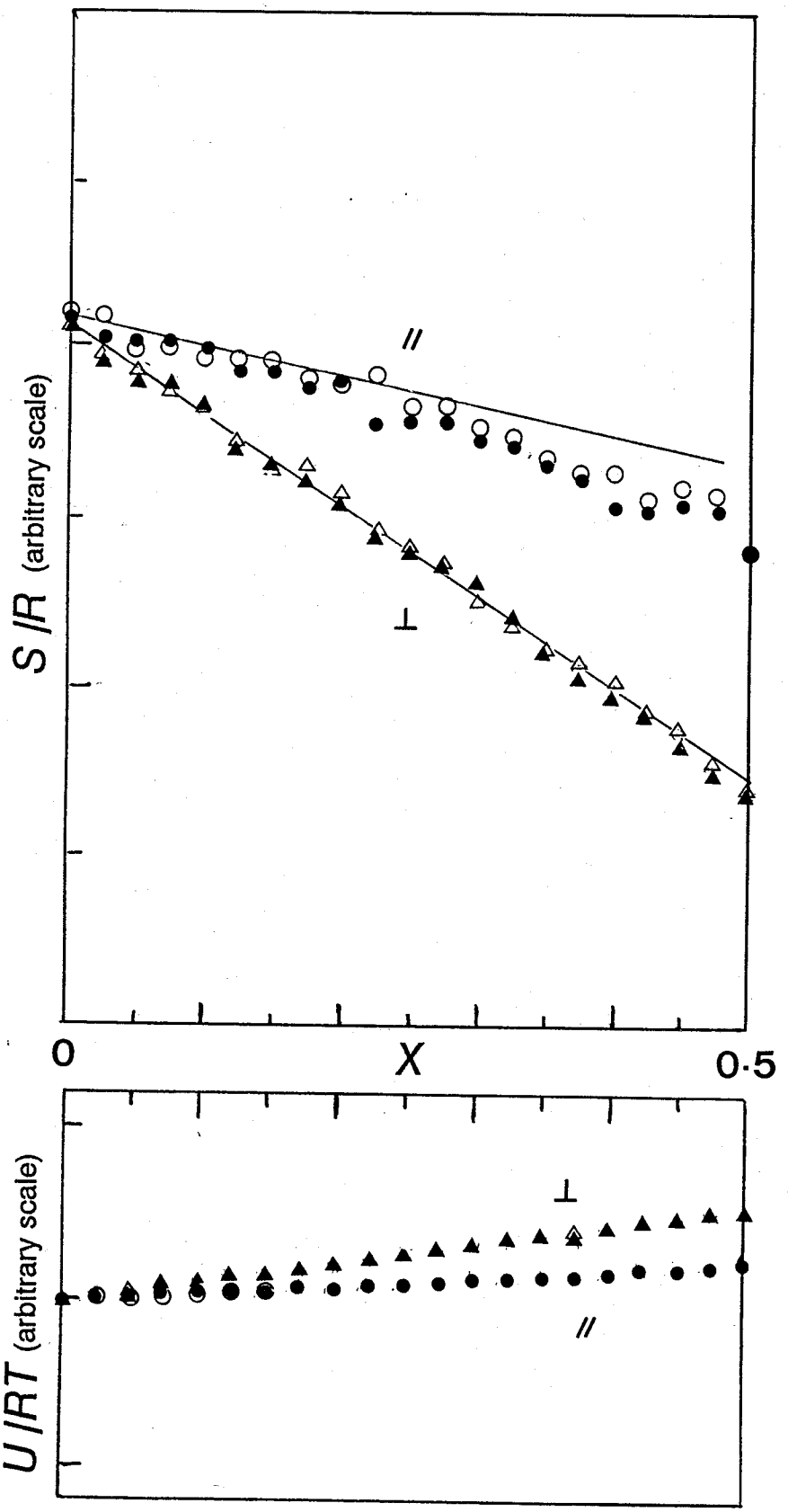

Fig.4.8c Calculated lattice entropy (top) and internal energy function (bottom) at various x based on the Model B. Circles indicate the values for the lattice, **s** // Z axis, and triangles the values for **s** ⊥ Z axis (see Fig.4.3). The values based on different random number series are shown by open and filled marks. Solid lines are drawn for the eye.

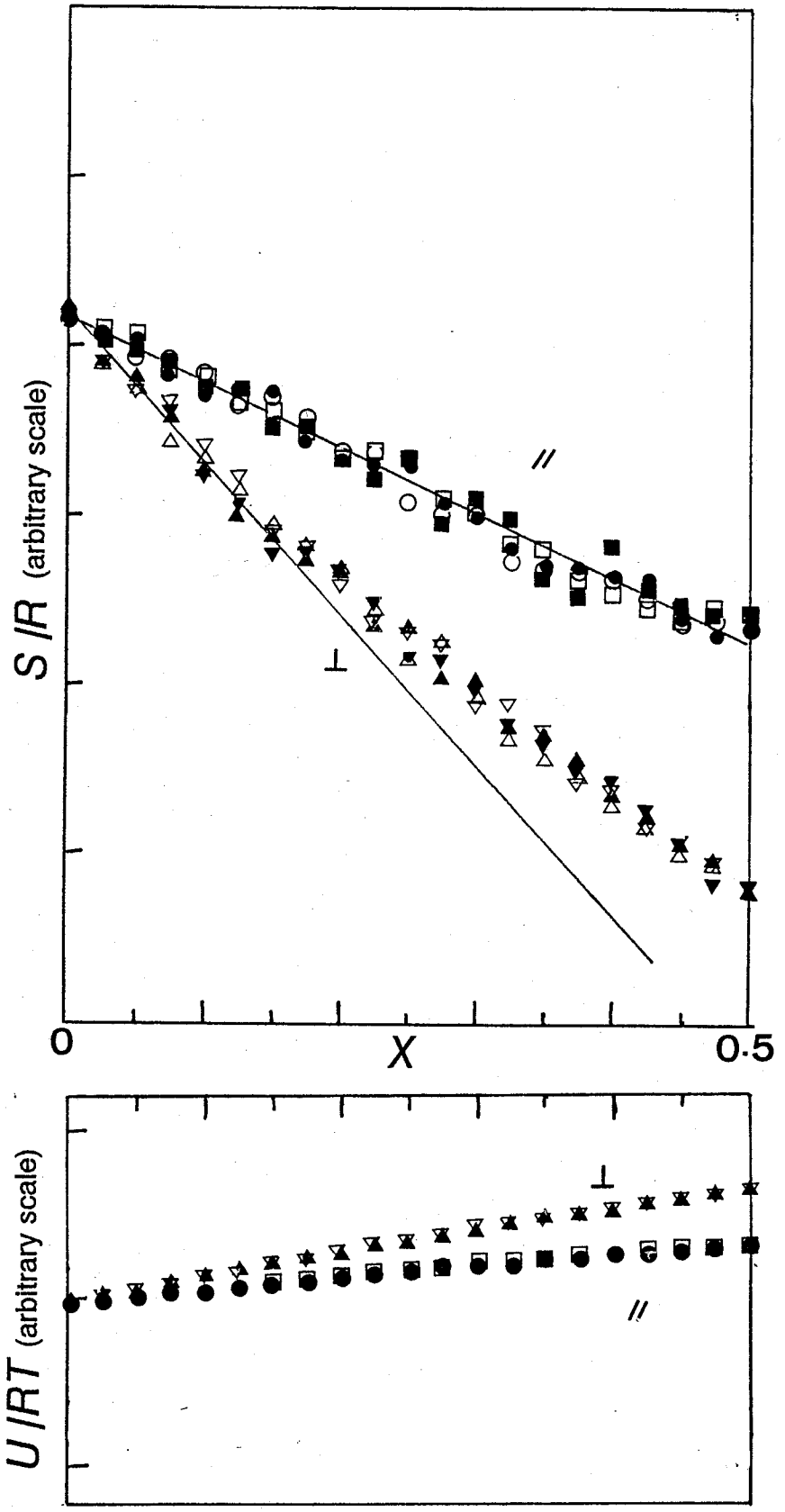

Fig.4.8d Calculated lattice entropy (top) and internal energy function (bottom) at various contents of dioxygen bonds (X) based on the model B'. Circles indicate the values for the lattice, **s** // Z axis, and triangles the values for **s** ⊥ Z axis (see Fig.4.3), and squares (**s** // Z) an inverted triangles (**s** ⊥ Z) indicate the values for lattices larger than the former two cases. The values based on different random number series are shown by open and filled marks. Solid lines are drawn for the eye.

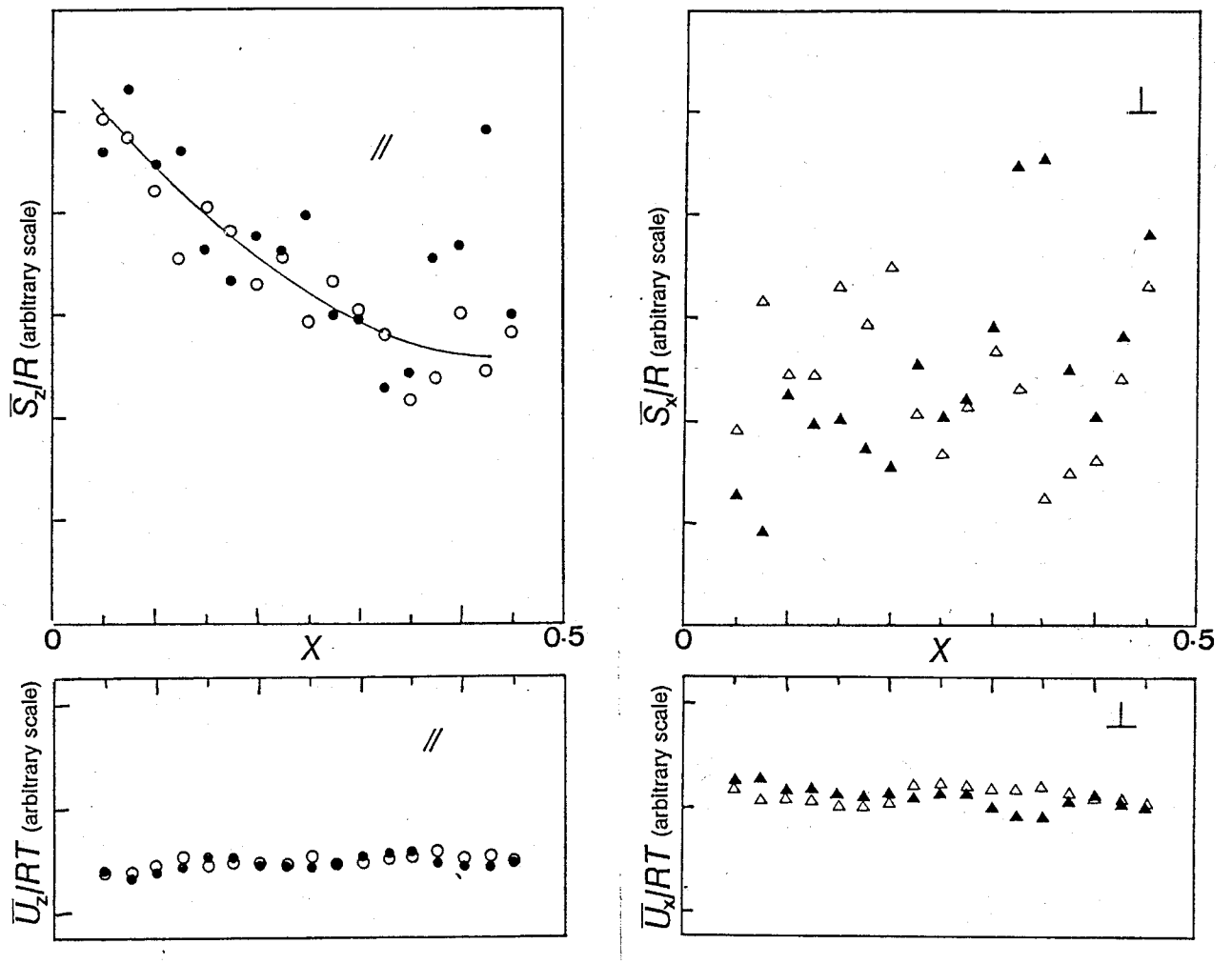

Fig.4.9a Calculated partial molar entropy (top) and partial molar internal energy function (bottom) at various x based on the **s** // Z lattice (left) and **s** ⊥ Z one (right) of the Model A. Meaning of marks are same in Fig.4.8a.

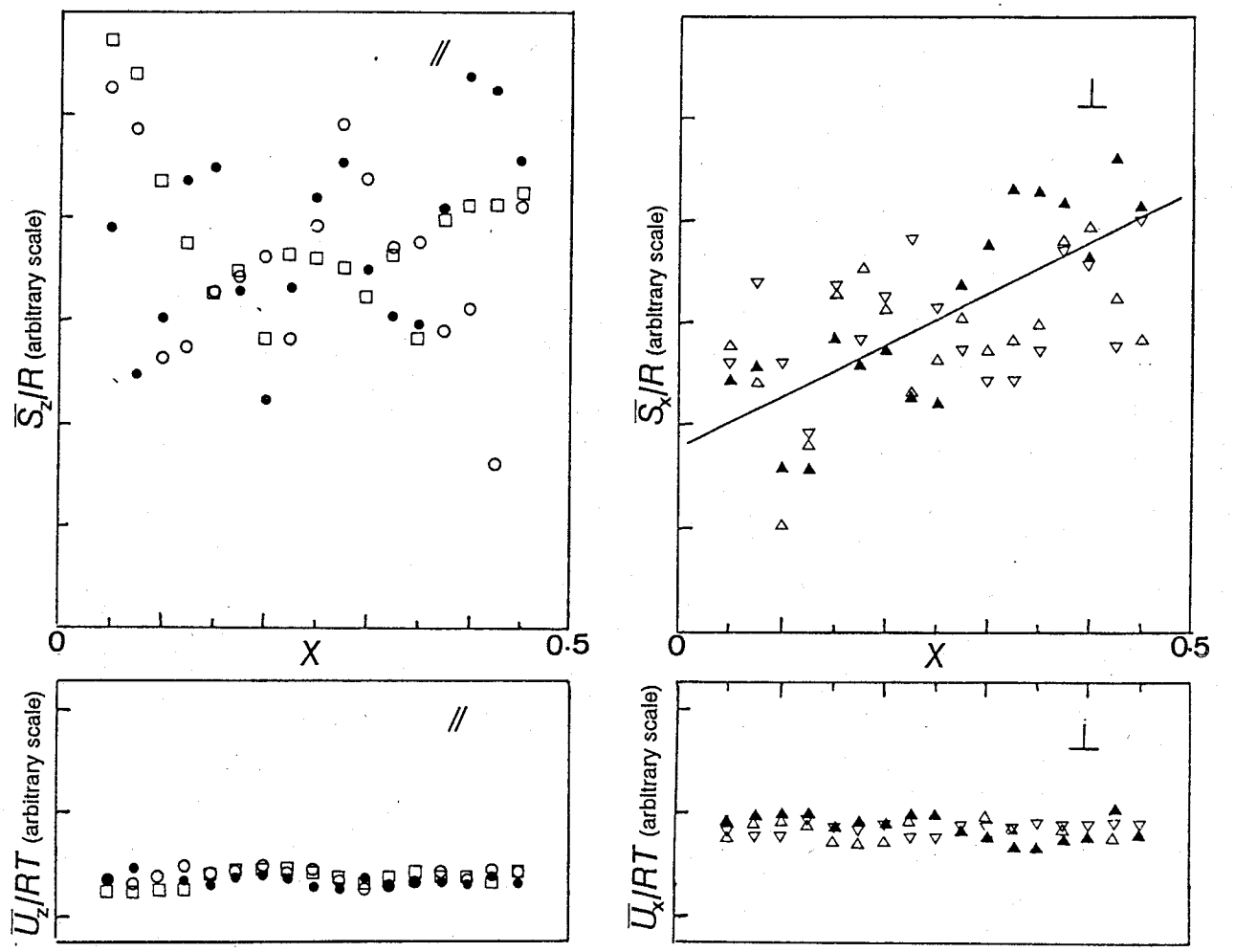

Fig.4.9b Calculated partial molar entropy (top) and partial molar internal energy function (bottom) at various x based on the **s** // Z lattice (left) and **s** ⊥ Z one (right) of the Model A'. Meaning of marks are same in Fig.4.8b.

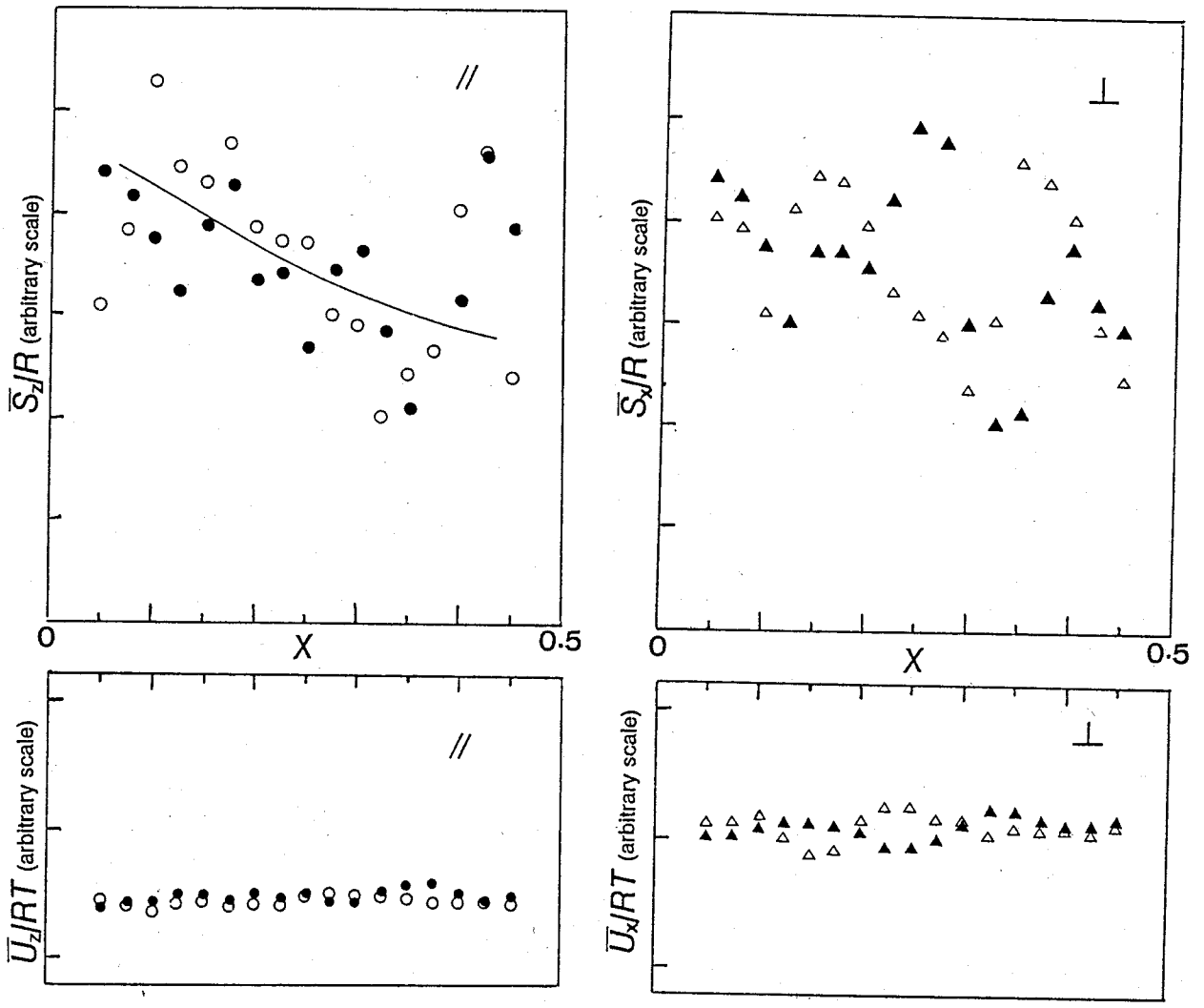

Fig.4.9c Calculated partial molar entropy (top) and partial molar internal energy function (bottom) at various x based on the **s** // Z lattice (left) and **s** ⊥ Z one (right) of the Model B. Meaning of marks are same in Fig.4.8c.

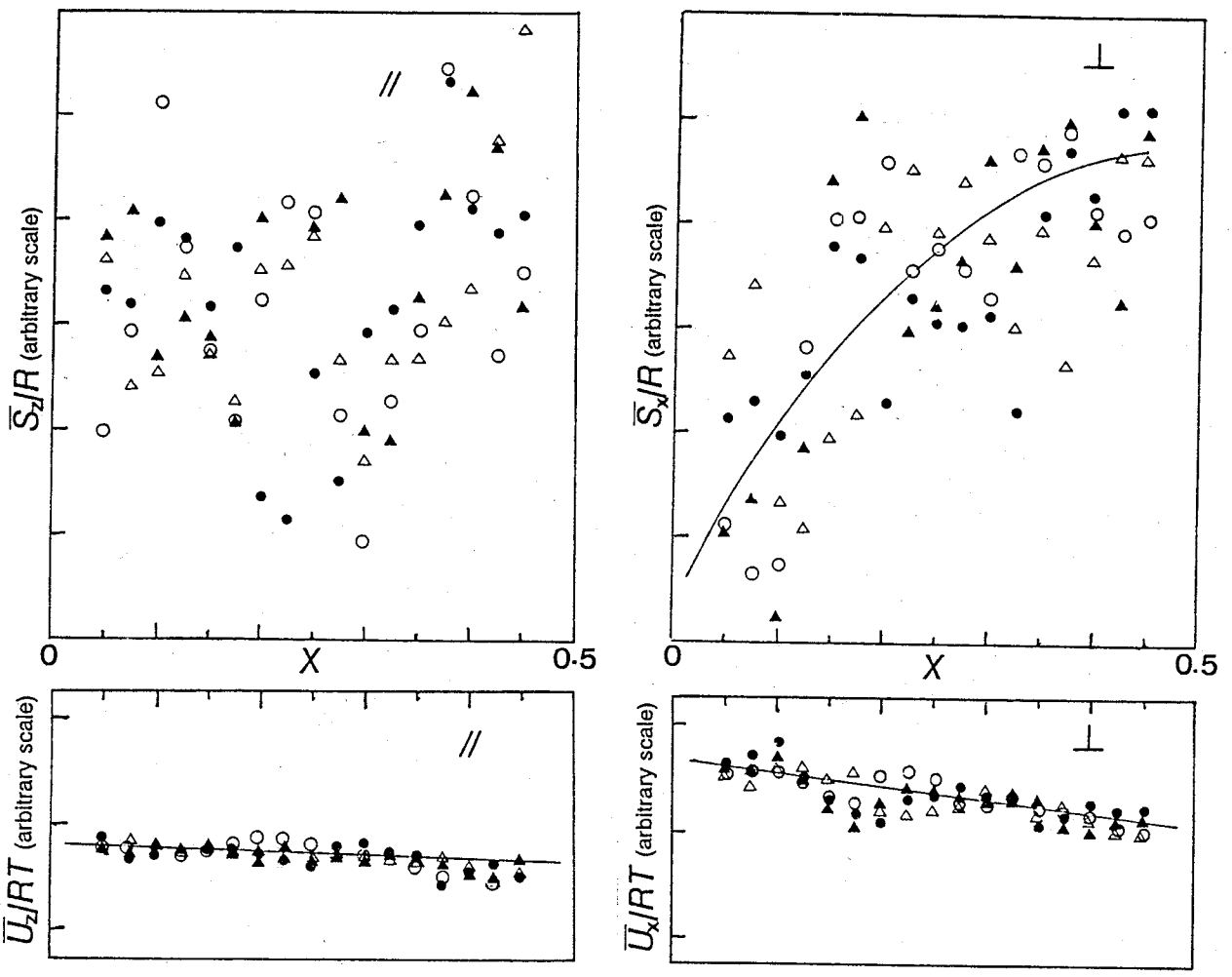

Fig.4.9d Calculated partial molar entropy (top) and partial molar internal energy function (bottom) at various x based on the **s** // Z lattice (left) and **s** ⊥ Z one (right) of the Model B'. Meaning of marks are same in Fig.4.8d.

References to Chapter 4

1. a) L.M.Atras, *J.Phys.Chem.Solids*, 29, 91 (1968).
   b) L.M.Atras, *ibid*, 29, 1349 (1968).
2. a) "*Hydrogen in Metals*", Vol.I and II, eds. G.Alefeld and J.Volkl, Springer-Verlag, Berlin, Heidelberg, New York (1978).,
   b) V.G.Vaks and V.G.Orlov, *J.Phys.F:Met.Phys.*, 18, 883(1988).
3. a) O.J.Kleppa, P.Denter and M.E.Melnichak, *J.Chem.Phys.*, 61, 4048 (1974). b) T.Kuji and W.A.Oates, *J.Less-Common.Met.*, 162, 251 (1984).
4. a) H.Inaba, A.Navrotsky and L.Eyring, *J.Solid-State Chem.*, 37, 67 (1981). b)I.A.Vasil'eva and I.S.Sukhushina, *J.Chem.Thermodyn.*, 7, 5 (1975).
5. P.Dean, *Rev.Modern Phys.*, 44, 127 (1972).
6. P.Dean and J.L.Martin, *Proc.Roy.Soc.*, 63, 471 (1960).
7. A.E.Martell and M.Calvin, "*Chemistry of the Metal Chelate Compounds*", Prentice Hall, New York, (1952), Chap.7.
8. S.Brucker, M.Calligaris, G.Nargin and L.Randaccio, *Acta Cryst.*, B25, 1671 (1969).
9. R.Deiasi, S.L.Holt, B.Post, *Inorg.Chem.*, 10 1498 (1971).
10. W.P.Schaefer and R.E.Marsh, *Acta Cryst.*, B25, 1675 (1969).
11. B.C.Wang and W.P.Schaefer, *Science*, 166, 1404 (1969).
12. D.N.Payton and W.M.Visscher, *Phys.Rev.*, 154, 802 (1967).
13. P.Dean and M.D.Bacon, *Proc.Roy.Soc.*, A283, 64 (1965).
14. A.I.Kitaigorodosky, "*Molecular Crystals and Molecules*", Academic Press, New York and London, (1973).

Chapter 5 Physico-chemical Studies on [Co(3-RO-SALEN)] (R=CH_3, C_2H_5) – O_2 Systems

5.1 Introduction

In 1946, Calvin *et al.*[1] reported that the [Co(3-RO-SALEN)]-O_2 systems (R=CH_3 or C_2H_5, Fig.5.1) gave isotherms without a two-phase region different from that of the [Co(SALEN)]-O_2 system. The isotherms suggest that the systems consist of a single nonstoichiometric phase, although they attributed them to insufficient attainment of equilibrium. They also reported that van't Hoff plots over different temperature ranges for the [Co(3-EtO-SALEN)]-O_2 system gave different partial molar enthalpies. Unfortunately, nature of such behavior of the nonstoichiometric phases has not been studied in detail since then.

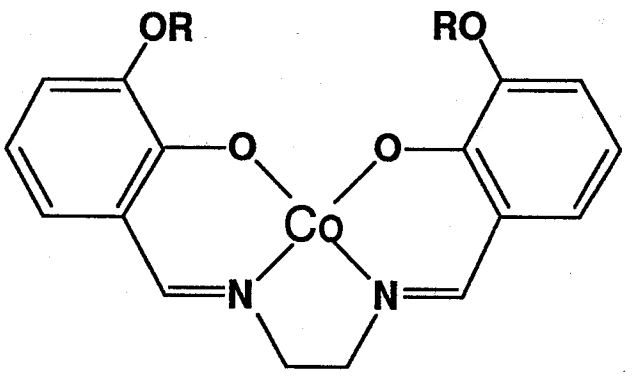

Fig.5.1 [Co(3-RO-SALEN)]

Gas-solid reaction calorimetry is a useful technique for the systems which show unusual temperature and composition dependence of thermodynamic values, because the technique enables us to obtain partial molar enthalpy and entropy at a given temperature without difficulties in pressure measurement in nonstoichiometric phase, such as drift of compoition during the measurement. In

this chapter, gas-solid reaction calorimetry was applied to [Co(3-RO-SALEN)]-dioxygen (O_2) system (R=CH_3 or C_2H_5) and their thermodynamic properties were discussed together with results from magnetic, spectroscopic, and powder X-ray diffraction measurement.

In the preliminaly experiment for the [Co(3-EtO-SALEN)]-O_2 system, shift in pressure and partial molar enthalpy was observed in every cycle when oxygenation-deoxygenation cycles were repeated without annealing after deoxygenation prior to every oxygenation run, and the partial molar enthalpy converged into the value much more negative than the original value. After storing fresh [Co(3-EtO-SALEN)] for about 1 year in the oxygenated form, equilibrium pressure and partial molar enthalpy for the sample also agreed with the converged values in the preliminary experiment. The [Co(3-MeO-SALEN)]-O_2 system for the sample stored for about 1 year in the oxygenated form also showed thermodynamic quantities quite different from those for the fresh sample. On the other hand, thermodynamic quantities for the systems of the fresh samples were reproducible when the samples were annealed for 24 hours at 373 K *in vacuo* after deoxygenation prior to every oxygenation run. However, the stored samples never showed thermodynamic properties of the fresh ones, even if they were annealed. Since the samples stored in the oxygenated form were found to be thermodynamically different from the fresh samples, experiments were conducted for both samples of each complex. In the following sections, [Co(3-RO-SALEN)] (R=CH_3 or C_2H_5) is abbreviated to "ME" for R=CH_3 and "ET" for R=C_2H_5, the "ME" and "ET" samples stored in their oxygenated forms are written as "MM" and "EM", respectively.

5.2 Experimental Results

5.2.1 Gas-Solid Reaction Calorimetry on the Systems; O_2 and Two Types of [Co(3-MeO-SALEN)] (ME and MM) and [Co(3-EtO-SALEN)] (ET and EM)

Thermodynamic measurements on the systems were carried out for absorption run at 274.75 K and 293.15 K for the ME-O_2 and MM-O_2 systems, and at 293.15 K and 323.15 K for both ET-O_2 and EM-O_2. For the ME-O_2 and ET-O_2 systems, the fresh samples prepared from [Co(3-RO-SALEN)]H_2O (R = CH_3, C_2H_5) were used, and they were annealed for 24 hours at 373K *in vacuo* after deoxygenation prior to every oxygenation run.

After every dose of dioxygen gas, the output voltage of calorimeter returned to the initial voltage within 5 hours, and it took about 1 day to find the equilibrium pressure by the method described in chapter 2. The experimental results are summarized in Table 5.1 and 5.2, where definition of dioxygen content, x_e and x_m, and the evaluation method of partial molar thermodynamic functions are identical with those in chapter 3. The equilibrium pressures, partial molar enthalpies and entropies of the systems are shown in Fig.5.2, Fig.5.3 and Fig.5.4, respectively.

All of the isotherms in Fig.5.2 show monotonous increase with increase in dioxygen content (x), which indicates that all the systems in this chapter consist of a single nonstoichiometric phase. Shape of isotherms of the ME-O_2 and ET-O_2 systems was similar to those reported by Calvin *et al.*[1]. Isotherms of the MM-O_2 and EM-O_2 systems were appreciably different from those of the

ME-O_2 and ET-O_2 systems. For the samples stored under their oxygenated form for 1 year, equilibrium pressure was higher in the MM-O_2 system than that of ME-O_2, while it was lower in the ET-O_2 system than that of the EM-O_2 system. In addition, oxygenation measurement was not possible beyond about x=0.25 (MM-O_2) and x=0.4 (EM-O_2) due to slowing down in the reaction rate, though isotherms seemed to be extended toward higher composition.

It is noticeable that the ME-O_2 and EM-O_2 systems exhibit considerable composition and temperature dependences of partial molar enthalpy and entropy as shown in Fig.5.3 and 5.4, which span about 20 $kJmol^{-1}$ for enthalpy and about 60 $JK^{-1}mol^{-1}$ for entropy. Although the ET-O_2 and MM-O_2 systems did not show such dependences in partial molar quantities, the values were quite different from those of the ME-O_2 and EM-O_2 systems.

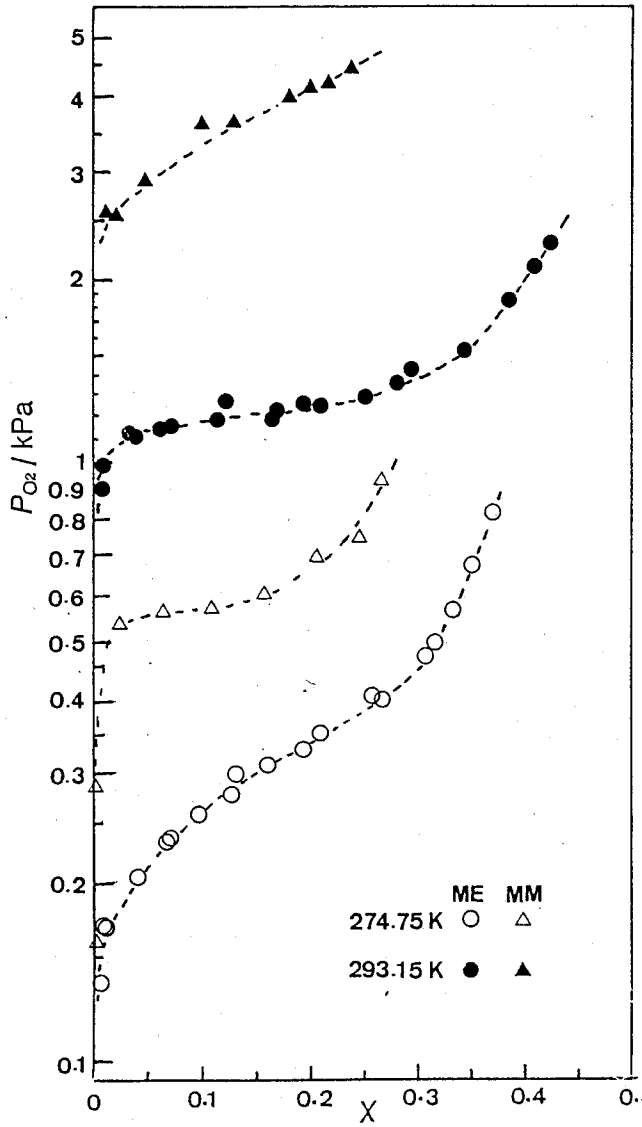

Fig.5.2a Isotherms of the ME-O_2(circle) and MM-O_2(triangle) systems at 274.75K(open marks) and 293.15K(filled maks)

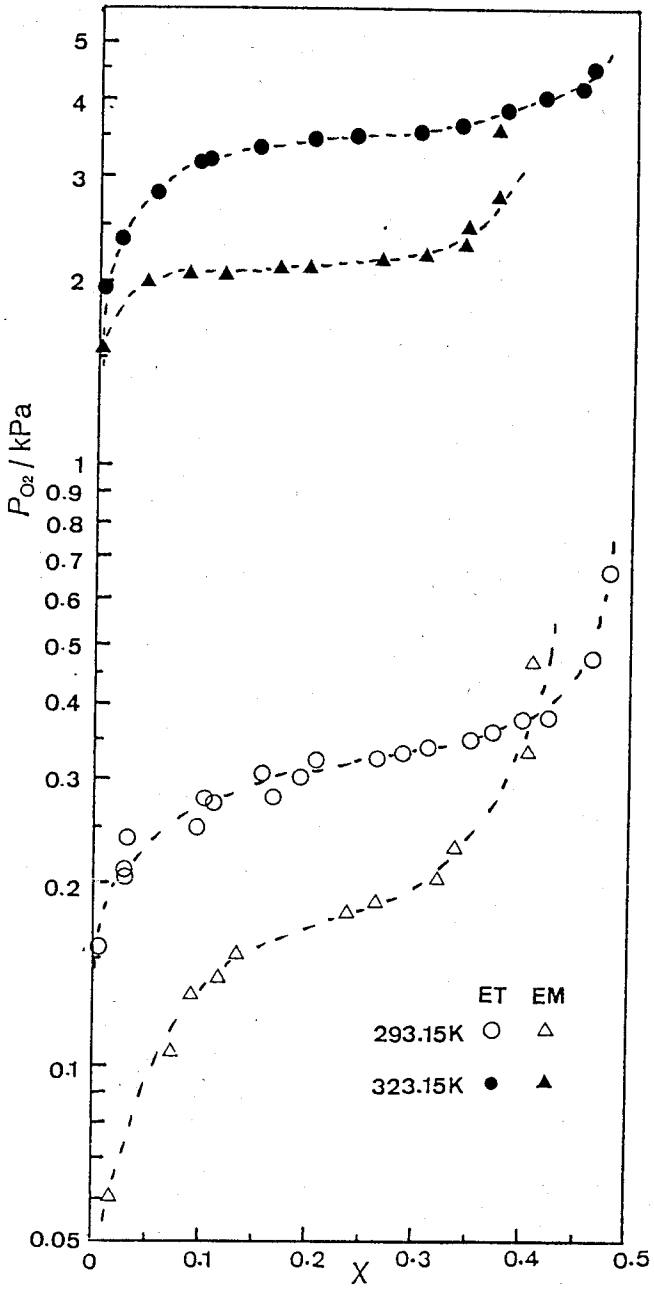

Fig.5.2b Isotherms of the ET-O_2(circle) and EM-O_2(triangle) systems at 293.15K(open marks) and 323.15K(filled marks)

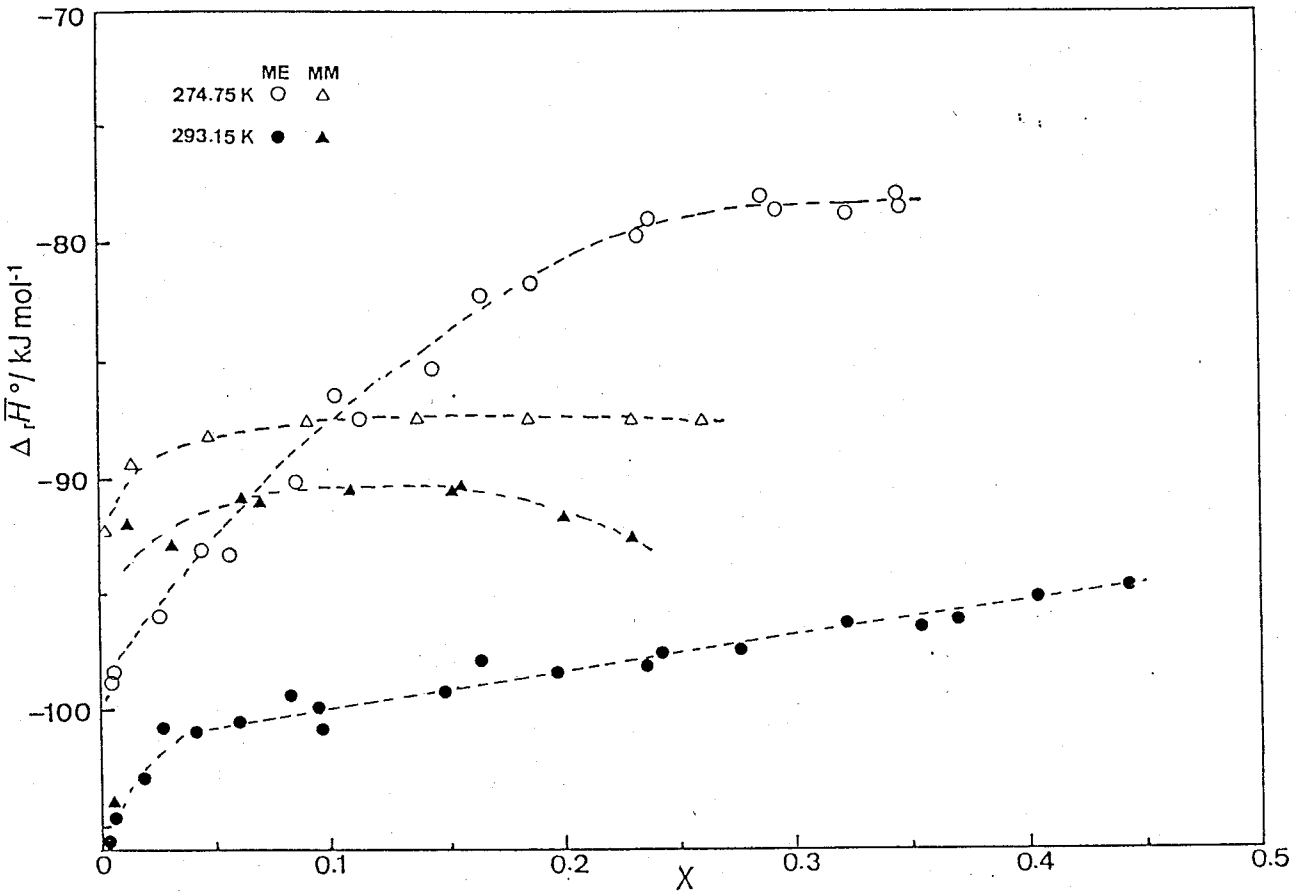

Fig.5.3a Partial molar enthalpies of the ME-O_2(circle) and MM-O_2(triangle) systems at 274.75K(open marks) and 293.15K(filled marks). Broken curves are drawn for the eye.

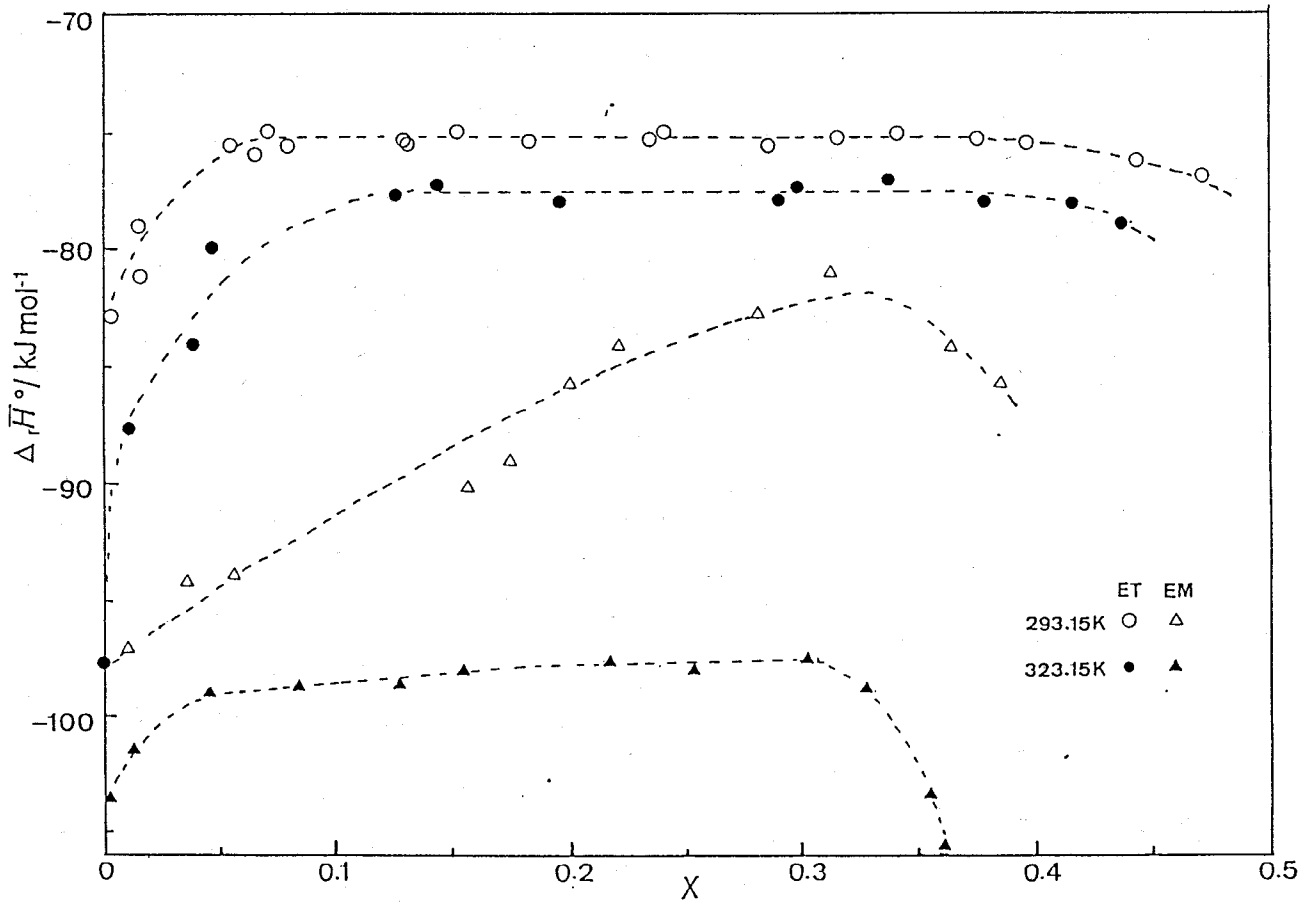

Fig.5.3b Partial molar enthalpies of the ET-O_2(circle) and EM-O_2(triangle) systems at 293.15K(open marks) and 323.15K(filled marks). Broken curves are drawn for the eye.

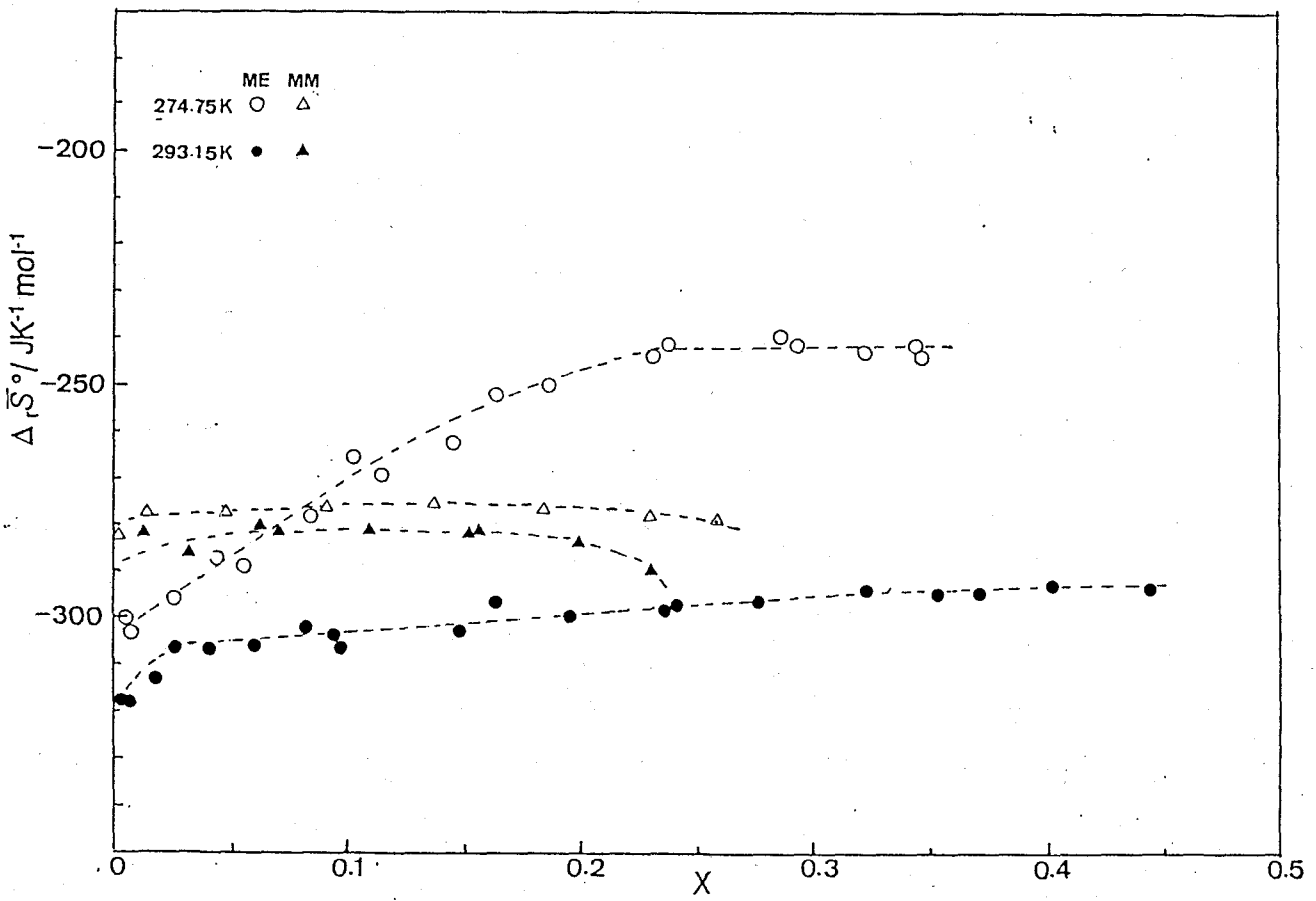

Fig.5.4a Partial molar entropies of the ME-O_2(circle) and MM-O_2(triangle) systems at 274.75K(open marks) and 293.15K(filled marks). Broken curves are drawn for the eye.

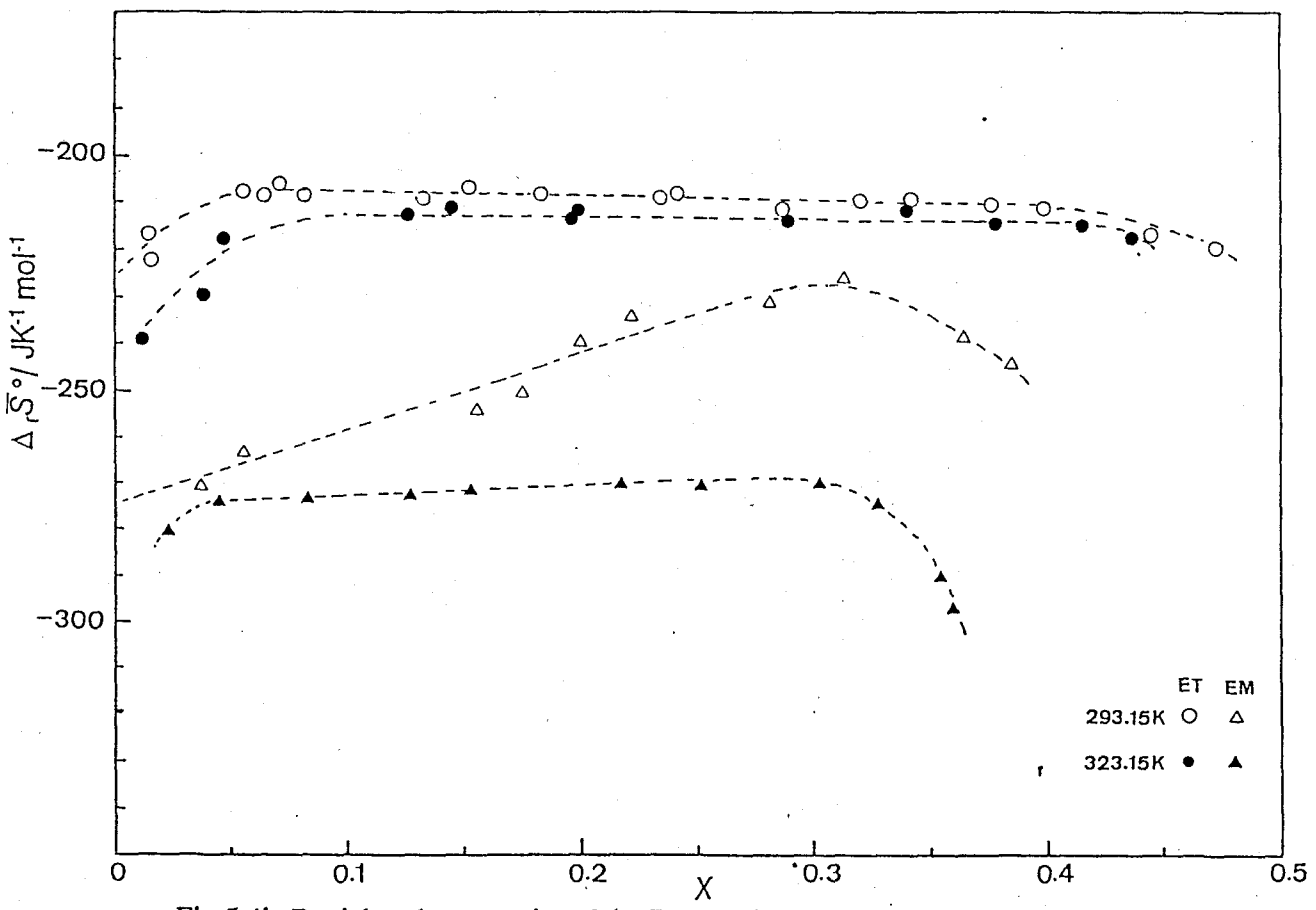

Fig.5.4b Partial molar entropies of the ET-O_2(circle) and EM-O_2(triangle) systems at 293.15K(open marks) and 323.15K(filled marks). Broken curves are drawn for the eye.

Table 5.1a Equilibrium pressure P_{eq}, partial molar Gibbs energy $\Delta_r \overline{G}^\circ$ and excess partial molar Gibbs energy $\Delta_r \overline{G}^E$ at dioxygen content x_e of the ME-O_2 system.

No.	x_e	P_{eq} / kPa	$\Delta_r \overline{G}^\circ$ / kJmol^{-1}	$\Delta_r \overline{G}^E$ / kJmol^{-1}
Series 1 at 274.75K				
1	0.01312	0.162	-14.674	-4.865
2	0.07191	0.236	-13.819	-8.345
3	0.13021	0.300	-13.272	-9.675
4	0.19306	0.332	-13.038	-11.020
5	0.26595	0.401	-12.606	-12.342
6	0.31654	0.501	-12.099	-13.183
7	0.37072	0.823	-10.964	-13.819
Series 2 at 274.75K				
1	0.00726	0.137	-15.062	-3.861
2	0.03929	0.204	-14.156	-7.044
3	0.06960	0.232	-13.857	-8.289
4	0.09742	0.260	-13.601	-9.037
5	0.12660	0.276	-13.462	-9.765
6	0.15973	0.311	-13.185	-10.356
7	0.20800	0.354	-12.892	-11.230
8	0.26072	0.405	-12.588	-12.194
9	0.30600	0.472	-12.234	-13.020
10	0.33453	0.559	-11.851	-13.472
11	0.35200	0.669	-11.437	-13.623
Series 3 at 293.15K				
1	0.03297	1.116	-10.957	-2.891
2	0.12092	1.241	-10.697	-6.583
3	0.19531	1.246	-10.688	-8.592
4	0.28171	1.344	-10.504	-10.650
5	0.42470	2.315	-9.179	-14.972
6	0.46019	3.271	-8.336	-17.277
Series 4 at 293.15K				
1	0.00613	0.901	-11.479	0.893
2	0.03945	1.102	-10.988	-3.411
3	0.07395	1.153	-10.878	-5.123
4	0.11286	1.175	-10.831	-6.469
5	0.17442	1.214	-10.752	-8.120
6	0.21027	1.226	-10.728	-9.012
7	0.25088	1.276	-10.631	-9.953
8	0.29300	1.413	-10.383	-10.845
9	0.34327	1.511	-10.218	-12.242
10	0.38656	1.839	-9.740	-13.463
11	0.40957	2.096	-9.421	-14.297
Series 5 at 293.15K				
1	0.01047	0.989	-11.251	-0.217
2	0.06401	1.144	-10.898	-4.705
3	0.16711	1.189	-10.803	-7.980

Table 5.1a' Partial molar enthalpy, entropy, Gibbs energy and excess partial molar entropy of the ME-O_2 system at mean dioxygen content x_m for each reaction.

No.	x_m	$\Delta_r \overline{H}^\circ$ / kJmol^{-1}	$\Delta_r \overline{G}^\circ$ / kJmol^{-1}	$\Delta_r \overline{S}^\circ$ / JK^{-1}mol^{-1}	$\Delta_r \overline{S}^E$ / JK^{-1}mol^{-1}
Series 1 at 274.75K					
1	0.00735	-98.53	-15.056	-303.8	-344.5
2	0.04381	-93.17	-14.111	-287.7	-312.6
3	0.10301	-86.44	-13.574	-265.2	-281.2
4	0.16385	-82.34	-13.167	-251.8	-261.7
5	0.23182	-78.65	-12.755	-243.5	-247.5
6	0.29309	-78.65	-12.354	-241.3	-239.7
7	0.34501	-77.96	-11.603	-241.5	-234.4
Series 2 at 274.75K					
1	0.00455	-98.76	-16.132	-300.7	-345.5
2	0.02546	-95.96	-14.430	-296.8	-326.6
3	0.05613	-93.31	-13.990	-288.7	-311.2
4	0.08480	-90.28	-13.709	-278.7	-296.8
5	0.11393	-87.53	-13.522	-269.4	-284.1
6	0.14547	-85.31	-13.227	-262.4	-274.0
7	0.18673	-81.73	-13.066	-249.9	-257.8
8	0.23748	-79.02	-12.722	-241.3	-244.8
9	0.28679	-78.06	-12.413	-238.9	-238.0
10	0.32322	-78.75	-12.007	-242.9	-238.3
11	0.34602	-78.57	-11.579	-243.8	-236.6
Series 3 at 293.15K					
1	0.01821	-102.9	-11.145	-313.0	-345.8
2	0.08165	-99.40	-10.869	-302.0	-320.6
3	0.16350	-97.85	-10.795	-297.0	-306.9
4	0.24189	-97.65	-10.653	-296.8	-299.9
5	0.35355	-96.48	-10.105	-294.6	-286.5
6	0.443556	-94.64	-8.731	-293.1	-268.4
Series 4 at 293.15K					
1	0.00378	-105.7	-12.658	-317.4	-363.7
2	0.02567	-100.8	-11.042	-306.3	-336.0
3	0.05979	-100.6	-10.914	-306.0	-323.4
4	0.09660	-100.7	-10.851	-306.7	-323.4
5	0.14869	-99.27	-10.761	-302.0	-313.3
6	0.19614	-98.53	-10.690	-299.7	-306.7
7	0.23484	-98.13	-10.669	-298.3	-302.1
8	0.27349	-97.41	-10.526	-296.4	-296.4
9	0.32286	-96.29	-10.285	-293.4	-288.8
10	0.36968	-96.19	-9.926	-294.3	-294.0
11	0.40436	-95.12	-9.456	-292.2	-276.6
Series 5 at 293.15K					
1	0.00603	-104.7	-11.521	-317.9	-360.2
2	0.04061	-100.9	-10.984	-306.7	-332.3
3	0.09380	-99.87	-10.854	-303.7	-320.7

Table 5.1b Equilibrium pressure P_{eq}, partial molar Gibbs energy $\Delta_r \overline{G}^\circ$ and excess partial molar Gibbs energy $\Delta_r \overline{G}^E$ at dioxygen content x_e of the MM-O_2 system.

No.	x_e	P_{eq} / kPa	$\Delta_r \overline{G}^\circ$ / kJmol^{-1}	$\Delta_r \overline{G}^E$ / kJmol^{-1}
Series 1 at 274.75K				
1	0.00189	0.160	-14.713	-0.395
2	0.02350	0.534	-11.954	-3.551
3	0.06522	0.562	-11.835	-6.083
4	0.11171	0.566	-11.821	-8.830
5	0.15859	0.600	-11.688	-8.830
6	0.20494	0.688	-11.374	-9.639
7	0.24590	0.729	-11.241	-10.484
8	0.26461	0.929	-10.689	-10.392
Series 2 at 293.15K				
1	0.00141	0.287	-14.264	1.733
2	0.02068	2.568	-8.926	0.373
3	0.10005	3.430	-8.110	-3.330
4	0.20056	4.131	-7.767	-5.805
Series 3 at 293.15K				
1	0.00983	2.581	-8.913	2.280
2	0.04891	2.943	-8.593	-1.617
3	0.08707	3.366	-8.266	-3.027
4	0.12778	3.638	-8.077	-4.168
5	0.17987	3.989	-7.852	-5.361
6	0.21421	4.192	-7.731	-6.115
7	0.23662	4.440	-7.591	-6.545

Table 5.1b' Partial molar enthalpy, entropy, Gibbs energy and excess partial molar entropy of the MM-O_2 system at mean dioxygen content x_m for each reaction.

No.	x_m	$\Delta_r \overline{H}^\circ$ / kJmol^{-1}	$\Delta_r \overline{G}^\circ$ / kJmol^{-1}	$\Delta_r \overline{S}^\circ$ / JK^{-1}mol^{-1}	$\Delta_r \overline{S}^E$ / JK^{-1}mol^{-1}
Series 1 at 274.75K					
1	0.00163	-92.33	-14.746	-282.4	-335.7
2	0.01446	-89.40	-13.108	-277.7	-312.5
3	0.04697	-88.14	-11.887	-277.5	-301.7
4	0.09094	-87.59	-11.827	-275.8	-293.2
5	0.13798	-87.34	-11.746	-275.1	-287.5
6	0.18422	-87.49	-11.514	-276.5	-284.6
7	0.22963	-87.50	-11.294	-277.4	-281.6
8	0.25912	-87.44	-10.851	-278.8	-280.4
Series 2 at 293.15K					
1	0.00355	-54.39	---	---	---
2	0.01189	-92.10	-8.916	-283.8	-320.3
3	0.06143	-90.86	-8.475	-281.0	-302.6
4	0.15170	-90.59	-7.974	-281.8	-292.9
Series 3 at 293.15K					
1	0.00533	-104.2	-11.397	-316.6	-360.0
2	0.03093	-92.87	-8.805	-286.8	-314.9
3	0.06951	-91.03	-8.399	-281.9	-302.2
4	0.10922	-90.52	-8.099	-281.2	-296.4
5	0.15677	-90.35	-7.952	-281.1	-291.7
6	0.19911	-91.81	-7.773	-286.7	-293.5
7	0.22953	-92.57	-7.636	-289.7	-293.9

Table 5.2a Equilibrium pressure P_{eq}, partial molar Gibbs energy $\Delta_r \overline{G}^\circ$ and excess partial molar Gibbs energy $\Delta_r \overline{G}^E$ at dioxygen content x_e of the ET-O_2 system.

No.	x_e	P_{eq} / kPa	$\Delta_r \overline{G}^\circ$ / kJmol^{-1}	$\Delta_r \overline{G}^E$ / kJmol^{-1}
Series 1 at 293.15K				
1	0.00422	0.156	-15.753	-2.459
2	0.03081	0.238	-14.728	-6.480
3	0.10514	0.273	-14.390	-9.780
4	0.15665	0.306	-14.108	-11.007
5	0.20904	0.319	-14.007	-12.260
6	0.26427	0.323	-13.982	-13.656
7	0.31114	0.339	-13.864	-14.856
8	0.37072	0.357	-13.735	-16.781
9	0.42380	0.380	-13.586	-19.320
10	0.46428	0.477	-13.030	-22.563
11	0.48067	0.664	-12.224	-24.670
Series 2 at 293.15K				
1	0.02804	0.212	-15.001	-6.502
2	0.11272	0.269	-14.426	-10.059
3	0.19156	0.302	-14.144	-11.953
4	0.28843	0.331	-13.919	-14.252
5	0.34946	0.345	-13.816	-16.057
6	0.40132	0.369	-13.656	-18.091
Series 3 at 293.15K				
1	0.03079	0.203	-15.106	-6.856
2	0.09741	0.248	-14.628	-9.758
3	0.16774	0.277	-14.357	-11.550
Series 4 at 323.15K				
1	0.00415	1.968	-10.555	4.148
2	0.09072	3.154	-9.287	-3.659
3	0.19858	3.467	-9.033	-6.814
4	0.29756	3.646	-8.998	-9.651
5	0.38104	3.820	-8.772	-12.606
6	0.44970	4.140	-8.556	-17.145
Series 5 at 323.15K				
1	0.02222	2.369	-10.056	-0.012
2	0.05342	2.807	-9.600	-2.188
3	0.09992	3.169	-9.274	-4.000
4	0.15124	3.351	-9.125	-5.545
5	0.24002	3.487	-9.017	-7.960
6	0.33963	3.635	-8.905	-10.999
7	0.41609	4.001	-8.648	-14.438
8	0.45679	4.443	-8.366	-17.779

Table 5.2a' Partial molar enthalpy, entropy, Gibbs energy and excess partial molar entropy of the ET-O_2 system at mean dioxygen content x_m for each reaction.

No.	x_m	$\Delta_r \overline{H}^\circ$ / kJmol^{-1}	$\Delta_r \overline{G}^\circ$ / kJmol^{-1}	$\Delta_r \overline{S}^\circ$ / JK^{-1}mol^{-1}	$\Delta_r \overline{S}^E$ / JK^{-1}mol^{-1}
Series 1 at 293.15K					
1	0.00236	-82.97	---	---	---
2	0.05561	-75.49	-14.691	-207.4	-230.0
3	0.08148	-75.57	-14.652	-207.8	-226.4
4	0.13157	-75.34	-14.290	-208.3	-221.2
5	0.18367	-75.39	-14.216	-208.7	-216.8
6	0.23442	-75.34	-13.996	-209.2	-213.0
7	0.28590	-75.61	-13.926	-210.4	-209.5
8	0.34168	-75.11	-13.826	-209.1	-202.3
9	0.39767	-75.59	-13.632	-211.4	-196.9
10	0.44435	-76.25	-13.504	-216.5	-191.6
11	0.47266	-76.25	-12.618	-219.5	-182.7
Series 2 at 293.15K					
1	0.01486	-79.04	-15.472	-216.8	-251.5
2	0.07138	-75.10	-14.667	-206.2	-226.2
3	0.15269	-74.97	-14.137	-207.5	-218.4
4	0.24080	-75.07	-13.993	-208.3	-211.5
5	0.31959	-75.30	-13.853	-209.6	-205.3
6	0.37610	-75.31	-13.741	-210.0	-198.9
Series 3 at 293.15K					
1	0.01622	-80.64	-15.374	-222.6	-256.5
2	0.06471	-75.85	-14.677	-202.7	-223.7
3	0.13326	-75.55	-14.277	-209.0	-221.8
Series 4 at 323.15K					
1	0.00224	-103.5	---	---	---
2	0.04752	-79.96	-9.686	-217.5	-241.5
3	0.14453	-77.30	-9.145	-210.9	-222.6
4	0.29880	-77.36	-8.995	-211.5	-209.4
5	0.33952	-77.13	-8.905	-211.1	-204.7
6	0.41556	-78.10	--8.650	-214.9	-197.6
Series 5 at 323.15K					
1	0.01121	-87.71	-10.360	-239.4	-276.4
2	0.03795	-84.08	-9.826	-229.8	-256.0
3	0.07138	-79.75	-9.449	-217.5	-237.5
4	0.12581	-77.82	-9.199	-212.4	-225.9
5	0.19577	-78.03	-9.039	-213.5	-220.6
6	0.28982	-77.96	-9.001	-213.4	-212.1
7	0.37804	-78.05	-8.782	-214.4	-202.9
8	0.43654	-79.08	-8.702	-217.8	-195.1

Table 5.2b Equilibrium pressure P_{eq}, partial molar Gibbs energy $\Delta_r \overline{G}^\circ$ and excess partial molar Gibbs energy $\Delta_r \overline{G}^E$ at dioxygen content xe of the EM-O_2 system.

No.	x_e	P_{eq} / kPa	$\Delta_r \overline{G}^\circ$ / kJmol^{-1}	$\Delta_r \overline{G}^E$ / kJmol^{-1}
Series 1 at 293.15K				
1	0.07286	0.106	-16.694	-10.898
2	0.11619	0.139	-16.031	-11.773
3	0.23777	0.170	-15.543	-14.526
4	0.32139	0.203	-15.113	-16.419
5	0.40553	0.329	-13.933	-18.588
Series 2 at 293.15K				
1	0.01731	0.0899	-17.096	-7.338
2	0.09123	0.131	-16.177	-11.090
3	0.13456	0.152	-15.821	-12.108
4	0.26552	0.187	-15.310	-15.017
5	0.33943	0.228	-14.830	-16.723
6	0.40949	0.468	-13.077	-17.948
Series 3 at 323.15K				
1	0.00388	1.564	-11.172	3.713
2	0.08382	2.064	-10.426	-4.516
3	0.16860	2.104	-10.375	-7.306
4	0.26297	2.161	-10.303	-9.905
5	0.34005	2.317	-10.116	-12.226
6	0.37031	2.761	-9.644	-12.984
Series 4 at 293.15K				
1	0.04521	2.014	-10.492	-2.557
2	0.11648	2.054	-10.439	-5.755
3	0.19685	2.112	-10.364	-8.097
4	0.30571	2.232	-10.216	-11.131
5	0.34582	2.451	-9.964	-12.293
6	0.37190	3.572	-8.952	-12.363

Table 5.2b' Partial molar enthalpy, entropy, Gibbs energy and excess partial molar entropy of the EM-O_2 system at mean dioxygen content x_m for each reaction.

No.	x_m	$\Delta_r \overline{H}^\circ$ / kJmol^{-1}	$\Delta_r \overline{G}^\circ$ / kJmol^{-1}	$\Delta_r \overline{S}^\circ$ / JK^{-1}mol^{-1}	$\Delta_r \overline{S}^E$ / JK^{-1}mol^{-1}
Series 1 at 293.15K					
1	0.03767	-96.24	-16.949	-270.5	-296.8
2	0.15614	-90.20	-15.763	-253.9	-264.5
3	0.19878	-85.81	-15.648	-239.3	-246.2
4	0.28168	-82.94	-15.133	-231.3	-230.8
5	0.36465	-84.33	-14.488	-238.2	-228.6
Series 2 at 293.15K					
1	0.01954	-97.07	---	---	---
2	0.05599	-93.97	-16.817	-263.2	-285.7
3	0.17462	-89.15	-15.713	-250.5	-259.5
4	0.22120	-84.23	-15.588	-234.1	-239.5
5	0.31373	-81.12	-14.932	-225.8	-222.1
6	0.38505	-85.89	-14.210	-244.5	-232.0
Series 3 at 323.15K					
1	0.00583	-122.4	---	---	---
2	0.04527	-99.02	-10.492	-270.0	-298.5
3	0.12684	-98.63	-10.426	-272.9	-286.4
4	0.21662	-97.64	-10.346	-270.2	-275.5
5	0.30235	-97.56	-10.223	-270.3	-267.8
6	0.35545	-103.59	-9.838	-290.1	-281.7
Series 4 at 323.15K					
1	0.02317	-101.6	-10.855	-280.7	-311.4
2	0.08324	-98.77	-10.427	-273.4	-291.7
3	0.15398	-98.09	-10.393	-271.4	-282.2
4	0.25238	-97.911	-10.313	-271.1	-273.3
5	0.32790	-98.98	-10.151	-274.9	-269.7
6	0.35959	-105.8	-9.784	-297.1	-288.2

5.2.2 X-ray Diffraction

Powder X-ray diffraction patterns of the ME-O_2 and MM-O_2 systems were recorded at 293 K, those of the ET-O_2 and EM-O_2 systems were at 293 K and 321 K. The samples with nonstoichiometric compositions were prepared at 293K by use of the preparative gas-titration system described in chapter 2. Those and unoxygenated samples were mixed with silicon powder as reference, and charged in the sample holder.

Recorded diffraction patterns are shown in Fig.5.5 and Fig.5.6. For all nonstoichiometric systems, samples with different dioxygen contents indicated similar patterns. This is consistent with their isotherms which showed that those systems consist of a single nonstoichiometric phase. Diffractions for the EM-O_2 system became appreciably broaden with increasing temperature from 293 K to 323 K, although similar shape of diffraction peaks were observed for the EM-O_2 system at 293K, and for the ET-O2 system at both 293 K and 323 K. The patterns for the MM-O_2 system at 293 K were also very broad except for a few strong diffractions.

All patterns were indexed as an orthorhombic system. The lattice parameters for the sample with x=0.31 in the MM-O_2 system were tentatively determined because of the limited number of diffractions and the serious broadness of peaks. Broadness of the peaks for the MM-O_2 system at 293 K and the EM-O_2 system at 321 K would also suffer from large uncertainty owing to broadness of peaks. The parameters are summarized in Table.5.3, and the variations in the cell volume are shown in Fig.5.7 and 5.8. The cell volumes at x=0 at 293K of the MM-O_2 and EM-O_2 system were 2.7% and 1.3% larger than those of the ME-O_2 and ET-O_2,

respectively. The cell volume at x=0 at 321 K of the EM-O_2 system was 10% larger than that at 293 K, while that of the ET-O_2 system at 321 K was 1.4% larger than that at 293 K. The changes in the cell volumes were less than 2% except the sample of the MM-O_2 system at x=0.31.

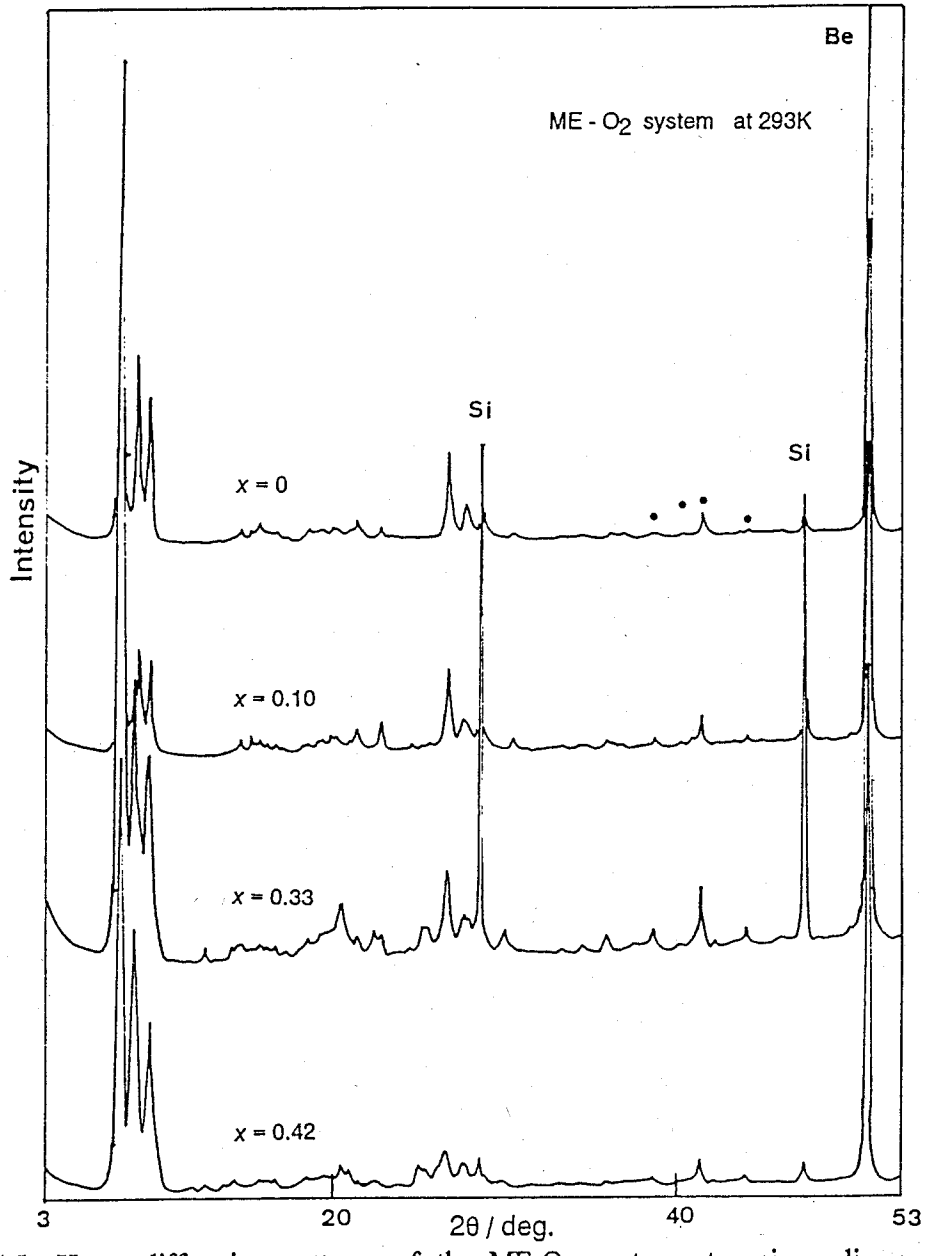

Fig.5.5a X-ray diffraction patterns of the ME-O_2 system at various dioxygen contents at 293K. Filled circles indicate diffractions from the sample holder.

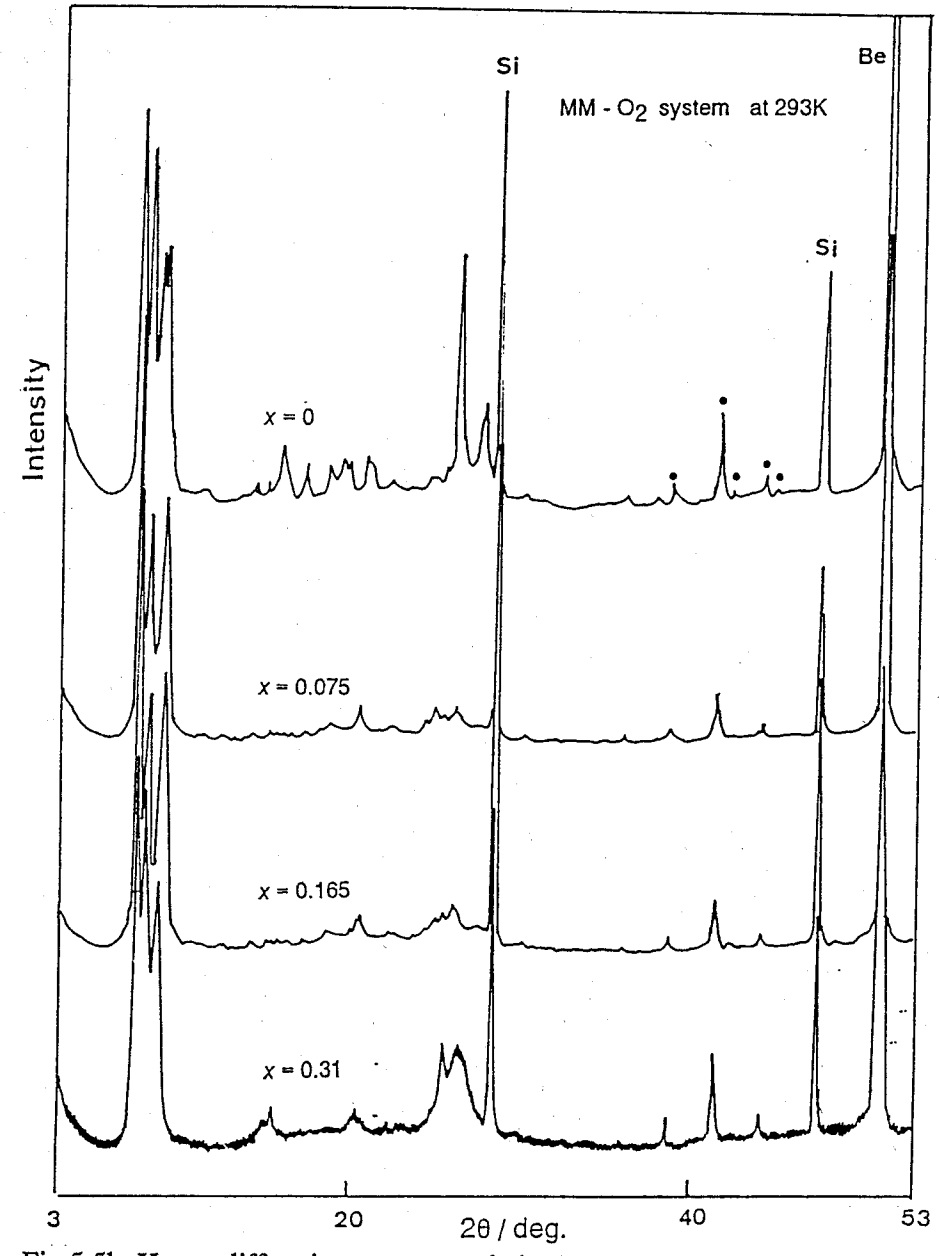

Fig.5.5b X-ray diffraction patterns of the MM-O_2 system at various dioxygen contents at 293K. Filled circles indicate diffractions from the sample holder.

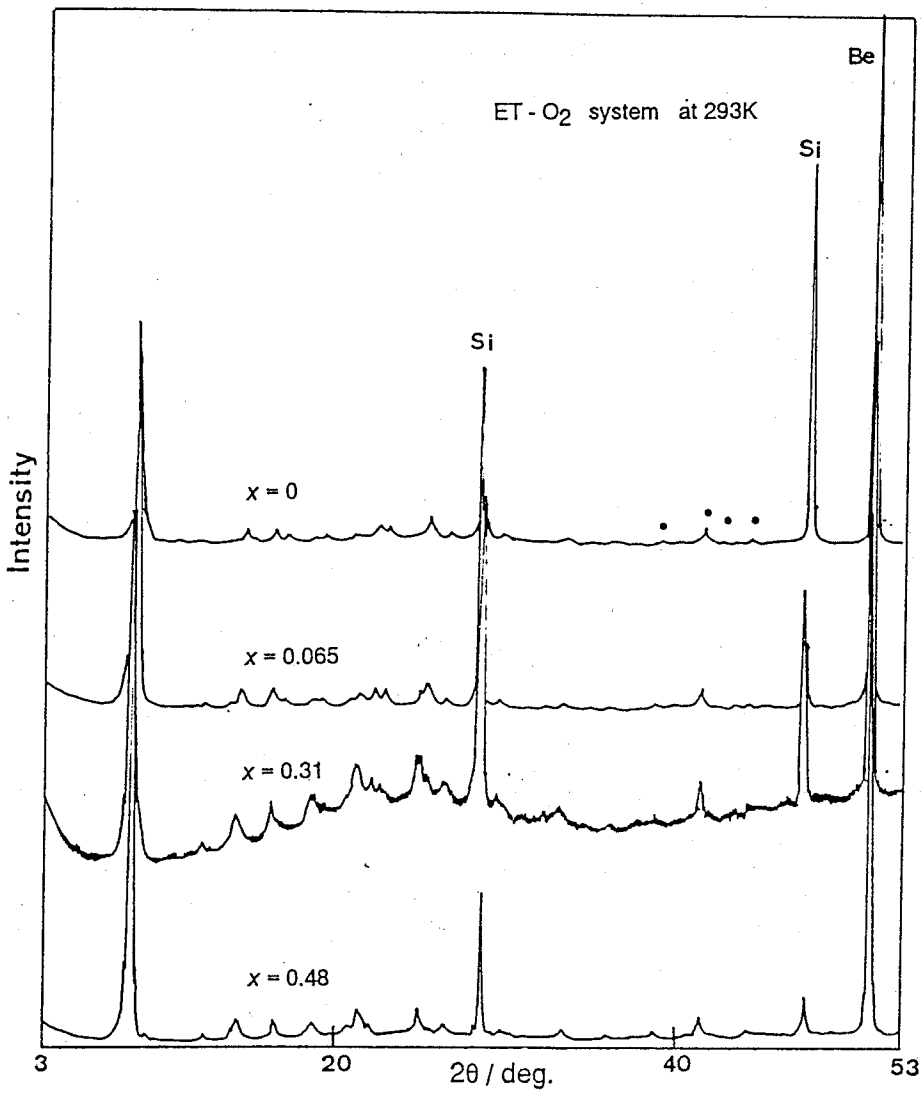

Fig.5.6a X-ray diffraction patterns of the ET-O_2 system at various dioxygen contents at 293K. Filled circles indicate diffractions from the sample holder.

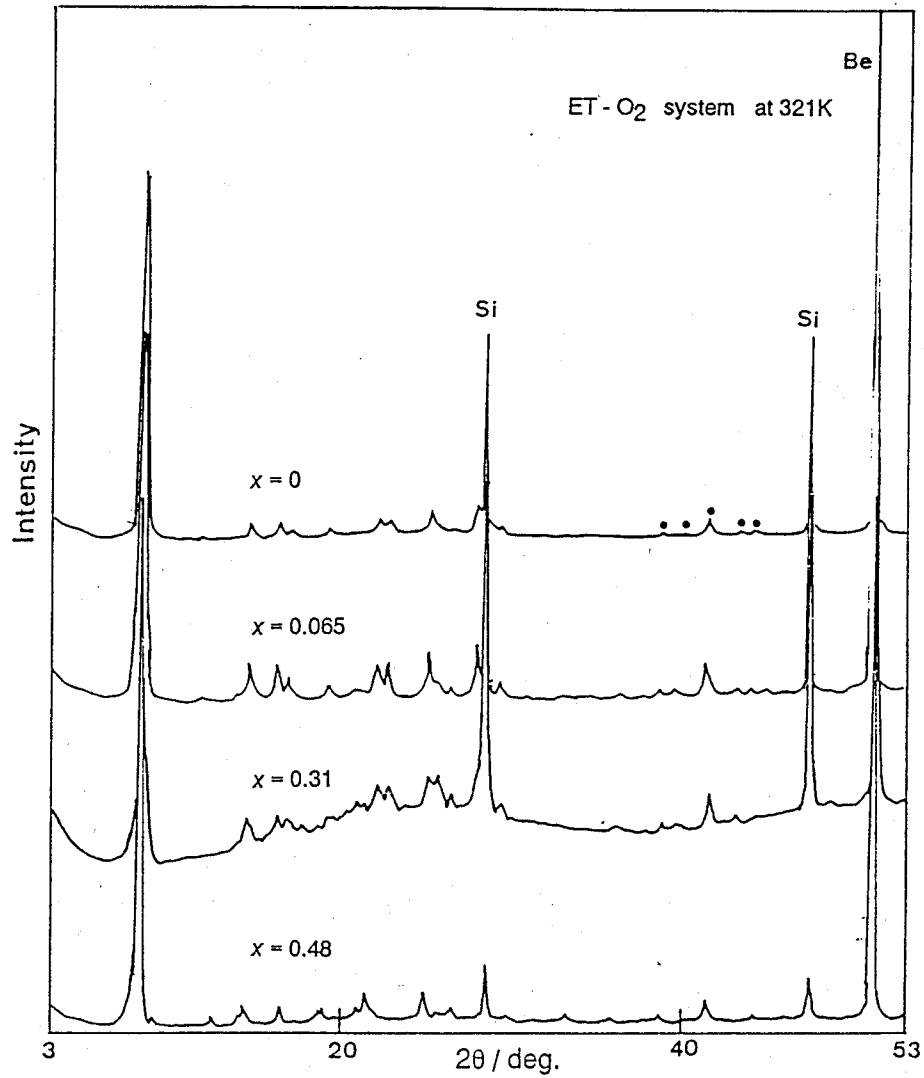

Fig.5.6a' X-ray diffraction patterns of the ET-O_2 system at various dioxygen contents at 321K. Filled circles indicate diffractions from the sample holder.

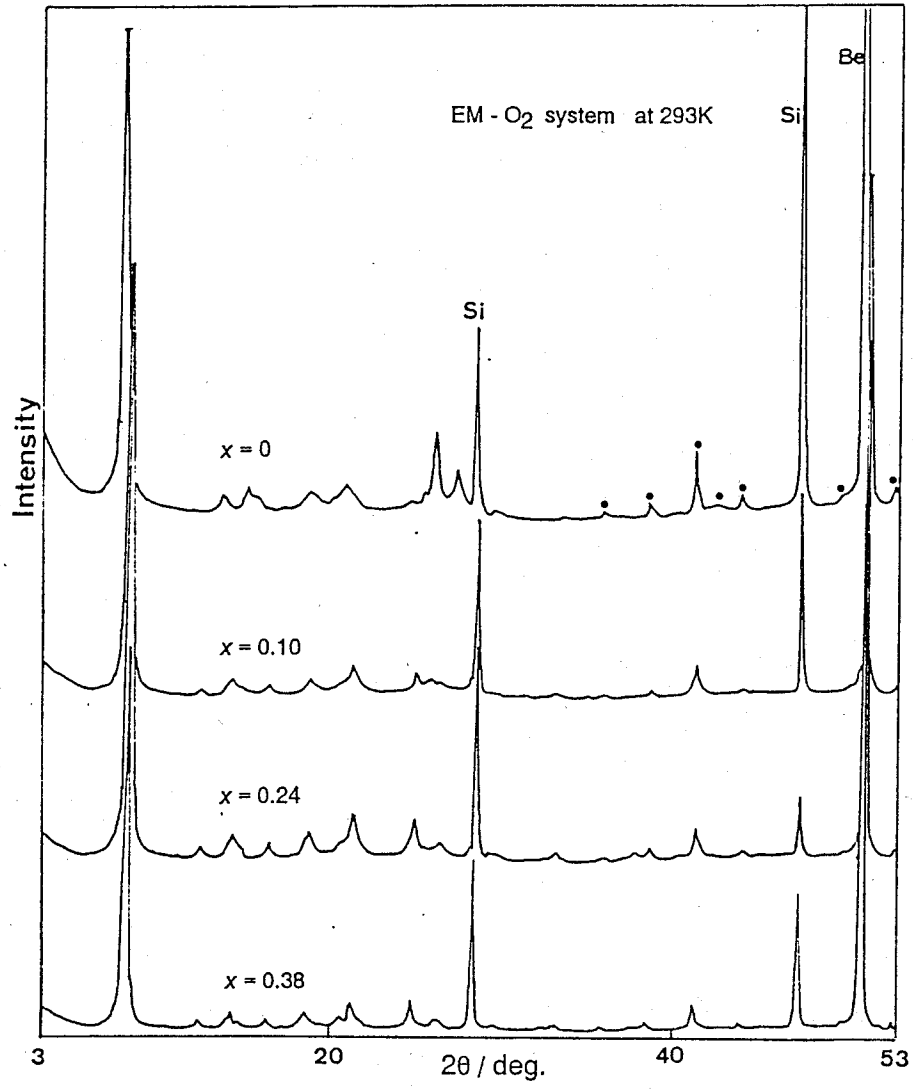

Fig.5.6b X-ray diffraction patterns of the EM-O_2 system at various dioxygen contents at 293K. Filled circles indicate diffractions from the sample holder.

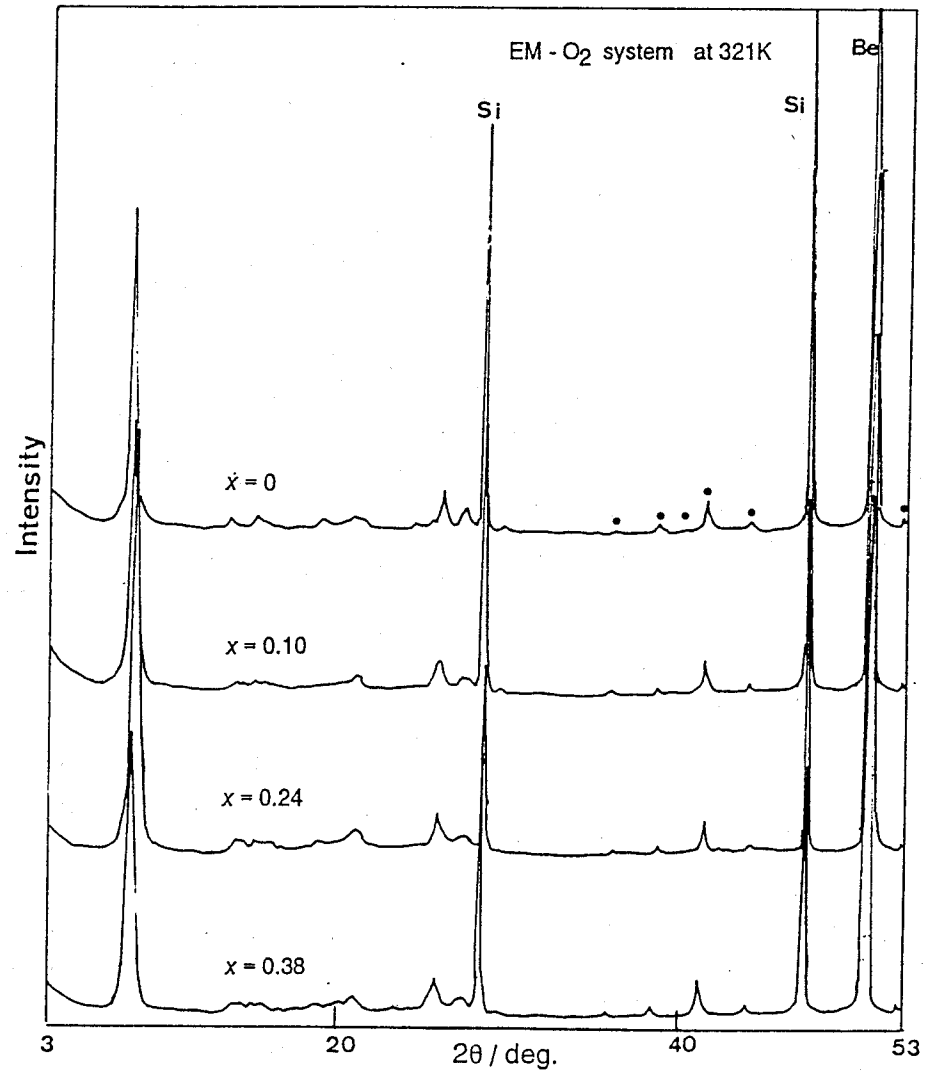

Fig.5.6b′ X-ray diffraction patterns of the EM-O_2 system at various dioxygen contents at 321K. Filled circles indicate diffractions from the sample holder.

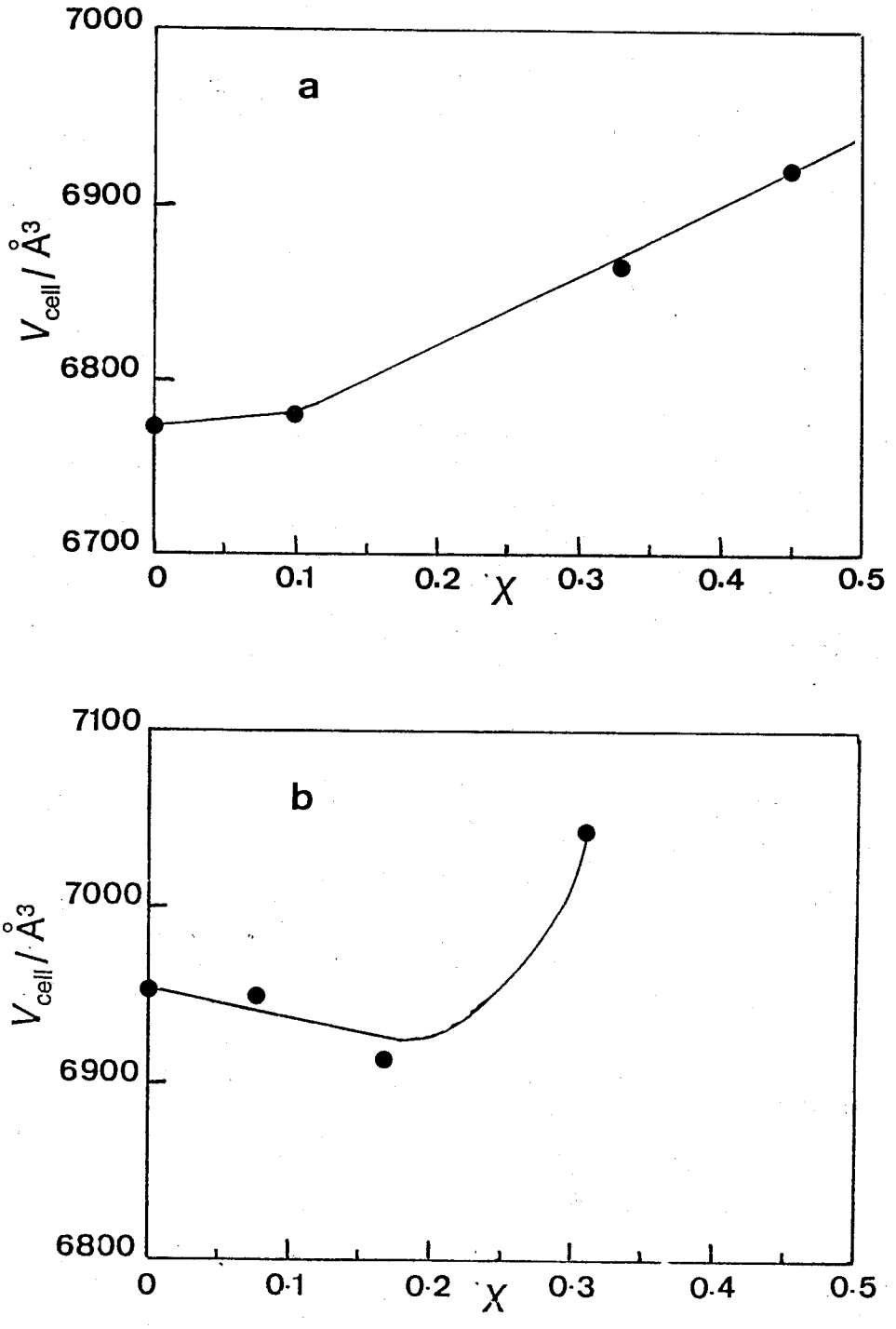

Fig.5.7 Dioxygen content dependence of the cell volume for the ME-O_2 (a) and the MM-O_2 (b) systems at 293K.

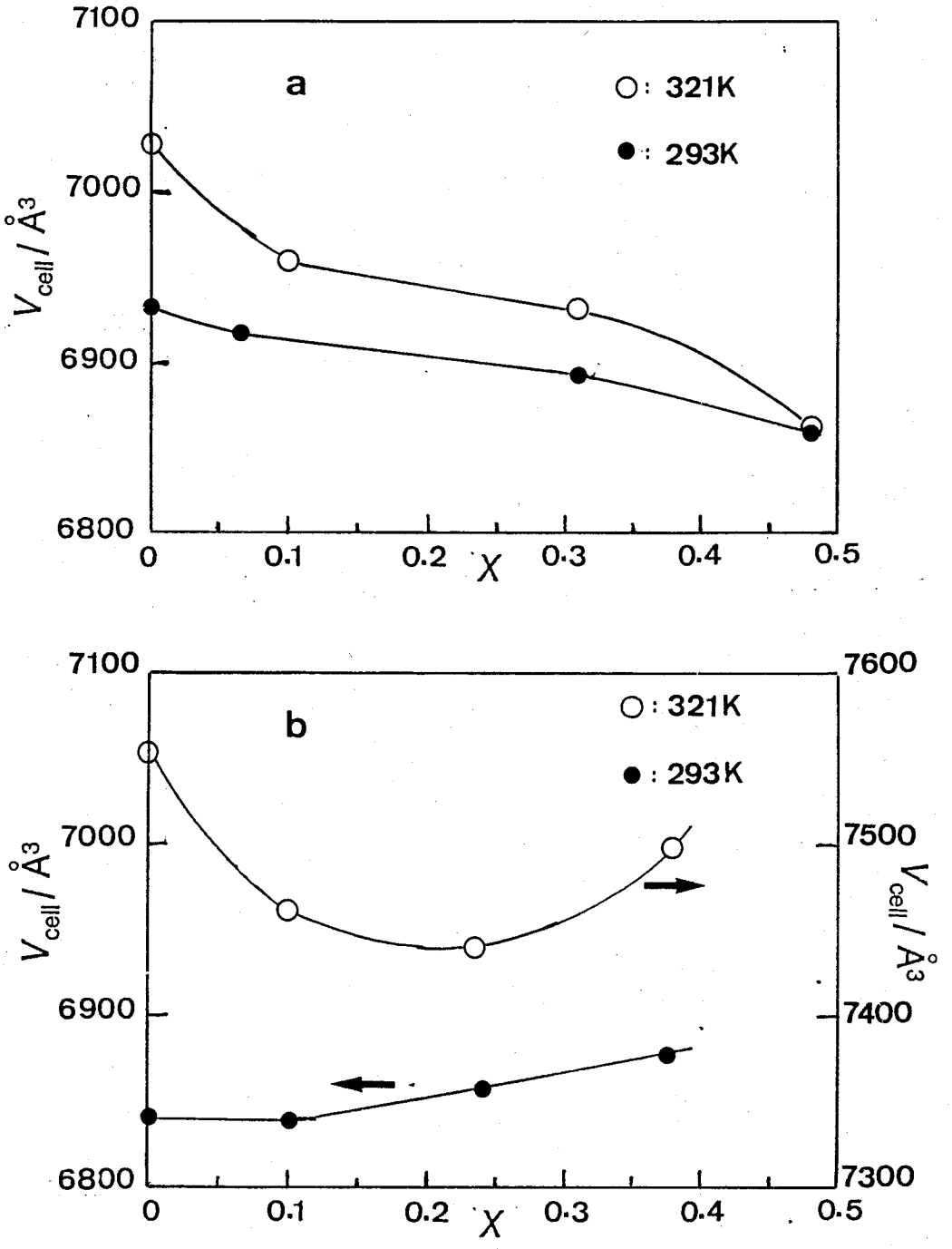

Fig.5.8 Dioxygen content dependence of the cell volume for the ET-O_2 (a) and EM-O_2 (b) systems at 293K (filled circles) and 321K (open circles).

Table 5.3 Lattice parameters and cell volume of the systems, ME-O_2, MM-O_2, ET-O_2 and EM-O_2 at various dioxygen contents. All diffraction patterns were indexed as an orthorhombic system.

System and Dioxygen content x	Latticd parameters a / nm	b / nm	c / nm	Cell volume V_{cell} / nm^3
ME-O_2 at 293 K				
x= 0	2.120	2.374	1.346	6.774
0.10	2.122	2.374	1.346	6.779
0.33	2.141	2.375	1.350	6.865
0.42	2.146	2.391	1.349	6.922
MM-O_2 at 293 K				
x= 0	2.178	2.370	1.349	6.964
0.075	2.171	2.350	1.362	6.950
0.165	2.161	2.343	1.366	6.917
0.27	2.220	2.357	1.347	7.046
ET-O_2 at 293 K				
x= 0	1.955	2.112	1.679	6.933
0.065	1.949	2.115	1.678	6.918
0.311	1.952	2.098	1.684	6.895
0.48	1.944	2.098	1.683	6.863
ET-O_2 at 321 K				
x= 0	1.963	2.119	1.689	7.027
0.065	1.962	2.096	1.693	6.961
0.311	1.953	2.103	1.688	6.933
0.48	1.944	2.095	1.684	6.860
EM-O_2 at 293 K				
x= 0	1.954	2.096	1.671	6.841
0.10	1.946	2.093	1.679	6.839
0.24	1.951	2.091	1.681	6.859
0.38	1.948	2.100	1.682	6.877
EM-O_2 at 321 K				
x= 0	1.942	2.202	1.766	7.550
0.10	1.950	2.214	1.728	7.458
0.24	1.955	2.201	1.729	7.440
0.38	1.951	2.216	1.734	7.498

5.2.3 Dioxygen Content and Temperature Dependence of Magnetic Susceptibility

Dioxygen content, x, and temperature dependencies of molar magnetic susceptibility of the ME, MM, ET and EM-O_2 systems were measured as described in section 2.5 and section 3.2.2.

Dioxygen content dependence was obtained at (291.1±2.5) K for the ME-O_2 system, (285.0±1.6) K for MM-O_2, (288.8±2.0) K for ET-O_2 and (284.9±1.0) K for EM-O_2. Molar magnetic susceptibility of the samples, X_m, and that of paramagnetic species, $X_m/(1-2x)$, are shown in Fig.5.9 and Fig.5.10. Diamagnetic nature of the oxygenated species in the ME-O_2 and ET-O_2 systems is suggested from dioxygen content dependences of X_m in Fig.5.9a and Fig.5.10a that converge on zero at x=0.5 at which all of the complex molecules form dimeric oxygenated species. Although X_m for the MM-O_2 and EM-O_2 systems (Fig.5.9b and Fig.5.10b) could not be extrapolated to x=0.5 owing to the lack of data at high dioxygen contents, the similarity in infrared spectra between the MM-O_2 and EM-O_2 systems and the ME-O_2 and ET-O_2 systems, respectively, as shown in the following section, shows that the nature of the cobalt-dioxygen bonds in the MM-O_2 and EM-O_2 system should be similar to that of the ME-O_2 and ET-O_2, respectively. Thus, the oxygenated species in the EM-O_2 and ET-O_2 systems are considered to be diamagnetic. As shown in those figures, magnetic susceptibility of paramagnetic species, $X_m/(1-x)$, increases with x. Order of the rate of increase was MM-O_2 = EM-O_2 > ET-O_2 > ME-O_2, and the slope of susceptibility at a given x became steeper at larger x.

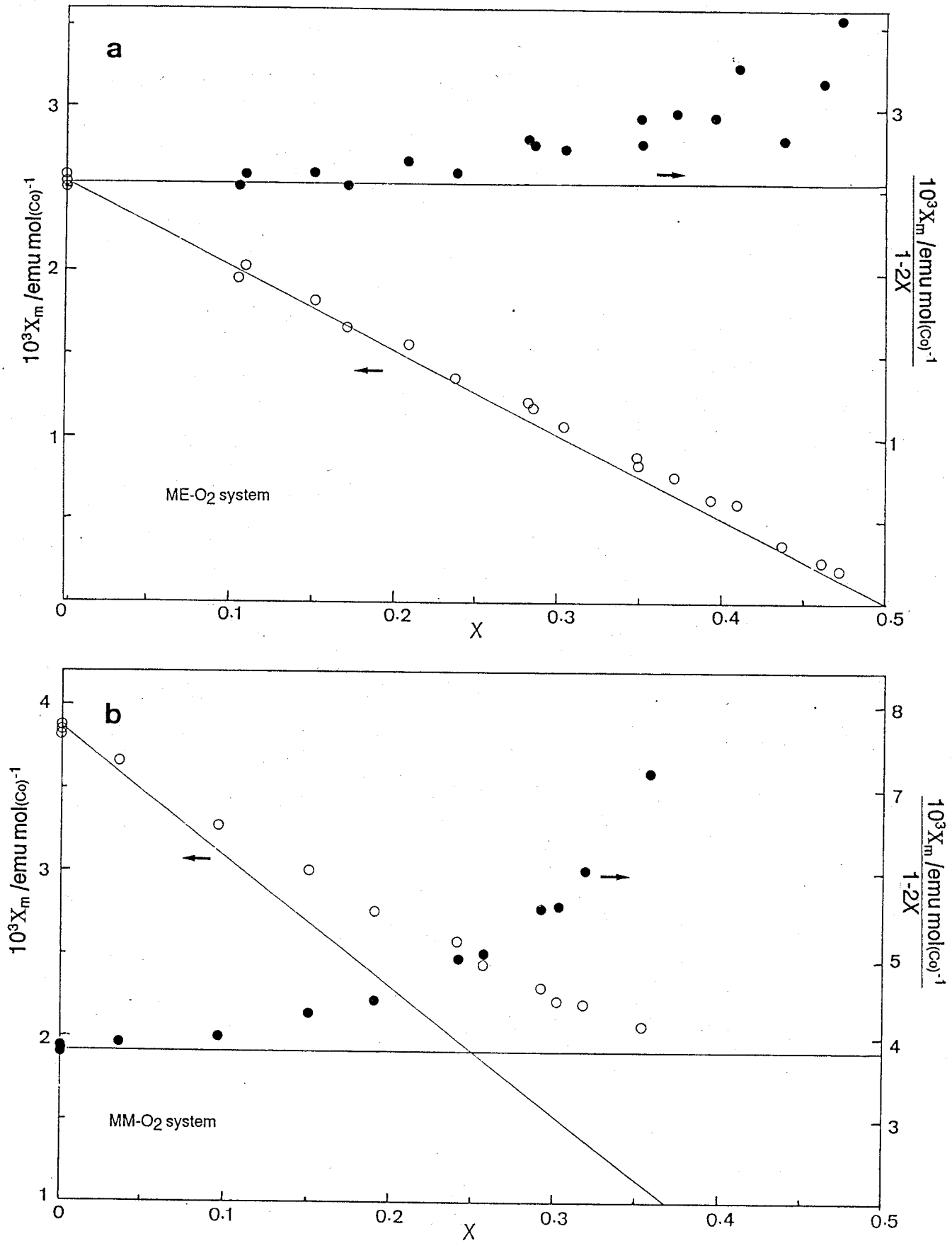

Fig.5.9 Dioxygen content dependence of molar magnetic susceptibility of the whole (open circles) and the paramagnetic (filled circles) for cobalt ions in the complex: a, ME-O_2 system at (291.1±2.5)K; and b, MM-O_2 system at (288.5±1.1)K. Solid lines indicate the values without formation of the species with higher magnetic susceptibility.

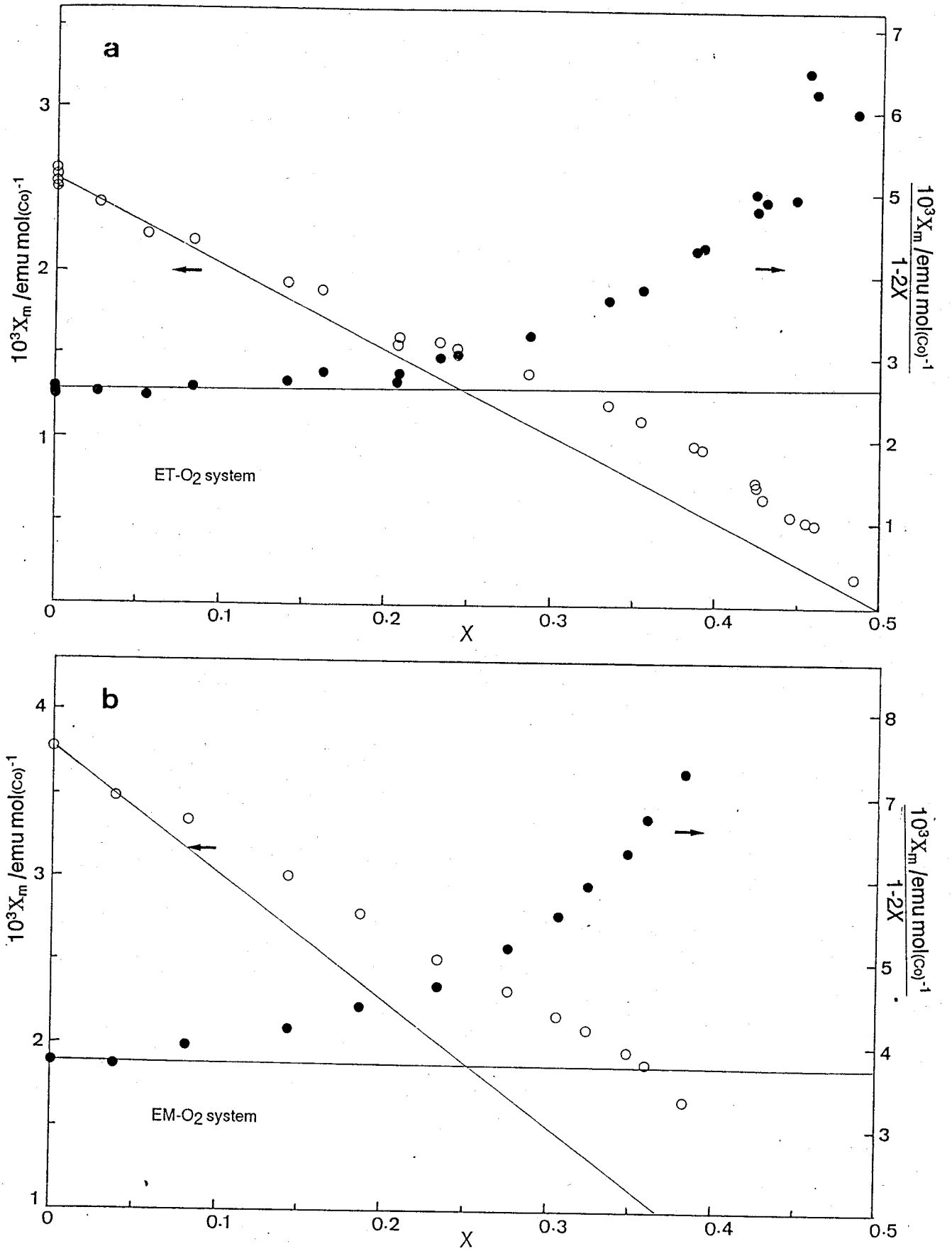

Fig.5.10 Dioxygen content dependence of molar magnetic susceptibility of the whole (open circles) and paramagnetic (filled circles) for cobalt ions in the complex: a, ET-O_2 system at (288.8±2.0)K; and b, EM-O_2 system at (286.7±0.7)K. Solid lines indicate the values without formation of the species with higher magnetic susceptibility.

Since planer [Co(3-RO-SALEN)] molecules are considered to form a column structure in which complex molecules are arranged face to face with each other as discussed in chapter 4. A model shown in Fig.5.11 is considered, where the complex molecules for which both of two adjacent complex molecules are oxygenated possess higher magnetic susceptibility, X_H, than other kinds of complex molecules. In a sample which consists of N complex molecules and xN dioxygen moieties, the number of oxygenated and unoxygenated complexes are xN and $(1-2x)N$, respectively. Therefore according to this model, the probability with which a complex molecules possesses the higher magnetic susceptibility X_H is $\{x/(1-x)\}^2$ at a given dioxygen content x. Plots of susceptibility of paramagnetic species with respect to $\{x/(1-x)\}^2$ form a straight line as shown in Fig.5.12 and Fig.5.13, respectively. Thus, an equation for interpolation of susceptibility of the systems is written as follows;

$$\frac{X_m}{1-2x} = \left\{\frac{x}{1-x}\right\}^2 \cdot X_{m0} + \left[1 - \left\{\frac{x}{1-x}\right\}^2\right] \cdot X_H \ , \qquad \text{(eq.5.1)}$$

where X_{m0} is the susceptibility at x=0. Parameters in eq.5.1 fitted to the measured systems are summarized in Table 5.4.

The magnetic susceptibilities evaluated according to the parameters given in Table 5.4 were used as reference values for temperature dependence measurements. Temperature dependences of the effective magnetic moment at various dioxygen contents are shown in Fig.5.14 and Fig.5.15. Temperature dependences of the magnetic moment of species with X_H are also shown in the figures.

Since X_H turns negative value in the lower temperature region, eq.5.1 is invalid in this region.

Table 5.4 $X_m(x=0)$, X_H, and μ_H for 1 mole of cobalt ion in the ME-O_2, MM-O_2, ET-O_2 and EM-O_2 systems which are determined by $X_m/(1-2x)$ vs. $\{x/(1-x)\}$ plots at room temperature. T_{av} is the average temperature at which the measurements were carried out.

system	T_{av} / K	$10^3 X_m(x=0)$ / emu·mol(Co)$^{-1}$	$10^3 X_H$ / emu·mol(Co)$^{-1}$	μ_H / μ_B
ME-O_2	291.1±2.5	2.51±0.13	3.76±0.21	2.96±0.17
MM-O_2	288.5±1.1	3.88±0.20	5.89±0.21	5.21±0.19
ET-O_2	288.8±2.0	2.56±0.13	6.84±0.55	3.98±0.32
EM-O_2	286.3±0.7	3.84±0.20	12.85±0.39	5.43±0.17

a)

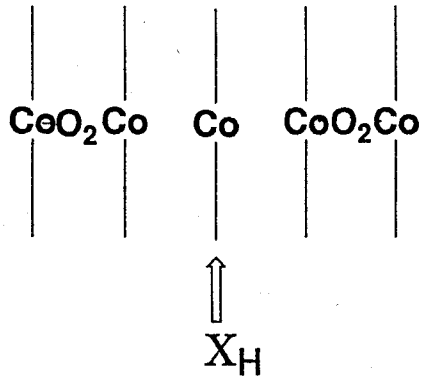

b)

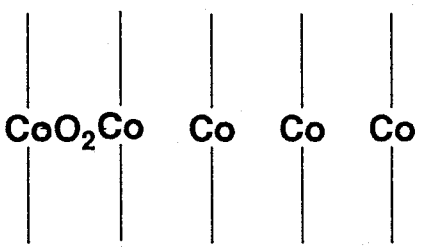

c)

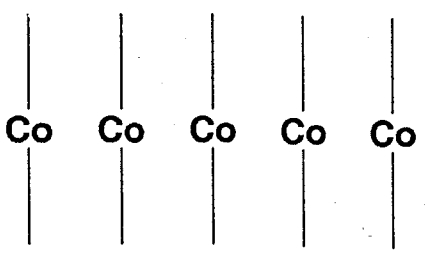

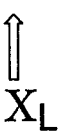

Fig.5.11 Dependence of magnetic susceptibility of a Co(II) complex molecule on its environment. Only the molecule for which both adjacent ones are oxygenated (as shown in a) shows higher susceptibility X_H than the value for the unoxygenated molecule in the unoxygenated crystal, X_L.

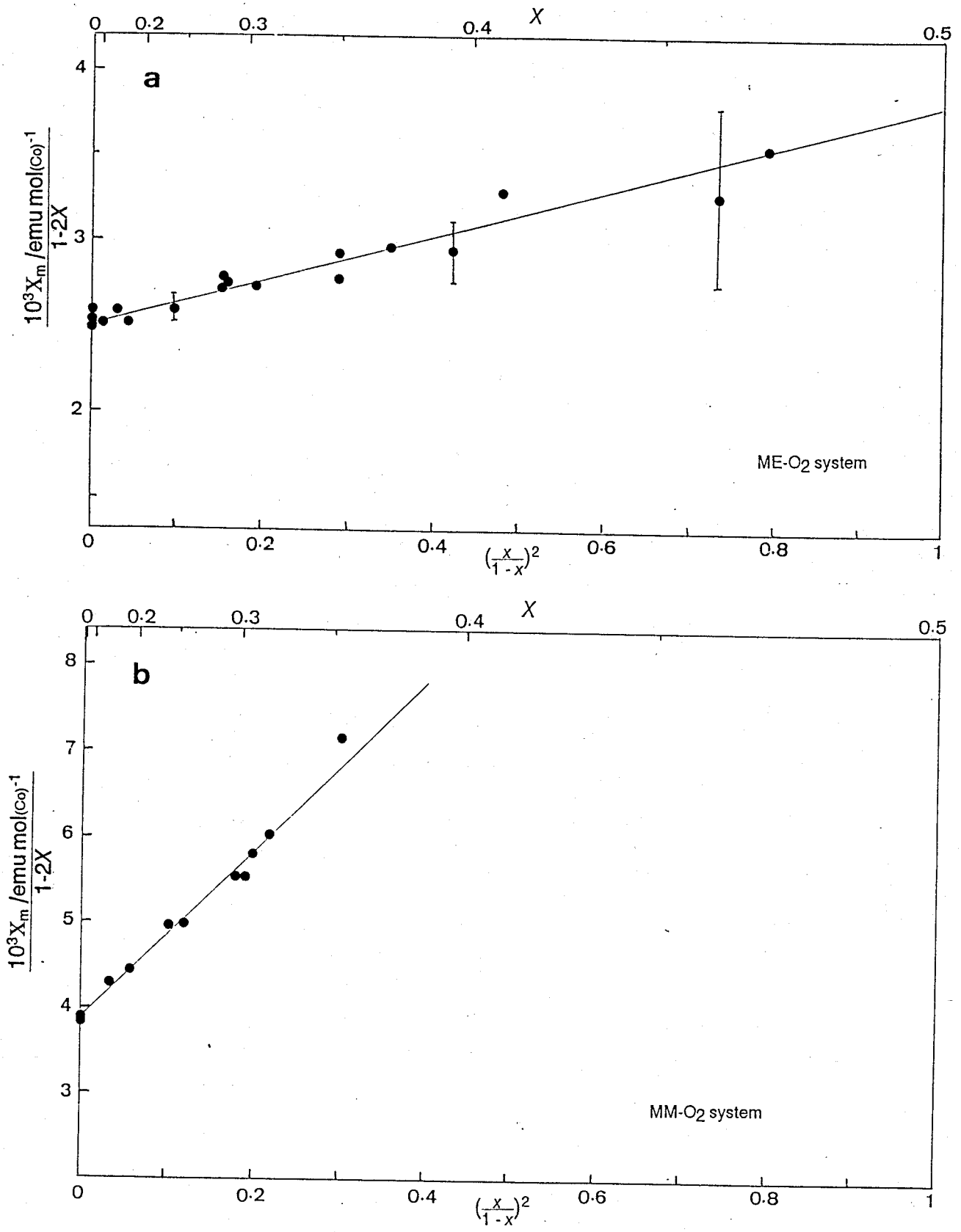

Fig.5.12 Plots of molar magnetic susceptibility of paramagnetic cobalt ions vs. $\{x/(1-x)\}^2$: a, ME-O_2 system at (291.1±2.5)K; and b, MM-O_2 system at (288.5±1.1)K. Solid lines indicate the value calculated by eq.5.1 with parameters in Table 5.4.

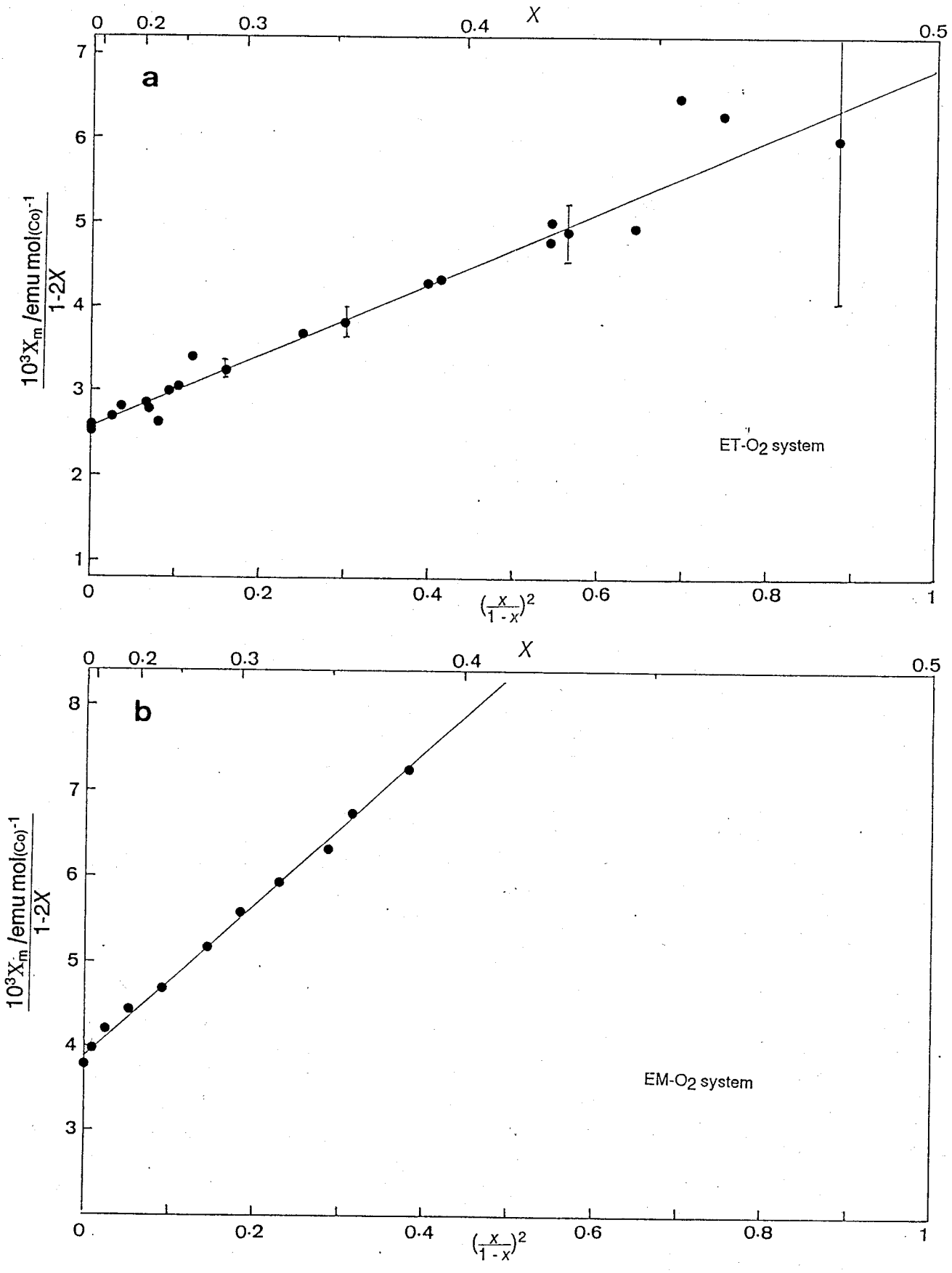

Fig.5.13 Plots of molar magnetic susceptibility of paramagnetic cobalt ions vs. $\{x/(1-x)\}^2$; a, ET-O_2 system at (288.8±2.0)K; and b, EM-O_2 system at (286.7±0.7)K. Solid lines indicate the value calculated by eq.5.1 with parameters in Table 5.4.

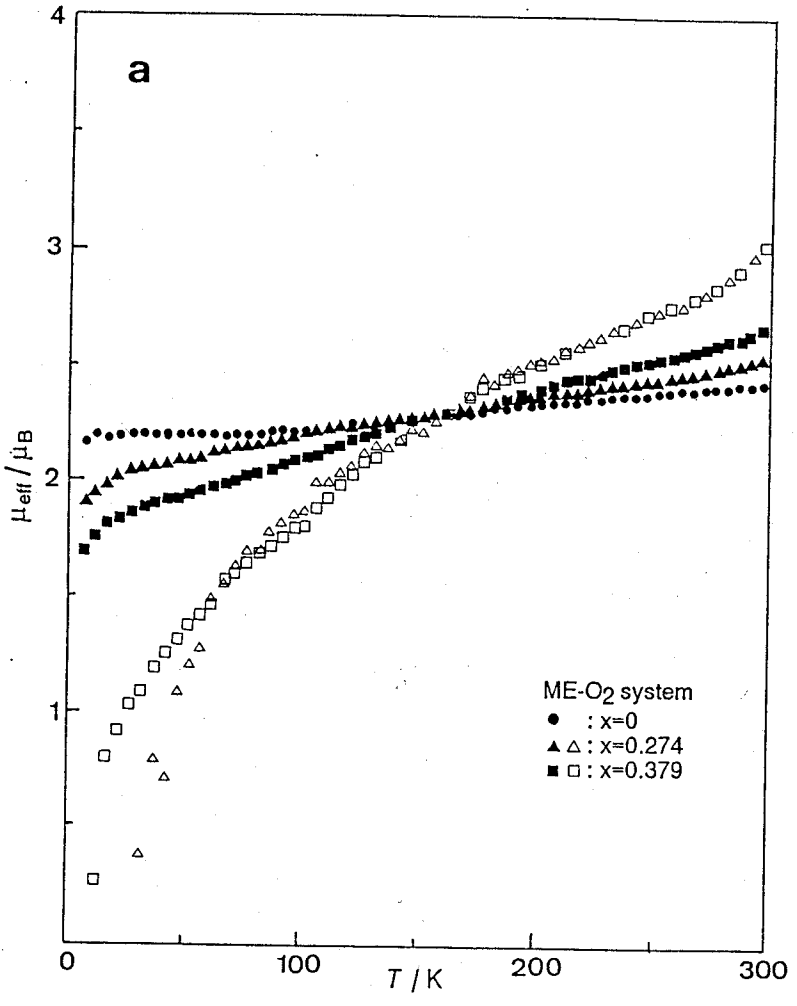

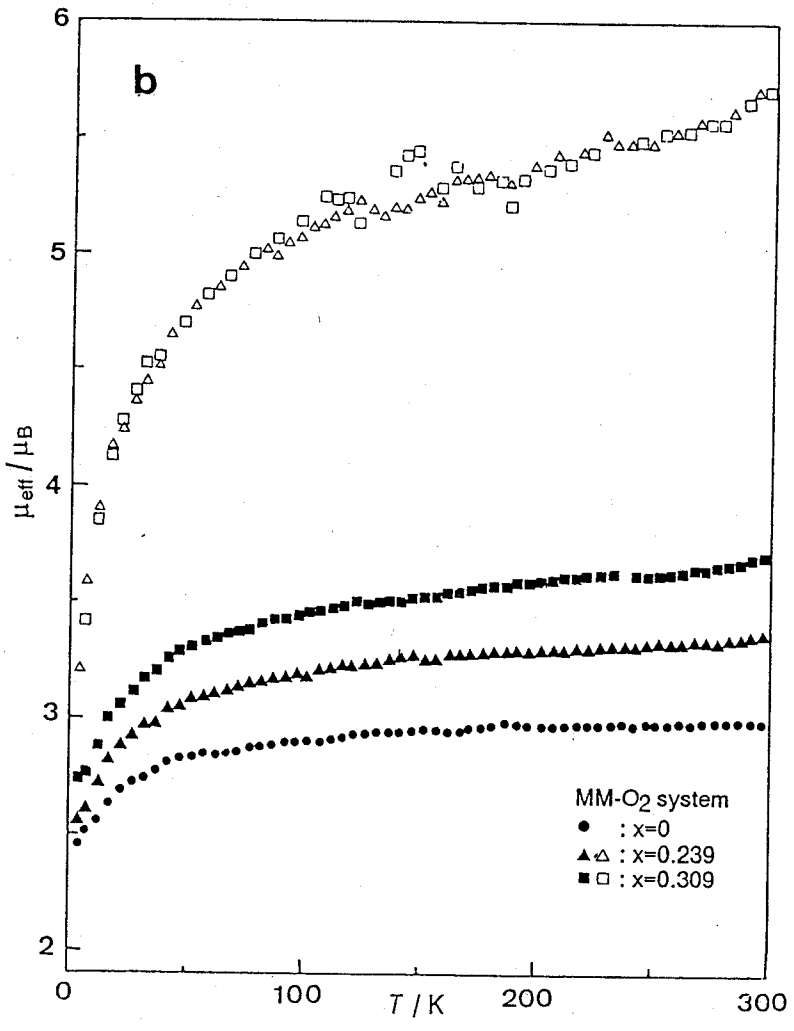

Fig.5.14 Temperature dependence of effective magnetic moment of paramagnetic species (filled marks) for the ME-O_2 (a) and MM-O_2 (b) systems at various dioxygen contents and that of species with higher susceptibility X_H (open marks corresponding to similar filled marks. See section 5.2.3).

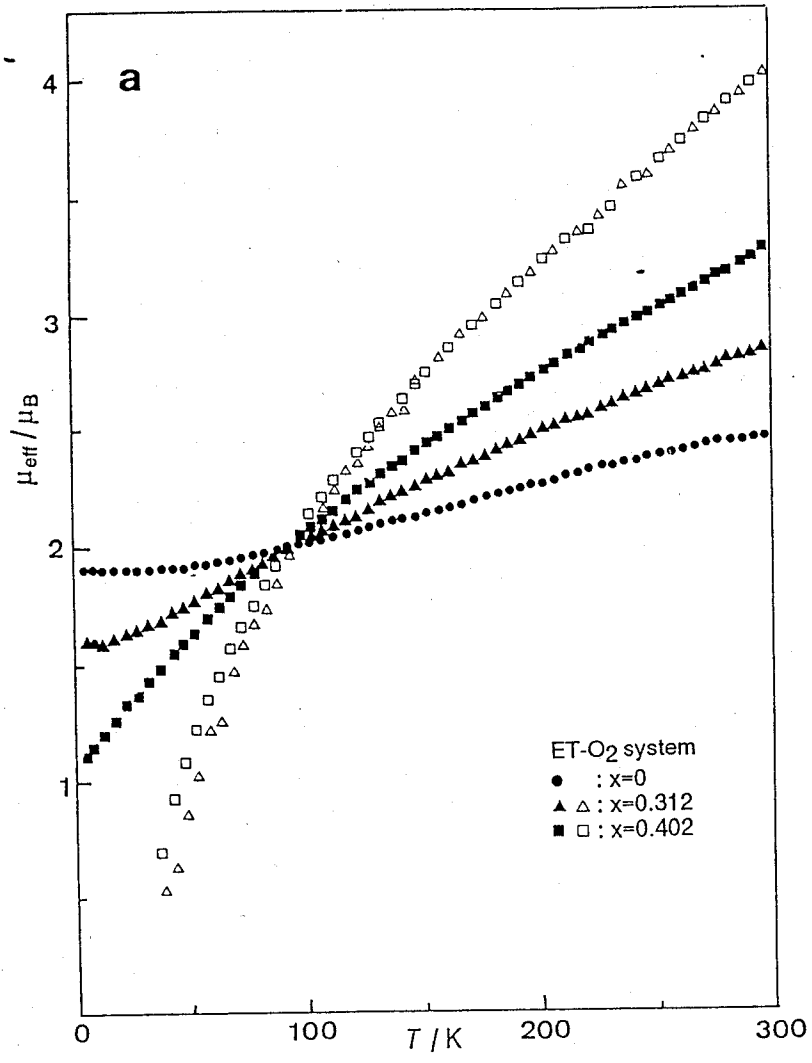

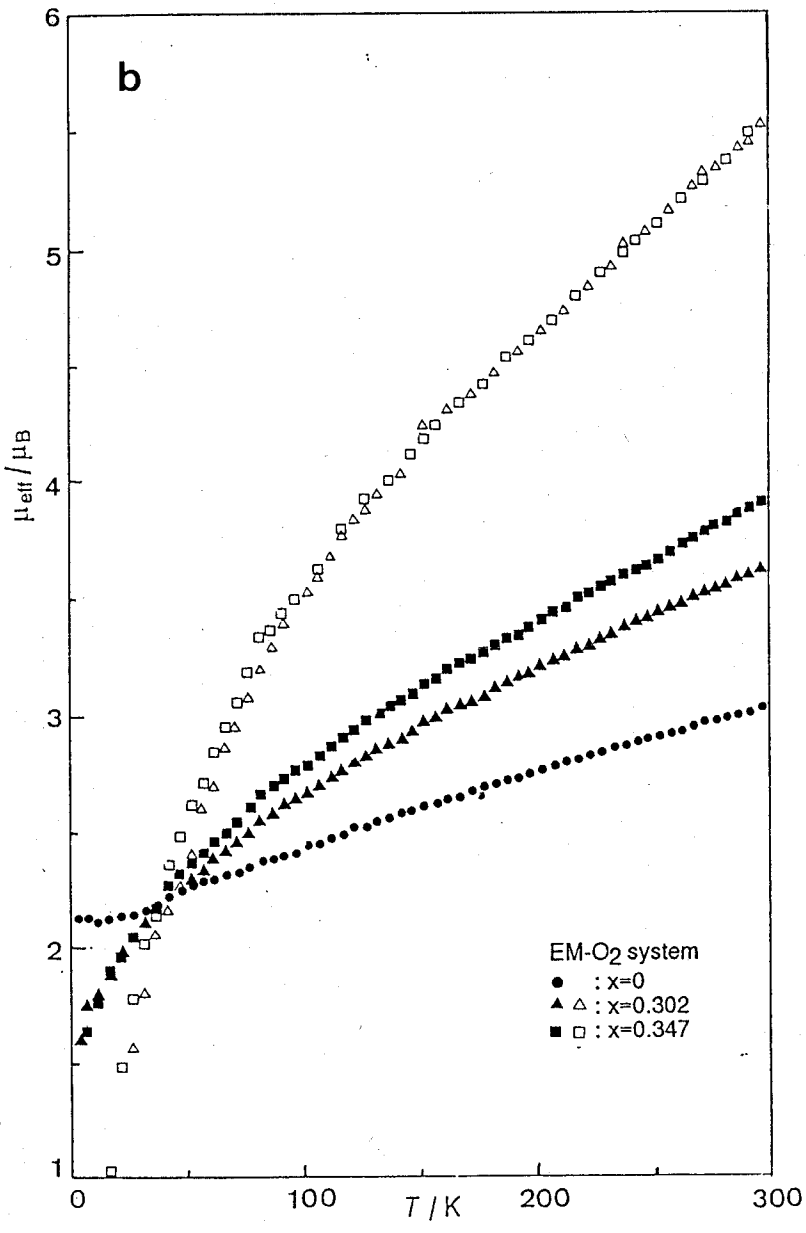

Fig.5.15 Temperature dependence of effective magnetic moment of paramagnetic species (filled marks) for the ET-O_2 (a) and EM-O_2 (b) systems at various dioxygen contents and that of species with higher susceptibility X_H (open marks corresponding to similar filled marks. See section 5.2.3).

5.2.4 Infrared Spectra

Infrared spectra for the ME-O_2 and MM-O_2 systems were recorded at 203 K, 273 K and 296 K, those for ET-O_2 and EM-O_2 at 203K, 296K and 323 K. The spectra from 400 cm^{-1} to 700 cm^{-1} and from 900 cm^{-1} to 1300 cm^{-1} of unoxygenated and oxygenated samples at various temperatures are shown in Figs.5.16 and 5.17. The spectra of the ME-O_2 system and the MM-O_2 system resemble each other for both unoxygenated and oxygenated state, except in the degree of broadness of the absorption peaks. Those of the ET-O_2 and EM-O_2 systems also resemble with each other. Since the absorption bands in the range 400-700 cm^{-1} of [Co(SALEN)] and its derivatives have been assigned to metal-ligand vibrations[2,3,4], similar assignment can be given to those of the present samples in this region. It is likely that they also involve contribution of the ethylene bridge of the complex molecules, because the bands indicated by "**d**" exhibited isotope shift by deuterating at the ethylene bridge (Fig.5.16c). The deuterization also resulted in isotope effects for the bands of ME-O_2 (x=0.45) near 850, 940, 970, 990, 1040, 1165 and 1390 cm^{-1} as shown in Fig.5.16c. Thus these band are attributable to deformation modes of the ethylene bridge.

Far infrared spectra from 30 cm^{-1} to 400 cm^{-1} were recorded at 296 K for unoxygenated and oxygenated samples of ME, MM, ET and EM, which are shown in Fig.5.18 (unoxygenated samples) and Fig.5.19 (oxygenated samples). Several bands with triangles (open and filled) in Fig.5.19 from 200 cm^{-1} to 400 cm^{-1} of [Co(3-MeO-SALEN-d_4)]$(O_2)_{0.45}$ indicated isotope shifts. Therefore the vibration of the ethylene bridge contributes to these bands. Although the complex molecules have the same chelate skeleton, spectra of the systems both at unoxygenated and oxygenated state

(Fig.5.18 and Fig.5.19, respectively) were slightly different from each other.

5.2.5 Raman Spectra

The recorded Raman spectra from 1300 cm^{-1} to 1500 cm^{-1} for the ME-O_2 system, the MM-O_2 system, [Co(3-MeO-SALEN)]H_2O and [Co(3-MeO-SALEN-d_4)]H_2O deuterated at the ethylene bridge are shown in Fig.5.20, and those for the ET-O_2 and EM-O_2 systems in Fig.5.21. Peaks indicated by circles show isotope shifts by deuteration at the ethylene bridge of [Co(3-MeO-SALEN)]H_2O, thus these peaks are assigned to vibrations of its methylene groups.

The intensity of those peaks was found to depend on temperature. The ratios of Raman intensity at 1360 cm^{-1} to that at 1440 cm^{-1} for the ME-O2, MM-O2, ET-O2 and EM-O2 systems and [Co(3-MeO-SALEN)]H_2O are shown in Table 5.5 and Table 5.6.

5.2.6 Diffuse Reflectance Spectra

Diffuse reflectance spectra at various dioxygen contents were recorded from 1500 nm to 500 nm at 296K as shown in Fig.5.22 and Fig.5.23. Dioxygen content dependences of the spectra were similar with each other. Increasing dioxygen content, a new band appeared at about 730nm, but it disappeared at higher dioxygen content. This composition dependence shows existence of the unoxygenated complex molecules subject to interaction from their environment. In the case of MM and EM (x=0), absorbance of the band at about 700 nm was found to increase relative to those of ME and ET as shown in Fig.5.24a and 5.25a. The spectra of MM and EM minus those of ME and ET, respectively, are shown in Fig.5.24b

and Fig.5.25b. Absorption bands are observed at about 720 nm for MM and at about 600 and 670 nm for EM.

Table 5.5 Ratio of Raman intensity of the peak at about 1360 cm^{-1} to that at about 1440 cm^{-1} for the ME-O_2, MM-O_2 systems and [Co(3-MeO-SALEN)]H_2O.

System and Dioxygen content x	$\frac{I(1360cm^{-1})}{I(1440cm^{-1})}$ at 202 K	at 296 K
ME-O_2		
x=0	1.27	1.48
x=0.45	0.93	1.02
MM-O_2		
x=0	0.83	0.97
x=0.24	0.76	0.90
[Co(3-MeO-SALEN)]H_2O	0.76	1.34

Table 5.6 Ratio of Raman intensity of the peak at about 1360 cm^{-1} to that at about 1440 cm^{-1} for the ET-O_2 and EM-O_2 systems.

System and Dioxygen content x	$\frac{I(1360\ cm^{-1})}{I(1440\ cm^{-1})}$ at 202 K	at 296 K	at 323 K
ET-O_2			
x=0	1.75	1.82	1.80
x=0.48	0.56	0.69	0.76
EM-O_2			
x=0	1.56	1.71	1.73
x=0.38	0.83	0.85	0.86

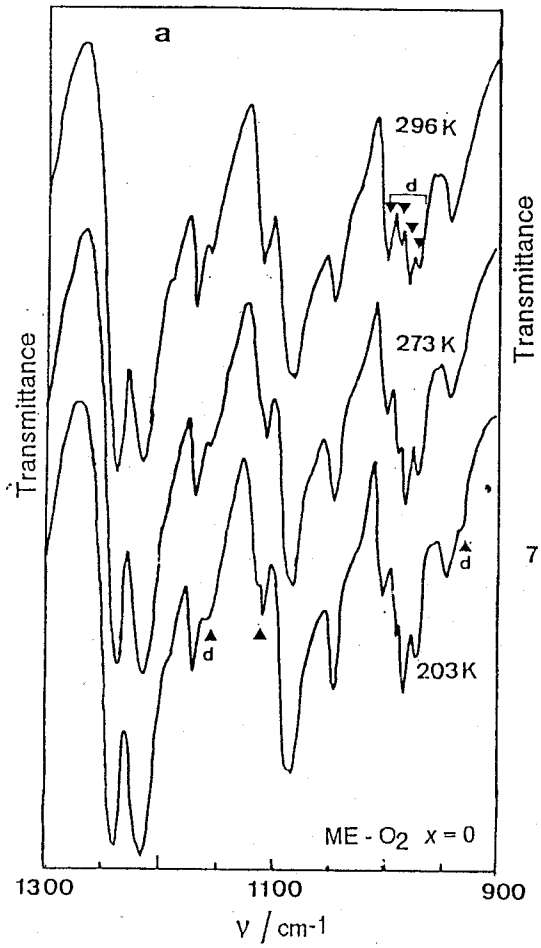

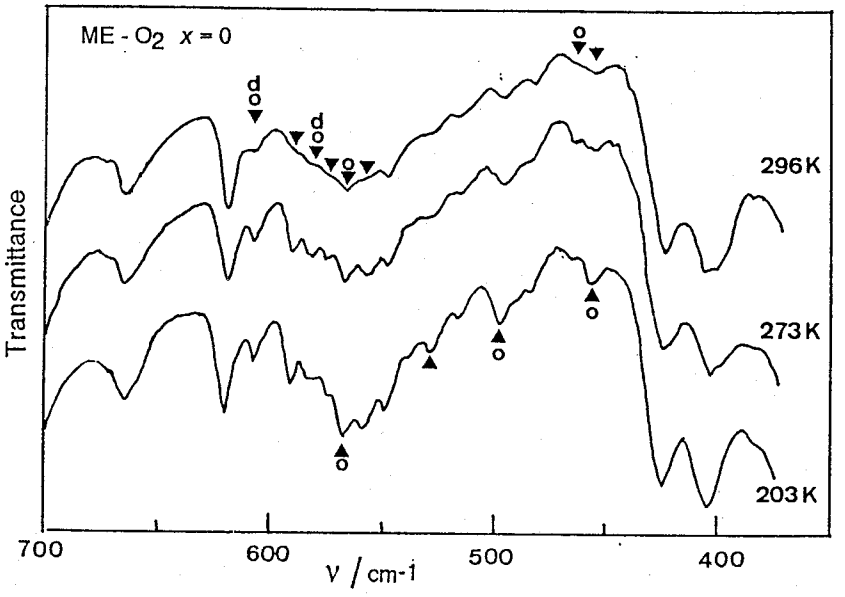

Fig.5.16a Infrared spectra (350-700cm^{-1} and 900-1300cm^{-1}) of the ME-O_2 system with x=0 at 203K, 273K and 296K. Triangles on the spectra at 296K and 203K indicate the peaks with shapes significantly different from the one at 273K. The peaks with "o" marks are also observed in the spectra of the ME-O2 system with x=0.45, and those with "d" marks showed isotope shift in the ME-O2 system with x=0.45.

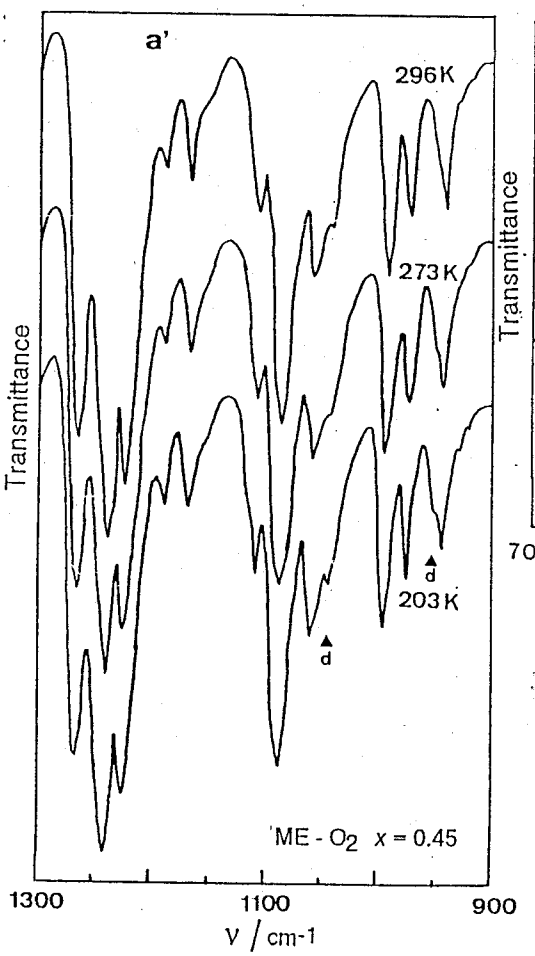

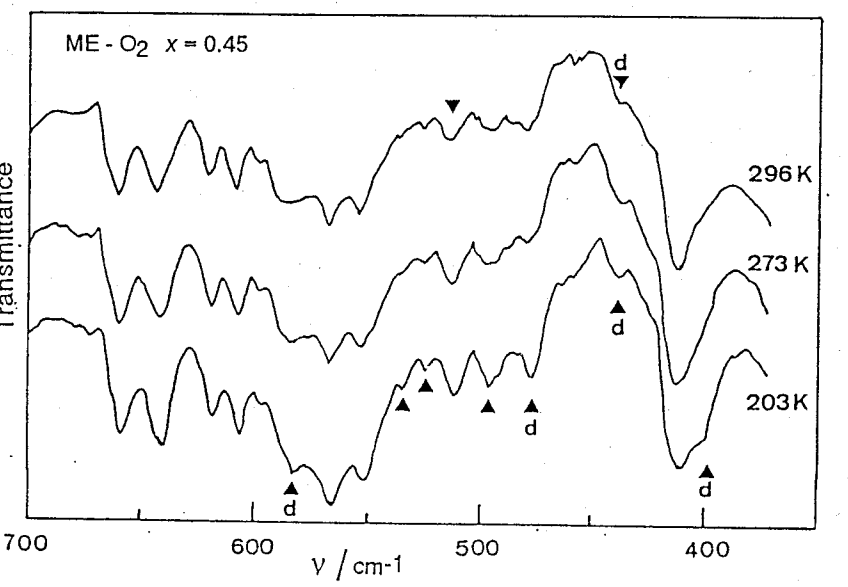

Fig.5.16a' Infrared spectra (350-700cm^{-1} and 900-1300cm^{-1}) of the ME-O_2 system with x=0.45 at 203K, 273K and 296K. Triangles on the spectra at 296K and 203K indicate the peaks with shapes significantly different from the one at 273K. The peaks with "d" marks showed isotope shift in the ME-O2 system with x=0.45.

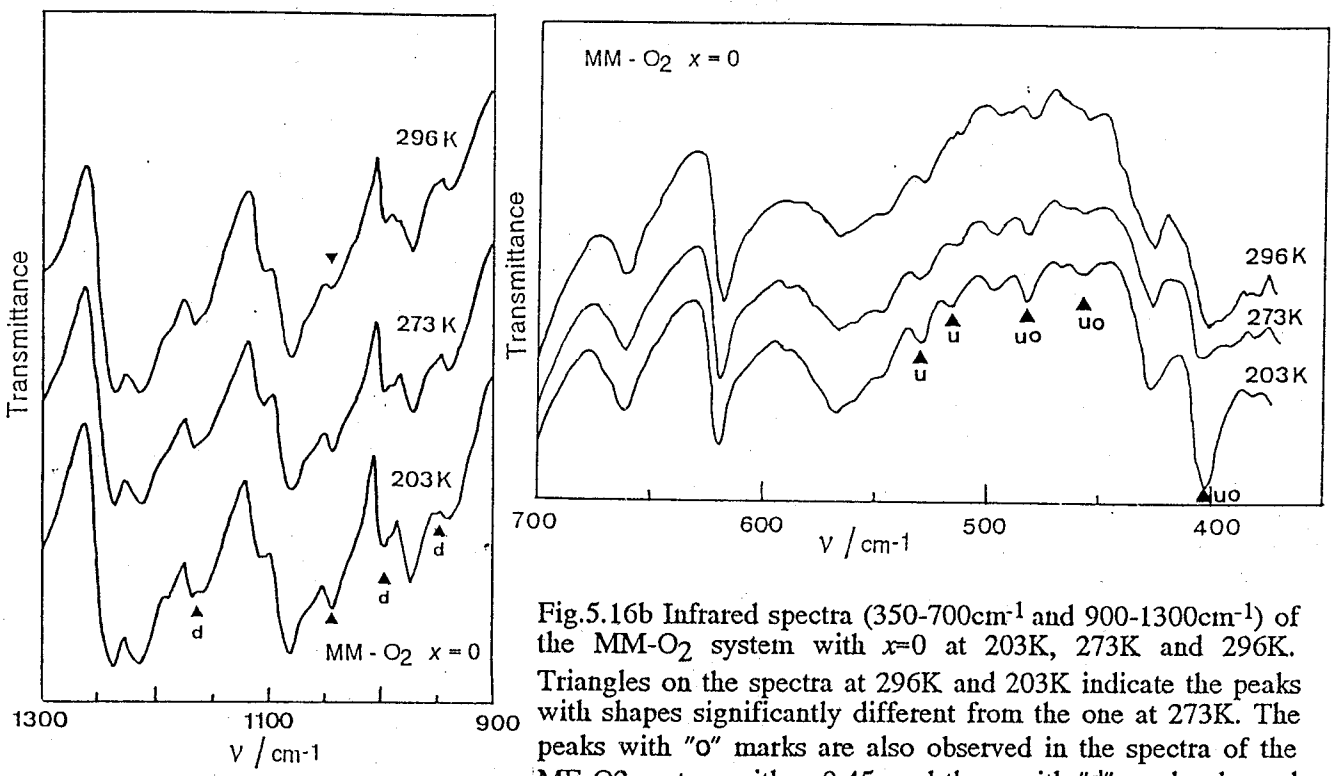

Fig.5.16b Infrared spectra (350-700cm^{-1} and 900-1300cm^{-1}) of the MM-O_2 system with x=0 at 203K, 273K and 296K. Triangles on the spectra at 296K and 203K indicate the peaks with shapes significantly different from the one at 273K. The peaks with "o" marks are also observed in the spectra of the ME-O2 system with x=0.45, and those with "d" marks showed isotope shift in the ME-O2 system with x=0.45.

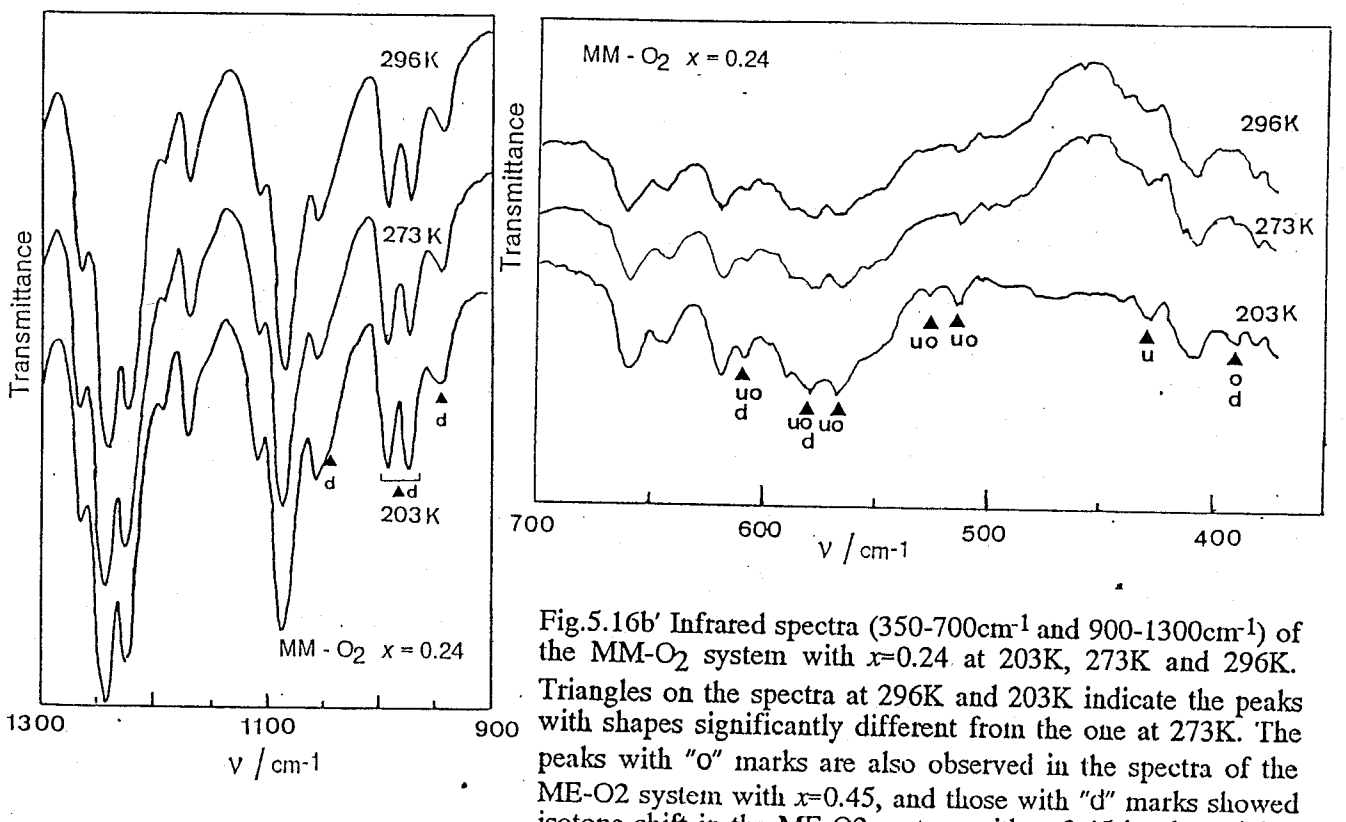

Fig.5.16b' Infrared spectra (350-700cm^{-1} and 900-1300cm^{-1}) of the MM-O_2 system with x=0.24 at 203K, 273K and 296K. Triangles on the spectra at 296K and 203K indicate the peaks with shapes significantly different from the one at 273K. The peaks with "o" marks are also observed in the spectra of the ME-O2 system with x=0.45, and those with "d" marks showed isotope shift in the ME-O2 system with x=0.45 by deuterizing at the ethylene bridge of the complex.

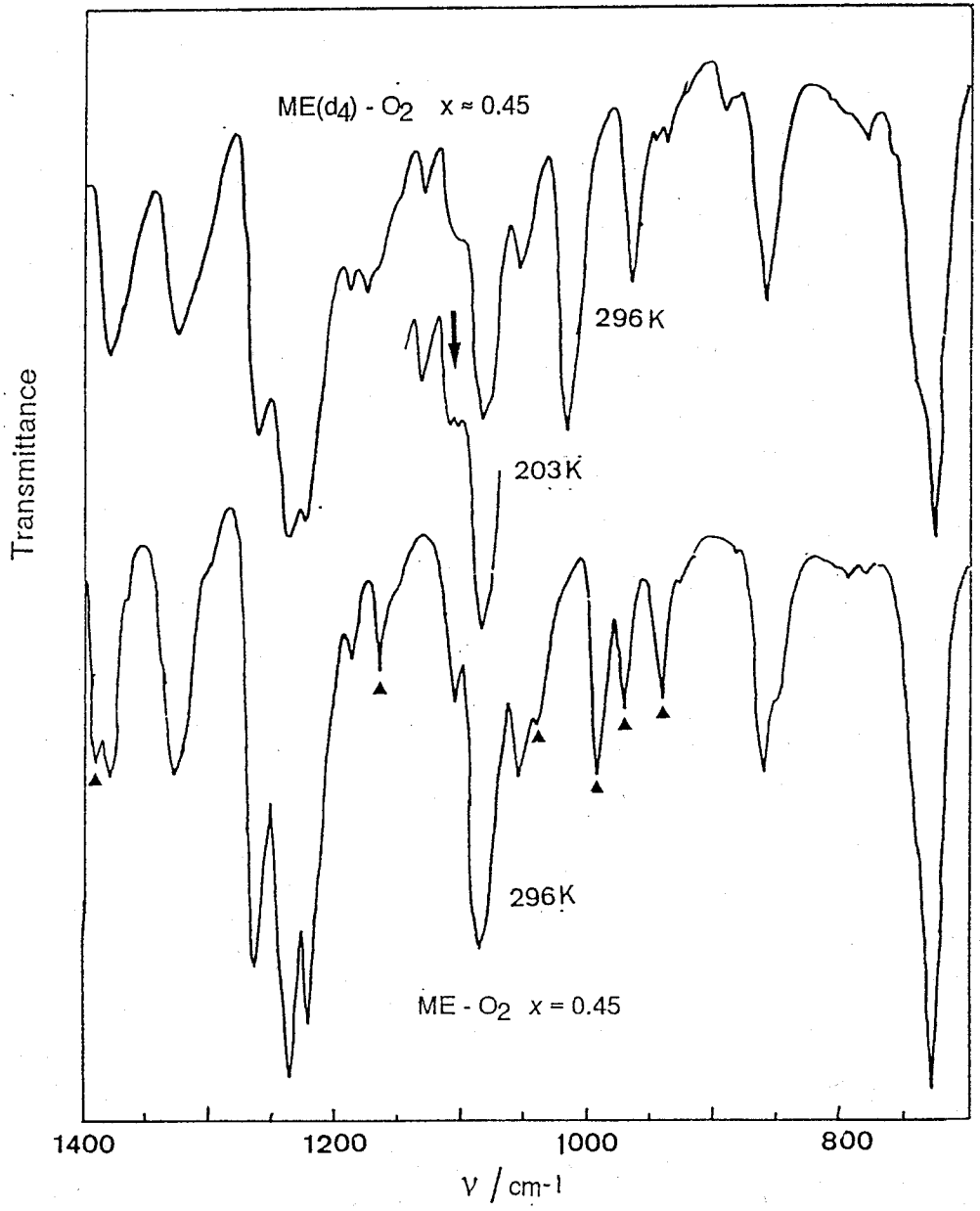

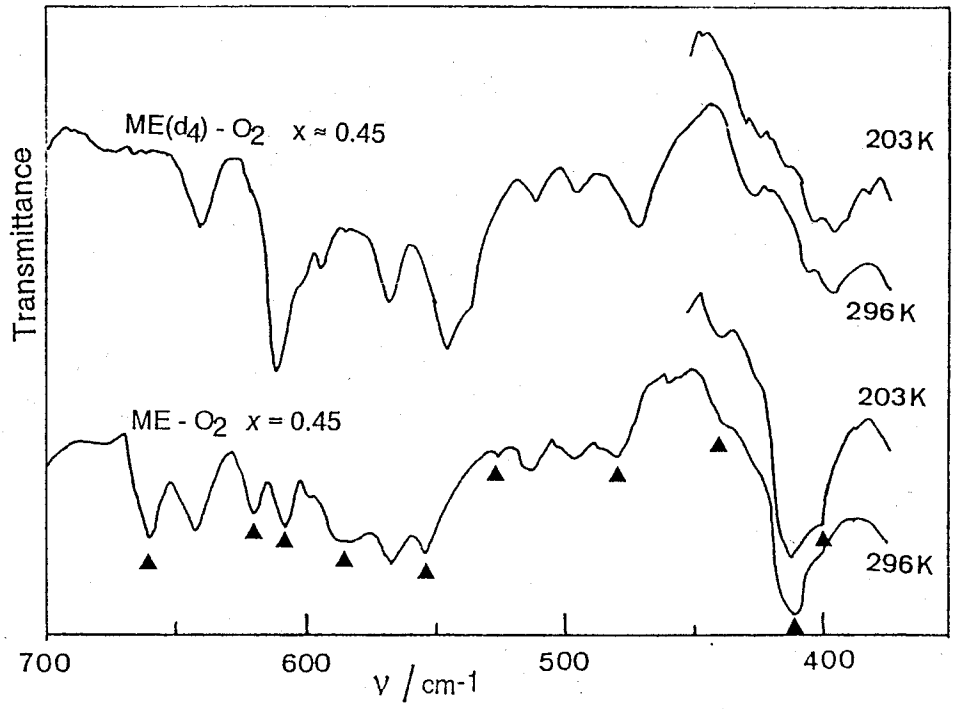

Fig.5.16c Infrared spectra (350-1400cm^{-1}) of [Co(3-MeO-SALEN-d$_4$)](O$_2$)$_{0.45}$ at 296K. Spectra at 203K in the region in which significant difference from the one at 296K was observed are shown together. Isotope shift was observed for the peaks indicated by triangles.

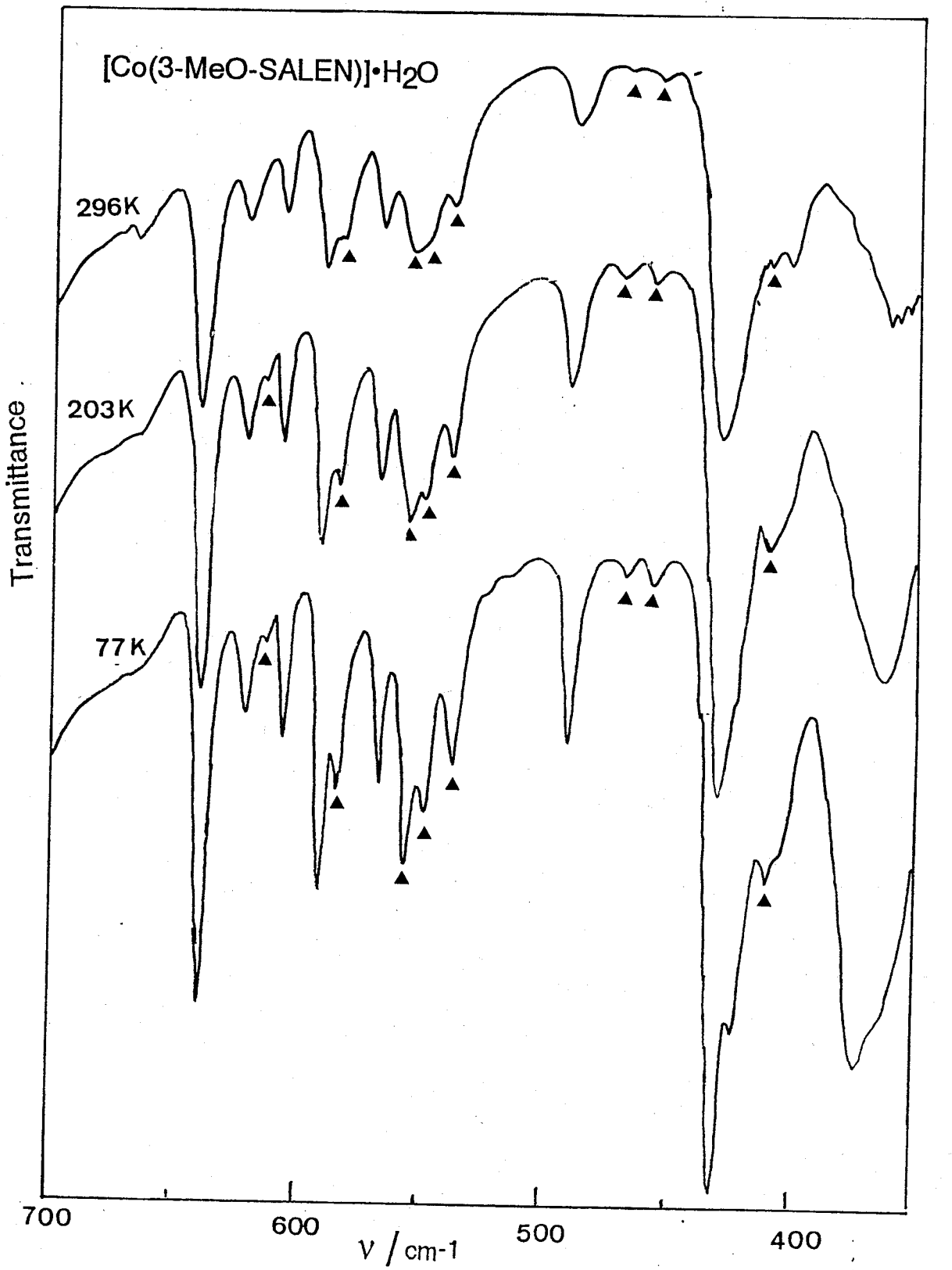

Fig.5.16d Infrared spectra (350-700cm^{-1}) of [Co(3-MeO-SALEN)]H_2O at 77K, 203K and 296K. The peaks indicated by triangles showed outstanding temperature dependence of their shape.

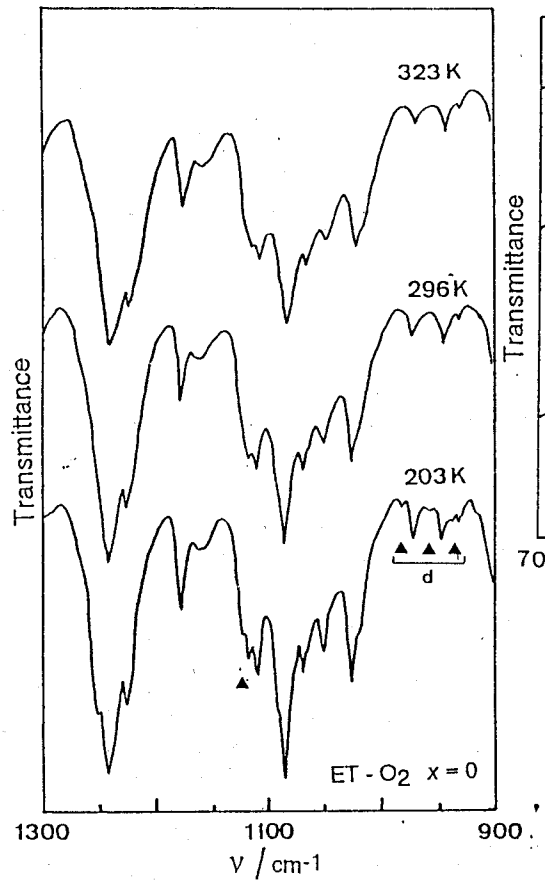

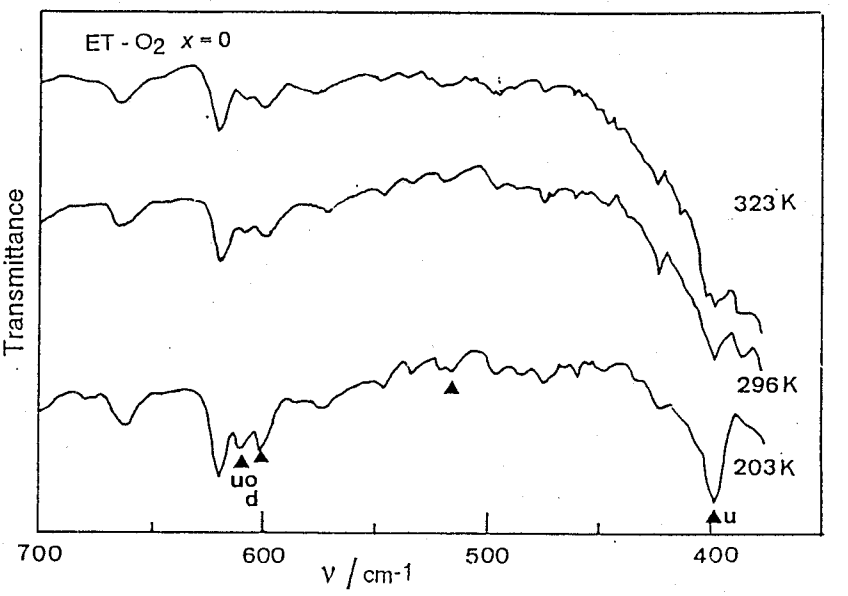

Fig.5.17a Infrared spectra (350-700cm^{-1} and 900-1300cm^{-1}) of the ET-O_2 system with x=0 at 203K, 296K and 323K. Triangles on the spectra at 323K and 203K indicate the peaks with shapes significantly different from the one at 296K. The peaks with "o" marks are also observed in the spectra of the ME-O2 system with x=0.45, and those with "d" marks showed isotope shift in the ME-O2 system with x=0.45.

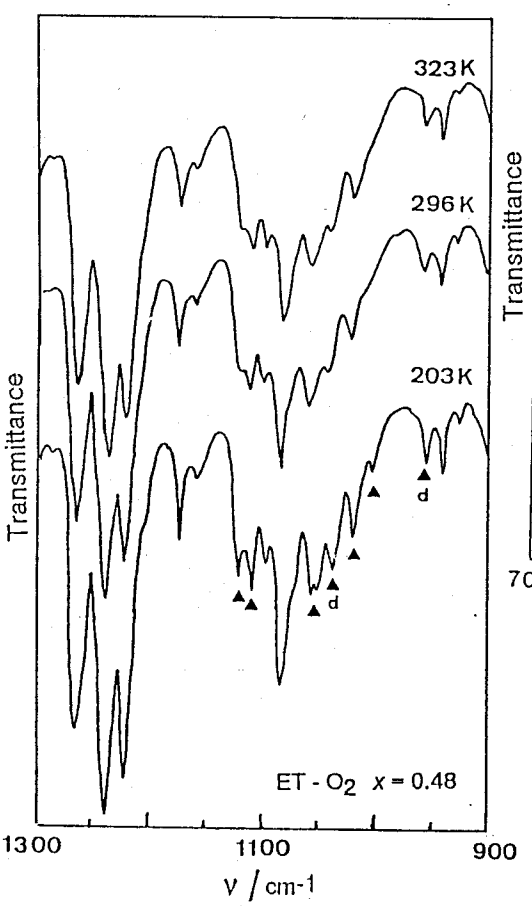

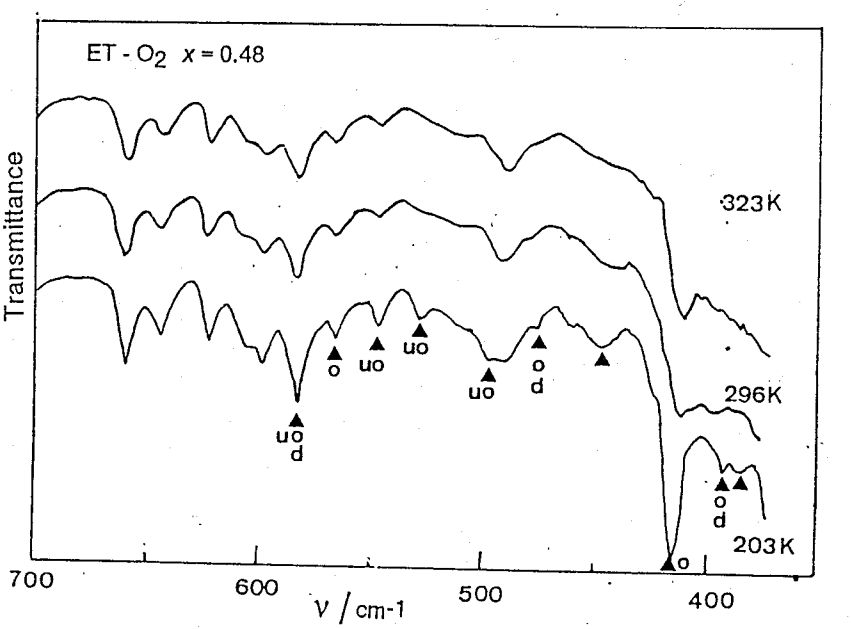

Fig.5.17a' Infrared spectra (350-700cm^{-1} and 900-1300cm^{-1}) of the ET-O_2 system with x=0.48 at 203K, 296K and 323K. Triangles and the marks "o" and "d" have the same meanings as in Fig.5.17a.

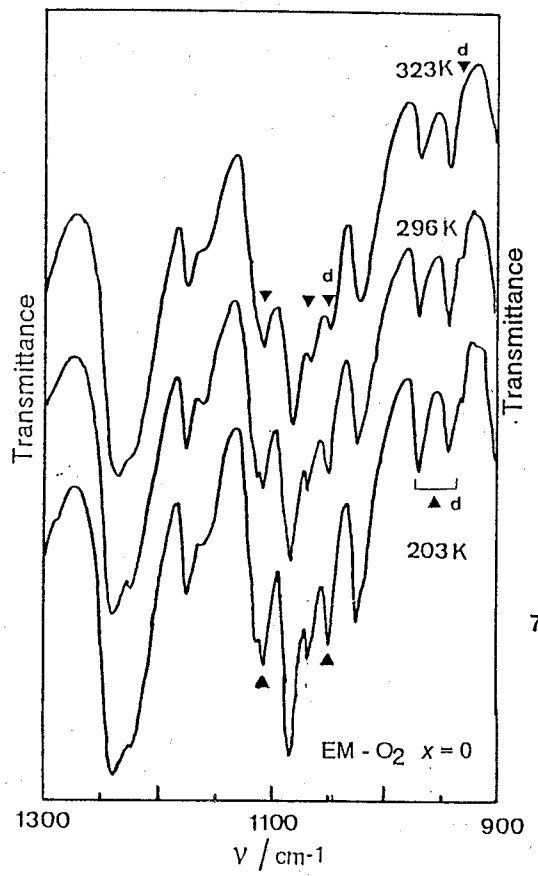

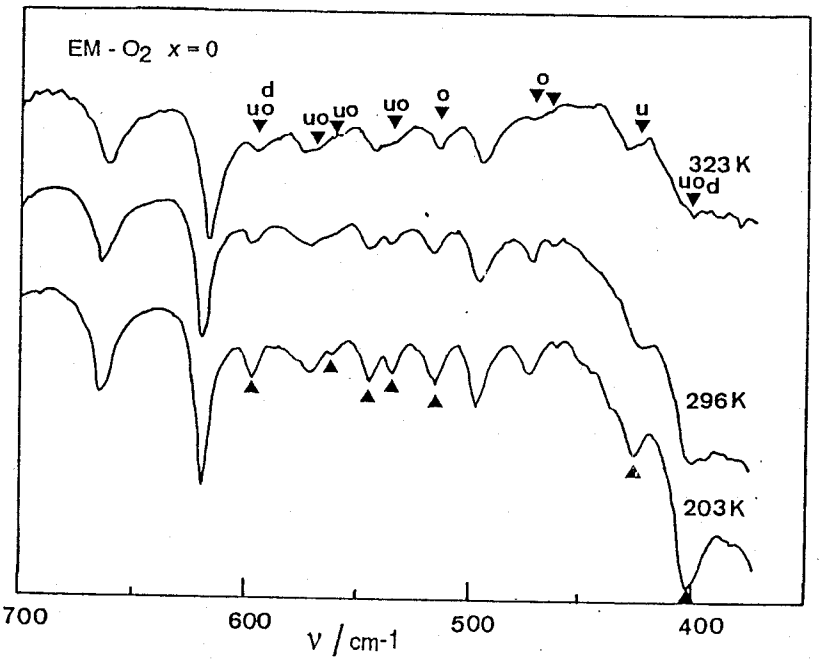

Fig.5.17b Infrared spectra (350-700cm^{-1} and 900-1300cm^{-1}) of the EM-O_2 system with x=0 at 203K, 296K and 323K. Triangles and the marks "o" and "d" have the same meanings as in Fig.5.17a.

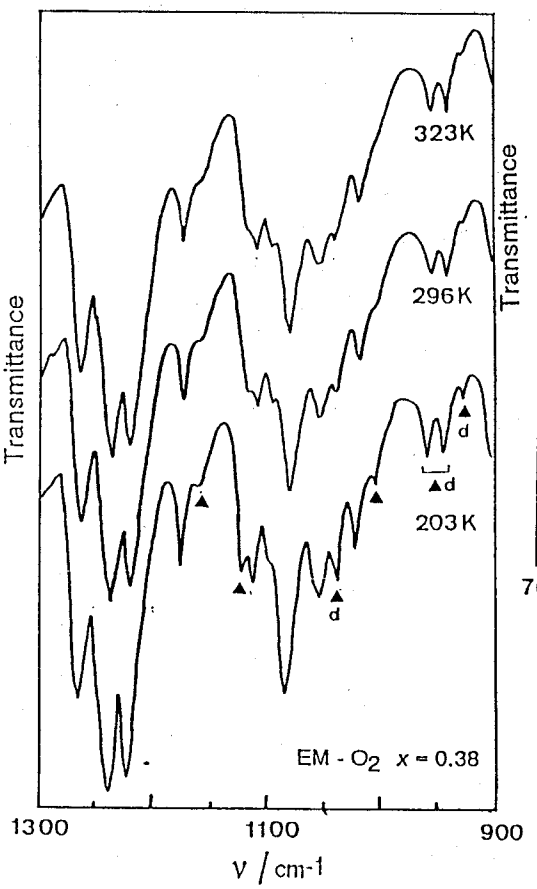

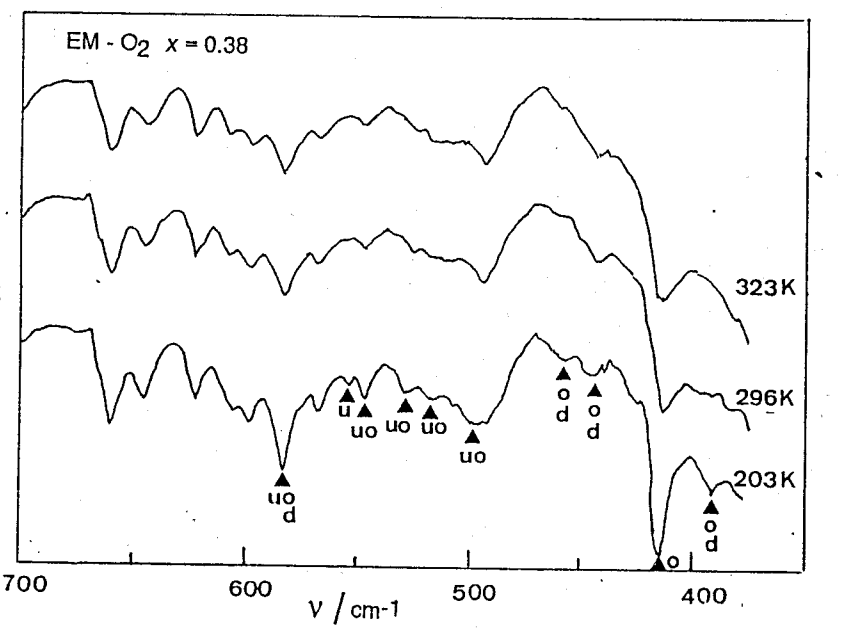

Fig.5.17b' Infrared spectra (350-700cm^{-1} and 900-1300cm^{-1}) of the EM-O_2 system with x=0.38 at 203K, 296K and 323K. Triangles and the marks "o" and "d" have the same meanings as in Fig.5.17a.

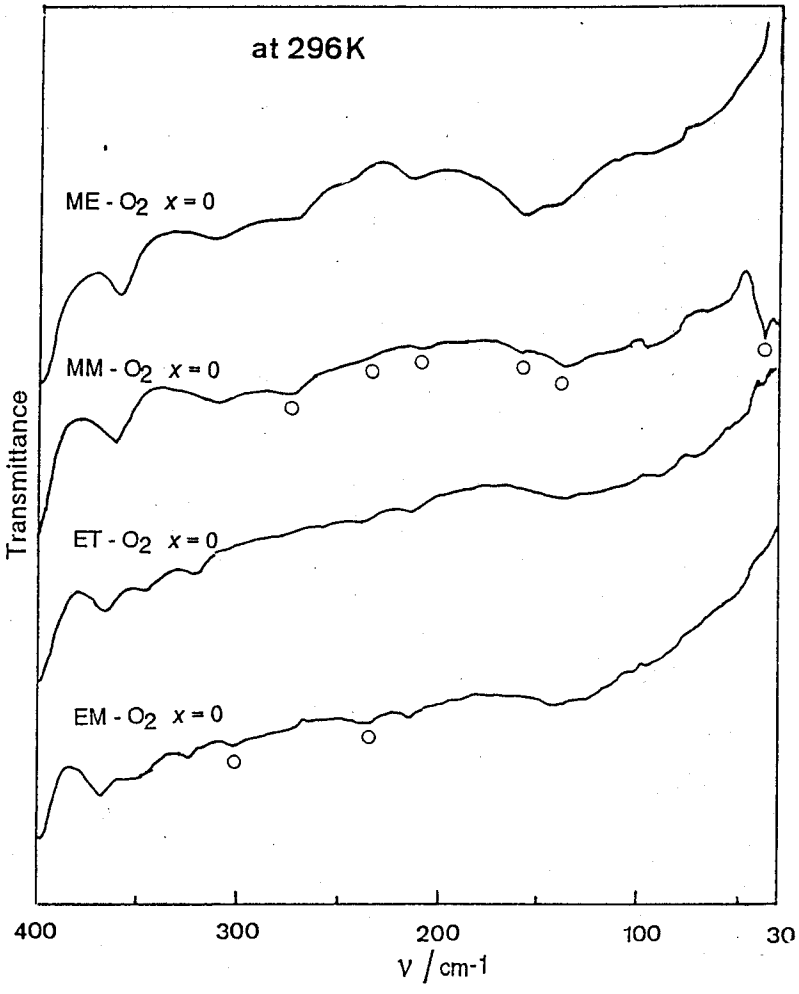

Fig.5.18 Far infrared spectra (30-400cm^{-1}) at 296K of unoxygenated ME, MM, ET and EM. Open circles on MM and EM indicate the peaks with wave numbers different from those of ME and ET, respectively.

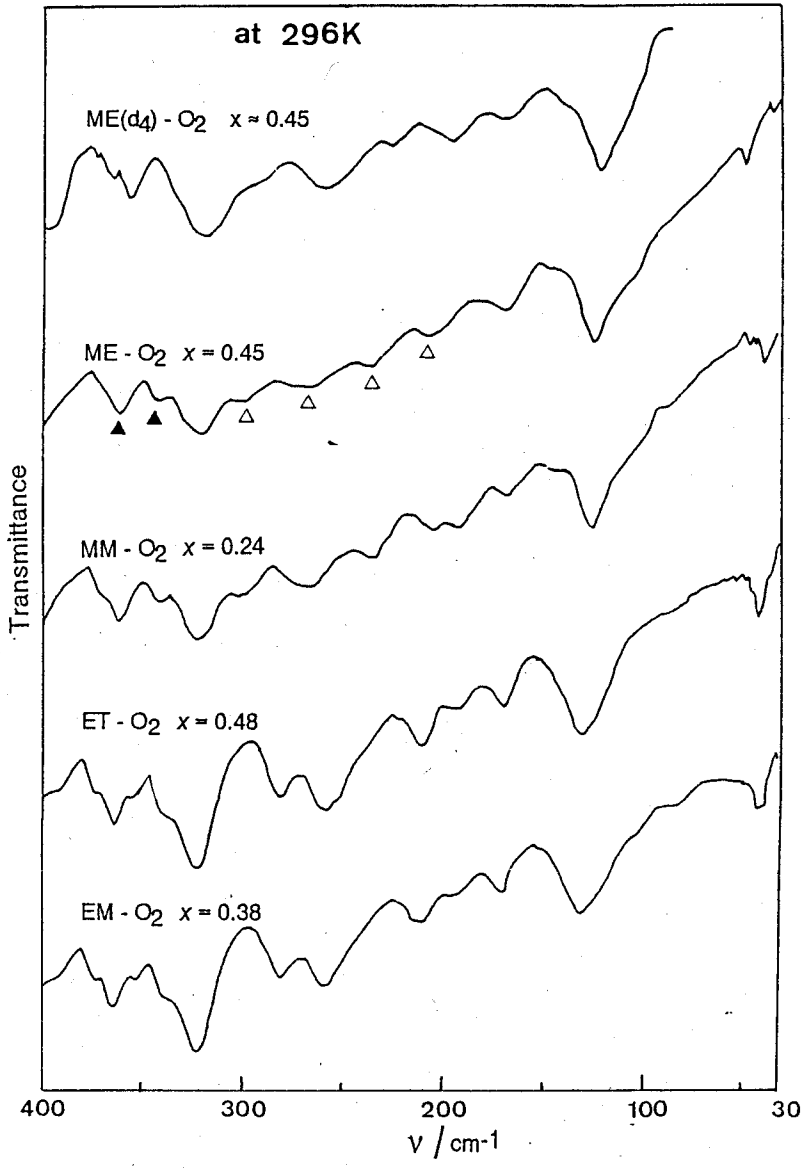

Fig.5.19 Far infrared spectra (30-400cm^{-1}) at 296K of oxygenated ME, MM, ET and EM and [Co(3-MeO-SALEN-d$_4$)](O$_2$)$_{0.45}$. Triangles on the spectrum of the oxygenated ME indicate the peaks with wave numbers different from that of its deutelated sample.

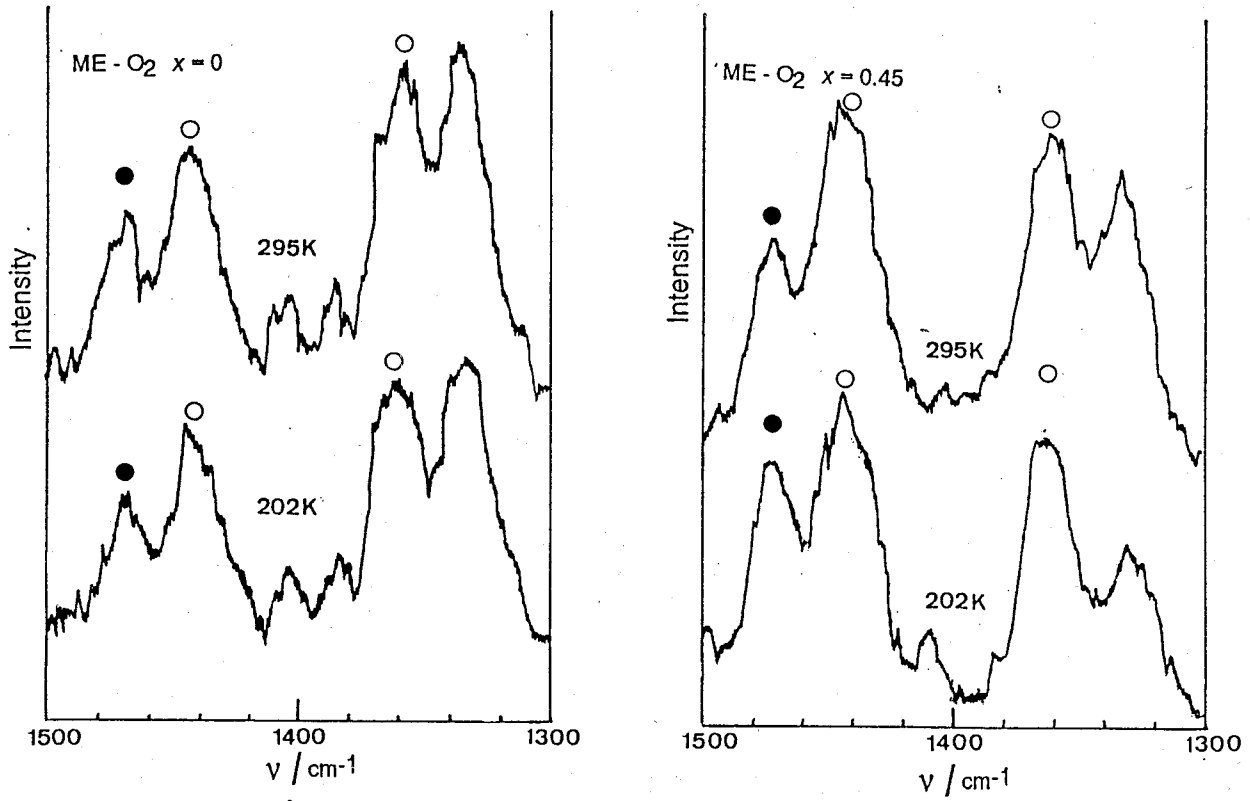

Fig.5.20a Temperature dependence of Raman spectra (1300-1500cm^{-1}) of the ME-O_2 system. Left side : x=0, and right : x=0.45. The peaks with circles indicated isotope shift by deuteration at the ethylene bridge as shown in Fig5.20c.

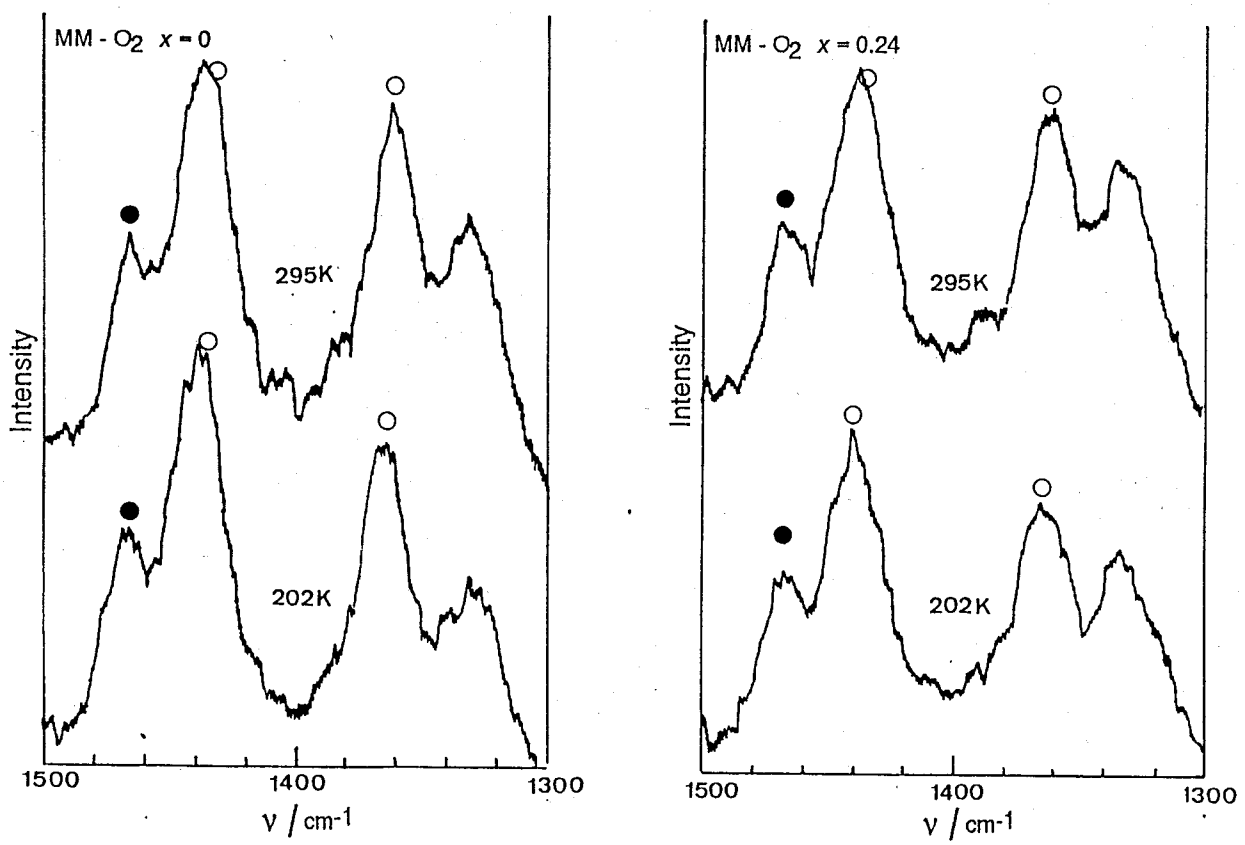

Fig.5.20b Temperature dependence of Raman spectra (1300-1500cm^{-1}) of the MM-O_2 system. Left side : x=0, and right : x=0.24. The meaning of the circles in this figure is the same as in Fig.5.20a.

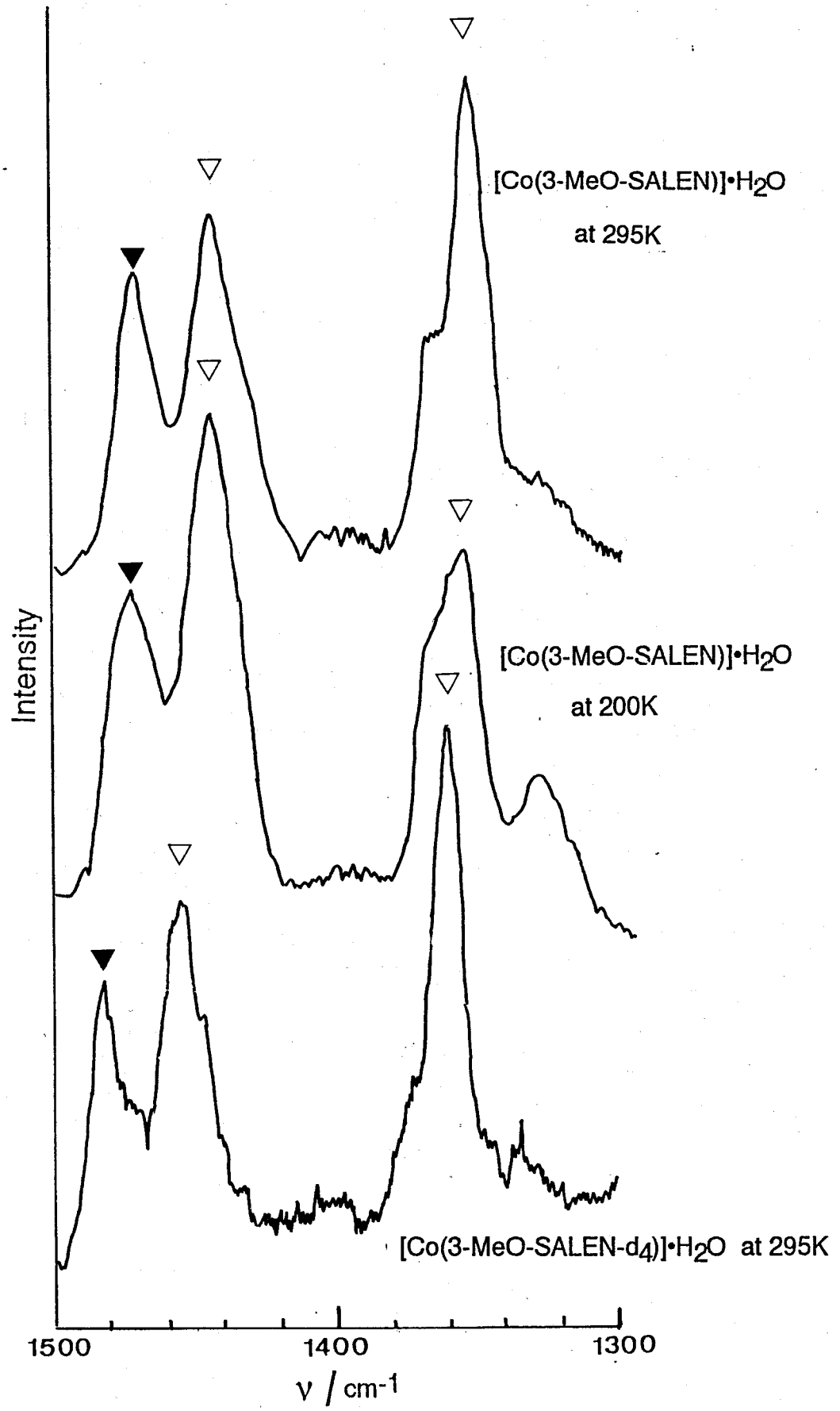

Fig.5.20c Temperature dependence of Raman spectra (1300-1500cm^{-1}) of [Co(3-MeO-SALEN)]H_2O and spectrum of [Co(3-MeO-SALEN-d_4)]H_2O at 296K.

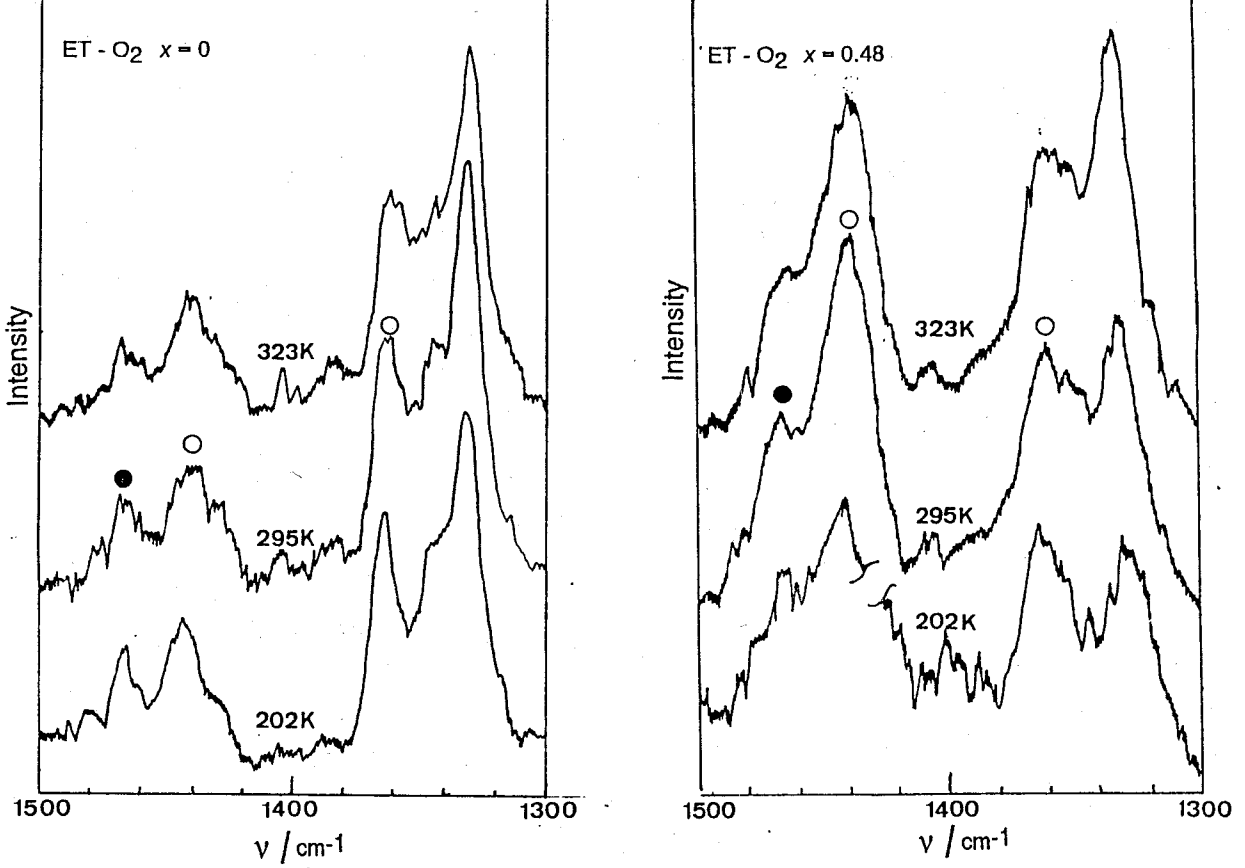

Fig.5.21a Temperature dependence of Raman spectra (1300-1500cm^{-1}) of the ET-O_2 system. Left side : x=0, and right : x=0.48. The meaning of the circles in this figure is the same as in Fig.5.20a.

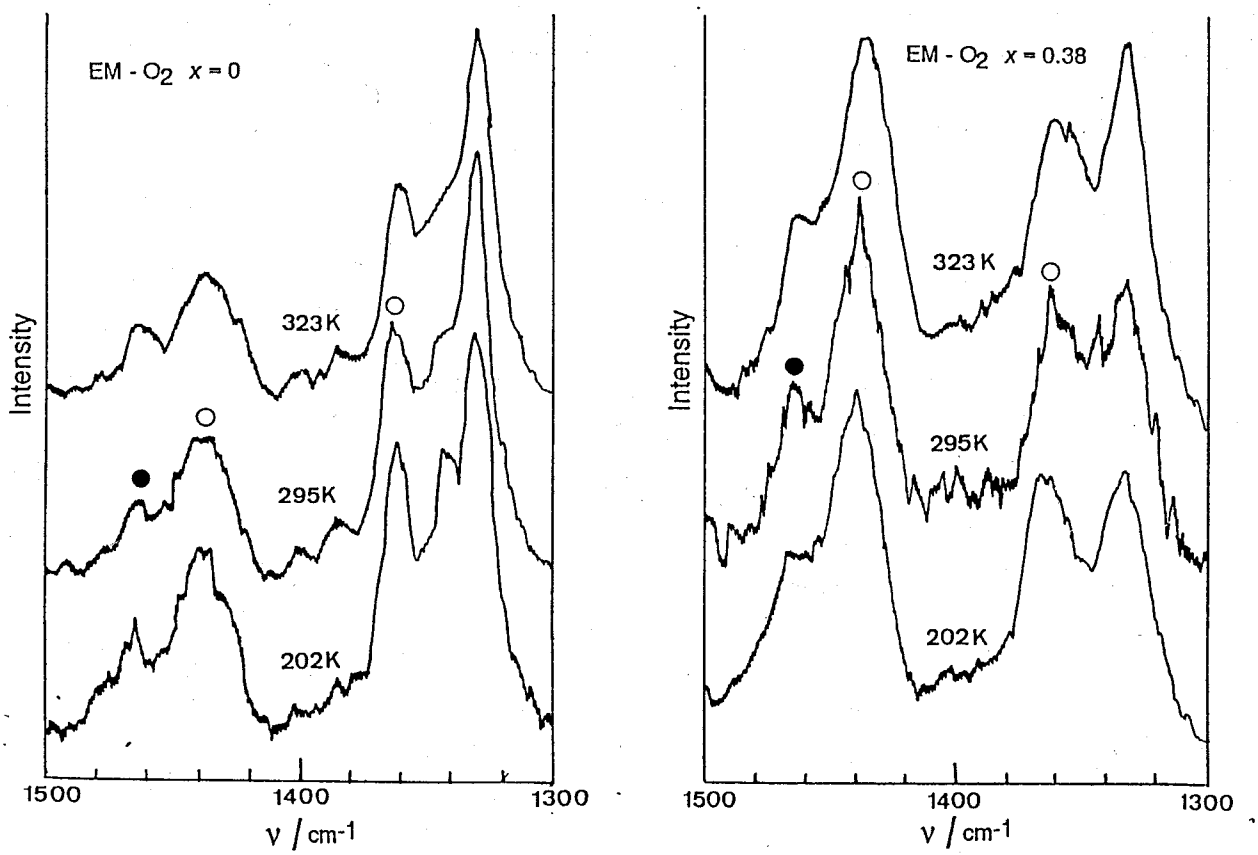

Fig.5.21b Temperature dependence of Raman spectra (1300-1500cm^{-1}) of the EM-O_2 system. Left side : x=0, and right : x=0.38. The meaning of the circles in this figure is the same as in Fig.5.20a.

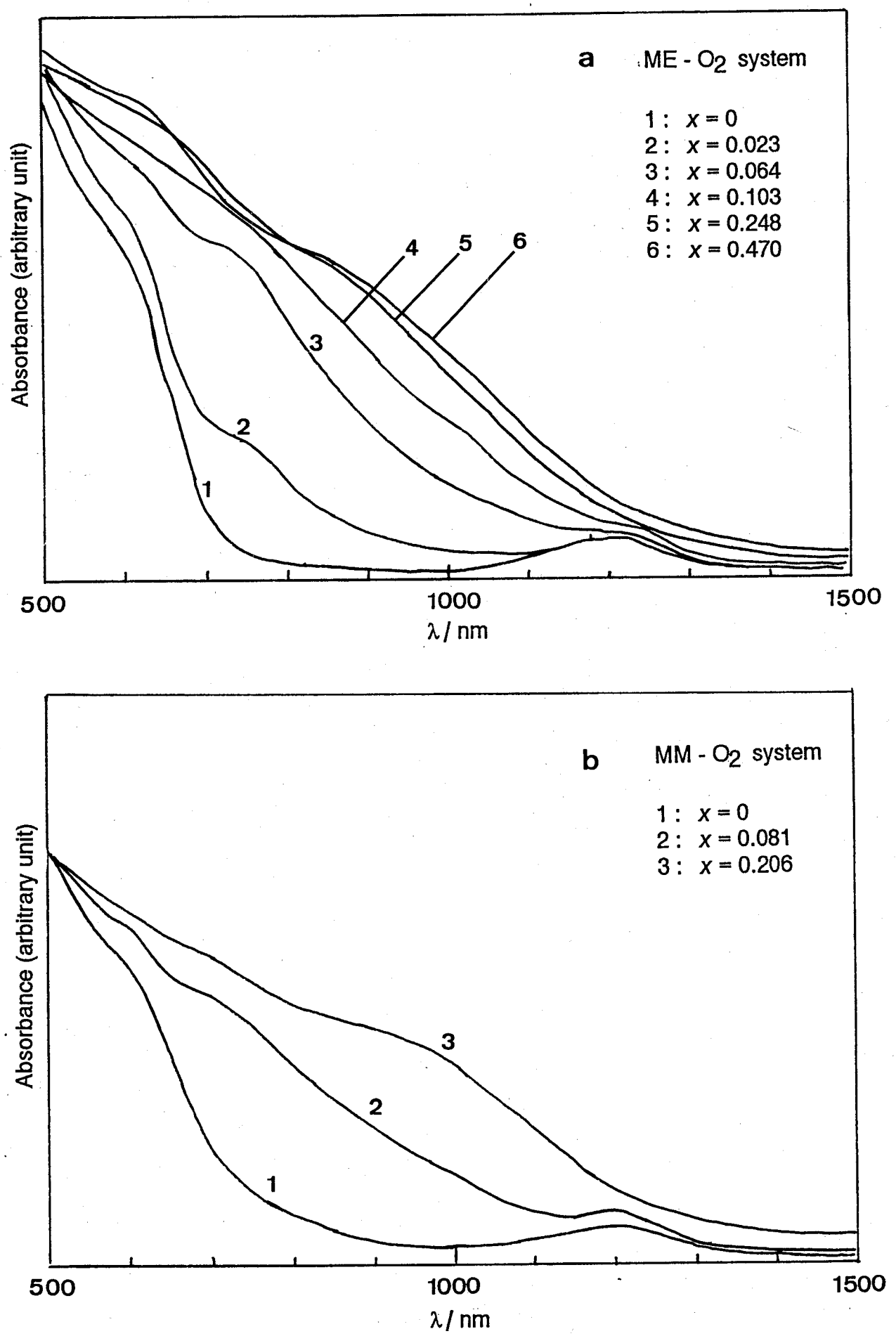

Fig.5.22 Diffuse reflectance spectra of the ME-O_2 (a) and MM-O_2 (b) systems at various dooxygen contents at 296K.

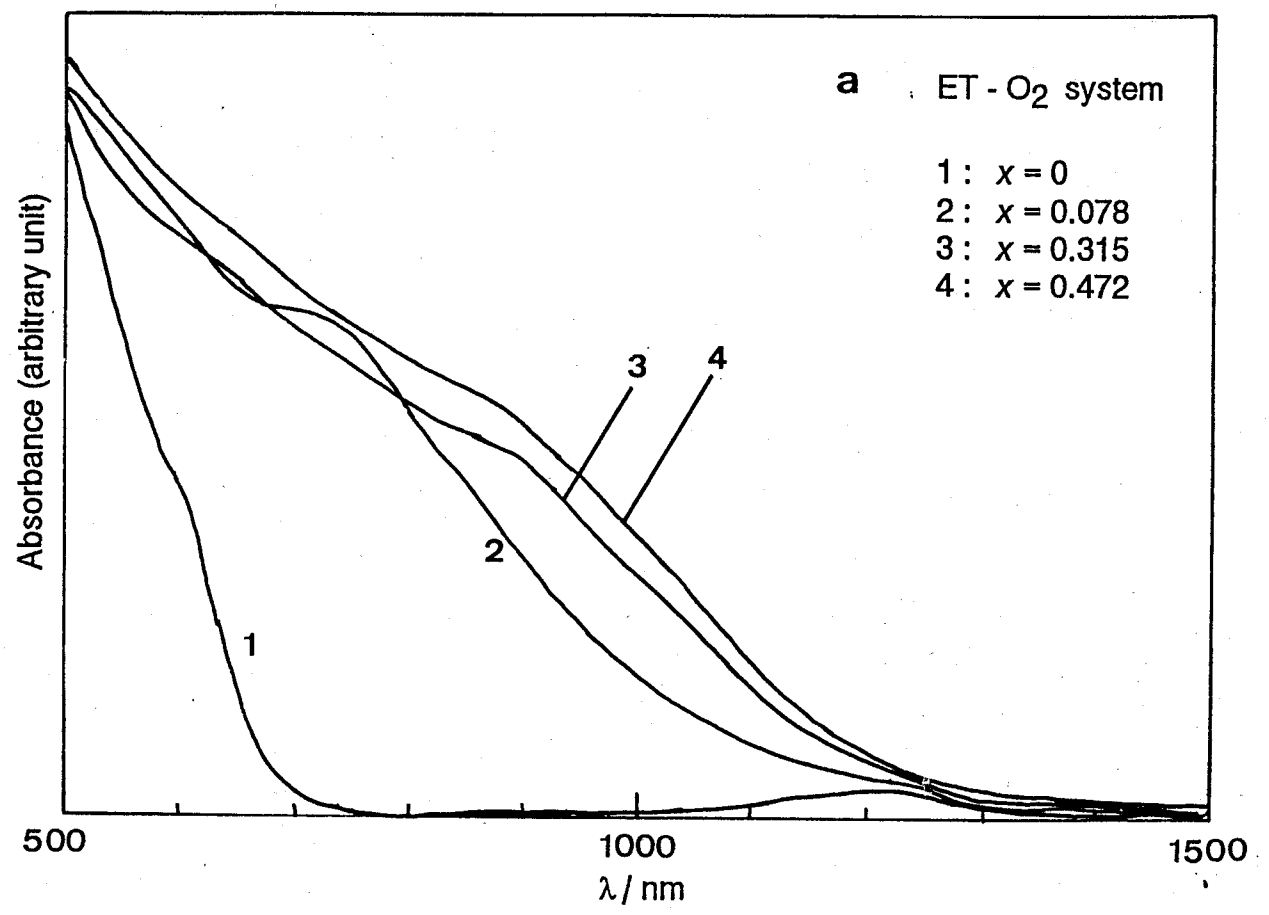

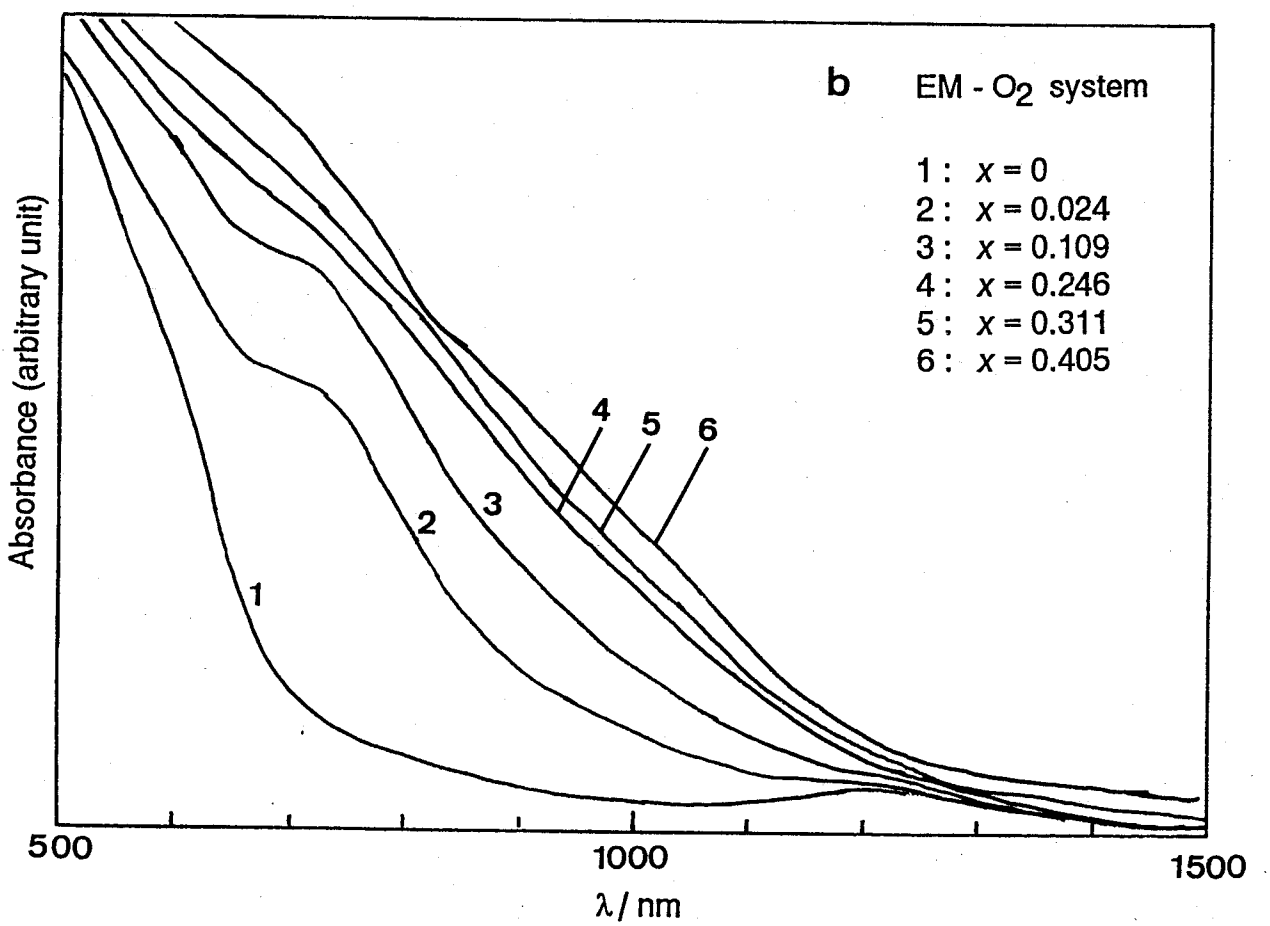

Fig.5.23 Diffuse reflectance spectra of the ET-O_2 (a) and EM-O_2 (b) systems at various dioxygen contents at 296K.

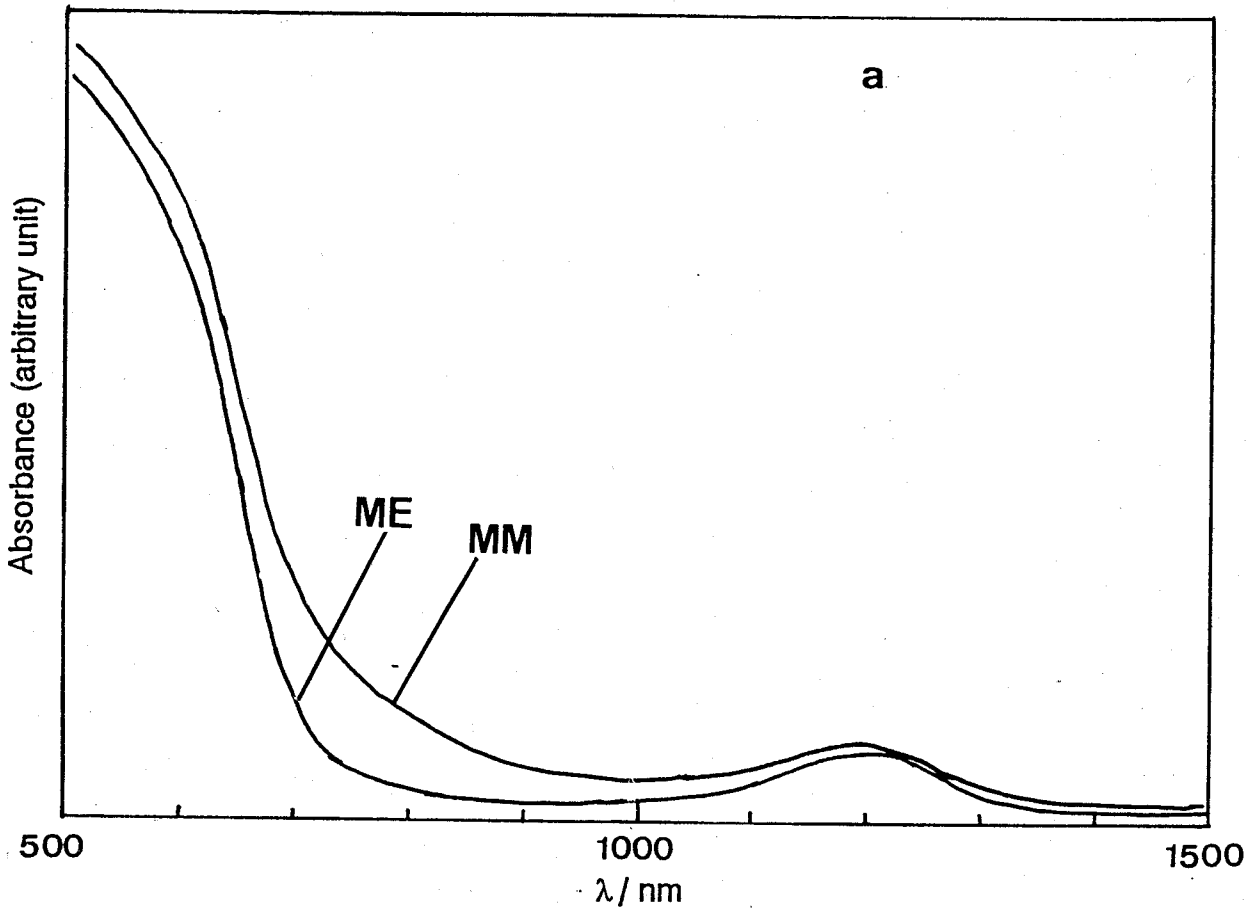

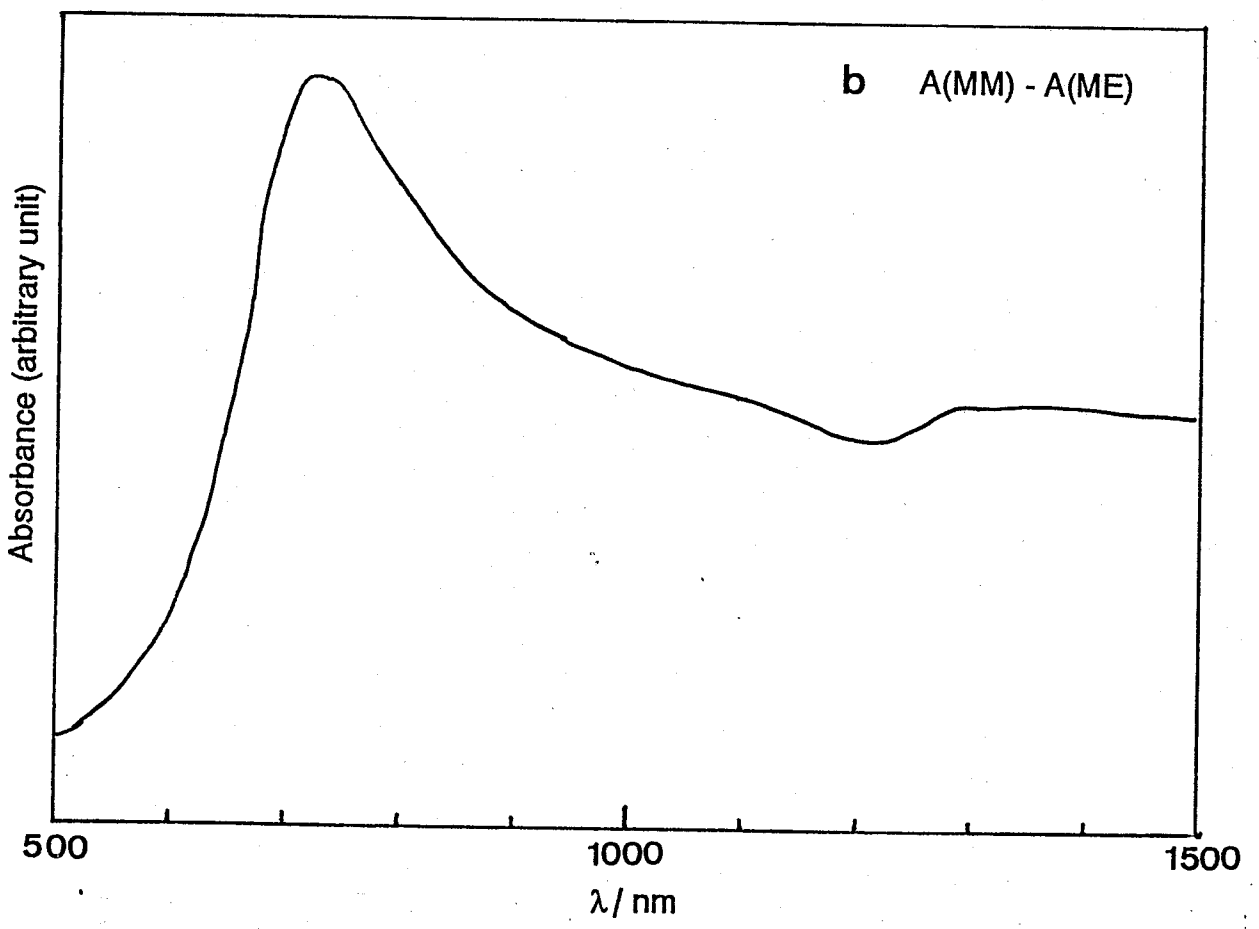

Fig.5.24 a: Comparison of diffuse reflectance spectra of ME and MM. b: the difference spectrum between MM and ME.

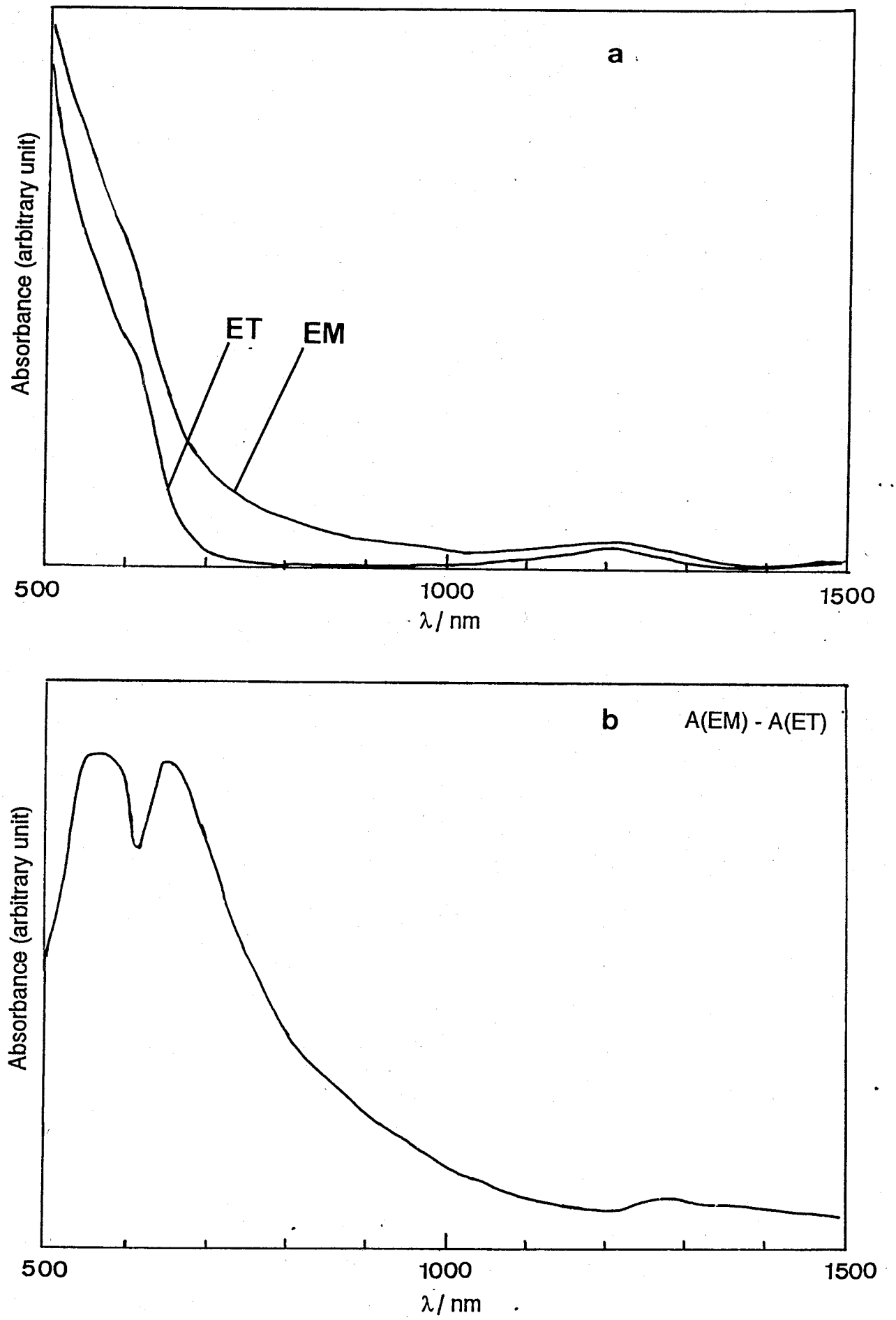

Fig.5.25 a: Comparison of diffuse reflectance spectra of ET and EM. b: the difference spectrum between EM and ET.

5.3 Discussion

5.3.1 Distribution of Dioxygens

As described in section 5.2.3, the magnetic susceptibility of paramagnetic species, $X_m/(1-2x)$, in the ME-O_2, MM-O_2, ET-O_2 and EM-O_2 systems linearly increases as a function of $\{x/(1-x)\}^2$ which is the probability with which both of two complexes adjacent to a unoxygenated complex in a column are oxygenated (Fig.5.11) and its magnetic moment is increased by interaction from both sides. Furthermore, the magnetic moments of an unoxygenated complex molecule located between the oxygenated ones with different x values, μ_H, agreed well each other above 200 K as shown in Fig.5.14 and 5.15. μ_H for the samples with different x values would show different temperature dependence and then μ_H vs. T plots would not coincide with each other over a finite temperature range, if the sample did not obey the model described here and in section 5.2.3 where μ_H at a given temperature is independent of x. Therefore the model is considered to be valid for the systems of interest. This also means that unoxygenated complexes and dimerized complex molecules with a dioxygen bridge should be uniformly distributed in the systems, because the linearity in $X_m/(1-2x)$ vs. $\{x/(1-x)\}^2$ plots is based on the assuming of random arrangement. The present model also states that dioxygen moieties are distributed over intermolecular gaps formed by complex molecules arranged like a column. Therefore the linearity in the real systems seen in Fig.5.12 and 5.13 suggests the random distribution of dioxygen moieties over their sites in the systems.

5.3.2 Cooperativity in [Co(3-RO-SALEN)] (R=CH_3, C_2H_5) - O_2 Systems

To start with, partial molar entropy of distribution based on the model given in the last section are derived. A system which consists of N complex molecules and $2xN$ with dioxygen moieties bonded to them is considered, where x is the dioxygen content or the ratio of number of dioxygen moieties to that of complex molecules and a dioxygen bonds to a couple of the complex molecules. In the system, there are $(1-2xN)$ unoxygenated complex molecules and xN of the oxygenated species which have the complex-O_2-complex structure, and the total number of molecules of both species is $(1-x)N$. Therefore entropy of distribution of the system are calculated as the entropy of mixing of the two kinds of species, which is given by eq.5.2:

$$S_{dis} = kN \ln \frac{\{(1-x)N\}!}{\{xN\}! \cdot \{(1-2x)N\}!} \quad , \qquad \text{(eq.5.2)}$$

where k is the Boltzmann constant. Using Stirling's relation, the entropy is written approximately as follows:

$$S_{dis} = kN\{(1-x)\ln(1-x) - x\ln x - (1-2x)\ln(1-2x)\} \quad . \qquad \text{(eq.5.3)}$$

The partial molar entropy of distribution of dioxygen moieties in the present system is derived from eq.5.3 as follows:

$$\bar{S}_{dis} = R \ln \frac{(1-2x)^2}{x\ (1-x)} \quad , \qquad \text{(eq.5.4)}$$

where R is the gas constant.

Since the distribution of dioxygen moieties in all the systems under study is described well by the random mixing of unoxygenated and oxygenated complex molecules as shown in the previous section, excess partial molar Gibbs energies, $\Delta_r\bar{G}^E$, are

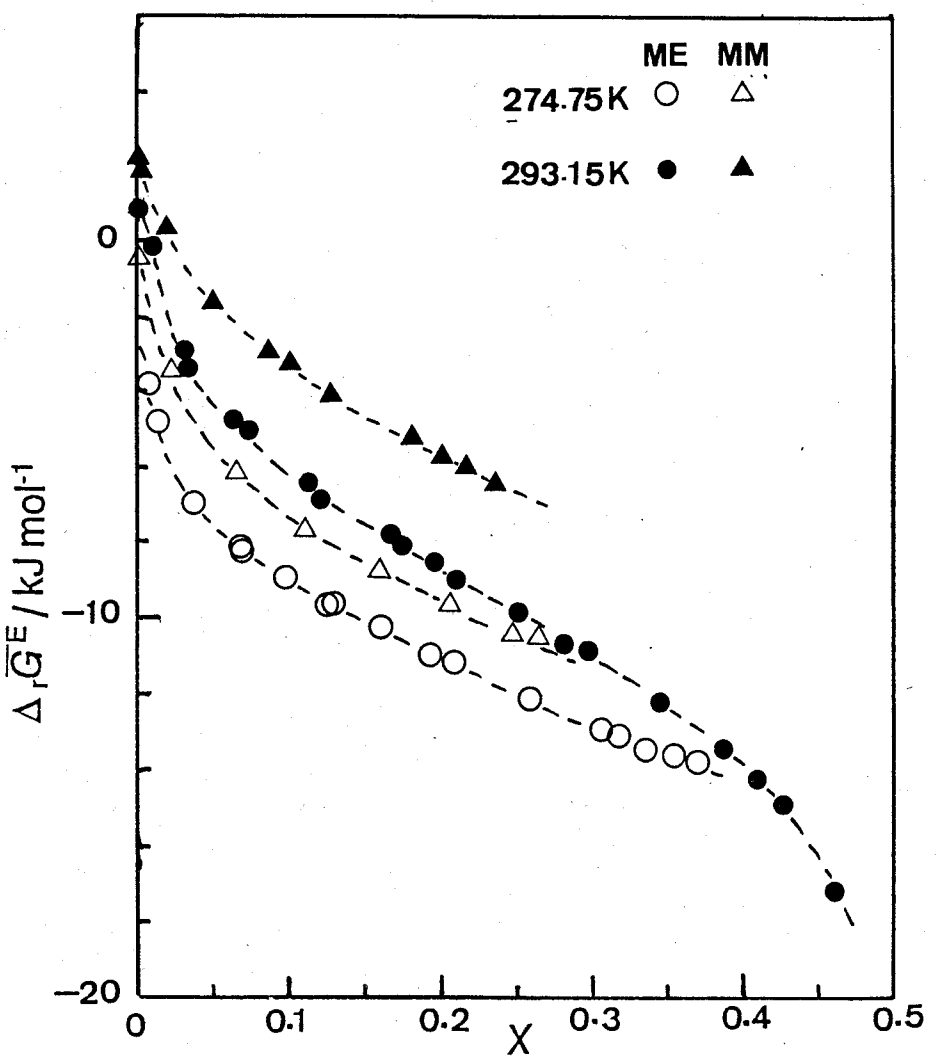

Fig.5.26 Excess partial molar Gibbs energy of the ME-O_2 (circles) and MM-O_2 (triangles) systems at 274.75K (open marks) and 293.15K (filled marks). Broken lines are drawn for the eye.

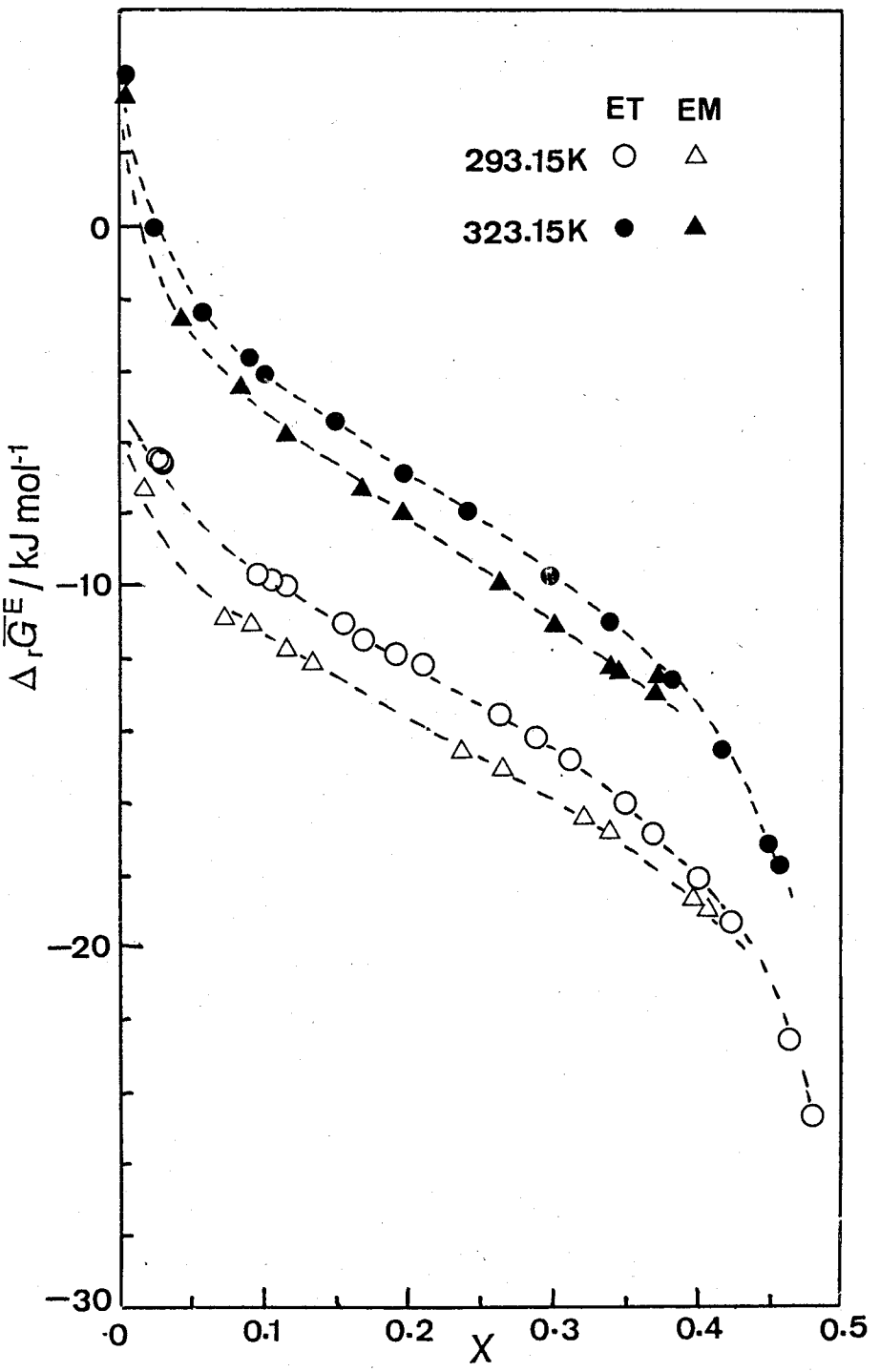

Fig.5.27 Excess partial molar Gibbs energy of the ET-O_2 (circles) and EM-O_2 (triangles) systems at 293.15K (open marks) and 323.15K (filled marks). Broken lines are drawn for the eye.

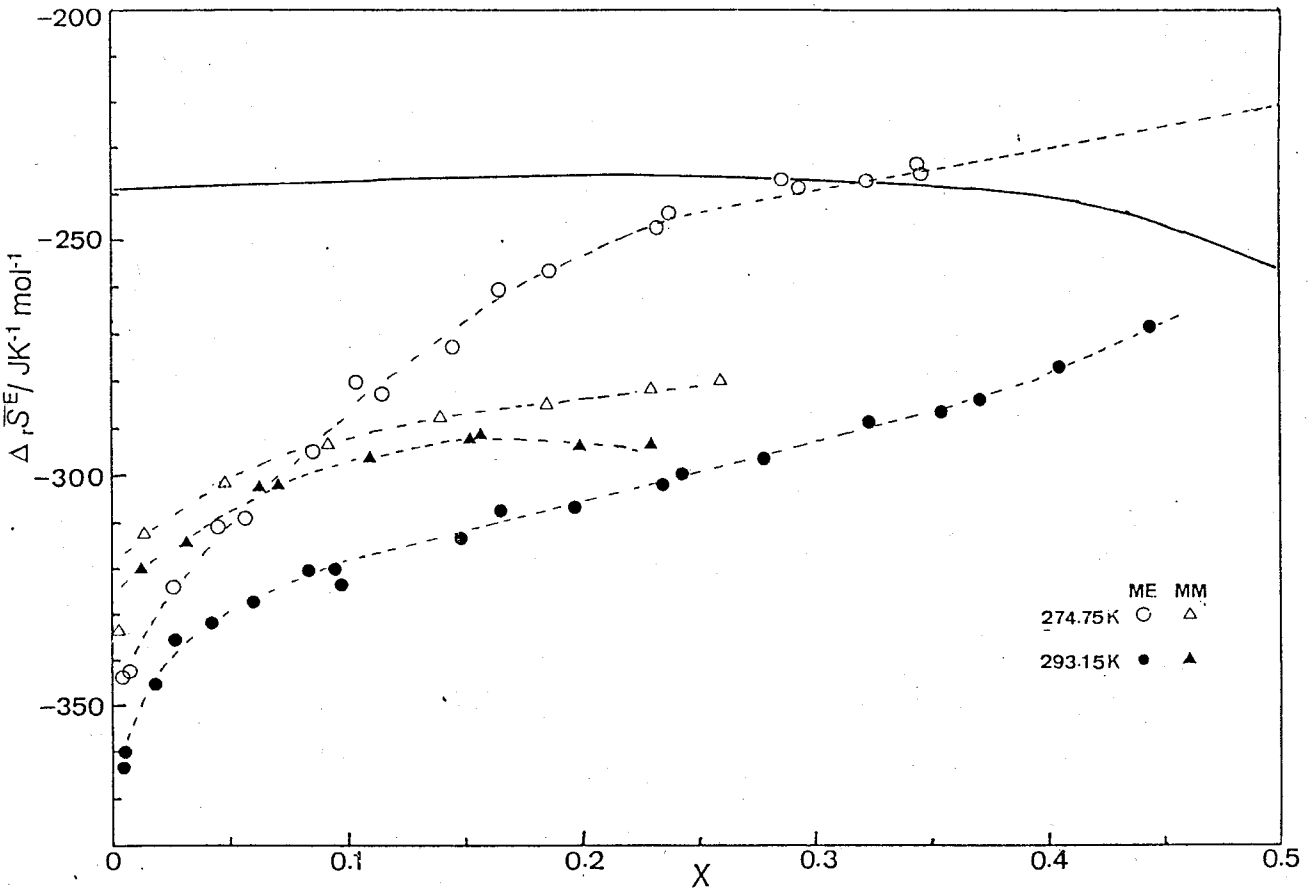

Fig.5.28 Excess partial molar entropy of the ME-O_2 (circles) and MM-O_2 (triangles) systems at 274.75K (open marks) and 293.15K (filled marks). Broken lines are shown for the eye. The solid curve shows the estimated value (see text).

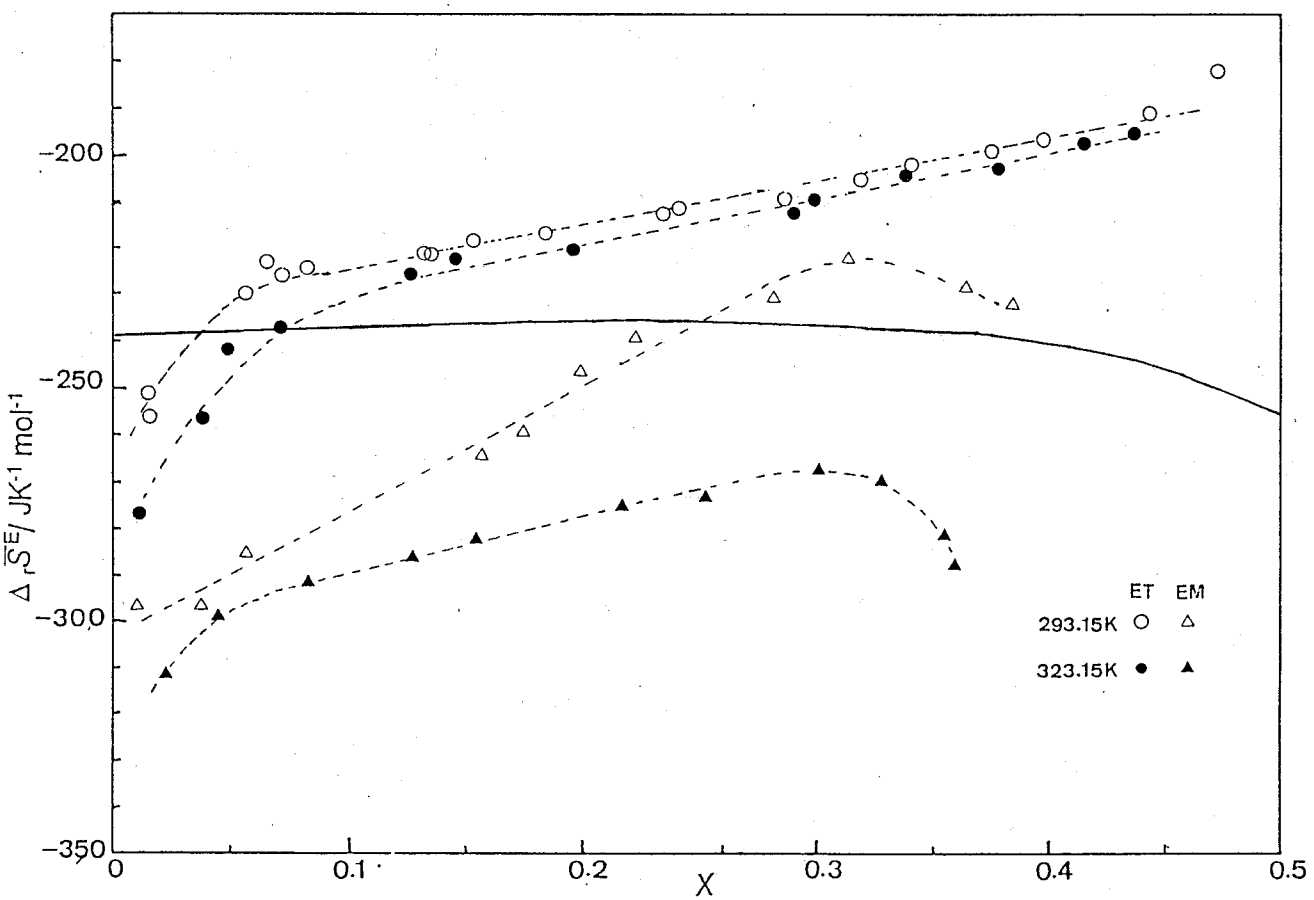

Fig.5.29 Excess partial molar entropy of the ET-O_2 (circles) and EM-O_2 (triangles) systems at 293.15K (open marks) and 323.15K (filled marks). Broken lines are shown for the eye. The solid curve shows the estimated value (see text).

obtained by subtracting partial molar Gibbs energy, $\bar{G}_{dis}$, of distribution (eq.5.5) from partial molar Gibbs energy of oxygenation, and shown in Fig.5.26 and 5.27.

$$\bar{G}_{dis} = -RT \ln \frac{(1-2x)^2}{x\ (1-x)} \quad . \qquad \text{(eq.5.5)}$$

Excess partial molar entropy, $\Delta_r\bar{S}^E$, is also calculated by subtracting eq.5.4 from partial molar entropy of oxygenation (Fig.5.4) as shown in Fig.5.28 and 5.29. These figures show the existence of cooperativity in the systems of interest, because all of the excess partial molar Gibbs energies decrease with the increase in dioxygen content x.

As a next step, cooperativity in the ET-O_2 system is considered. The fact that the partial molar enthalpy for the system is independent of dioxygen content for the system with $x>0.1$ shows that the cooperativity arises from an entropy term of the Gibbs energy. In fact, since excess partial molar entropy of the system (Fig.5.29) increased with increase in x, the partial molar Gibbs energy will be decreased by increasing x.

Partial molar enthalpy and entropy arising from volume expansion results in a similar contribution to the partial molar Gibbs energy at room temperature as discussed in chapter 3, while appreciable dioxygen content dependence was observed only for the excess partial molar entropy. Thus cooperativity in the entropy term of the ET-O_2 system is also attributable to the effect of linkage formation between an adjacent couple of complex molecules by a dioxygen moiety to the lattice spectrum as discussed in chapter 3 and 4. In addition, the distribution of dioxygen for this system would correspond to model B' in chapter 4, because

cooperativity was observed in the model. In this model, an interaction between oxygenated complex molecules and the neighboring one is required. Such interaction is suggested by the facts that high spin species are formed with increasing x (Figs.5.9 and 5.10), and that an appreciable increase in the absorbance at about 720nm are attributable to unoxygenated complexes interacting with the environment was found by adding a small amount of dioxygen gas ($x<0.2$) as shown in Fig.5.22 and 5.23 and section 5.2.6.

The ME-O_2, MM-O_2, ET-O_2 and EM-O_2 systems indicated similar composition dependence of excess partial molar Gibbs energy as shown in Figs.5.26 and 5.27, although partial molar enthalpies (Fig.5.3) and entropies (Fig.5.4) of those systems exhibited various composition dependence. This fact suggests that dioxygen content dependences of enthalpy and entropy compensate each other, and that only the cooperative interaction is observed. In analogy with the ET-O_2 system, the cooperativity in the ME-O_2, MM-O_2 and EM-O_2 systems would result from the dimerization of complex molecules by dioxygens.

5.3.3 An Estimation of Excess Partial Molar Entropy of Oxygenation for [Co(3-RO-SALEN)](R=CH_3, C_2H_5)-O_2 Systems

Generally the majority of excess partial molar entropy for a gas-solid reaction system results from loss of translational and rotational entropy of the gas phase, S_{trans} and S_{rot} (>0). Other minor contributions in the [Co(3-RO-SALEN)](R=CH_3, C_2H_5)-O_2 reaction systems can be divided into the following terms: disappearance of entropy of electronic spin multiplicity of dioxygens and unoxygenated cobalt ions, Co^{2+}, by oxygenation;

$\Delta_r\bar{S}_{spin}$, change in entropy of lattice vibration; $\Delta_r\bar{S}_{lattice}$, and that of intramolecular vibrational modes; $\Delta_r\bar{S}_{vib}$.

S_{trans} and S_{rot} can be calculated by statistical mechanics as follows[5]:

$$S_{trans} = R\left[\frac{5}{2} + \ln\left\{\left(\frac{2\pi mkT}{h^2}\right)^{3/2}\frac{V}{N_A}\right\}\right], \qquad \text{(eq.5.6)}$$

and

$$S_{rot} = R\left\{1 + \ln\frac{8\pi^2 IkT}{\sigma h^2}\right\}, \qquad \text{(eq.5.7)}$$

where T is the temperature of the system, R is the gas constant, k is the Boltzmann constant, h is the Plank constant, N_A is the Avogadoro constant, m is the mass of dioxygen (5.315×10^{-26} kg), V is the molar volume of dioxygen gas ($0.0224\times T/273$ m^3), I is the moment of inertia of an dioxygen (1.936×10-46 kgm^2) and σ=2 is the number of rotational degree of freedom.

In the present reaction systems, the reaction product of the systems is diamagnetic (see section 5.2.3 and reference 5, while the spin state of an dioxygen is triplet and that of a low-spin Co^{2+} ion of the unoxygenated complex is doublet.[5,6] Since an dioxygen reacts with two Co^{2+} ions, the entropy change by oxygenation is evaluated as $-(R\ln3 + 2R\ln2)$. In addition, since the species with higher magnetic susceptibility, X_H, are formed in the systems as described in section 5.2.3, the contribution from formation and disappearance of the species with X_H to $\Delta_r\bar{S}_{spin}$, $\Delta_r\bar{S}_{HL}$, should be taken into account. Since the probability of forming the species with X_H is $\{x/(1-x)\}^2$, the mole fraction of complex molecules with X_H is given by

$(1-2x)\{x/(1-x)\}^2$. Assuming quartet spin state for the species for simplicity, the contribution is expressed as follows:

$$\Delta_r \bar{S}_{HL} = \frac{\partial}{\partial x}\left\{(1-2x)\left(\frac{x}{1-x}\right)^2 (R\ln 4 - R\ln 2)\right\}$$
$$= \left\{\frac{x}{(1-x)^2}\cdot\left(\frac{1-2x}{1-x}\right) - (1-2x)\left(\frac{x}{1-x}\right)^2\right\}\cdot R\ln 2 \quad . \qquad \text{(eq.5.8)}$$

The magnetic moment of the species with X_H for the ME-O_2 system at 291.1K shown in Table 5.4, 2.96μ_B, is close to the value for triplet spin state, 2.83μ_B. However eq.5.8 was used for $\Delta_r\bar{S}_{HL}$ of the system, because triplet and quartet spin states have similar entropies, 9.1 $JK^{-1}mol^{-1}$ and 11.5 $JK^{-1}mol^{-1}$, respectively. Thus, for simplicity, the partial molar entropy related to change in spin multiplicity is given as follows:

$$\Delta_r \bar{S}_{spin} = -R(\ln 3 + 2\ln 2) + \Delta_r \bar{S}_{HL} \quad . \qquad \text{(eq.5.9)}$$

Assignments of intramolecular vibrational modes below 700cm^{-1} of which shifts significantly contribute to the entropy are not clear. However, no temperature dependence of wave numbers of the peaks in the region was observed for the unoxygenated and oxygenated samples of the ME-O_2 (Figs.5.16a and a') and EM-O_2 (Figs.5.17b and b') systems, although those systems exhibited considerable temperature and dioxygen content dependences of the thermodynamic quantities as shown in Figs.5.3 and 5.4. No considerable difference in wave numbers of infrared vibrations between the ME-O_2 and MM-O_2 systems, and between the ET-O_2 and EM-O_2 systems, as shown in Figs.5.16, 5.17, 5.18 and 5.19. Therefore wide shift of the low frequency modes would not contribute to the thermodynamic quantities for the [Co(3-RO-SALEN)]-O_2 systems

significantly. Only three vibrational modes related to a dioxygen in the oxygenated [Co(SALEN)] have been reported as follows[7]; $\nu(O_2)$ = 1011 cm^{-1}, ν(CoO,sym.) = 533 cm^{-1} and ν(CoO,asym.) = 370 cm^{-1}. And the OO stretching mode of dioxygen gas is known as $\nu(O_2$ gas) = 1580 cm^{-1} [8,9]. Tentatively, entropy due to these modes, $\Delta_r\bar{S}'_{vib}$, was evaluated as Einstein oscillators as follows:

$$\Delta_r \bar{S}'_{vib} = S(\nu(O_2)) + S(\nu(CoO,sym.)) + S(\nu(CoO,asym.)) - S(\nu(O_2,gas)), \quad \text{(eq.5.10)}$$

where

$$S(\nu(x)) = R\left\{\frac{u\exp(-u)}{1-\exp(-u)} - \ln(1-\exp(-u))\right\}, \quad \text{(eq.5.11)}$$

and $u = hc\nu/kT$.

The partial molar entropy arising from the change of the lattice vibration, $\Delta_r\bar{S}_{lattice}$, is unknown, but may be considered to be a large negative value due to linkage formation between two complex molecules with a dioxygen in the oxygenation reaction. Since both of the [Co(SALEN)]-O_2 systems did not show appreciable shift of absorption bands in the infrared spectra in their nonstoichiometric regions as described in section 3.2.4, the contribution from intramolecular vibrational modes is expected to be minor. Thus eq.5.12 is the least negative estimation of the magnitude of $\Delta_r\bar{S}'_{lattice}$ for the [Co(3-RO-SALEN)]-O_2 systems:

$$\Delta_r \bar{S}'_{lattice} = \Delta_r \bar{S}^E([Co(SALEN)], x\rightarrow 0.5) - \{\Delta_r \bar{S}'_{vib} - R(\ln 3 + 2\ln 2)\}, \quad \text{(eq.5.12)}$$

where $\Delta_r\bar{S}^E$([Co(SALEN)], $x\rightarrow$0.5), -238 $JK^{-1}mol^{-1}$, is the excess partial molar entropies of the [Co(SALEN)]-O_2 (SP-O_2 and SC-O_2) systems extrapolated to x=0.5, the first term in the braces is the change in the entropy arising from streching vibration related to dioxygen moieties given by eq.5.10, and the second

term in the braces arises from the loss of spin multiplicity of two cobalt ions (S=1/2) and an dioxygen (S=1). This lattice term, $\Delta_r\bar{S}'_{lattice}$, includes the minor contribution from change in the frequency of the intramolecular vibrations of [Co(SALEN)] by oxygenation effectively, according to the estimation.

An estimation of excess partial molar entropy of oxygenation for 1 mol of dioxygen, $\Delta_r\bar{S}^{E'}$, may be given by eq.5.13:

$$\Delta_r \bar{S}^{E'} = (-S_{trans} - S_{rot}) + \Delta_r \bar{S}'_{vib} + \Delta_r \bar{S}'_{lattice} + \Delta_r \bar{S}_{spin} . \qquad \text{(eq.5.13)}$$

Eq.5.13 is considered to be an estimation of the least negative value of magnitude of the whole excess partial molar entropy, because the term, $\Delta_r\bar{S}'_{lattice}$, is the least negative estimation. Eq.5.13 is valid, if the case where excitations of new intramolecular motions do not take place.

The excess partial molar entropies at 274.75 K and at 293.15 K estimated by eq.5.13 are shown by solid curves in Fig.5.28 and Fig.5.29, respectively. The components of the estimated values at x=0.3 and the experimental values in Fig.5.28 and Fig.5.29 at x=0.3 are shown in Fig.5.30. The estimated values are lower in magnitude than the experimental one for the ET-O_2(at 293.15 K and 323.15 K) and ME-O_2 (at 274.75 K) systems. This fact is in conflict with eq.5.13 as the estimation of the most negative whole partial molar entropy. Therefore positive contributions to the partial molar entropy must be taken into account. Since the [Co(3-RO-SALEN)] (R=CH_3 or C_2H_5) molecule has many degrees of freedom of intramolecular motion such as out-of-plane vibration of the chlate skeleton and hindered lotation of the alkoxy groups, excitation of those intramolecular motions is expected as a possible origin. Disordered structure for the ethylene bridge

in [Co(3-MeO-SALEN)]H_2O[10] suggests possility of contribution from such intramolecular motions for the present reaction systems.

In the following sections, intramolecular motions of the complex molecules and contribution from them to partial molar thermodynamic quantities are discussed.

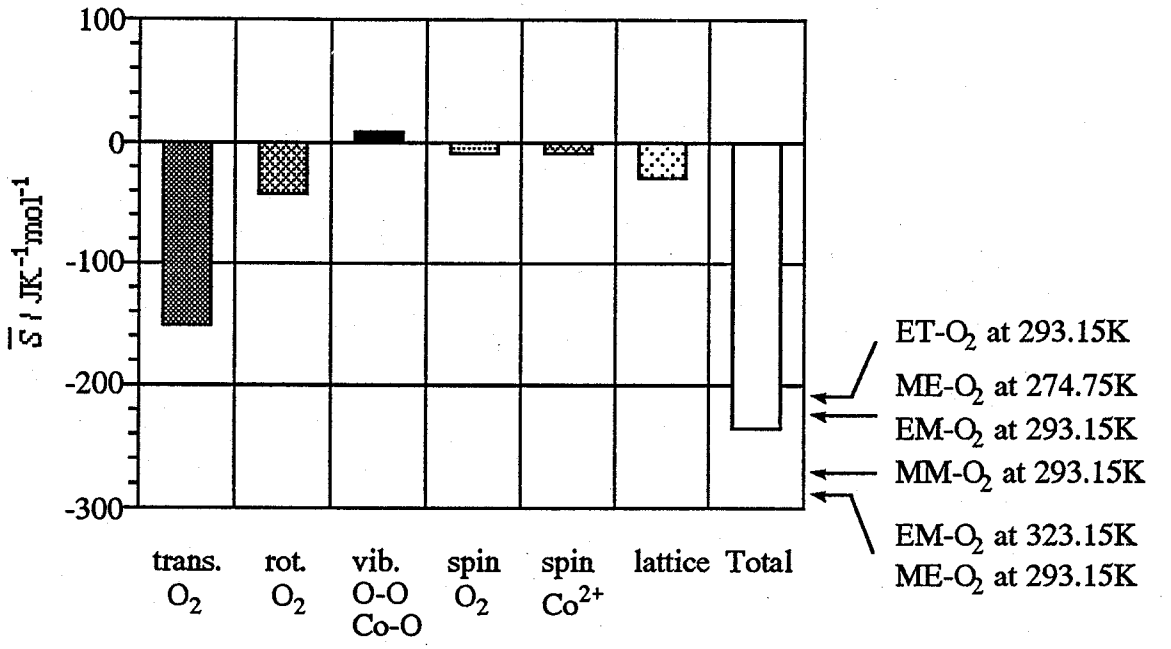

Fig.5.30 Total excess partial molar entropy at 293.15 K and x=0.3 (white bar) and contributions to it. The bars with the terms, "trans. O_2" and "rot. O_2", show the contributions from the traslational and rotational motions of dioxygens given by eq.5.6 and eq.5.7, respectively. The bar with the term, "vib. O-O Co-O", shows that from the vibrations of the O-O and Co-O bonds given by eq.5.10. The bars with the terms, "spin O_2" and "spin Co^{2+}", show those from spin multiplicities of dioxygens and Co^{2+} ions. The spin contributions is given by eq.5.9. The bar with the term, "lattice", shows that from the lattice vibration at 293.15 K and x=0.5 estimated by eq.5.12. The arrows on the right hand of this figure indicated the experimental total excess partial molar entropies of the ME-O_2 (274.75 K, 293.15 K), MM-O_2 (293.15 K), ET-O_2 (293.15 K) and EM-O_2 (293.15 K, 323.15 K) with x=0.3.

5.3.4 Thermodynamic Properties and Intramolecular Motion in [Co(3-RO-SALEN)] (R=CH_3, C_2H_5)-O_2 Systems

5.3.4.1 Outline of Thermodynamic Properties of the Present Systems.

As shown in Fig.5.3 and 5.4, partial molar enthalpy and entropy of the ME, MM, ET and EM-O_2 systems were significantly dependent on temperature T, dioxygen content x and materials. For example, the difference between minimum and maximum values in partial molar quantities for the ME-O_2 system at 274.75 K and the EM-O_2 system at 293.15 K is about 20 $kJmol^{-1}$ in enthalpy and about 60 $JK^{-1}mol^{-1}$ in entropy, while enthalpies at 293.15 K (ME-O_2) and at 323.15 K (EM-O_2) were approximately independent of dioxygen content at about -98 $kJmol^{-1}$. On the other hand, the ME-O_2 system at 293.15 K, MM-O_2, ET-O_2 and EM-O_2 at 323.15 K have a wide plateau region as shown in Fig.5.3 and 5.4, while their partial molar quantities were considerably different.

In spite of such variety in change of thermodynamic functions, their changes were similar in magnitude between the ME-O_2 and EM-O_2 systems as seen in Fig.5.3 and 5.4.. In addition, similar differences in enthalpy and entropy were observed between the plateau regions of the ME-O_2 system (at 274.75 K and 293.15 K) and the ET-O_2 and EM-O_2 systems at 323.15 K. These facts suggest that the variety should be attributed to a mechanism in common with both systems of 3-methoxy and 3-ethoxy derivatives. However, the contribution from motional excitation of alkoxy groups would be excluded, because it would depend on the alkyl chain length.

5.3.4.2 Temperature Dependence in Vibrational Spectra and Intramolecular Motion

Temperature dependence of the infrared spectra of the present systems correspond to the changes in the partial molar enthalpies and entropies. In this section, relationship between intramolecular motions and temperature dependence of their vibrational spectra and thermodynamic quantities will be discussed.

ME-O_2 system

The ME-O_2 system showed quite different composition dependence of the partial molar enthalpy between 274.75 K and 293.15 K. For the unoxygenated sample, decrease in temperature from 293K to 273 K brought about the splitting of a broad band at about 570 cm^{-1} (assigned to chelate ring deformations) and the change in transmittance for bands from 900 cm^{-1} to 1000 cm^{-1} (CH_2 deformations of the ethylene bridge) as shown in Fig.5.16a corresponding to the enthalpy change, while minor change in the spectrum between 273 K and 203 K was observed. On the other hand, sharpening of the several bands of the oxygenated sample of it was observed between 273 K and 203 K, although outstanding change was not observed between 293 K and 273 K. Since some peaks indicating temperature dependence of their line shape showed isotope shift by deuteration at the ethylene bridge, these changes is considered to be related to motions of the chelate skeleton involving the ethylene bridge.

Corresponding to those changes in the infrared spectra, the ratios of the Raman intensity at 1360 cm^{-1} to that at 1440 cm^{-1} were found to decrease by lowering temperature from 295 K to

202 K in both the unoxygenated and oxygenated samples (Table 5.5). For the monohydrate [Co(3-MeO-SALEN)]H_2O, the ratio between the Raman intensity at 1360 cm^{-1} to that at 1440 cm^{-1} also varied with temperature (Table 5.5). Furthermore, the infrared spectrum also exhibited splitting and sharpening in its several bands by lowering temperature from 296 K to 203 K as shown in Fig.5.16d. Since Calligaris *et al.* reported statistically disordered structure of the ethylene bridge at room temperature[10], the change in intensities of the Raman and infrared spectra is attributable to a change in the motional state of dynamic puckering of the ethylene bridge.

Considering these facts, motions of the chelate skeleton including the ethylene bridge is considered to be excited in the unoxygenated crystal at least above 296 K and in the oxygenated one above 273 K. Hence, at 273 K, the intramolecular motions are more excited for the oxygenated sample than for unoxygenated sample. This means that the motions are excited with adding dioxygen to the unoxygenated sample, because the partial molar quantities for the ME-O_2 system varied with dioxygen content smoothly as shown in Figs.5.2, 5.3 and 5.4. On the other hand, at 293K, the motions are considered to be excited over whole dioxygen content range ($0 \leq x \leq 0.5$).

The ratio of the Raman intensity at 1360 cm^{-1} to 1440 cm^{-1} of the oxygenated sample was smaller than that of the unoxygenated sample even at 203 K, though opposite relation in it was expected according to above discussion because the motions of the chelate skeleton of the unoxygenated sample would not be excited. This contradiction would arise from variety in the environment of the complexes in the oxygenated sample owing to its nonstoichiometry.

MM-O_2 system

For the unoxygenated and oxygenated samples of the MM-O_2 system, minor temperature dependence of the absorption bands between 350 cm^{-1} and 700 cm^{-1} and between 900 cm^{-1} and 1100 cm^{-1} (Fig.5.16b and b') were observed between 273 K and 203 K, although the spectra between 350 cm-1 and 700 cm-1 were broad. According to the discussion on the ME-O_2 system, the motions of the chelate skeleton seems to be somewhat excited above 203K for the unoxygenated and oxygenated samples. However, since outstanding difference in temperature dependence of the spectra was not observed, it is difficalt to discuss the levels of excitation of the intramolecular motions for both samples.

EM-O_2 system

For an unoxygenated sample of EM-O_2 system, the absorption bands in the metal-ligand vibration region became outstanding on decreasing temperature from 323 K to 296 K, and a band in CH_2(ethylene bridge) deformation region appeared at 932 cm^{-1}, and the band at 1107 cm^{-1} at 323 K split into two bands as shown in Fig.5.17b. On cooling from 296 K to 203 K, several bands in the region also become sharp. On the other hand, outstanding changes in the spectra of the oxygenated sample were observed between 296 K and 203 K as shown in Fig.5.17b', and spectra at 323 K and 296 K were broad and had similar shapes and transmittances. Therefore motions related to the chelate skeleton are appreciably excited between 296 K and 323 K in the unoxygenated state, and similar excitation also takes place below 296K. On the other hand, such motions are sufficiently excited above 296 K in the

oxygenated state, while they may not be excited at 203 K. Similar to the ME-O_2 system, the motions are excited with adding dioxygen to the unoxygenated sample at 296 K, while excited over whole dioxygen content range ($0 \leq x \leq 0.5$) at 323 K.

Decrease in the ratio of the Raman intensity at 1360 cm^{-1} to that at 1440 cm^{-1} and sharpening of the peak at 1470 cm^{-1} with a filled circle were observed for the unoxygenated sample by lowering temperature from 293 K to 203 K as shown in Table 5.6 and Fig.5.21b. These observation also suggest the change in motional state of the ethylene bridge. The discrepancy in temperature range between the Raman result and other observations is considered to be due to heating of the sample by laser beam.

ET-O_2 system

For the oxygenated sample, new bands appeared and some peaks became sharp in the range 350-700 cm^{-1} on cooling from 296 K to 203 K, and gave spectra (Fig.5.17a') similar to the oxygenated sample of the EM-O_2 system (Fig.5.17b'). The spectra of this region at 296 K and 323 K resemble each other, and also resemble to those of the oxygenated sample of the EM-O_2 system at the same temperature. In the region from 900-1300 cm^{-1}, appreciable change in spectra was found for the oxygenated sample on cooling from 296 K to 203 K (Fig.5.17a'), while slight changes in the spectrum were observed for the unoxygenated sample (Fig.5.17a). Therefore, in the ET-O_2 system, motions of the chelate skeleton of the complex molecules in the oxygenated sample are considered to be excited on heating from 203 K to 293 K.

Change in the vibrational spectrum of the unoxygenated sample of the ET-O_2 system (Fig.5.17a) was not appreciable compared to

that of the oxygenated sample (Fig.5.17a'), while only a few minor change in the spectrum on cooling to 203K were obserbed. In addition, the Raman scattering peak at 1470 cm^{-1} related to CH_2 deformation of the unoxygenated sample (Fig.5.21a) was sharper at 323 K and 293 K than that of the EM-O_2 system in which the motions are excited at 323 K. Thus, according to the discussion for the other systems, the motions of the chelate skeleton seems to be excited scarecely within measured temperature range.

Consequently, the motions of the chelate ringe skeleton at 296 K and 323 K are more excited for the oxygenated sample than for the unoxygenated one. Therefore, the motions of the chelate ringe skeleton are considered to be excited with adding dioxygen to the unoxygenated sample at both 296 K and 323 K.

5.3.4.3 Temperature and Dioxygen Content Dependence of Partial Molar Enthalpy and Entropy

As shown in the foregoing section, temperature dependence of the partial molar enthalpy and entropy of the studied systems corresponds to change in the motional state of the chelate skeleton. Excitation of such motions with increasing dioxygen content will result in appreciable positive contribution to both partial molar entropy and enthalpy. According to discusion in section 5.3.4.2, the enthalpies and entropies owing to the intramolecular motions for the unoxygenated and oxygenated (at the highest dioxygen content) samples are expected as shown in Figs.5.31a-f. In addition, schematic figures on the partial molar quantities of the corresponding systems are also shown in Figs.5.31a'-f'. Although intramolecular motions should be discussed according to excess entropy described in section 5.3.2,

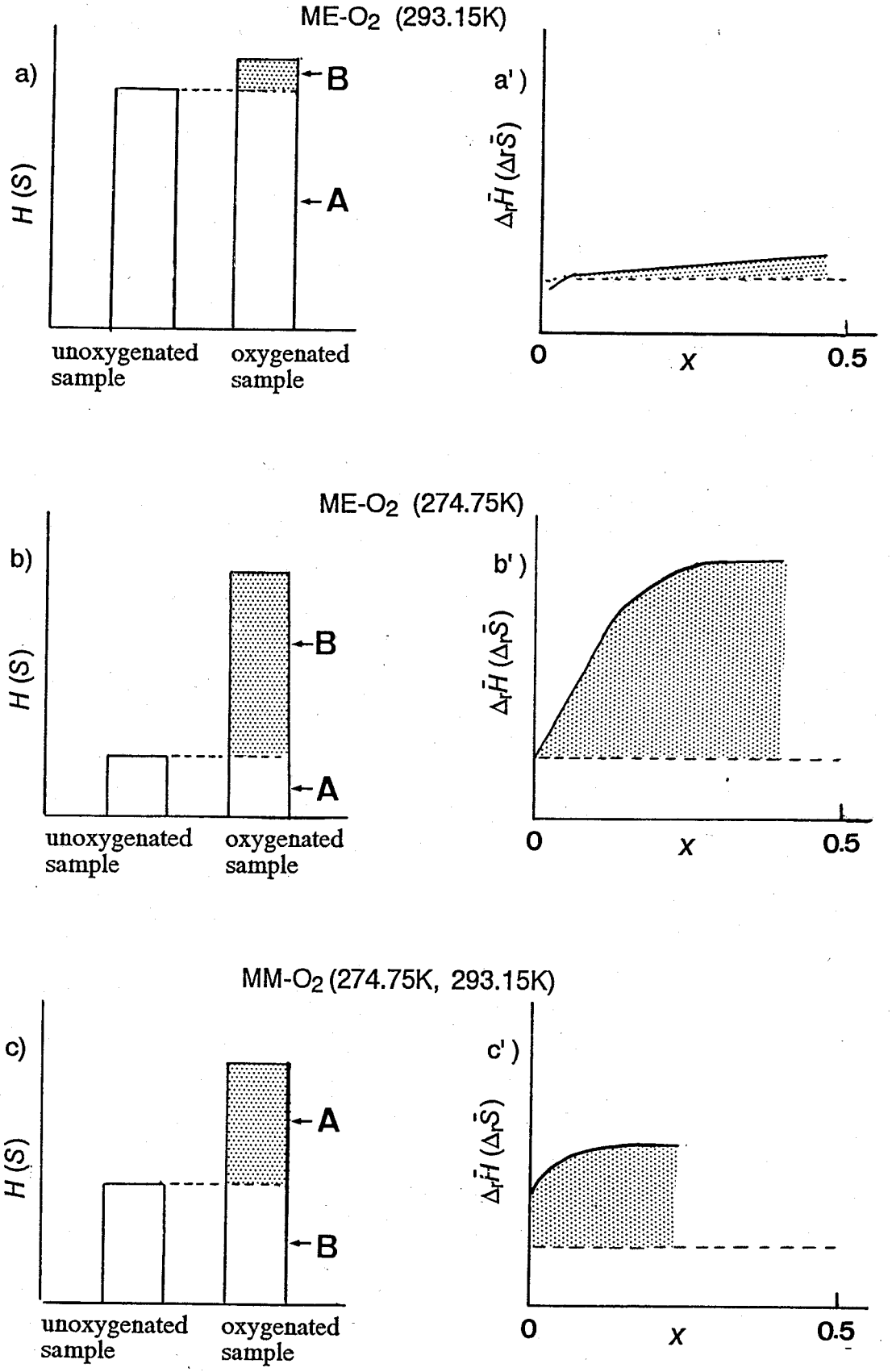

Fig.5.31 a)-f) : Schematic diagrams of enthalpy and entropy of the unoxygenated and oxygenated samples for the ME-O_2, MM-O_2, ET-O_2 and EM-O_2. The shaded regions (B) show additional enthalpy and entropy of the oxygenated samples relative to the unoxygenated samples (A). (to next page)

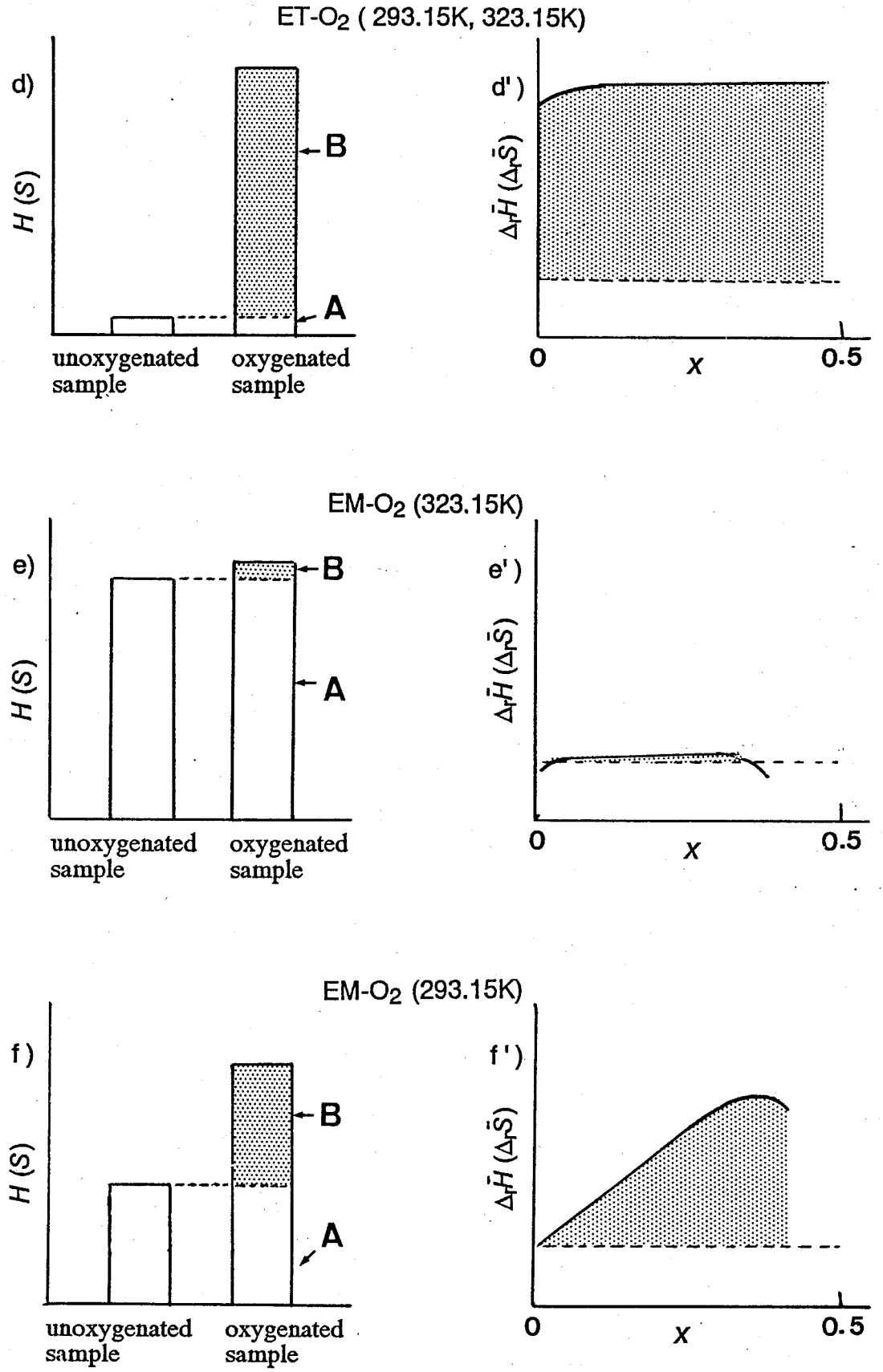

a')-f') : Schematic figures of the experimental partial molar enthalpy and entropy of the systems corresponding to a)-f), respectively. The broken lines show the estimated partial molar quantities without contributon from intramolecular motions of the complex molecules. The areas of the shaded regions show enthalpy and entropy gains by oxygenation upto the highest dioxygen content from the unoxygenated state. These areas correspond to the areas of the region B in a)-f).

differences in partial molar entropy between the present systems are not easily understood because of the significant dioxyge content dependence of the excess partial molar entropies arising from change in the lattice vibration. Since the same distribution of dioxygen in the complex crystal can be employed for the present systems as described in section 5.3.1, partial molar entropies instead of the excess quantities are used in order to discuss intramolecular motions. Moreover, since the partial molar enthalpies and entropies exhibited similar dioxygen content dependences as shown in Fig.5.3 and Fig.5.4, the two quantities are shown by the same lines for convenience.

For the ME-O_2 system at 296 K, both the unoxygenated and oxygenated samples are considered to possess much enthalpy and entropy (Fig.5.31a) because of the excited nature of the intramolecular motions at the temperature. Although the motions for the oxygenated sample at 273 K is excited similar to those at 296 K, the motions for the unoxygenated sample at 273 K is not excited as much as those at the higher temperature. Therefore the unoxygenated sample at the lower temperature is considered to possess much smaller than those at the higher temperature (Fig.5.31b). Because of the partially excited nature of the motions at the lower temperature, the unoxygenated sample would possess somewhat motional enthalpy and entropy. As described in section 5.3.4.2, the EM-O_2 system also showed similar change in the level of excitation of the intramolecular motions for the unoxygenated sample between 296K and 323K. Hence the diagram on enthalpy and entropy of the unoxygenated and oxygenated samples for the EM-O2 system is expected to be similar to that for the ME-O2 system as shown in Figs.5.31e and f.

According to above discussion, the unoxygenated samples of the ME-O_2 and EM-O_2 systems at the lower temperatures must gain much additional enthalpy and entropy (the shaded region in Figs.5.31b and f) through their oxygenation. Since enthalpy and entropy for the oxygenated sample with the dioxygen content are given by integration of the partial molar quantities from the unoxygenated state to the highest dioxygen content, the positive additional enthalpy and entropy for the oxygenated sample mean positive sifts in the corresponding partial molar quantities. Thus wide shifts in the partial molar enthalpy and entropy for the lower temperatures (ME-O_2: 274.75 K and EM-O_2: 293.15 K) and narrow ones for the higher temperatures (ME-O_2: 293.15 K and EM-O_2: 323.15 K) are expected.

Since the small dioxygen content dependences of the partial molar quantities at the lower temperatures (Figs.5.31a' and e') would result from slight higher enthalpy and entropy of the oxygenated sample relative to the unoxygenated one (the shaded regions in Figs.5.31a and e, the values determined by extrapolation to the unoxygenated state are employed as the values without contributions from intramolecular motions (broken line) because of significant uncertainty at about the unoxygenated state and the highest dioxygen content. Thus, approximately, the shaded regions in the Figs.5.31a', b', e' and f' are considered to correspond to the additional enthalpy and entropy shown by the shaded regions in Figs.5.31a, b, e and f, respectively. One can find that the expected trends of the partial molar quantities agree well with the trends of the positive shifts and the areas of the shaded regions shown in Figs.5.31a', b', e' and f'.

Additional enthalpy and entropy for the oxygenated sample of the ET-O_2 system are also expected at both 293.15 K and 323.15 K as shown in Fig.5.31d, because of the excited nature of the intramolecular motions for the oxygenated sample and the less excited nature of those for the unoxygenated one as described in section 5.3.4.2. This expectation is consistent with the wide positive shift (Fig.5.31d') in the partial molar quantities from the values (broken line) without contribution from the intermolecular motions which is determined for the EM-O_2 system at 323.15 K. Since the shaded region in Fig.5.31d' is the largest among the [Co(3-RO-SALEN)](R=CH_3, C_2H_5)-O_2 systems, the largest additonal enthalpy and entropy are expected for the oxygenated sample of the ET-O2 system (Fig.5.31d).

For the MM-O_2 system, the thermodynamic quantities could not estimated according to the spectral results as described in section 5.3.4.2. However, excitation of the intramolecular motions are expected for the unoxygenated and oxygenated samples at 296K and 273K. If difference between the experimental curve and the broken line in Fig.5.31c' arises from the excitation of the intramolecular motions, appreciable additional enthalpy and entropy would be expected as shown in Fig.5.31c.

Consequently, for the ME-O_2, EM-O_2 and ET-O_2 systems, it is qualitatively suggested that the variety of the partial molar quantities result from defference in the excitation level of the motions of the chelate skeleton of the complex molecules. For the MM-O_2 systwm, similar excitaion would be involved in the thermodynamic quantities. However, at the present stage, it is ambiguous what mechanism controlls the dioxygen content

dependence of the partial molar quantities for the ME-O_2 system at 274.75 K and the EM-O_2 at 293.15 K.

5.3.5 Differences between the fresh (ME and ET) and stored (MM and EM) samples

The fresh 3,3'-dialkoxy derivatives of [Co(SALEN)], ME and ET, were significantly different from the samples stored for 1 year under dioxygen (MM and EM). The stored samples exhibited changes in temperature and dioxygen content dependence of their thermodynamic values caused by excitation of vibration of the chelate skeleton (Fig.5.2, 5.3 and 5.4). They also exhibited their crystallographic features different from their fresh samples (powder diffraction patterns shown in Fig.5.5 and 5.6, and cell volumes shown in Fig.5.7 and 5.8), increase in molar magnetic susceptibility (Fig.5.9 and 5.10) and new absorption bands in diffuse reflectance spectra of their unoxygenated state (Fig.5.24 and 5.25). Although the infrared spectra of the MM-O_2 and EM-O_2 systems resemble to those of the ME-O_2 and ET-O_2 systems, respectively, shifts in wave number of some bands, and a few new bands were observed in far infrared region (Fig.5.18 and 5.19).

The difference between their electronic spectra and that between magnetic properties reflects change in the environment of the cobalt ion. However, the unoxygenated samples of MM and EM did not indicate exchange interaction between cobalt ions as found in $[Co(SALEN)]_2$[11] (Fig.5.32). This fact excludes the possibility of coordinative interaction to a cobalt ion by the salicylic oxygen atom of the adjacent complex molecule for MM and EM, which is also supported by the minor change in vibrational

spectra between the fresh and stored samples to that between the $[Co(SALEN)]_2$ dimer and its monomer.

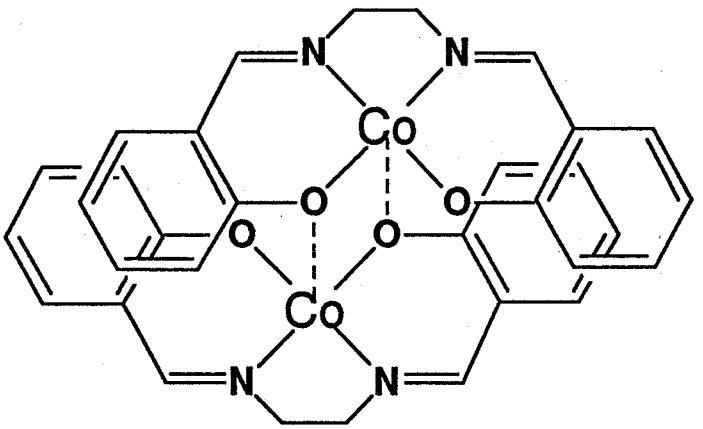

Fig.5.32 $[Co(SALEN)]_2$ dimer

Another possible origin of the differences is distortion of the chelate skeleton. The far infrared spectra of the methoxy and ethoxy derivative were different each other in the wave number of the chelate skeleton vibration band which indicated isotope shift by deuterating the ethylene bridge of the methoxy derivative as shown in Fig.5.18 and Fig.5.19, although they have a similar ligand which is only different from their alkoxy groups on their aromatic ring. This observation indicates that their alkoxy groups should affect the vibration of the chelate skeleton. Structural difference is suggested from the difference in the powder X-ray diffraction patterns and cell volumes between the fresh and stored samples. Therefore change in crystal packing around their alkoxy groups is considered to cause distortion of their chelate skeleton, and consequently, the vibrational modes of the chelate skeleton and the electronic structure of the cobalt ion would be perturbed.

References to Chapter 5

1. E.W.Hughes, W.K.Wilmarth and M.Calvin, *J.Am.Chem.Soc.*, 68, 2273 (1946).

2. K.Ueno and A.E.Martell, J.Phys.Chem., 59, 998 (1959); *ibid.*, 60, 1270 (1956).

3. D.B.Powell and N.Sheppard, *J.Chem.Soc.*, 112 (1967).

4. J.A.Faniran, K.S.Patel and J.C.Bailar,Jr., *J.Inorg.Nucl.Chem.*, 36, 1547 (1974).

5. M.Calvin and C.H.Barkelew, *J.Am.Chem.Soc.*, 68, 2267 (1946).

6. A.Earnshaw, P.C.Hewlett, E.A.King and L.F.Larkworthy, *J.Chem.Soc.*(A), 241 (1968).

7. M.Suzuki, T.Ishigro, M.Kozuka and K.Nakamoto, *Inorg.Chem.*, 20, 1993 (1981).

8. R.D.Jones, D.A.Summerville and F.Basolo, *Chem.Rev.*, 79, 139 (1979).

9. E.C.Niederhoffer, J.H.Timmens and A.E.Martell, *Chem.Rev.*, 84, 137 (1984).

10. M.Calligaris, G.Nardin and L.Landaccio, *J.Chem.Soc.Dalton Trans.*, 1903 (1974).

11. G.O.Carlisle, G.D.Simpson, W.E.Hatfield, Van H. Carwford and R.F.Drake, *Inorg.Chem.*, 14, 217 (1975).

Chapter 6 Summary

Physico-chemical studies were carried out on the gas-solid reaction systems between dioxygen and a series of solid-state synthetic oxygen carriers; [Co(SALEN)], [Co(3-RO-SALEN)] (R=CH_3 and C_2H_5), which form dimeric oxygenated species having a Co-O-O-Co linkage. Special attention was paid to cooperativity in their nonstoichiometric phases and intramolecular motion in the [Co(3-RO-SALEN)]-O_2 systems.

The partial molar Gibbs energy, enthalpy and entropy of oxygenation were determined by means of equilibrium pressure measurement and gas-solid reaction calorimetry. Magnetic and spectroscopic properties and powder X-ray diffractions as a function of dioxygen content and temperature were measured in order to clarify the situation of the complex molecules and the distribution of dioxygen in their crystals. Lattice dynamics calculation was performed on finite random lattices which are models of the present systems in order to study the effect of Co-O-O-Co linkages on their thermodynamic functions of and cooperativity in these systems.

In chapter 3, two kinds of [Co(SALEN)] which were prepared from its pyridine and chloroform adducts, were studied. They reacted with dioxygen up to Co:O_2=2:1, and gave similar phase relation, a two-phase region in low dioxygen contents and a one-phase nonstoichiometric region in high dioxygen contents, though small differences were found in their thermodynamic and magnetic properties which would be attributable to a slight difference in molecular packing. In their nonstoichiometric regions, their partial molar enthalpy was independent of dioxygen content, while

cooperativity in those systems was observed. On the other hand, since increase in their partial molar entropy with increasing dioxygen content results in decrease in their partial molar Gibbs energy, the dioxygen content dependence of the entropy term was found to be an origin of their cooperativity. These variations in thermodynamic functions were explained as contribution from change in lattice spectrum due to linkage formation between two adjacent complex molecules by a dioxygen moiety, through the lattice dynamic calculation described in chapter 4.

In chapter 5, studies on two types each of [Co(3-MeO-SALEN)] ("ME" and "MM") and of [Co(3-EtO-SALEN)] ("ET" and "EM") are described, where ME and ET are the fresh samples annealed prior to every oxygenation run, while MM and EM are the samples stored for 1 year in their oxygenated forms. The systems between dioxygen and those samples consist of a nonstoichiometric phase for which random mixing of oxygenated and unoxygenated complex molecules was suggested from dioxygen content dependence of magnetic susceptibility. However, the systems indicated appreciable difference in thermodynamic quantities, magnetic susceptibility, vibrational and electronic spectra, and X-ray diffraction patterns. The difference between those fresh sample (ME and ET) and stored sample (MM and EM) would be attributable to difference in packing of the alkoxy groups. The ME-O_2 system exhibited considerable temperature dependence of the partial enthalpy and entropy between 274.75 K and 293.15 K. At 293.15 K, these thermodynamic values were almost independent of dioxygen content, while those increased about 20 $kJmol^{-1}$ (in enthalpy) and 60 $kJmol^{-1}K^{-1}$ (in entropy) with increasing dioxygen content.

However, the MM-O_2 system did not indicate appreciable temperature and dioxygen content dependence between 274.75 K and 293.15 K. The ET-O_2 system did not show dioxygen content dependence at both 293.15 K and 323.15 K. However, the EM-O_2 system showed quite different dioxygen content dependence of thermodynamic values between 293.15 K and 323.15 K, which is similar to those for the ME-O_2 system.

The ET-O_2 system gave partial molar enthalpy independent of dioxygen content. Thus the cooperativity observed in the system was attributed to contribution from the entropy term resulted from the dimerization of the complex molecules by dioxygens, as suggested from the lattice dynamics described in chapter 4. Since the partial molar Gibbs energies of the ME-O_2, MM-O_2 and EM-O_2 systems showed dioxygen content dependence similar to the ET-O_2 systems, the dioxygen content dependences of partial molar enthalpies and entropies of the systems compensate each other, and cooperative interaction by dioxygen binding would be also suggested for the systems. For the ET-O_2 system and the ME-O_2 system (at 293.15 K), estimation of the partial molar entropy excluding the statistical entropy of random distribution of dioxygen suggested positive shift in the partial molar entropy with increasing dioxygen content.

Temperature of vibrational spectra for the unoxygenated and oxygenated samples of the systems showed that the positive contribution to partial molar enthalpy and entropy was attributable to excitation of intramolecular motions of the chelate skeleton of the complex molecules. For the ME-O_2, ET-O_2 and EM-O_2 systems, the experimental results agreed well with trends of the positive shift of the partial molar quantities

expected from the temperature dependence of vibrational spectra for the unoxygenated and oxygenated samples of the systems. For the MM-O_2 system, the motions would contribute to the partial molar quantities. However, at the present stage, it is ambiguous what mechanism controlls the dioxygen content dependence of the partial molar quantities for the ME-O_2 system at 274.75 K and the EM-O_2 at 293.15 K.

Consequently, cooperativity arising from linkage of a pair of complex molecules by a dioxygen was found in the systems between dioxygen and [Co(3-X-SALEN)] (X=H, OCH_3 and OC_2H_5). In addition, it was suggested that intramolecular motions also contributed to the thermodynamic property of the systems involving the alkoxy derivatives. These phenomena would contribute to oxygenation reaction of solid-state oxygen carriers, such as iron(II) picket fence porphyrins.